Spring 2014

Experimental and computational investigation of flow of pebbles in a pebble bed nuclear reactor

Vaibhav B. Khane

Department: Chemical and Biochemical Engineering

EXPERIMENTAL AND COMPUTATIONAL INVESTIGATION OF FLOW OF PEBBLES IN A PEBBLE BED NUCLEAR REACTOR

by

VAIBHAV B. KHANE

A DISSERTATION

Presented to the Faculty of the Graduate School of the

MISSOURI UNIVERSITY OF SCIENCE AND TECHNOLOGY

In Partial Fulfillment of the Requirements for the Degree

DOCTOR OF PHILOSOPHY

in

CHEMICAL ENGINEERING

2014

Approved by:

Muthanna H. Al-Dahhan, Advisor
Joseph D. Smith
Xinhua Liang
Joontaek Park
Gary E. Mueller

ABSTRACT

The Pebble Bed Reactor (PBR) is a 4th generation nuclear reactor which is conceptually similar to moving bed reactors used in the chemical and petrochemical industries. In a PBR core, nuclear fuel in the form of pebbles moves slowly under the influence of gravity. Due to the dynamic nature of the core, a thorough understanding about slow and dense granular flow of pebbles is required from both a reactor safety and performance evaluation point of view.

In this dissertation, a new integrated experimental and computational study of granular flow in a PBR has been performed. Continuous pebble recirculation experimental set-up, mimicking flow of pebbles in a PBR, is designed and developed. Experimental investigation of the flow of pebbles in a mimicked test reactor was carried out for the first time using non-invasive radioactive particle tracking (RPT) and residence time distribution (RTD) techniques to measure the pebble trajectory, velocity, overall/zonal residence times, flow patterns etc. The tracer trajectory length and overall/zonal residence time is found to increase with change in pebble's initial seeding position from the center towards the wall of the test reactor. Overall and zonal average velocities of pebbles are found to decrease from the center towards the wall. Discrete element method (DEM) based simulations of test reactor geometry were also carried out using commercial code EDEM^{TM} and simulation results were validated using the obtained benchmark experimental data. In addition, EDEM^{TM} based parametric sensitivity study of interaction properties was carried out which suggests that static friction characteristics play an important role from a packed/pebble beds structural characterization point of view. To make the RPT technique viable for practical applications and to enhance its accuracy, a novel and dynamic technique for RPT calibration was designed and developed. Preliminary feasibility results suggest that it can be implemented as a non-invasive and dynamic calibration methodology for RPT technique which will enable its industrial applications.

ACKNOWLEDGEMENTS

I wish to express my heartfelt gratitude and deep appreciation to Dr. Muthanna H. Al-Dahhan, my advisor, who guided me diligently and patiently through my PhD studies. He has been extremely helpful throughout and a constant source of knowledge and motivation. I have learned a great deal from him. He is becoming younger and I am becoming older day-by-day. I wish I can steal some of his energy and enthusiasm before graduating. He assigned me with number of challenging things such as proposals writing and I have learned something which will help me throughout my career.

I would also like to thank my committee members Dr. Joseph Smith, Dr. Xinhua Liang, Dr. Joontaek Park, and Dr. Gary Mueller for their support, co-operation and valuable inputs which helped me in shaping my research work. Special thanks to Dr. Mueller in guiding me with DEM based simulation work. I cannot imagine carrying out experimental work without great help from Mr. Adam Lenz. Also, I would like to thank to Dept. of Energy for a research grant **NERI-08-043** and my department for providing me with financial support to carry out this work. My department secretaries Julia, Krista and Marlene helped me with numerous things during my studies and would like to thank them. Also, I would like to thank staff of Graduate Studies, International Affairs and Curtis laws Wilson Library for helping and guiding me throughout my stay. I would like to thank to all my friends, colleagues for always being there for me and for making my studies at Missouri S&T memorable. Special thanks to Dr. P.K. Jain and Dr. James D. Freels from ORNL for mentoring me during my stay at ORNL.

This was a challenging journey and I would like to thank my wife Sfurti who accompanied me at every stage of this tightrope walk. I owe a lot to her and I don't think I am capable of paying it back to her. My son Aadi is the most beautiful thing happened to us and his silent co-operation with my studies is beyond appreciation. He has been great source of luck, hope, and motivation during my PhD studies. Most importantly, I would like to thank my Pappa, Mummy, Sachindada , Rupalivahini and Parshwa for everything they have done for me; without them none of this would have been possible.

TABLE OF CONTENTS

LIST OF ILLUSTRATIONS

LIST OF TABLES

NOMENCLATURE

Symbol	Description
D	Reactor diameter, inches
d_p	Particle diameter, inches
F_{ij}	Contact force between particle i and j
F_{nij}	Normal component of contact force between particle i and j
F_{tij}	Tangential component of contact force between particle i and j
V_{ij}	velocities
V_{wall}	Velocity at the wall
$V_{centreline}$	Velocity at the centerline
H	Reactor height, inches
$R_{run,\ calib}$	Cross-correlation coefficient
r/R	Dimensionless radial position
E	Young's modulus
G	Shear modulus
U	Superficial flow velocity
k	Stiffness
C	Damping coefficient

Greek letters

ξ	Overlap
ξ_t	Overlap in tangential direction
ξ_n	Overlap in normal direction
β	Half-cone angle
ϕ	Peak to total (Photo-peak) ratio
τ	Dead time of detector
ε	Total detection efficiency
Ω	Solid angle subtended by the detector surface at the tracer location
μ	Attenuation coefficient
μ_{static}	Coefficient of static friction

$\mu_{rolling}$	Coefficient of rolling friction
ν	Poisson ratio
ρ	Particle density
ε_{avg}	Mean/average/bulk porosity
Δt_c	Critical time-step
ΔP	Pressure drop
ν	Kinematic viscosity

Abbreviations

PBR	Pebble Bed Reactor
PBMR	Pebble Bed Modular Reactor
VHTR	Very High Temperature Reactor
RPT	Radioactive Particle Tracking
RTD	Residence Time Distribution
DEM	Discrete Element Method
MFI	Mass Flow Method
AARE	Absolute Averaged Relative Error
ROI	Region of Interest
CV	Control Volume
NIM	Nuclear Instrumentation Module
CAMAC	Computer Automated Measurement and Control
EDEM™	Experts of Discrete Element Method
COR	Coefficient of restitution
CFD	Computational Fluid Dynamics

1. INTRODUCTION

Nuclear energy will play a crucial role in achieving future global energy demands due to rapidly depleting fossil fuels, growing concerns about global warming and climate change issues, and sustainable development point of view. Electricity generation by nuclear means is a proven technology and is becoming more popular due to its zero greenhouse gas emission. Nuclear energy is the only proven large-scale non fossil fuel source of energy and is capable of meeting rapidly increasing global energy demands. Over the years nuclear power plant technology evolved into four different distinct generations as demonstrated in Figure 1.1 and outlined below.

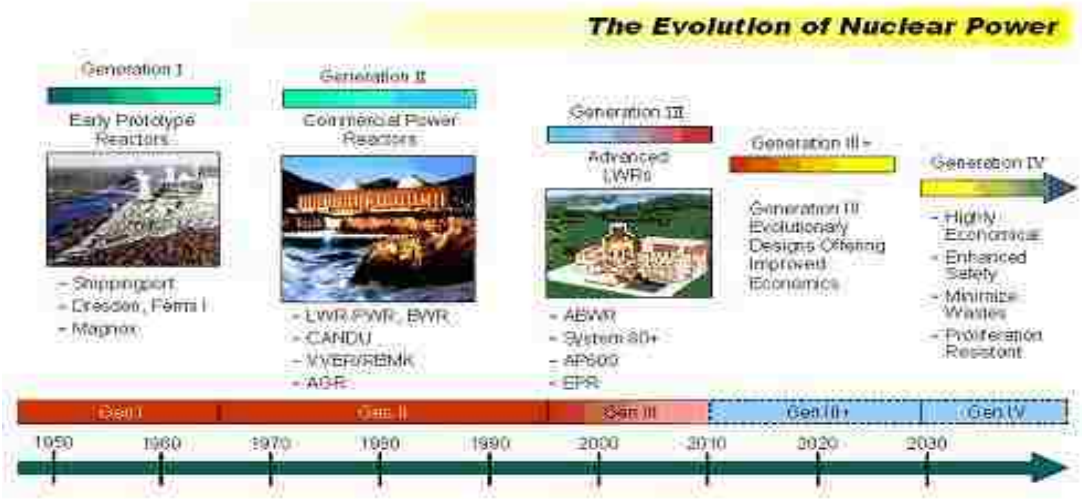

Figure 1.1. Evolution of distinct generations of nuclear power over the years (US Department of Energy annual report for Gen IV reactors, 2011)

- **First generation** (~1950-1970) – consists of prototypes and demonstrated safe generation of electricity by nuclear means.
- **Second Generation** (~1970-2030) – consists of current operating plants which went under power up-rating and life extension
- **Third Generation** (~2000 and on) – consists of deployable improvements to current reactors mainly passive safety systems were used
- **Fourth generation** (2030 and beyond) – also known as Gen-IV reactors consists of advanced and new reactor systems

Current reactors in operation around the world fall under second or third-generation systems, with most of the first-generation systems having been retired or revamped to second or third generation reactors in past. Gen IV reactors are nuclear reactor designs currently being researched around the world. A number of innovative reactor concepts were considered initially and six designs were finalized as Gen IV candidates. These designs meet the goals of Gen IV initiative started by the Generation IV International Forum (GIF). The main features of these designs are as follows: nuclear safety, higher resistance to proliferation of fissile materials, minimum radioactive waste generation, efficient and economical design reducing the cost to build and operate such plants. These designs demand extensive research in order to prove their safety and reliability. The very high temperature (VHTR) reactor is one among these six designs and is uses gaseous coolant. They are either prismatic block reactors or pebble bed reactors and are discussed in detail in the following sections. It is noteworthy to mention that the focus of this work is on pebble bed reactors.

1.1. VERY HIGH TEMPERATURE REACTOR

The very high temperature reactor (VHTR), or high temperature gas-cooled reactor (HTGR), is one of the Generation IV reactor types that is graphite-moderated and helium cooled, using TRISO (Tri-isotropic) uranium fuel particles. The VHTR can have a design outlet temperature of 900^{o}-1000^{o}C. The high outlet temperatures of VHTR's find numerous applications in process heating and hydrogen production via the thermochemical sulfur-iodine cycle beside higher thermal efficiency of electrical power generation. There are two main versions of VHTR's: Prismatic modular reactors (PMR) and pebble bed reactors (PBR).

1.1.1 Prismatic Type VHTR Design. In a typical prismatic block type VHTR design (600Megawatt thermal GT-MHR), graphite hexagonal blocks (which are either fuel or reflector blocks) are stacked on top of each other to form columns (Figure 1.2) and the hexagonal arrangements of those columns form the core of a prismatic block type VHTR design (Shenoy,1996 , INL,2008). Each fuel block has circular holes for fuel and coolant that are aligned axially with those of the other blocks over the entire length of the column. The fuel holes contain the fuel pellets made of the TRISO particles, while the coolant holes are aligned axially to form coolant channels. The central and side graphite blocks in the prismatic core are replaceable reflectors while those at the outer periphery are permanent side graphite reflectors placed between the side replaceable reflectors and the core wall. Helium at 500 °C enters the reactor from its bottom part, flows to the upper part of the core through the inlet riser holes in the permanent side reflectors, cools the active core from top to bottom, and finally exits through the lower plenum at high temperature (900-1000 °C) (Figure 1.3).

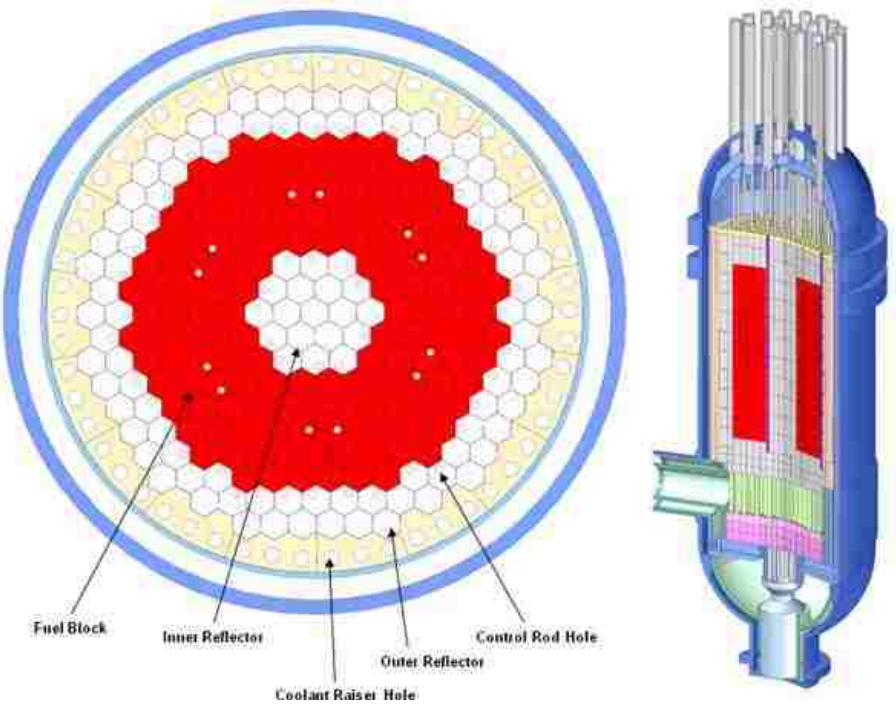

Figure 1.2 Typical prismatic type VHTR core configuration (Lee et al., 2010)

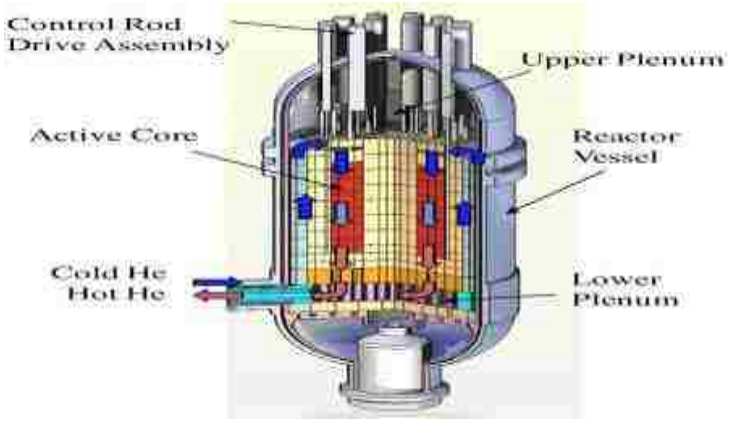

Figure 1.3. Helium flow path in typical prismatic type VHTR (Tak et al., 2011)

1.1.2. Pebble Bed Type VHTR Design. The pebble bed reactor (PBR) concept was conceived and developed at Oak Ridge National Lab (ORNL) (ORNL Review-nuclear power and research reactors). Nuclear fuel is in the form of spherical pebbles and these pebbles move under the influence of gravity. Pebbles leaving the reactor are recycled based on the utilization of fissile materials. Germany pursued the concept of PBR further and built 15 MWe demonstration reactor Arbeitsgemeinschaft Versuchsreaktor (AVR) at Jülich Research Centre in Jülich, West Germany in late 60's (Sen and Viljoen, 2012). Based on operational experience from AVR, Thorium High Temperature Reactor rated at 300 MW (THTR-300) was constructed in early 80's. THTR-300 was shut down after 4 years. Operational experience reveled that both reactors faced problems such as significantly higher temperature, radioactive dust production and associated contamination, and blockage of pebbles. In 2004, Eskom-South African government owned electrical utility company announced development of Pebble Bed Modular reactor (PBMR) project. Each module of PBMR has 400MWth rating (165 MWe) and modular feature allows faster construction times. PBMR project was abandoned in 2010 due to lack of funds. China has an operating 10-megawatt high temperature reactor (HTR-10) based on the pebble bed design at Tsinghua University and plans to construct a commercial 250-megawatt unit in near future (South China Morning Post, 05/10/2004). PBMR was being considered as one of the candidates for Next Generation Nuclear Plant (NGNP) - Generation IV initiative by U.S. Dept. of Energy (DOE) along with the prismatic block high temperature reactor (US DOE Report, 2002). Both these VHTR designs contain their fuel in the form of TRISO fuel particles (Boer, 2009). The uranium dioxide fuel particles (~450 μm in diameter) are coated with four

layers of carbon and silicon carbide the TRISO (TRi-ISOtropic) coating- which acts as "the primary containment" of fission products. The coated particle is having ~900-950 µm in diameter (Figure 1.4).

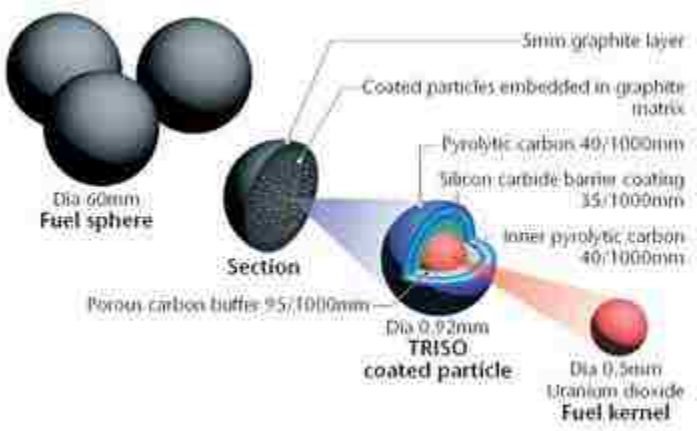

Figure 1.4. Fuel element design for PBR (**http://www.pbmr.co.za**)

In a typical pebble bed type VHTR design, about 11000-15000 LEU (lightly enriched uranium) TRISO fuel particles (8-10% U-235 by wt.) are mixed with graphite powder to form a fuel pebble having diameter of 6cm (Figure 1.4). Graphite is used because of its excellent structural characteristics at high temperature and its ability to slow down neutrons to the speed required for the nuclear fission reaction to take place. The reactor is filled with approximately 460,000 pebbles (fuel and graphite reflector). In the central region graphite pebbles are present whereas; in the annular region fuel pebbles are present. Both fuel and graphite pebbles move in the core under the influence of gravity (Figure 1.5).

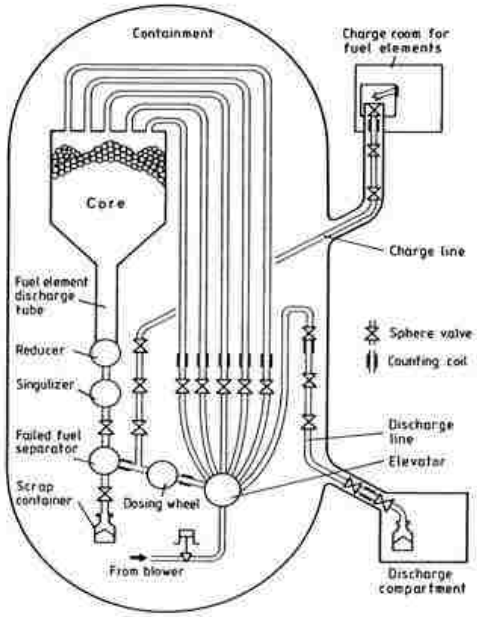

Figure 1.5. Typical Pebble bed reactor configuration (http://web.mit.edu/pebble-bed)

The fuel pebbles are continuously re-circulated through the core and are monitored for burn-up (Terry et al., 2002). Helium gas moves downwards through complex interconnected network of voids formed between pebbles and removes the heat from the fuel (Yang et al. 2009). After each pass through the reactor core, the fuel pebbles are examined to determine the amount of fissionable material left in it. If a pebble still contains certain usable amount of the fissile material, it is returned to the top of the reactor for a next pass. The returned radial placement position of pebble depends on fissile material content in that pebble. This continuous re-circulation feature eliminates the need to shut down the reactor for refueling. Also, it helps in the efficient utilization of fissile material due to which high burn-up can be achieved. The continuous refueling feature is the main advantage of a PBR design over other core designs, including

prismatic versions based on the same fuel design concept. The work carried out as a part of this research involves experimental and computational investigation of slow and dense granular flow in pebble bed reactors (PBR's).

1.1.3. Moving Bed Reactors. Moving bed reactors are used in the chemical and petrochemical industries to replace deactivated catalysts with new or regenerated catalysts and to gasify bio-mass and non-conventional feedstock's in these reactors. They are analogous to pebble bed reactors (PBR's). They find applications in multiphase reaction systems where there is significant catalyst decay and require continual regeneration, replacement of the catalyst and gasification of bio-mass while the bed is moving downward. Catalysts are introduced into the reactor at the top and fall through the reactor under the influence of gravity. The spent catalysts are withdrawn from the bottom of the reactor for regeneration/disposal (Fogler, 2005) while ash from biomass gasification process is removed from the bottom. Catalyst particles are typically between $1/8$ and $1/4$ inch in diameter. The main difference between PBR's and moving bed reactors used in chemical industries is the size of particles: pebbles are bigger in size (6 cm in diameter) as compared to catalysts which are much smaller in size. There are different configurations of moving bed reactors used in hydro-desulphurization of heavy oils (e.g. Shell's residue hydro-processing technology using bunker-flow reactor and online catalyst replacement (OCR) technology from Chevron etc.) (Sie, 2001). Generally, fresh/regenerated catalyst or bio-mass and non-conventional feed-stock enters at the top of the moving bed reactor and then moves through the reactor as compact packed-bed. For catalytic reaction, the catalysts keep on deactivating due to chemical reaction while moving through the reactor until they exit the reactor. They are then sent to the

regenerator and returned back to the reactor or they are disposed as solids waste. If required, fresh catalysts are added to the reactor at the top. As mentioned earlier, the work carried out as a part of this research is focused on pebble bed nuclear reactors. However, it would also benefit moving bed reactors used in the industry other than nuclear industry.

1.2.MOTIVATION

A granular material is defined as a collection of solids or grain particles. In such materials, most of the particles are in contact with some of their neighboring materials (Rao and Nott, 2008). Flow of such granular materials is known as a granular flow. Granular materials exhibit solids-type behavior when at rest, whereas exhibits partial fluid-type behavior when flowing. e.g. Granular materials will flow from vessels under the influence of gravity but the mass flow rate will be approximately independent of head of the material above it. This kind of behavior can be attributed to the friction between particles and between particles and the wall. Due to the complex behavior, there is still lack of unified theory for granular materials. The core of a pebble bed reactor (PBR) has a cylindrical shape with a conical bottom hopper which contains an exit opening for the pebbles and the cooling gas (Li et al., 2009). Such kind of geometrical configuration is also known as a *bunker*. The granular flow in a PBR or moving bed reactors is an example of slow and dense type granular flow under the influence of gravity with long-lasting frictional contacts. The basic physics governing it is not yet fully understood and relies on experimental investigations and numerical simulation methods such as discrete element method (DEM) to extract useful information.

In most nuclear reactors, including the prismatic block type high temperature reactor core, the fuel element is stationary and coolant moves through a pre-defined channel geometry formed between fuel elements, control rods, the reactor pressure vessel and other structural elements. The dynamic core of a PBR is a cause of concern from safety analyses and licensing point of view. Hence, an investigation of pebbles flow field is of paramount importance and is required for basic reactor design calculations, estimation of fuel burn-up and core power distributions, to devise refueling strategies, and safety analyses and assessment (Rycroft et al., 2006). It is crucial to have full knowledge about pebbles flow field in terms of Lagrangian trajectories, overall and local residence time distribution, velocities, and stagnant zones, if any. Conventional optics based velocimetry techniques are of limited use for investigation of granular flow in a PBR; as these systems are dense and opaque. Hence, many of previous studies (Kadak and Bazant, 2004 , Yang et al., 2009, Li et al., 2009) were carried out using half-model or 180° model of actual PBR. Due to an additional transparent wall in such half models, actual granular flow is not very well mimicked. Particles at the mid-plane transparent wall were tracked visually and in an intermittent manner in such half-models. In some of previous studies (Gatt,1973; Kadak and Bazant, 2004; Shehata, 2005) collimated detector based radioactive particle tracking technique was used to track the motion of pebbles in a scaled PBR model. These studies provided limited information about pebbles path-lines or trajectories and were performed on scaled down PBR geometries. Experimental investigation in scaled-down geometries can provide benchmark data for validation of current computational methodologies associated with granular flows. These validated computational methodologies can then be used to carry out high fidelity

simulations of actual scale PBR geometry. Hence, there is a need to perform integrated experimental and computational study of a granular flow in a scaled down PBR geometry. Experimental study involving 3-D scaled-down cold flow PBR set-up (without flow of any gaseous coolant) mimicking continuous recirculation of pebbles will be needed as a first attempt. By tracking motion of individual pebbles, path and time dependent position information about pebbles can be obtained. This information will be important from burn-up estimation, devising re-fuelling strategies for steady state core design point of view. The time spent by pebbles at particular position in the core (local residence time) and total time taken by pebbles from their entry in the core to its exit from the core (global residence time) will be crucial information for estimation of burn-up. Residence time distribution (RTD) study can provide further insight on non-idealities associated with pebbles flow in the core. A stagnant/dead zone may exist in the pebble bed reactor near the transition from cylindrical to conical section. Pebbles in the stagnant zone will be moving extremely slow or may be stand-still. This can lead to hot spots in the core, possibility of severe irradiation damage and subsequent release of radioactive fission products from the pebbles. Hence, identification of stagnant zones and estimation of its extent is of paramount importance from PBR safety point of view. Ideal PBR operation should have nil or smallest size stagnant/dead zones.

Radio-isotopes based non-invasive techniques such as radioactive particle tracking (RPT) and residence time distribution (RTD) techniques are capable of providing useful information about granular flow in a PBR in a non-invasive manner. They can provide detailed information about pebble flow fields, overall and local residence time distribution of pebbles, stagnant zones and their sizes, and many other

parameters (Al-Dahhan, 2009). Study of slow and dense granular flow in a cold-flow recirculation experimental set-up using advanced radio-isotopes based flow visualization techniques is one of the main objectives of this work. Designing and development of continuous cold-flow pebble recirculation experimental set-up, which mimics the flow operation of PBRs, was carried out as a part of this study. The distribution of solids and voids in the bed plays an important role from coolant dynamics and reactor neutronics point of view. The spatial distribution of solids will determine the neutron flux profile and hence, heat generation rate due to fission. The coolant gas flows through the complex interconnected network of voids and knowledge about radial and axial porosity variation profile is required for study of coolant dynamics. It will be important to characterize local bed structure and also to check the effect of pebble movement on the distribution of solids and voids. The slow and dense granular flow in a PBR is currently approximated by the study of static packed beds (duToit, 2002). However, there are no such experimental studies in the open literature to support the conclusions of the published research. Hence, there is a need to compare packing characteristics between static packed beds and the moving beds of PBRs. This issue has been addressed to some extent in this work.

Discrete Element Method (DEM) simulations are based on a modified version of model developed by Cundall and Strack (1979). DEM calculations alternate between the application of Newton's second law of motion and force-displacement law at the contact points. DEM requires calculation of contact forces, which are evaluated using phenomenological contact models. A contact model describes how elements behave when they come into contact with each other. There is a lack of contact force models

developed from the first principles (Rao and Nott, 2008) and this demands assessment of contact force models with experimental benchmark data, which is another main objective of this work. A computational study using experts in discrete element method (EDEM^{TM}) - a commercial DEM code from DEM Solutions Ltd., UK was carried out. Also, the calculation of contact forces demands accurate input of various interaction properties which needs to be determined by developing simple experimental set-ups, in case of their unavailability (Li et al., 2005). This is necessary to ensure fair assessment of simulations with experiments. In any DEM based analysis, first step is to pack particles inside a confined geometry. Reliable numerical analysis of fixed/packed beds is a challenging engineering task due to the complexity of bed structure. Accurate representation of complex 3-D packed beds structure is essential; since local flow and transport characteristics of the fluid flowing through the voids are closely coupled with the local bed structure. Also, nature of packing affects subsequent motion of particles in granular flows. There is a need to perform a comparison study of numerically simulated packing structures with available benchmark data and was carried out as a part of this work. Radial porosity variation profile is a good indicator of local bed structure and was used along with mean porosity values for structural characterization of beds. Also, EDEM^{TM} (Discrete Element Method based commercial code) based parametric sensitivity study of interaction properties was carried out to determine sensitivity of packed bed structural properties to interaction properties and highlight important interaction properties from experimental determination and from a reliable EDEM^{TM} based simulation point of view.

It is of interest to identify the flow pattern in systems involving flow of granular materials such as bunker-type geometries. If there is a simultaneous motion of all

particles without any stagnant zones, mass flow occurs (Figure 1.6.a). Usually, for the hoppers with steep walls (smaller values of half cone angle -β) mass flow is observed. On the other hand, if there is a rapid movement of material surrounded by either stagnant or slowly moving particles, funnel/core flow occurs (Figure 1.6.b).

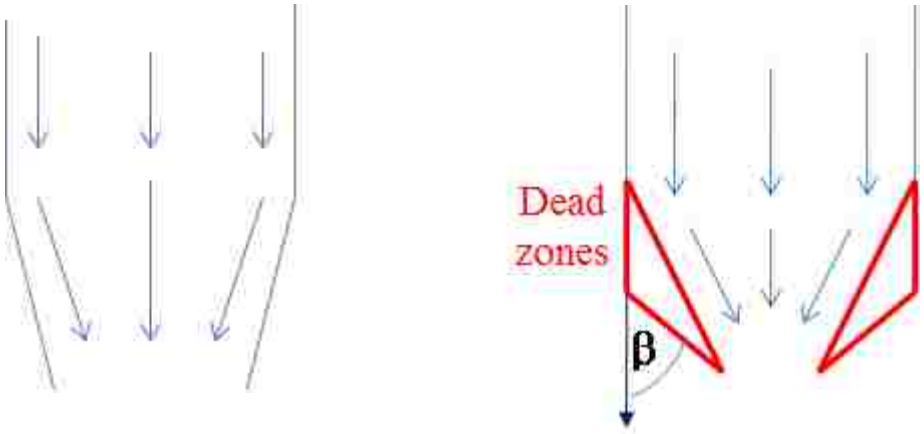

a. Mass flow b. Funnel flow

Figure 1.6. Flow patterns observed in Bunkers

The simultaneous presence of stagnant and moving zones makes it difficult to model such systems due to the requirement of different sets of governing equations for two zones. Usually, for the hoppers with shallow walls (larger values of half cone angle -β) funnel/core flow is observed (Nedderman, 1992). Hence, there is a need for reliable and detailed experimental data which can be used as a benchmarking data for DEM based simulations besides advancing the understanding of the interplay phenomena of the pebbles dynamics. Such benchmarking data can be obtained using advanced radioactive

particle tracking technique which are suitable for opaque systems like pebble bed reactor. Such benchmarking data will not be only useful to validate the simulation results carried out in this work but also in assessment of reported codes and models such as PEBBLES. However, radioactive particle tracking (RPT) technique, a versatile non-invasive flow mapping technique, has limited applicability for commercial applications due to its existing time consuming, static, and invasive calibration methodology that must be performed before actual RPT experiments. In existing calibration methodology, the radioactive tracer particle used for tracking study is held static at known locations by different means (manual/automatic calibration apparatus) and photo-peak counts in the detectors are recorded. This radioactive tracer particle moves during actual RPT experiments. The static calibration methodology generates a calibration curve, i.e. a map of counts vs. the tracer-detector distance, which is then used to reconstruct the locations and Lagrangian trajectories of the radioactive tracer. Hence, there is an error associated with position reconstruction of a moving particle using static calibration data. To make the RPT technique viable, advancement in existing RPT calibration methodology is essential to make it non-invasive and dynamic. This was another main objective of this work. As a part of this work, design and development of novel and dynamic RPT calibration equipment, which is a synergistic combination of fixed non-collimated detectors based RPT technique and collimated detectors based RPT technique, was carried out.

1.3.OBJECTIVES

The main objective of this work is to design and develop cold flow continuous pebble recirculation experimental set-up mimicking cold flow operation of a PBR, and implement advanced radioisotopes-based flow visualization techniques such as RPT and residence time distribution (RTD) around it to extract detailed information about pebbles flow field for benchmarking simulation methodologies related to the granular flow. To make the RPT technique viable for practical applications, advancement in RPT technique's calibration methodology is essential and is one of main objectives of this work. In order to achieve the above mentioned objectives, following tasks as outlined in Figure 1.7 were carried out as a part of this work.

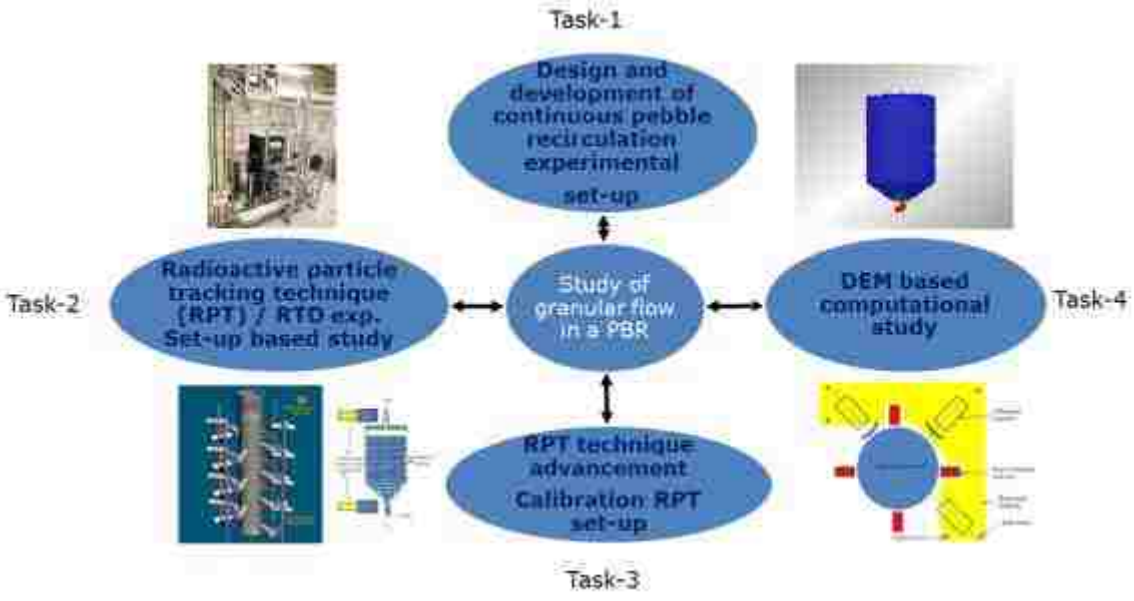

Figure 1.7. Planned tasks for an integrated study of granular flow in a PBR

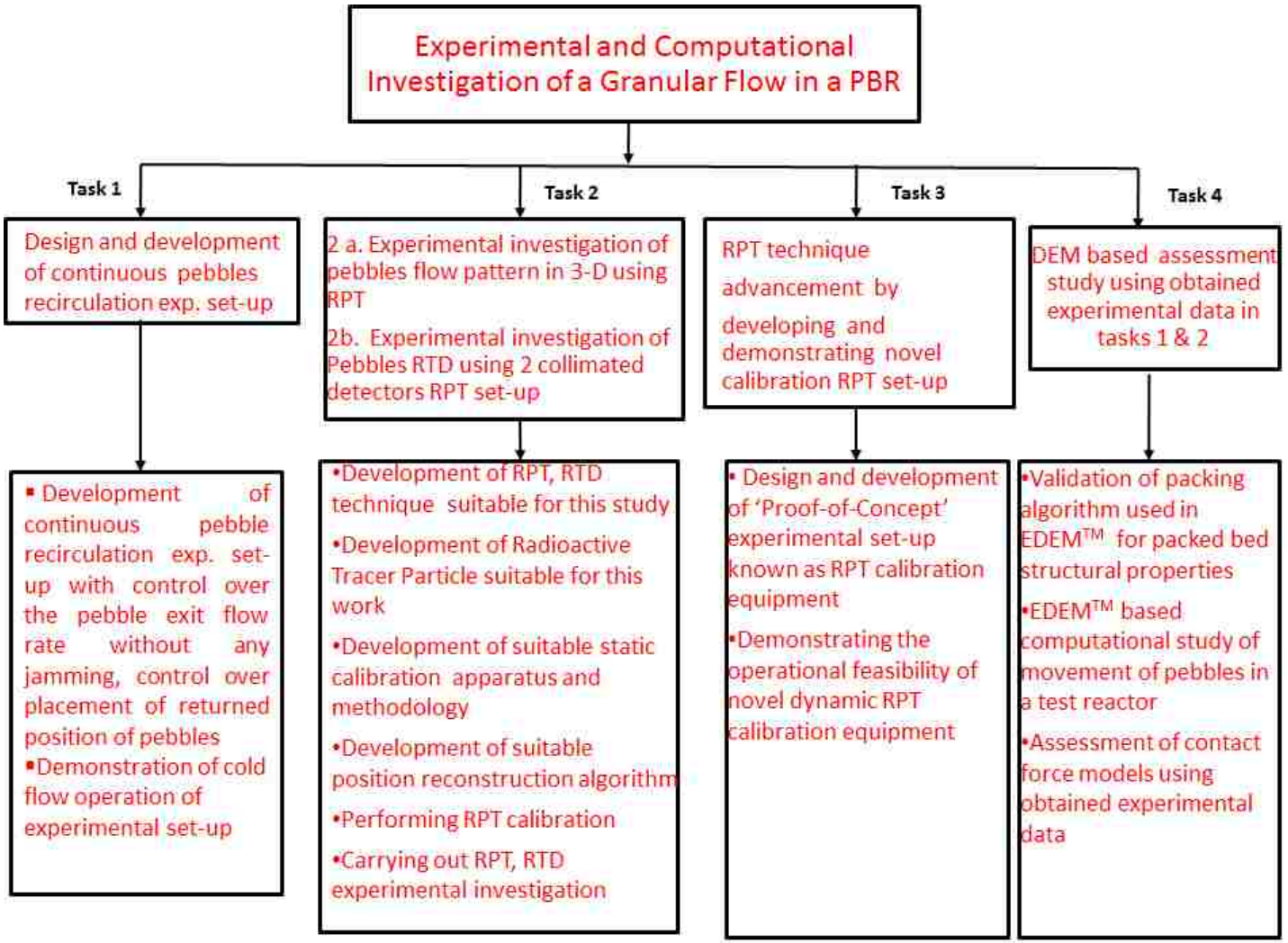

Figure 1.8 Tasks and sub-tasks planned and executed as a part of this work

This research work is divided into 4 main tasks. Various sub-tasks planned under each task are tabulated in Figure 1.8. These tasks and sub-tasks will be elaborated in details in respective sections devoted for each task. Description about each task is as follows:

Task 1: Development of a continuous pebble recirculation experimental set-up to demonstrate cold flow operation of a PBR, having control over pebble's exit flow rate without any jamming and placing returned pebble at any desired location in a non-violent manner

Sub-task 1a: Development of continuous pebble recirculation experimental set-up with above mentioned features

Sub-task 1b: Demonstration of cold flow operation of experimental set-up

Task 2: Investigation of pebble flow dynamics by implementing advanced radioisotopes based flow visualization techniques around continuous pebble recirculation experimental set-up

Sub-task 2a: Development of RPT, RTD technique suitable for this study

Sub-task 2b: Development of radioactive tracer particle suitable for this work

Sub-task 2c: Development of suitable static calibration apparatus and methodology

Sub-task 2d: Development of suitable position reconstruction algorithm

Sub-task 2e: Performing RPT calibration

Sub-task 2f: Carrying out RPT and RTD experimental investigation and to provide benchmark data for validation of models and codes such as PEBBLES

Task 3: RPT technique advancement by developing and demonstrating a novel, dynamic and non-invasive calibration RPT set-up which synergistically combines conventional RPT technique with collimated detector based RPT technique

Sub-task 3a: Design and development of 'proof-of-concept' experimental set-up known as RPT calibration equipment

Sub-task 3b: Demonstrating the operational feasibility of the novel dynamic RPT calibration equipment

Task 4: Assessment of contact force models used in DEM based simulations using experimental benchmark data obtained in task 2 and further assessment of simulation results

Sub-task 4a: Validation of packing algorithm used in EDEM^{TM} for packed bed structural properties

Sub-task 4b: EDEM^{TM} based computational study of movement of pebbles in a test reactor

Sub-task 4c: Assessment of DEM contact force models using obtained experimental data

1.4. THESIS ORGANIZATION

Section 2 provides detailed literature review of previous experimental and DEM based studies related to dense and granular flow in a PBR. Also, previous experimental studies and continuum models related to granular flow in a PBR such as kinematic model (used widely) are reviewed.

Section 3 describes the design and development of cold flow continuous pebble recirculation experimental set-up and its need, inlet and exit control mechanism, salient features of this set-up.

Section 4 presents experimental study carried out using advanced radio-isotopes based flow visualization techniques such as RPT and RTD. Detailed description about these techniques such as various components of these techniques, electronic data acquisition system, and position reconstruction algorithms has been covered in this Section. Obtained results about pebbles flow field are discussed in detail in this Section.

Section 5 discusses the issue and challenges with conventional RPT calibration methodology and need for novel dynamic calibration RPT equipment. Detailed design and development of novel hybrid calibration RPT equipment and its various components such as mechanical structure, motion control and radiation detection system, data collection and processing programs are described in detail. Preliminiary operational feasibility results obtained using calibration RPT equipment, its advantages and limitations are also discussed in this Section.

Section 6 discusses DEM simulation methodology, need for validation of packing algorithm used in EDEM^{TM}, experimental determination of interaction properties for interactions of interest, EDEM^{TM} based validation and parametric sensitivity study of

interaction properties for simulation of realistic packed bed structures, EDEM^{TM} based study of granular flow in a scaled down pebble bed reactor and obtained results, identification of flow patterns and assessment of contact force models used in DEM simulations using experimental benchmark data.

Section 7 summarizes the research findings of work presented as a part of this dissertation and concludes with recommendations for future work.

2. LITERATURE REVIEW

Flow of pebbles under the influence of gravity in a pebble bed reactor is an example of slow and dense type granular flow. The moving core of a PBR is a cause of concern from safety and performance evaluation point of view, which demands basic understanding about the physics governing dense granular flow. In the slow flow regime, the solids fraction is high (dense) and contact forces between neighboring particles last over a long time (slow) (Rao and Nott, 2008). This poses challenges in experimental investigation of granular flow using conventional optical techniques and due to which very few number of experimental studies related to this topic were carried out. A few number of DEM based computational studies of granular flow in a PBR can be found in the open literature. However, there are many DEM based studies of granular flow in a bunker or silo type geometries. The objective of this section is to present previous studies which are directly related to this work, their findings, especially shortcomings which helped in shaping this work. This literature review consists of

- Previous experimental studies and measurement methods related to pebbles flow in a PBR
- A brief review of DEM
- Previous DEM based studies related to pebbles flow in a PBR
- A review of continuum based kinematic models

This review not only lays down necessary foundation for the objectives of the current work but also provides suitable inputs to make this study more relevant to PBR technology.

2.1. PREVIOUS EXPERIMENTAL STUDIES AND MEASUREMENT METHODS

There are few number of experimental studies related to investigation of granular flow in a PBR. These studies are discussed in chronological order in next paragraphs.

2.1.1. Gatt's Study. An experimental study was performed at Australian Atomic Energy Commission (Gatt, 1973) to track pebbles trajectories at pre-defined intervals of time from the outside in recirculated randomly packed beds. A radioactive tagged pebble was seeded into the system at the top of the bed and allowed to follow the motion of pebbles. It was tracked from the outside at pre-defined intervals of time using tracking device mounted on a moving platform. This tracking device consisted of 3 well-collimated scintillation detectors. The main objectives of this study were:

1. To track the motion of individual pebbles seeded in the bed under different operating conditions and bed parameters and to provide information about associated velocity field
2. To provide information about overall residence time in terms of transit number for different seeding radius. Transit number is defined as the number of pebbles recirculated between the seeding of the radioactive tagged pebble and its exit from the bed, expressed as a fraction of total number of pebbles in the pebble bed (Gatt, 1973)
3. To define the boundaries of plug flow zone, pipe zone, dead or stagnant zone and the pipe feed zone
4. To determine effect of extractor rotation on the pebble motion

Experimental set-up used for this study consisted of an aluminum cylinder of 30 inch in diameter and 60 inch in height with a conical base and single axial outlet. Different bases of 15°, 25°, 35° and 45° cone angles (measured from the horizontal) were used. Spherical and aspherical pebbles of 1 inch or 0.75 inch diameter pebbles press

formed from plastic bonded zirconite sand were used in this investigation. Aspherical pebbles were used to mimic worn fuel pebbles. Random and relatively loose packings having void fraction of ~0.404 were constructed. In order to avoid scatter of returned pebbles, an entry mechanism was designed to ensure that entry of pebble was nearly vertical and possessed negligible inlet velocity. An extraction device was designed to remove the pebbles from the bottom at a controlled flow rate without jamming. It consisted of a raised cylindrical center surrounded by troughs which can exactly align to pebbles themselves. During extractor rotation, elongated hole allows a pebble above it to fall into rotating pipe attached to extractor and removes pebble from the system. This device is very important in this kind of study and a modified version of it has been used in the experimental set-up designed and developed as a part of current work. A radioactive tagged pebble used in this study used cobalt-60 isotope and has same sphericity, diameter, specific gravity and surface finish as that of pebbles used. Gamma rays emitted by radioactively tagged pebble while following the motion of pebbles were recorded and motion of tagged pebble was tracked using a pebble tracker device which consisted of three well collimated scintillation detectors mounted on a moving platform. The detector at the center was used to identify the vertical position (z co-ordinate) of tagged pebble, whereas other two detectors capable of swinging around vertical axis provided angular positions (θ_1 and θ_2). In this manner, this tracking device provided all the three position co-ordinates of tagged pebbles in a non-invasive manner. This tracking technique is also known as collimated version of RPT technique. RPT is the best suited technique for this PBR study, as it has no limitations on operating conditions, opacity, system design and configuration. In Gatt's work, magnetic tapes, analog electronics were

used to collect experimental data which might have limited continuous tracking ability. A total of 204 separate experiments were carried out to investigate different aspects of pebbles dynamics. The trajectories of pebbles through the pebble bed were found to be streamlined and there was a little interference or crossing between pebbles trajectories. The obtained results were analyzed to identify boundaries of four different flow zones observed during discharge of granular material from silos. Deutsch (1967a) suggested that flow domain can be divided into four different zones: pipe, pipe feed, dead and plug flow zones (Figure 2.1).

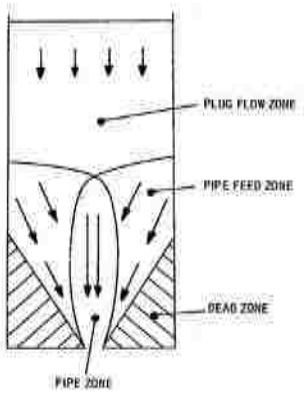

Figure 2.1. Flow zones (Deutsch, 1967a)

Pipe zone is just above the opening in the bottom of silos and all the pebble exits the vessel via pipe zone. The velocity of pebbles in this region is pre-dominantly vertically downwards. There is a plug flow zone well above the bottom opening in which velocity profile is nearly uniform except for a boundary layer effect. The pebbles within

this zone move as a solid mass. Also, there is a pipe feed zone which feeds pebbles from plug flow zone to pipe zone and is characterized by gain in the radial velocity component towards center . Also there is a dead/ stagnant /very slowly moving zone of pebbles close to the transition between cylindrical and bottom section. Pebbles in this zone are moving very slowly or at stand-still condition. Dead zones are detrimental to the safety of pebble bed reactors and their extent can be minimized by suitable half-cone angle of conical bottom. The dead zone extent is also function of friction between pebbles and between pebble and reactor wall. Gatt's experimental results confirmed existence of such four flow zones suggested by Deutsch (1967a). It was found that with increase in bottom opening diameter volume of the pipe zone was increased. Larger dead zones were observed for smaller base cone angle. Also, pipe zone size and its upper limit moved further into the vessel at smaller base cone angle. The variation in lower end of plug flow zone is found to diminish as base cone angle was increased and actual lower end position of the plug flow zone was found to be closer to the base at higher base cone angle. Analysis of experimental data for pebbles velocity suggested that there was very slow and intermittent movement of pebbles everywhere except near the bottom conical base. In general, very small resultant velocities were observed in upper cylindrical section and increased as pebbles descended towards the bottom conical section. Also, it was found that pebbles velocity increases as it nears the center of the bed. The influence of extractor rotation on the flow of pebbles was checked by an examination of the circumferential component of pebble velocity in the region of extractor and no visible sign of such effect was reported. Due to walls of container, there is a wall effect in terms of local voidage which is felt up to 5 pebble diameters from the wall. Due to this, annular region moves

slower than the center part of bed. This wall effect was characterized in terms of transit numbers for different initial seeding position. The transit number is defined as the number of pebbles recirculated between the seeding of a radioactively tagged pebble in the bed and its exit from the bed, expressed as a fraction of the bed inventory. For a given base angle, transit number was found to increase as the pebble seeding position changed from the Centre of the bed to the wall (Gatt, 1973).With increase in base cone angle, transit number of pebbles seeded near the wall was found to be closer in magnitude to the transit number of pebbles seeded near the center.

Gatt's study is one of the important study as far as investigation of granular flow in a PBR is considered. In Gatt's study, continuous recirculation experimental set-up mimicking flow of pebbles in an actual pebble bed reactor was developed and used in actual experiments. Such a set-up is essential for study of granular flow in a PBR and one of the main task of current work is to design and develop continuous pebbles recirculation experimental set-up._Experimental set-up used in Gatt's study had the provision of extracting pebbles at a controlled flow rate without jamming. This study was performed in early 1970's and limited capability of electronics and computer hardware might have prevented continuous tracking of pebbles. Continuous pebbles recirculation experimental set-up designed and developed as a part of current work is having salient features such as control over pebbles exit flow rate without jamming, capability to place returned pebble in a non-violent manner at desired radial location across top section of bed and offers space for implementation of advanced radio-isotopes based flow visualization techniques. Detailed description about this set-up is provided in Section 3. Gatt's study tracked radioactively tagged pebbles positions at a given intervals

of time using collimated detector based RPT technique. This version of RPT technique has some inherent limitations such as upper limit on tracking speed due to dynamically moving platform and lower counts are recorded due to collimated detectors (Shehata, 2005). As a part of this work, stationary scintillation detectors based RPT technique is implemented around continuous pebbles recirculation experimental set-up to track tagged pebbles (radioactive tracer) continuously and useful information about motion of pebbles. Is extracted. In this version of RPT technique, an array of scintillation detectors is arranged strategically around the system under investigation. The detectors used are stationary and non-collimated which overcome one of main limitations of Gatt's study. Non-collimated version of RPT technique faces challenges due to existing time-consuming, static and invasive calibration methodology. As a part of this work novel, dynamic and in-situ calibration equipment for RPT technique is designed and its operational feasibility is demonstrated. This set-up also known as calibration RPT equipment synergistically combines non-collimated and collimated versions of RPT technique. Gatt's study provided valuable inputs while designing and developing calibration RPT equipment. Also, Gatt's study provided useful information while designing and developing continuous pebble recirculation experimental set-up. Gatt's study was performed before the development of DEM based numerical simulation methodology, which is widely used for investigation of granular flows (Cundall and Strack, 1979). This was one of the main limitations of Gatt's study. In this work, an integrated experimental and DEM based study are carried out and simulation results are assessed with experimental benchmark data obtained by RPT technique.

2.1.2. Study at M.I.T. Students in Nuclear Engineering Department at Massachusetts Institute of Technology (M.I.T) carried out experimental study of pebbles flow dynamics as a part of design project (MIT Nuclear Engineering Design Report, 2002). A granular flow and dropping dynamics in the scaled-down pebble bed modular reactor (PBMR) was studied as a part of such design project. The main objective of the study was to investigate whether the fuel and graphite pebbles in bi-disperse core concept will move in a streamlined manner or in a random haphazard fashion. Three experimental models: 180° half-model, three-dimensional opaque model and continuous flow experimental set-up (180 ° half-model) with dynamic central column (scaled down by 1 to 10 ratio of the actual size pebbles) were designed and an experimental investigation was carried (Kadak and Bazant, 2004). In case of 180° half-model and continuous flow experimental set-up with dynamic central column, visual tracking of pebbles at the mid-plane transparent wall was carried out. 180° half-model suffers from 'wall effect' which alters the overall flow behavior. In order to overcome this 'wall effect', study in a full three-dimensional opaque cylinder was also carried out. Effect of different bottom cone angles, and exit opening diameters were studied as a part of study carried out at M.I.T. A radioactive tracer consisting of 1 mCi of Sodium-24 (Na-24) was tracked from the outside using two collimated scintillation detectors mounted on a wooden platform to extract useful information about pebbles motion path. There was a horizontal imager, which consisted of a NaI scintillation detector, a lead collimator with narrow vertical slit and associated electronics. It was used to determine x and y co-ordinates of tracer. Also, there was a vertical imager which consisted of a NaI scintillation detector, a lead collimator with narrow horizontal slit and associated electronics. It was used to determine

z co-ordinate of a tracer. The experimental set-up used to track tracer uses two scintillation detectors, whereas total three collimated detectors were used to track tracer in Gatt's work. The position accuracy of this imaging system was found to be within one pebble diameter. The experiments consisted of seeding tracer in the top of the core at a defined location, adding few layers of pebbles above the tracer, repetitive draining of the pebbles from the core for fixed amounts of time and finding the position of the tracer using imager at the end of each drain. Half-model visual tracking experiments reported that exit hole diameter does not affect the flow paths of pebbles. It was found that larger the exit opening diameter, faster the pebbles move while maintaining fair paths in the core. It was found that there is no effect of refueling or recirculation on the pebble streamlines. This confirmed that flow path of pebbles are governed by the paths taken by the pebbles below it and not affected by the pebble motion above it. This is in accordance with kinematic equations used to describe these kinds of flows. It was reported that the pebble paths are not dependent on bottom cone angle and nearly flat velocity profiles were observed. This observation is questionable and can be attributed to the mid-plane wall effect which affects the pebbles motion. This aspect of their investigation needs further investigation in 3-D model. Also, these experiments did not capture pronounced concavity in velocity radial profile which was reported in the previous design reports of PBMR (PBMR Safety Analysis Report, 2000). A maximum lateral pebble motion or diffusion in the straight cylindrical section of one pebble diameter was reported in this study. This study lacked continuous recirculation experimental set-up having control on exit flow rate. Most of the work was carried out in 180° half model, which suffers from the wall effect. Draining of marbles for fixed amount of time and then stopping the

draining to track Na-24 tracer was carried out in 3-D opaque model using collimated scintillation detectors. This experimental study was carried out with no connection to any DEM based computational study. DEM simulations can make use of experimental data of this study for an assessment of contact force models. Ultimately, DEM based codes will be used to carry out pebbles flow analysis in a full-scale reactor model. In this work, an experimental and DEM based computational study of granular flow in a continuous pebble re-circulation experimental set-up is carried out and obtained results are compared with each other.

2.1.3 Study at Tsinghua University. HTR-10 is a 10 MWth prototype pebble bed reactor at Tsinghua University in China (Xu and Sun, 1997). It was made critical in December 2000 and was operated at full power for the first time in January 2003. To understand more about characteristics of pebbles flow, phenomenological experiments were carried out in a two dimensional 1:5 scaled down model of a pebble bed core (Yang et al., 2009) at Tsinghua University. The experimental set-up used was equivalent of an axial central slice of the 3-D scaled model. Investigation about the establishment of two region arrangement, and existence of stagnant zones was carried out. Also, general characteristics of pebbles flow in a PBR were analyzed based on the visual observations. Effect of different cone angles and different surface roughness's of pebbles on pebbles flow dynamics was investigated experimentally. Black and colorless glass pebbles having diameter $1/5^{th}$ of actual pebbles were used. A stable two-region arrangement of the core was established and maintained during experiments. Stagnant zones were observed in the corner of the experimental set-up. The motion of pebbles in the pebble bed is reported to be of collective type and intermittent. Pebbles motion paths were reported to be of

streamline form. Also, investigations in taller experimental vessel were performed to verify the feasibility of two-region design (Jiang et al., 2012). Additionally, DEM based study was carried out to verify experimental observations and effect of different cone angles was carried out. The stable establishment and maintenance of the two region arrangement was verified experimentally and also by DEM simulations. It was found that existence and size of stagnant zone strongly depends on the base cone angle. Size of stagnant zone was found to decrease with increase in the base cone angle. Physical mechanism behind flow of pebbles was investigated experimentally by four basic forms of the phenomenological methods such as central area method, side area method, pre-filled stripes method, and pre-filled core method (Yang et al., 2012). These phenomenological methods are traditional approach to study the dense pebble flow by virtue of interface features of different areas composed of differently colored pebbles. This method is widely used in the study of pebbles flow. Also, DEM simulations for different cone angles and different friction coefficients were carried out. Effect of friction coefficient on overall flow field was found to be very complicated and demanded further detailed investigation. Stagnant zone was reported as a main reason for observing non-uniformity in the overall flow field of pebbles.

The main limitation of the work carried out at Tsinghua University was use of two dimensional experimental set-up instead of actual three dimensional geometry. Pebbles flow in the two dimensional geometry is not same as actual flow of pebbles in the reactor core and obtained findings may not be applicable for a practical reactor design. The results obtained provided basic information about pebbles flow in a reactor core. Visual observation of pebbles movement was the main reason behind use of two dimensional

experimental set-up. There is a need to use advanced flow visualization techniques such as radioactive particle tracking (RPT) for the investigation of pebbles flow. It is worth to mention that RPT is the only best suited technique for this study of granular flow in a PBR, as it has no limitations on operating conditions, opacity, system design and configuration. This is one of the main motivations for the use of RPT for investigations of pebbles movement in current work.

2.1.4 Other Studies. At North Carolina State University (NCSU), study of granular flow in a PBR was carried out using three well-collimated detectors based radioactive particle tracking technique similar to the tracker used in Gatt's study (Shehata, 2005). The main aim was to explore technique's potential and its limitations through some error and sensitivity analysis. The collimated detectos based tracking system was designed and built at the Center for Engineering Applications of Radioisotope (CEAR), NCSU. It was reported that three detectors based tracking system has potential to be used in investigation of pebbles flow fields in a PBR. Its advantages and limitations as compared to conventional RPT were discussed. In another continuation work at CEAR (Wang, 2011), a dual measurement system for tracking flow of pebbles in a PBR was developed. Three collimated scintillation detectors based tracking system, as discussed before, was implemented to study pebbles flow path in a scaled down test reactor. Also, six non-collimated detectors based multiple radioactive particle tracking technique, which utilizes detector response function (DRF) generator feature in a modified MCNP5 (Monte-Carlo 'N' particle – radiation transport code), was developed and used to study pebbles motion in a scaled down test reactor. A comparison of results obtained using collimated and non-collimated detectors based RPT technique

with Gatt's study was made and good agreement about trajectories results was reported. This study lacked continuous pebbles recirculation experimental set-up and integration with DEM based simulation study.

In another work at Beijing Forestry University in China (Li et al., 2009), combined DEM and experimental study of flow of pebbles was carried out in a transparent semi-cylindrical silo. Particles at the transparent wall were visually tracked. Comparison between DEM and experimental results was carried out and a good agreement was found between them. DEM based simulations require input of various material and interaction properties. In case of its unavailability, interaction properties need to be determined by developing simple experimental set-ups involving same materials (Li et al., 2005). This determination of interaction properties were carried out in this combined DEM and experimental study. This is necessary to ensure fair assessment of experiments with simulations and this determination of interaction properties is carried out as a part of current work and is explained in detail in Section 6. The main limitations of this combined DEM and experimental study carried out at Beijing Forestry University in China was the use of semi-cylindrical geometry and the use of visual tracking technique.

It is clear from the above review of previous experimental studies and measurement methods that there is a need to carry out three-dimensional pebbles flow dynamics study by implementing advanced flow visualization techniques such as RPT around continuous pebbles recirculation experimental set-up mimicking flow of pebbles in a PBR. Also, there is a need to couple experimental study with DEM based study for

an assessment of phenomenological contact models. This is the main motivation behind current work.

2.2. MODELS RELATED TO GRANULAR FLOW

Models related to granular flow can be broadly classified into two types:

1. Continuum models
2. Discrete models

Continuum model treats the granular material as a continuous medium whereas; discrete models treat the granular material as a collection of particles. Discrete models appear more realistic description of granular systems than the continuum models. DEM simulations belong to discrete models related to granular flow. However, application of discrete models requires knowledge about contact forces for particle-particle and particle-wall interaction. There is a lack of contact force models developed from the first principles (Rao and Nott, 2008) and this demands assessment of contact force models using benchmark experimental data. Also, it is computationally intensive to simulate systems involving large number of particles using discrete models. However, continuum models are less computationally intensive. Despite these limitations, discrete models have been used due to their advantageous features such as systems with complicated geometries can be studied, particle-scale attributes such as shape, poly-dispersity, and deformation characteristics can be incorporated very easily etc. Due to these features, discrete models are popular models. On the other hand, continuum models does not suffer from limitations of discrete model but may not be the realistic description of actual system in some cases involving smaller size particles (order of few millimeters). Hence, both the models have their own advantages and limitations. In discrete models, Newton's

laws of motion is applied to each particle and its motion is followed in time. Overlaps between particles and between particles and wall are allowed and are resisted by normal and shear forces. This approach was introduced by Cundall and Strack (Cundall and Strack, 1979) and is termed as a distinct element method (DEM). It is more often called as discrete element method in the literature and is used widely. The DEM calculation cycle (Figure 2.2) consists of the following steps: 1. Model Generation: Particles are packed inside container 2. Determination of the total forces acting on each particle using a force balance method that considers various forces such as friction, weight, contact, and others 3. The resultant force acting on each particle is determined from which new velocities and positions of each particle are found out using Newton's second law of motion and numerical integration methods. The whole exercise is then repeated for newly obtained particle positions and so on until final simulation time is reached. Hence, DEM calculations alternate between Newton's second law of motion and resultant forces calculation. By tracking the motion of each individual particle, detailed information about the system behavior across a range of time-scales and length-scales can be obtained. The key assumption made in any DEM based simulations (Cundall and Strack, 1979) is that disturbances cannot propagate further than particle's immediate neighbors for a sufficiently small time step of simulation, which is usually a fraction of critical time step (Δt_c). This critical time step is derived by considering the speed of Rayleigh wave which is assumed to transfer all of the energy across a system (Li et al., 2005). For such smaller steps, velocities and accelerations of a particle are assumed to be constant for given time step and resultant forces on any particle are determined exclusively by its interaction with the particles with which it is in contact.

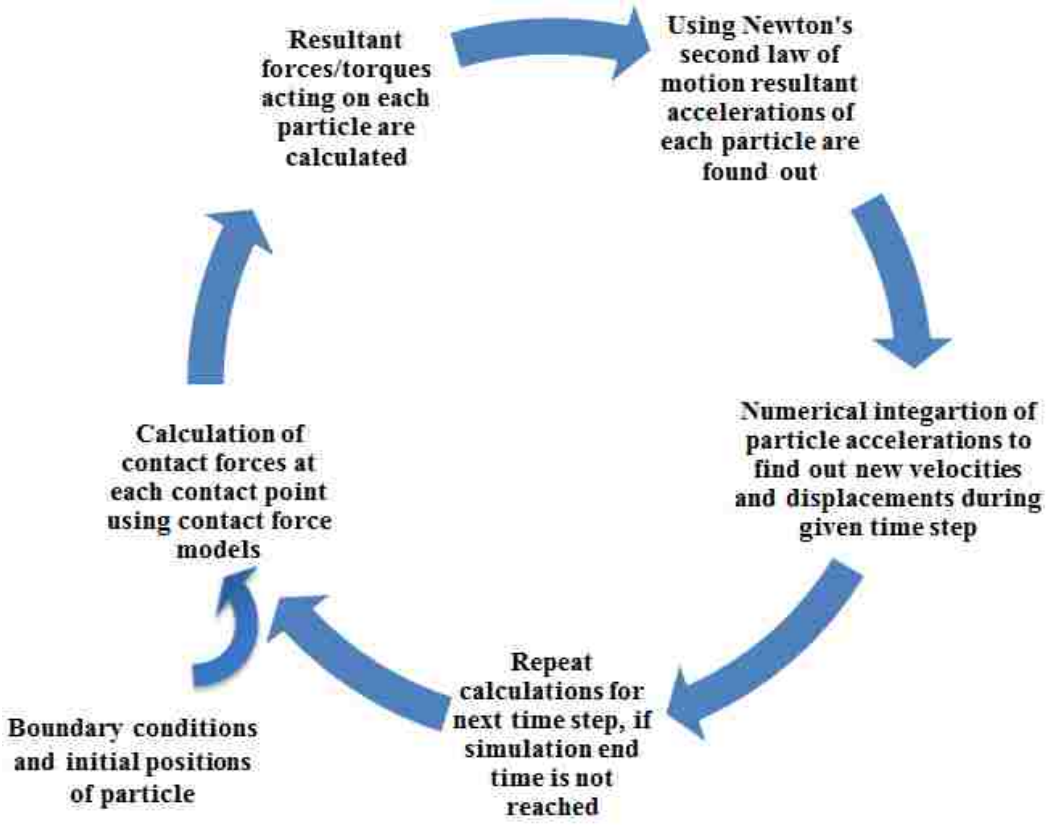

Figure 2.2 DEM Calculation cycle

Figure 2.3a represents typical situation involving particles and wall. Figure 2.3b represents tangential and normal forces acting on respective particles due to interaction with the wall. Figure 2.3c represents various normal and tangential contact forces acting on particle 'A' due to its interaction with the wall and other particles. The resultant force acting on each particle is calculated by considering various forces acting on each particle such as normal and tangential contact forces, weight, buoyancy and drag forces due to interaction with interstitial fluid. Newton's laws of motion are applied to each particle to find out resultant accelerations from which new velocities and positions during respective time step are found out by using suitable numerical integration schemes.

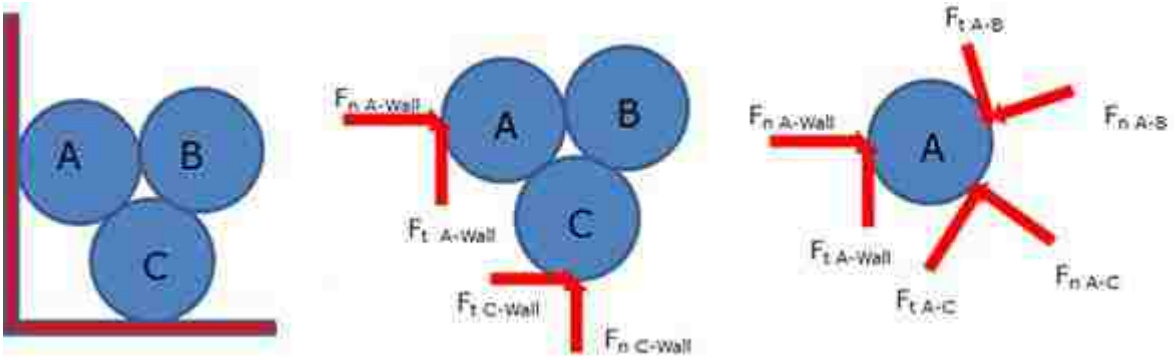

a **b** **c**

Figure 2.3 Forces acting for particle-particle and particle-wall interaction

2.3. PREVIOUS DEM BASED STUDIES

A detailed description about DEM simulation methodology and associated equations can be found in Section 6 devoted to DEM based study of granular flow in a PBR.A few number of DEM based studies of granular flow in a PBR can be found in the open literature. They are as follows:

2.3.1. Study at M.I.T. Rycroft et al. (2006) at M.I.T performed full-scale, discrete element simulations of actual geometries, with 6 cm diameter actual size pebbles exiting from the cylindrical vessel with conical bottom having angles of 30° and 60°. Various important issues related to reactor design, such as the sharpness of interface between fuel and moderator pebbles, horizontal diffusion of pebbles, effect of geometrical parameters on the streamlines, the porosity distribution, effect of container wall, residence time distributions were investigated (Rycroft, 2007). In actual PBR's, pebbles are individually removed from the conical bottom at a very slow rate, typically one pebble per minute. It is infeasible to carry out DEM based simulations at such

slower rates. Previous experimental work by Choi et al. (2004) has shown that features of the slow and dense granular flow are governed by geometry and packing constraints. The geometry of the flow profile is not altered by the overall flow rate. This suggests that pebbles flow path are not a function of exit flow rate. Hence, a faster flow regime was studied in all of the previous DEM based simulations related to a PBR. This DEM based simulation study investigated effect of bottom half-cone angle, feasibility of bi-disperse core concept, effect of wall friction on flow characteristics of a granular flow.

Large-scale Atomic/Molecular Massively Parallel Simulator (LAMMPS) code was used in Rycroft's DEM simulations. Hertzian contact model is claimed to be used in these DEM based simulations. Values of stiffnesses were chosen to be constant to avoid intensive computations. This is one of the main drawbacks of this work. Linear spring stiffnesses were used which conflicts with their claim as Hertzian contact as it uses nonlinear spring. Hertzian contact model calculates normal and tangential stifnesses depending upon the overlaps and is explained with necessary equations in Section 6 in detail. Values of friction coefficient for particle-particle and particle-wall interaction were chosen to be 0.7. There is no basis for selecting these values of interaction parameters. In some cases, value of friction coefficient for particle-wall interaction was set to zero to check effect of frictionless wall on the flow of pebbles. In any DEM based simulations, first step is to pack particles inside confined geometry. It is necessary to assess the packing characteristics with the previous experimental and numerical benchmark data. Unfortunately, this is lacking in DEM based study of Rycroft (2007). It is important to validate numerically simulated packing structures, since nature of packing (tightly packed vs. loosely packed) affects subsequent motion of particles. In

current work, numerically simulated packing structures are compared with previous benchmark data using suitable indicators such as overall or mean porosity, radial porosity variation profile.

DEM simulation results about mean velocity profile suggested that there is a uniform plug flow region in the upper cylindrical region and a non-uniform converging flow in the lower conical region. For a conical section, half-cone angle is one-half of the angle subtended at the apex point by a circular base of cone. In case of geometry with wider cone (i.e. half cone angle of 60°), region of slowly moving pebbles at the sharp corner (transition from cylindrical to conical portion) was observed. Also, velocity profiles in the upper cylindrical region were roughly uniform across the container. A boundary layer of slower velocities, several particle diameters wide, was observed in the upper region. A more smoother transition from plug-type flow to non-uniform converging flow was observed in the wider cone (i.e. half cone angle of 60°) as compared to the case of geometry with narrower cone (i.e. half cone angle of 30°). Kinematic model is perhaps the only continuum theory available in open literature for predicting the mean flow profile in a slowly draining silo (Nedderman and Tüzün, 1979). This will be described in detail in the next section devoted to continuum models. Rycroft et. al compared their DEM simulation results for the mean flow profile with kinematic model and identified limitations of kinematic models in describing DEM results. Kinematic model failed to describe boundary layer, several particle diameters thick, of lower velocities in the upper cylinderical region. Also, kinematic model failed to capture rapid transition from the upper plug flow region to converging region in lower region observed in DEM based simulations.

Also, diffusion of pebbles across streamlines was reported by measuring mean-squared horizontal displacements away from the streamlines as a function of the vertical co-ordinate. It was quantified in terms of increase in the variance of r co-ordinate of tracked particles from the variance at the initial height. No diffusion was observed in the upper cylindrical region which was consistent with the observation of plug-type flow in the upper region. It confirmed that packing in this region is essentially plug like and particles are locked with their neighbors while moving. Radial spreading was observed near the lower conical region where converging flow exists. The height where the amount of radial diffusion started to increase significantly was found to be function of bottom conical angle. In case of geometry with wider cone (i.e. half cone angle of 60°), this transition was significantly above the sharp corner (transition from cylindrical to conical portion), whereas in case of geometry with narrower cone (i.e. half cone angle of 30°), and this transition was observed almost at level with the sharp corner.

Most of previous structural characterization studies were carried out on static sphere packings (Mueller, 1992; Goodling et al., 1983; Mariani et al., 2009). The slow and dense granular flow encountered in a PBR is currently approximated by the study of static packed beds (duToit, 2002). However, there are no such experimental studies that were carried out to support the conclusions of the published research. Hence, there is a need to compare packing characteristics between static packed beds and the moving beds encountered in PBRs (packed beds with slow and dense granular flow). This aspect is investigated as a part of current work using calibration method of RPT technique. Rycroft et al. (2006) studied, for the first time, the distribution of local volume fraction and associated porosity. Local porosity affects helium flow in the core and hence

associated thermal-hydraulics of a PBR. It was observed that local packing fraction is mostly close to 63% in the center of upper region, suggesting that plug-like region of nearly jammed and rigid state. Lower density regions along the walls were observed due to partial crystallization or also known as *wall effect*. A fairly rapid transition based on local packing fraction, between a region of nearly plug flow and a less dense lower region of shear flow in the funnel, was observed in the geometry with wider cone angle (i.e. half cone angle of 60°). This observation was consistent with the observation based on velocity profiles. Local ordering in the flowing packings due to partial crystallization, also known as *wall effect*, within several pebble diameters from the wall were observed and are consistent with previous experiments (Mueller, 1992, Goodling, 1983) and simulations (Mueller, 2005, duToit, 2002).

Effect of wall friction on behavior of pebbles near the walls was investigated in half-size geometry. Two different values of wall friction (μ_w): 0 (frictionless) and 0.7 were used in these simulations and other parameters of simulation were kept the same. It was observed that boundary layer of slower velocities was removed in case of frictionless wall and perfectly uniform velocity profile was observed in the upper portion of the reactor. Also, increased radial ordering was observed due to frictionless wall. In lower conical region, more curved velocity profile was observed for the case of wall with friction.

Knowledge about pebbles residence time is crucial from fuel burn-up estimation point of view. Rycroft et al. (2006) studied residence time distributions (RTD) based on combination of plug flow model and kinematic model and compared with DEM simulations. A fat tail type RTD was observed for fuel pebbles which were in qualitative

agreement with the predictions based on kinematic model. The probability density was sharply peaked near the shortest residence time (τ_{min}). This was corresponding to pebbles, near the central axis, traveling the shortest distance at the highest velocity. Longest waiting times were associated with pebbles near the wall. Longer path of travel and smaller velocities were observed for pebbles near the wall and is the main reason for those longest waiting times. Narrower residence time distributions were predicted by DEM simulations for the case of narrower cones (i.e. half cone angle of 30°) as compared to the case of wider cones (i.e. half cone angle of 60°).

Rycroft et al. (2006) carried out intensive DEM based computational study of granular flow in a PBR. However, these results were not compared with experimental benchmark data due to its unavailability. It is essential as contact force models used in DEM simulations are phenomenological in nature and demands assessment. Interaction parameters used in this DEM work were not determined experimentally and their experimental determination is required to ensure fair assessment of simulations with experiments. Also, there is a need to validate DEM simulated packing structures using available benchmark data before carrying out simulations of a granular flow in a PBR. This is also missing from this study. The above mentioned missing aspects are incoroporated while carrying out this work.

2.3.2 Idaho National Laboratory (INL) – PEBBLES Code Development. PEBBLES is a DEM based code developed by Idaho National Laboratory which simulates packing of pebbles and flow of pebbles into PBR (Cogliati and Ougouag, 2006) . This code was developed mainly to conduct pebble bed reactor specific studies. This is the main difference between PEBBLES code and any other DEM based code

used to simulate granular flow. This code has the ability to model earthquakes and assess its impact on core configuration and to extract pebbles at the bottom of the reactor and recirculate them back to the reactor. Also, it can compute dance-off factors (Kloosterman and Ougouag, 2005) and was used in the modeling of the first criticality of HTR-10 reactor. It uses 'Linear Spring' contact force model details about which can be found in PhD thesis of Dr. Cogliati (Cogliati, 2010). This code is used to test the models of HTR-10 and PBMR-400 reactors. PEBBLES code can provide information about location of pebbles as a function of time and can be used to generate pebbles flow paths in the core. In addition, it can be used to evaluate packing fraction and its spatial fluctuations in the pebble bed. PEBBLES properly reproduces oscillatory behavior of radial porosity profile due to the wall effect and mean/average porosities of previous experimental work (Benenati and Brosilow, 1962). Any DEM code should properly reproduce oscillatory behavior of radial porosity variation profile. It is a good indicator of local packed bed structure and is used in current work along with mean porosity values for structural characterisation of EDEM^{TM} simulated packing structures. Cogliati and Ougouag (2006) reported that there is a strong dependence of packing density on friction coefficients and material parameters. Accurate input of these parameters related to graphite pebbles must be obtained and provided as an input to PEBBLES code. It was reported that higher values of friction results into lower packing frictions (loose packing). The code was used to calculate the evolution of the packing fraction during an earthquake (Cogliati and Ougouag, 2007). The neutronics behavior of a pebble bed reactor depends on the packing fraction of the pebbles. To simulate earthquakes in PEBBLES, the walls of the reactor were displaced with time, which was to shake the bed . This affected the contact force

for pebble-wall interactions. It was found that there was an increase in packing fraction of the pebbles in a pebble bed reactor after earthquake occurs. This increase is slower and smaller than the increase shown by the previous bounding calculations. This study made use of relatively simple linear spring contact force model in DEM simulations. The friction parameter values used were not determined experimentally. The results of this study lacks assessment with experimental benchmark data. However, it is the only DEM based code for PBR specific applications and can provide data specific to nuclear reactor analyses.

2.3.3. Combined DEM and Experimental Study. In a combined DEM and experimental study of pebbles flow in a PBR at Beijing Forestry University in China, a semi-cylindrical silo made of perspex was used (Li et al., 2009). A faster gravity flow regime of mono-sized glass beads in this semi-cylindrical silo was simulated using DEM. Non-linear Hertzian contact model was used in these simulations. This DEM study was carried out along with experimental study on similar geometries. Visual tracking at the transparent wall was carried out in the experimental investigation. A comparison of trajectories obtained for DEM simulations and using experimental results suggested a good agreement and reported that DEM modeling is capable of simulating real flow in an actual PBR. The main limitation of this study is use of semi-cylindrical geometry which suffers from additional wall effect. Also, the packing characteristics of numerically simulated packing structures were not validated with available experimental data.

2.3.4 Pebble Flow Simulation Based on a Multi-Physics Model at Rensselaer Polytechnic Institute (RPI). Recently, a multi-physics model based on coupling between DEM and CFD methods is developed and reported in the open literature (Li and Ji, 2010,

Li and Ji, 2011). DEM is used to simulate granular flow in a PBR and CFD is used to simulate coolant dynamics and to obtain the distribution of coolant velocity and pressure. DEM and CFD are fully coupled through the calculation and exchange of pebble-coolant interactions at each time step. In this manner, a fully coupled multi-physics computational framework is formulated (Li and Ji, 2013). Non-linear Hertzian contact model is implemented in DEM to simulate contact behavior of pebbles. A collective dynamics based method is used for initial packing of the pebbles and for subsequent high-fidelity pebble flow simulations (Li and Ji, 2012). In this method, pebbles are packed by two processes: a sequential generation process which allows overlaps and an overlap elimination process, which is based on a simplified normal contact force model. Overlap elimination process provided an adaptive and efficient mechanism to eliminate the overlaps and thus packs tens of thousands of pebbles within few minutes. Applications of this new method to pack pebbles in two types of pebble bed designs (HTR-10 and PBMR-400) were studied. Packing results exhibited radial and axial porosity distributions similar to the dynamic equilibrium packing state produced by the DEM simulations. Also, simulation results suggested that flow of pebbles in a PBR is streamlined and vertical speed of pebbles movement is the function of radial seeding distance of pebble and decreases from the center to the periphery. This work is still in progress.

There are many DEM based studies of granular flow in a silo geometry (Balevičius et al., 2011) (Xu et al., 2002) (Anand et al., 2008). However, González-Montellano et al. (2010) carried out DEM simulations of granular flow in a planar silo to evaluate velocity profiles at different levels, to check the influence of different cone angles and the

coefficient of static friction on the flow patterns. These parameters significantly influence the flow pattern in silos. A slice of a silo with a hopper at its base was simulated in EDEM^{TM}. Hertz-Mindlin (no-slip) contact model with viscous damping and frictional slider in tangential direction is used. For the analysis of flow patterns, different methods such as direct observation of discharge, parameters such as velocity profile and mass flow index (MFI) were evaluated and analyzed. Though, this study is not directly applicable, it lays down foundation to analyses methods used in Section 6 of current work and hence is reviewed. Mass flow index (MFI) is defined as follows

$$\text{MFI}= \frac{Vwall}{Vcentreline} \qquad (2.1)$$

where, v_{wall} – velocity at the wall, $v_{centreline}$ -velocity at the centerline

According to Johanson and Jenike (1962), mass flow is observed for values of MFI > 0.3, whereas funnel flow is observed for values of MFI < 0.3. It is possible to visually assess the predicted flow pattern by dividing silo into different horizontal layers colored alternatively with two contrasting colors. This helps in identifying the relative particle movement and predict flow pattern. These predicted flow patterns were compared with expected flow pattern from the Eurocode (EN 1991–4). These charts were developed by Jenike (1964, 1961) using continuum models and predicts the flow pattern based on hopper angle, friction between particles, and between particle and wall. Flow patterns predicted based on DEM results were found to be in general agreement with the expected flow pattern from the eurocode. A combination of different values of wall friction and hopper wall angle of inclination (or half-cone angle) produces different flow patterns in DEM simulations.

The review of DEM based studies related to granular flow in a PBR highlights following things: There is a need to validate DEM simulated packing structures before carrying out simulation study of pebbles flow. Also, all DEM code requires input of various material and interaction properties and in case of their unavailability, it needs to be determined experimentally by developing simple experimental set-ups involving same materials. This is necessary to ensure fair assessment between simulations and experiments. Also, contact force models used in DEM codes are phenomenological and needs to be assessed with experimental benchmark data. All the aspects mentioned above are essential and are lacking partially or completely in previous DEM based studies of granular flow in a PBR. In the current work, an attempt has been made to incorporate all the missing aspects of previous computational work.

2.4. CONTINNUM KINEMATIC MODELS

Flow of pebbles in a PBR is very complex phenomenon due to long-lasting contacts with their neighbors. Flow of pebbles is pre-dominantly governed by the geometry and packing constraints (Choi et al., 2004), material and interaction properties, particularly static friction characteristics (Lee, 2011). Continuum approach, where the particles are replaced by a single phase continuous medium, is used extensively for static and granular flow problems. The presence of interstitial fluid is ignored in the continuum approach. Balance laws for mass, linear and angular momentum, and energy are derived based on continuum mechanics. These equations have too many unknown variables and needs constitutive equations to describe the behavior of materials. These constitutive equations rely on experimental data to incorporate modifications suitable to particular

problem of interest. An empirical kinematic model (Nedderman and Tüzün, 1979) is the widely used continuum model to predict the mean velocity in silos of different shapes. In this model, it is assumed that the horizontal velocity (u) is proportional to the horizontal gradient($\nabla_\perp$) of the downward vertical velocity (v)

$$u = b\,\nabla_\perp\, v \qquad (2.2)$$

where b = 'diffusion length' which is a material parameter typically, in the range of one to three particle diameters. This parameter describes energy dissipation due to collisions of particles. The main idea behind equation 2.2 is that particles diffuse from region of low to high vertical velocity, where there is more free volume and more local rearrangements to accommodate their collective motion. Incompressible continuity equation approximation when applied to equation 2.2 gives a diffusion equation for downward vertical velocity (equation 2.3).

$$\frac{\partial v}{\partial z} = b\nabla_\perp{}^2\, v \qquad (2.3)$$

This equation is analogous to diffusion equation where 'z' co-ordinate acts as a time. Equation 2.9 can be solved by specifying appropriate boundary conditions. Kinematic model is successful in predicting fast granular flows. It has been found that there is a reasonable agreement between kinematic model predictions and the DEM flow profiles (Choi et al., 2005) near the bottom of wider silos but fails to capture effect of geometry. It cannot describe the observed boundary layer of slow velocities closer to the wall which is seen in DEM simulations. The parameter 'b' is reported to depend on the geometrical configurations and cone angle has significant effect on its value. Value of 'b' is found out by fitting of data otained using experimental investigations of granular flow. The kinematic model fails to describe the rapid transition from plug flow in the upper

cylindrical region to converging flow in the bottom conical region and is the main limitation of kinematic model (Rycroft et al., 2006). A new kinematic model proposed by Lee et al. (2009) combines the compressible continuity equation with phenomenological velocity relationship proposed by Nedderman and Tüzün (1979). Approximate solutions to this new kinematic model yields non-Gaussian velocity profiles for finite variations in density. These observations were consistent with previous experimental observations (Choi et al., 2004, Choi et al., 2005, Beverloo et al., 1961). Results of this new kinematic model also suggested that density field can play important role in slow and intermittent granular flow in a PBR and can have an effect on pebbles jamming in a PBR. However, it still relies on value of parameter 'b' which needs to be determined from experimental investigations in similar geometries.

2.5. CONCLUDING REMARKS

It is clear from above literature review that there is a strong need for integrated experimental and DEM based study of granular flow in a PBR. For experimental investigation, continuous pebble recirculation experimental set-up mimicking three-dimensional dense and granular flow in a PBR needs to be designed and developed. Due to the dense and opaque nature of granular medium, conventional optics based velocimetry techniques are of limited use in such study. Hence, advanced radioisotopes based flow visualization techniques such as RPT, which does not have any limitations in such flows, needs to be used for such experimental investigation. Experimental data obtained using radioisotopes based techniques needs to be used for assessment of phenomenological contact force models used in DEM. These contact force models are

not derived from first principles and need assessment with experimental benchmark data. In any DEM based analysis, first and important step is to properly pack the particles inside the container. Nature of packing affects subsequent motion of particles and is necessary to validate numerically simulated packed bed structures with available benchmark data using suitable indicator of local bed structure such as radial porosity variation profile. Also, the calculation of contact forces demands accurate values of various interaction properties, which needs to be determined by developing simple experimental set-ups, in case of their unavailability. The main focus of this study is to address the mentioned shortcomings of previous experimental and numerical studies and advance the knowledge and understanding about the granular flow present in a PBR. Design and development of continuous pebble recirculation experimental set-up mimicking cold flow operation of a PBR is carried out as a part of this study and its design and development is described in detail in Section 3. Advanced radio-isotopes based flow visualization techniques such as RPT are implemented around continuous pebble recirculation experimental set-up in order to get detailed information about pebbles flow field. Obtained experimental data about pebbles flow field is used for assessment of contact force models used in DEM based simulations. This assessment of DEM contact force models using experimental benchmark data will be an important step towards validation and use of DEM based full-scale reactor simulations for safe and economical design of a PBR technology.

3. DESIGN AND DEVELOPMENT OF COLD FLOW CONTINUOUS PEBBLES RECIRCULATION EXPERIMENTAL SET-UP

The pebble bed reactor (PBR) technology involves continuous recirculation of pebbles under the influence of gravity in the reactor core. As mentioned earlier, this continuous recirculation feature eliminates the need to shut down the reactor for refueling. Based on burn-up, fuel pebbles are returned back to the core to a particular radial position for effective utilization of fissile material. Each fuel pebble re-circulates through the core about 10 number of times and spends 1000 days before it can be discharged (Kadak, 2005). The continuous recirculation of fuel pebbles is the distinct advantageous feature of pebble bed version over prismatic one, which is based on the same fuel design concept. An investigation of granular flow in a PBR is of paramount importance from reactor neutronics and thermal hydraulics point of view. Hence, there is a need for a cold flow experimental set-up that mimics the cold flow operation of the granular flow in a PBR and is the main focus of this section.

Literature review suggested that such a set-up is essential for this study and is missing from some of previous investigations. Design and development of such an experimental set-up is not trivial activity and is a very challenging task. Such development demanded substantial time and effort. The current version of continuous pebble recirculation set-up is designed and developed by taking into account advantages and shortcomings of experimental set-ups used in previous studies.

3.1. LIMITATIONS OF THE REPORTED EXPERIMENTAL SET-UP USED IN PREVIOUS STUDIES

Experimental set-up used in Gatt's study (Gatt, 1973) consisted of an aluminum cylinder with a concave base and single axial outlet. In order to avoid scatter of returned pebbles, an entry mechanism was designed to ensure that entry of pebble was nearly vertical and possessed negligible inlet velocity. This is one of important feature from actual PBR operation point of view, and this feature is incorporated in the continuous pebbles recirculation experimental set-up designed as a part of this work. In Gatt's study, an extraction device was designed and incorporated to remove pebbles from the bottom at a controlled flow rate without jamming. Exit flow rate control mechanism used in the developed continuous pebble recirculation experimental set-up is an evolved version of this extraction device.

Experimental set-up involving half and full three-dimensional scaled down model of an actual PBR were used in the experimental study carried out at M.I.T (Kadak and Bazant, 2004). There was no continuous and automatic recirculation of exiting pebbles. Typical experiment in a study carried out at M.I.T. consisted of: draining for fixed time duration, and then stopping draining for tracking, visual tracking at mid-plane transparent wall for half-model / using two detectors based imager mounted on a moving platform for full three-dimensional model, and again draining for next time step and so on. Also, an exit flow rate of 120 pebbles per minute was maintained during experimental investigation which is significantly higher than that of actual PBR. To compare the packing characteristics of static and moving pebble beds, it is essential to mimic slow granular flow. Continuous pebble recirculation experimental set-up designed as a part of this work has control over its exit flow rate. In the current work, an exit flow rate of one

pebble exiting every five seconds is used which can be set to the desired exit flow rate used in PBR (one pebble exiting every thirty sec or higher). The main reason to use exit flow rate of one pebble exiting every five seconds is to avoid experiments of prolonged duration. A continuously rotating conveyor is used in current work for continuous recirculation of exiting glass marbles, which are used to represent the pebbles in this study. Such continuous system with adjustable exit flow rate of pebbles is missing from previous studies which allow carrying out experiments in an automatic manner. Experimental set-up used in other previous studies suffers from one or all of the above mentioned limitations and hence discussion about them is avoided. Table 2.1 summarizes previous experimental set-ups, their salient features and main limitations.

Table 3.1 Summary of previous experimental studies related to pebbles flow in a PBR

No.	Study	Salient Features	Limitations
1	Gatt's study (1973)	• 3-D scaled down model • Exit flow control mechanism • Use of tracker to track movement of tagged pebbles at pre-defined interval of time • Continuous recirculation of pebbles	• No integration with DEM simulations study • Old hardware and electronics posed limitations
2	M.I.T study (2002)	• 2-D and 3-D scaled down model • Faster flow regime was mimicked • Visual tracking method used in 2-D model • 2 collimated detector based tracking in 3-D model	• 2-D model suffers from 'wall-effect' • No integration with DEM simulations study • Slower flow of pebbles and continuous recirculation missing
3	Tsinghua University study (2009)	• 2-D scaled down model • Visual tracking method used with colored pebbles • Integration with DEM simulations study	• Advanced flow imaging techniques, capable of providing crucial information missing • 2-D model suffers from 'wall-effect'

3.2. DESIRED FEATURES OF AN EXPERIMENTAL SET-UP FOR STUDY OF GRANULAR FLOW IN A PBR

The desirable experimental set-up should mimic the slow flow of pebbles under the influence of gravity. It has been reported that coarse particles are less affected by the fluid drag force than fine particles (Rao and Nott, 2008). Hence, there is no need to mimic downward flow of gaseous coolant through interstitial cavities for the investigation of slow and dense granular flow in a PBR. As mentioned earlier, due to prolonged experimentation time it is not practical to carry out experimental investigation at an actual exit flow rate of one pebble every thirty seconds and experimentally feasible exit flow rates need to be used. Also, extracted pebbles needs to be returned back to the top of the reactor automatically and continuously in a non-violent manner. The returned position should be controllable. Flow of pebbles in a pebble bed reactor is an example of dense type granular flow and hence advanced radioisotopes based flow visualization techniques, which have no limitations from system opacity, are only one to properly investigate flow dynamics. Hence, the set-up should offer sufficient space for implementation of such radioisotopes based techniques for experimental investigation.

3.3. DESIGN AND DEVELOPMENT OF COLD FLOW CONTINUOUS PEBBLE RECIRCULATION EXPERIMENTAL SET-UP

The design and development of cold flow continuous pebbles recirculation experimental set-up (Figure 3.1), modality pivotal to this research, has been evolved with various attempts and designs in order to overcome properly the limitations of previous studies. It mimics the slow flow of pebbles (glass marbles of ½" in diameter) in the pebble bed test reactor of 1foot in diameter and 1 foot in height.

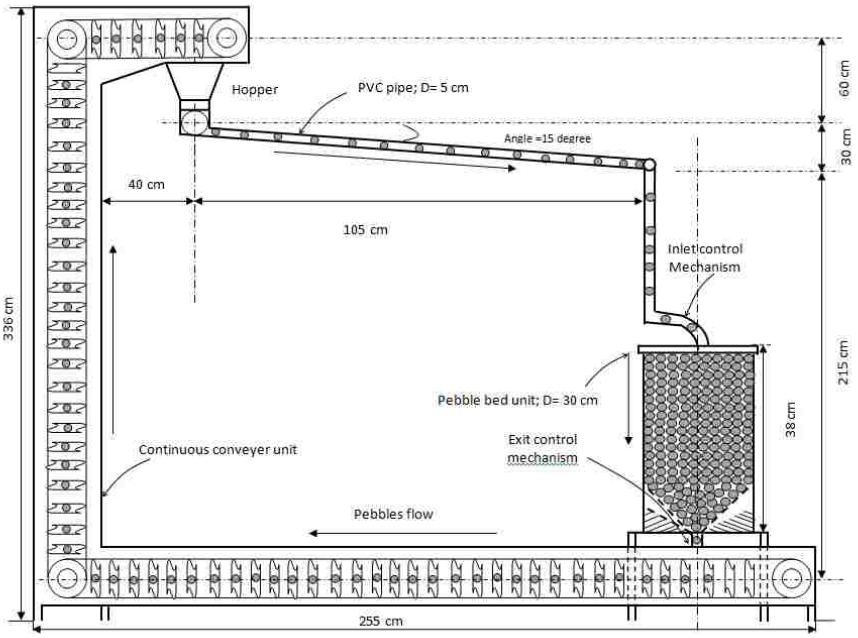

a. Schematic diagram.

b. actual picture (with earlier version of inlet control mechanism)

Figure 3.1 Continuous pebble recirculation experimental set-up

However, the set-up and its key mechanical components can be scaled up to accommodate large diameter and taller reactors and larger diameter of pebbles (upto 6 cm diameter pebbles). The main reason to choose these dimensions of test reactor is from experimental feasibility point of view. The residence time of pebbles in the core is an important parameter from various neutronic and safety related considerations. This can be controlled by controlling the exit flow rate of pebbles and control over radial position of returned pebbles. This set-up is operated as a cold flow module where glass beads represent pebbles. The spherical solids (1/2" diameter glass beads having density of 2.5 g/cm^3 representing pebbles having density of 1.8 g/cm^3) flow under the influence of gravity and circulate continuously. An adjustable speed conveyer shown in Figure 3.1 returns pebbles from the exit point to the top of the core. This set-up has following features:

- The pebbles flow and their residence time is controllable and adjustable. This demanded design, development and implementation of an exit flow control mechanism which should not hinder continuous recirculation of pebbles. This is the critical design feature of this set-up and demanded significant effort in conceptual design, machining, and, development of numerous exit control mechanical designs. The performance of some of the mechanisms was limited under actual operating conditions. Finally, a mechanical design based on rotary vane type cup is developed and its satisfactory operation is demonstrated at slower exit flow rate conditions. The details about different versions and evolution to the final working mechanism and mechanical design with schematic diagram are explained in next paragraphs.

- The pebbles exiting the test reactor can be returned to the top of the reactor continuously and automatically. Returned pebbles can be placed at any desired location across the top cross-section in a ‘non-violent’ manner (i.e. a returned pebble should not jump and change its position). This is an important feature from RTD study point of view and is required in actual PBR for implementation of devised refueling strategies for effective utilization of fissile material and other neutronic considerations such as power peaking related issues, flux flattening considerations, etc. (Boer, 2009). Also, it was observed in the past experimental study (Kadak and Bazant, 2004) that pebbles move radially after hitting other pebbles due to its fall from certain height and a mixing zone is formed. This mixing zone is prone to power peaking and should be avoided. Hence the pebbles need to be returned back to the core without violent motion. Various designs of tubing structure and joints have been tried and tested to reach to the final mechanism that provides the desired performance. The newly developed inlet control mechanism thus designed returns the pebble at user defined radial location and ensures that its entry is vertical and with negligible velocity.
- The set-up and the design of its conveyer provides the needed space around the test reactor to implement advanced radioisotopes based techniques. This is the key feature; as these advanced radiometric techniques require substantial space for implementation around the experimental set-up and is considered while designing this set-up.

Detailed information about inlet control mechanism, exit flow control mechanism designs and evolution to final exit control mechanism is explained in next paragraphs.

a. Side view

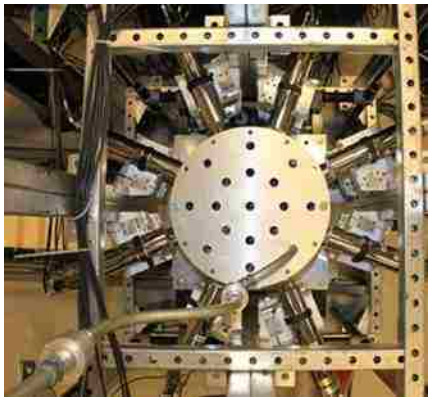

b. Top view

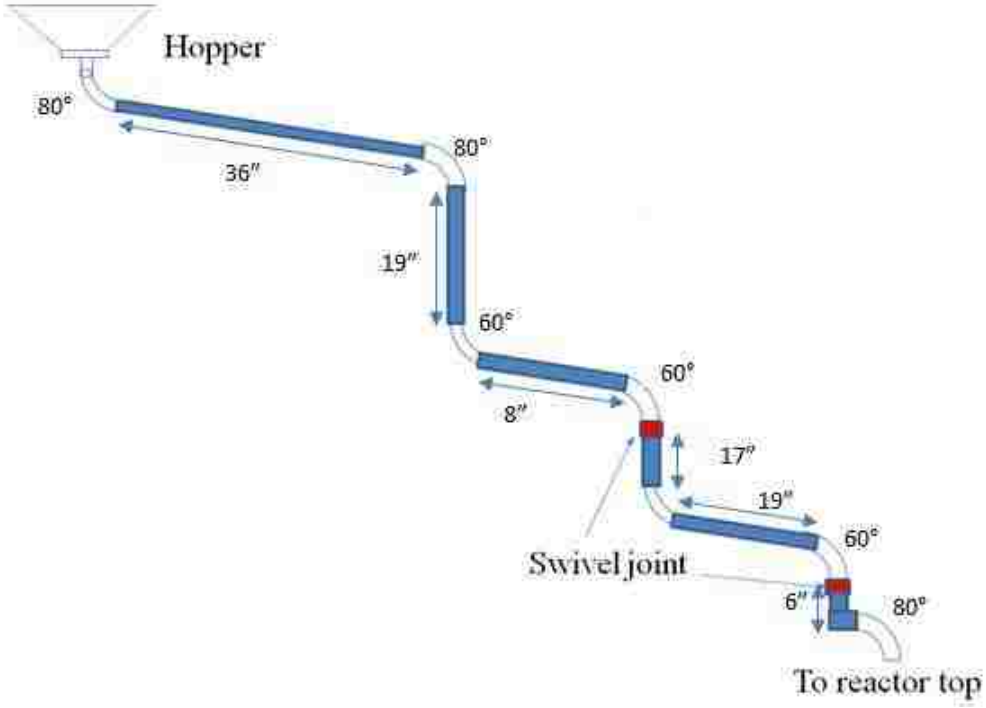

c. Schematic diagram with key dimensions

Figure 3.2 Inlet control mechanism

3.3.1 Inlet Control Mechanism. The purpose of an inlet control mechanism is to place the returned pebble at user defined radial locations with negligible vertical velocity and in a non-violent manner. Current design of an inlet control mechanism (Figure 3.2) consists of an inclined pipe connected at one end to the bottom of the hopper and its other end is connected to the top of the test reactor through vertical pipe section, swivel joints and elbows. The 80° elbow connects the other end of a pipe to a hole in the top plate mounted on the test reactor. The tubing has swivel joint mechanisms which allow slowing down and placing the returned pebbles at desired radial positions across the top surface of the test reactor.

3.3.2. Exit Control Mechanism. The purpose of an exit control mechanism is to control the exit flow rate of pebbles without any jamming and thus, residence time of pebbles in the reactor. Figure 3.3 shows previously developed exit control mechanism. A large number of different designs consisting of various mechanical components and mechanisms are tried to achieve this objective. Brief information about different designs tried and evolution to final mechanism can be found out in next subsections. The first subsections describe the previous designs and attempts and the following sub-section discusses the final and successful design and mechanism.

3.3.2.1. Evolution of exit control mechanism. Many attempts and various designs have been tried and failed. However, through the process of failed designs and evolution problems were identified and overcame. In these designs, the flow area available for flow of marbles is controlled using combination of fixed-moving parts having matching holes.

a. Primitive slider mechanism

b. Slider-disc mechanism

c. Two disc mechanism

d. Serrated cup mechanism

Figure 3.3. Previously developed exit control mechanisms in chronological order

The moving part, which is a rotary disc is rotated slowly by an electric motor (Dayton Model-4Z134). During one rotation of the disc, the hole in the moving and stationary part matches with each other which allow marbles to exit. In this manner, the rate of marbles coming out of the reactor can be controlled by controlling speed of rotation. The rotary disc shaped parts used in the previous versions are shown in Figure 3.3.a. thru Figure 3.3.c. All these versions suffered from jamming problem even though exit flow rate was controllable and hence, prevented continuous recirculation of pebbles.

In initial designs, matching hole was at some distance from central vertical axis of the test reactor. The holes were beveled to allow for smooth entry of pebbles in the opening but did not help to overcome jamming problem. Hence, it was decided to replace the rotary disc used in previous designs with a cup having central hole and radial slots (Figure 3.3.d). This central hole was then connected to a chute having inside diameter (Thin- wall still conduit) of 0.615", which is slightly bigger than diameter of glass marbles (Figure 3.4a.) The other end was connected to a solenoid operated sliding opening. The frequency of operation of this opening is controlled by a programmable timer. The main idea behind this mechanism is that it will sweep pebbles in the vicinity during its rotary movement which will avoid jamming and direct them towards Centre. Pebbles will get inside chute connected to the centre hole and will leave the system. The exit flow rate of pebbles will be determined by the frequency of solenoid operation which can be set by the user. In this manner, exit flow rate of pebbles can be controlled without any jamming problem. However, this design did not work satisfactorily under partially filled reactor conditions and suffered from occasional pebble jamming problem. The jamming problem could be due to the locking of pebbles in troughs provided in the rotary cup due to the heavy weight of marbles from the top. Hence, a modification to exit control mechanism was made based on discussion with Dr. Gardner's research group at North Carolina State University (NCSU). In their design, a rotary cup having impressions matching pebbles is used. This rotary cup sweeps pebbles in the vicinity and impressions in the cup helps in transporting pebbles to the central opening. The minimum exit flow rate achievable with their mechanism is 60-100 pebbles every minute which is higher for planned PBR study.

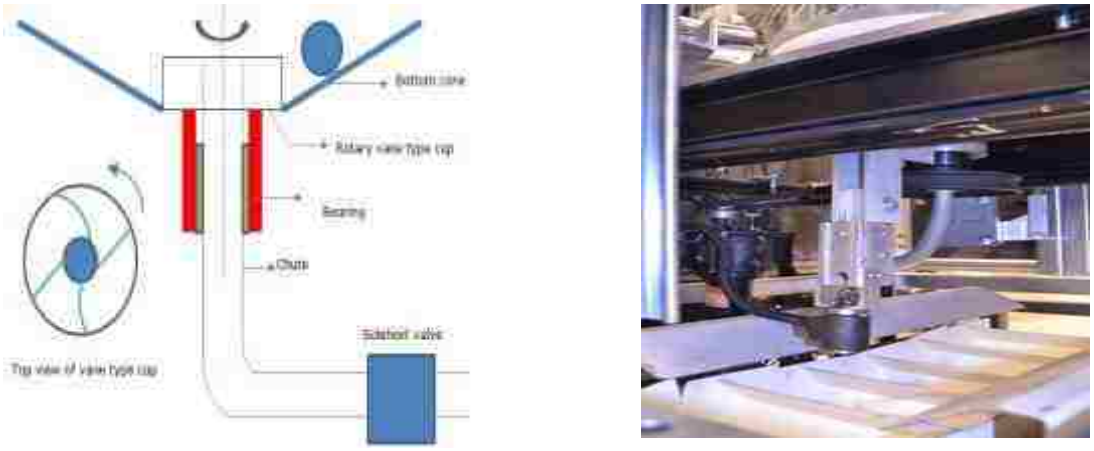

a. Schematic diagram b. Actual picture

Figure 3.4 Current exit control mechanism

This design used significantly larger opening and resulted into higher exit flow rates. Hence, previous radial slot design is upgraded to a rotary vane-type cup (Figure 3.4). The rotary vane type cup has two vanes. It sweeps and transports pebbles in the vicinity to the central opening in the cup of one pebble diameter and is explained in detail in next paragraphs.

3.3.2.2. Final developed exit control mechanism. This final mechanism consists of a rotary vane type cup (Figure 3.5.a, 3.5.b) installed at the opening in the conical bottom portion and connected to a solenoid operated valve whose frequency of operation can be controlled by a programmable timer (OMEGA-PTC 13). The pebbles trapped in between these vanes are directed towards the central opening during the rotation of vane-type cup without getting jammed. This central opening in the cup is connected to a solenoid operated sliding opening via extractor tube (Figure 3.4). This vane type cup offers smooth surface to flow of pebbles and slow rotation of cup has very little effect on

the motion of glass marbles. This cup is rotated slowly by means of a belt and pulley mechanism driven by an electric motor (Figure 3.5.c). These pebbles are extracted one at a time into the chute/extractor tube connected to the central opening in vane-type cup. This central opening is slightly bigger than one marble diameter and streamlines glass marbles in the extractor tube. There is a solenoid valve at other end of this extractor tube whose timing of operation is controllable. The operation of solenoid valve is controlled by a panel mount programmable timer. The extractor tube discharges marbles in the bins of recirculating conveyor which takes them back to the reactor.

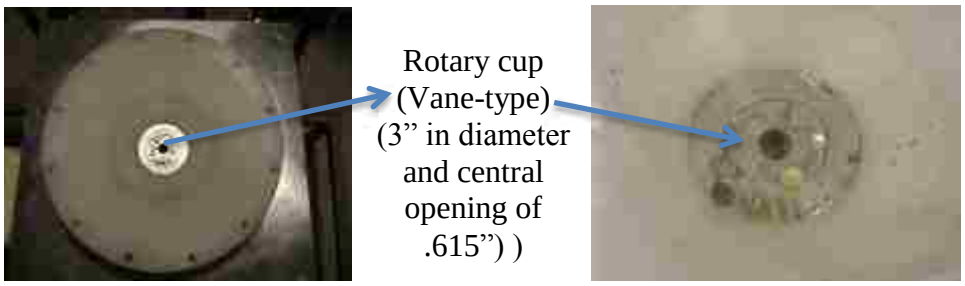

a. Top view of rotary vane-type cup

b. Closer view rotary vane-type cup

c. Exit control mechanism along with chute, slider and solenoid valve

d. Slot in the chute to remove broken marbles

Figure 3.5 Pictures of Rotary vane- type cup based exit control mechanism

This design worked satisfactorily under partially and fully filled reactor conditions and continuous operation of test reactor at slower exit flow rate of one pebble every five seconds is demonstrated.The performance during these trials is found to be satisfactory, except some minor problems such as marbles chipping off. These chips caused jamming in the extractor tube connecting exit of the reactor to the solenoid valve. The possible reasons for this marbles chip-off could be due to falling of marbles from height, mechanically weak marbles, and or defective marbles. To overcome this problem, a slot is machined (Figure 3.5.d) in the extractor tube. The main idea behind this slot is that it will remove chips, broken marbles from the set-up before it can reach to the solenoid valve operated sliding opening. Continuous recirculation experimental set-up is tested for continuous operation and is found to operate satisfactorily without any jamming problem. This is considered as one of the major achievements with regard to the design and development of continuous recirculation experimental set-up.

3.3.3. Test Reactor Geometrical Parameters Selection. In pebble bed reactors, oscillatory variation of radial porosity is reported in many previous works and is observed up to 5 pebble diameters from the wall (Mueller, 1992; Goodling et al., 1983; Mariani et al., 2009). Beyond 5 pebble diameters, there are minor fluctuations observed in the radial porosity. Hence, the effect of wall is not felt beyond 5 particle diameters. Also, glass marbles of 1/2" diameter having density ~2.5g/cm^3 are found suitable to start with from tracer preparation point of view and representing actual pebbles flow (actual density of pebbles ~1.8 g/cm^3). The diameter of test reactor is selected based on considerations of representing the wall effect as nature of packing will affect subsequent flow of pebbles. Large diameter test reactor will have significant attenuation demanding

stronger radioactive source and hence avoided in this work. One foot diameter of test reactor will yield diameter aspect ratio (which is defined as a ratio of inside cylinder diameter to the pebble diameter) of 23.9. Such an aspect ratio is capable of introducing wall-effect induced oscillatory variation in radial porosity observed in an actual reactor. Exit flow rate of one pebble every five seconds is chosen to represent slow granular flow in actual pebble bed reactor. Height-to-diameter ratio (H/D) of 2 or larger will yield into long duration radioactive particle tracking (RPT) experiments. There is a head independence of pressure and flow rate reported in previous studies related to a granular flow (McCabe et al., 1993). This is due to the static friction between wall and the particles. As coefficient of static friction increases, significantly higher head independence of pressure and flow rate is observed (Luo et al., 2010). Thus, Height-to-diameter ratio (H/D) of 1 is selected for this study. The bottom cone angle has significant influence on flow of pebbles and presence of dead zones. During evolution of exit control mechanism, it is found that bottom cone angle also affects the jamming of pebbles in bottom section. Half-cone angle of 60° is chosen based on previous studies (Gatt (1973), Wang (2010) and found to be less prone to jamming problem.

3.4. DESCRIPTION OF FINAL CONTINUOUS PEBBLES RECIRCULATION EXPERIMENTAL SET-UP

The pebble bed test reactor made of acrylic (1foot outer diameter with 11.95 inch inside diameter and 1foot in height) is filled with ½” glass marbles and is mounted on a stand (Figure 3.6). An exit control mechanism described previously is installed at the bottom opening in the cone.

Figure 3.6 Continuous pebbles recirculation experimental set-up at Missouri S&T along with implementation of RPT technique

An exit flow rate of one pebble every five seconds is used in all experiments. The glass marbles coming out of opening in extractor tube, which is operated by a solenoid operated slider, falls into a conveyor bin just below the reactor. From there, the glass marble is transferred back to the hopper at the top via adjustable speed conveyor (TipTrak from UNITRAK). Conveyor bin releases glass marbles in this hopper. Marbles are then transferred to the top of the reactor via inlet control mechanism which consists of straight and elbow sections of one pebble diameter tube. This inlet control mechanism also has three swivel joints. The inlet control mechanism is connected to a top plate (diameter matching with the reactor) having 17 holes. These holes are provided to return the pebble at 17 different radial positions. The vertical leg of conveyor belt is kept at a

sufficient distance (~150cm) away from the test reactor. This allows ease in implementation of techniques such as radioactive particle tracking (RPT), residence time distribution (RTD), computed tomography (CT), gamma-ray densitometry (GRD) and calibration RPT equipment around the test reactor. These advanced radiometric techniques require substantial space for implementation around the experimental set-up. Figure 3.6 shows implementation of RPT technique around this continuous pebble recirculation set-up. A significant effort in number of trial and different versions of mechanical designs has been put in the development of continuous pebbles recirculation experimental set-up at Chemical and Bio-chemical Engineering Dept. at Missouri S&T. The current set-up has improved capability to control the exit flow rate of glass marbles, mimicking pebbles, without any jamming. Also, the inlet control mechanism returns the pebble at different radial positions in a non-violent manner. This experimental set-up is a unique research facility operated as a cold flow module. This experimental set-up is used for implementation of advanced radiometric techniques such as radioactive particle tracking (RPT) and residence time distributions (RTD) set-up and new calibration RPT technique. This set-up is tested for continuous operation and found to work satisfactorily without any jamming. This set-up can be modified to operate as a moving bed reactor used in chemical and petro-chemical industries.

3.5. SUMMARY

The design and development of cold flow continuous pebbles recirculation experimental set-up, modality pivotal for implementation of RPT and RTD techniques and calibration RPT equipment, is carried out to mimic the flow of pebbles in PBR. This

set-up currently handles ½" glass marbles which can be extended to actual size pebbles of 6cm in diameter, if required. This set-up can be modified to accommodate larger diameter and taller columns. Automatic and continuous re-circulation of glass marbles, mimicking pebbles, is achieved and demonstrated at a slower flow rate. This continuous recirculation experimental set-up has following salient features

- Control over pebbles exit flow rate without jamming
- Capability to place returned pebble at a pre-defined radial position in a non-violent manner using inlet control mechanism
- Offers space for Implementation of RPT and RTD technique and calibration RPT set-up

Furthermore, the developed set-up can be modified to be operated as a moving bed used in chemical and petroleum industries.

4. EXPERIMENTAL INVESTIGATION OF PEBBLES FLOW FIELD USING RPT AND RTD TECHNIQUES

As mentioned earlier, In a Pebble Bed Reactor (PBR), heat source i.e. nuclear fuel is in the form of a spherical pebble and moves in the core under the influence of gravity. Helium gas moves through the voids formed in between the pebbles and removes heat generated due to nuclear fission from the fuel. Hence, an investigation of pebbles flow field is of paramount importance from reactor neutronics and coolant thermal hydraulics point of view (Rycroft et al., 2006). A comprehensive experimental study of pebbles flow field will not only significantly advance current understanding of the PBR technology but also provide a valuable information and benchmark data from reactor safety assessment and performance evaluation point of view. The design and development of a continuous pebble re-circulation experimental set-up (Khane et al., 2010), which simulates the flow of pebbles in a pebble bed test reactor was carried out and already described in Section 3. Glass marbles of ½" diameter were used and re-circulated continuously. The cold-flow continuous pebble re-circulation experimental set-up, a unique research facility that has control over pebbles exit flow rate and capability to place returned pebble at different radial positions. Radioactive Particle Tracking (RPT) and two detectors based residence time distribution (RTD) are radioisotopes based non-invasive flow mapping techniques, were implemented around continuous pebble re-circulation experimental set-up (Khane et al., 2011). RPT technique makes use of γ-rays emitting single or multiple radioactive particles (also known as radioactive tracer particle). The motion of radiotracer particle is followed, in the 3-D domain of the whole system, by using either collimated or non-

collimated scintillation detectors (Al-Dahhan,2009 ; Shehata and Gardner, 2007). RTD set-up is capable of measuring pebbles overall residence time in a non-invasive manner. Both of these radioisotopes based techniques together are capable of providing extensive information about pebble's flow field, including overall and local residence time distribution, stagnant zones, pebble occurrence, Lagrangian trajectory, etc. In this section, detailed information about these radio-isotopes based techniques and their various components, implementation of these techniques around continuous pebble re-circulation experimental set-up and the obtained results using these techniques about granular flow in a pebble bed test reactor are discussed.

4.1. RADIOACTIVE PARTICLE TRACKING (RPT) TECHNIQUE

4.1.1. Introduction to RPT Technique. In general, RPT technique uses a single or multiple radioactive particles emitting γ-rays (i.e. radiotracer particle) whose motion is followed in the 3-D domain of the whole system by using either collimated or non-collimated scintillation detectors (Lin et al.,1985 ; Gatt ,1973;, Vesvikar,2006). A tracer particle dynamically similar to the tracked phase is made-up of irradiated Scadium-46, Gold-198, Cobalt-60 or another isotope of a gamma ray emitter. If the tracer is mimicking solids phase, it should have same size, shape, density and surface finish as that of solids phase. If tracer is mimicking liquid phase, it should be as small as possible and should have same density as that of liquid phase. The non-collimated detectors based RPT has been demonstrated extensively in previous studies on multiphase flow systems of practical interest. The instantaneous tracer position is identified by simultaneously monitoring photo-peak counts received by a set of non-collimated sodium iodide (NaI)

scintillation detectors which are arranged strategically around the system (Moslemian et al., 1992; Al-Dahhan, 2009). The counts received in each detector are a function of the distance between the detector and the particle, and attenuating material inventory present between the tracer and the detector. The forward problem of finding instantaneous position of particle based on intensities received at the detectors is solved by performing calibration experiments. RPT calibration experiments, which are performed prior to actual RPT experiments, are carried out at the same operating conditions as that of actual experiment to mimic the radiation attenuation in the system. The radioactive tracer is placed at various known locations and the counts received at each detector are recorded. Using this information calibration curves, which are essentially distance-count map for each detector, are established. The instantaneous position of the tracer then can be found out with the help of various in-house developed position reconstruction algorithms (Devnathan (1991), Degalessan (1997), Rados (2003), Rammohan (2002), Ong (2003), Bhusarapu (2005), Shaikh (2007), Han (2007), Vesavikar (2006) and calibration curves. Using this instantaneous position data, Lagrangian trajectories, instantaneous and time averaged velocity field and various turbulent parameters (Reynolds stresses, turbulent kinetic energy, turbulent eddy diffusivities, etc.) can be determined. It is noteworthy to mention that RPT is the only non-invasive and quantitative measurement technique capable of providing full description of 3-D flow field in highly opaque reactors and can provide particle Lagrangian velocities throughout the domain.

4.1.2. Classification of RPT Technique. There are mainly two types of RPT techniques.

1. Non-collimated detector based RPT technique

2. Collimated detector based RPT technique

The collimated version of RPT consists of a set of three well collimated detectors mounted on a horizontal platform. This platform can be moved vertically up and down to search for the radioactive tracer particle and to identify its z-co-ordinate with the help of horizontal slit collimated detector fixed to moving platform. The other two collimated detectors are having vertical slit and can be swung about a pivot point to track the radioactive particle in the planar domain (identified by horizontal slit collimated detector), and provides information about in-plane position coordinates of tracer. This method relies on identifying instantaneous position of a tracer particle corresponding to instantaneous peak in the count rate data without any need for *a priori* calibration. This technique does not suffer from radiation detection problems which are usually associated with high count rates. Also, this method doesn't require any *in-situ* calibration to identify the instantaneous particle position. This technique involves real time tracking of unknown motion of tracer particle. Hence, its performance is limited due to upper limit on particle tracking speed (Shehata, 2005). The count rate reduces drastically due to narrow width collimators and needs to be compensated by stronger radioactive source which is cause of concern from radiation safety and handling point of view and or by installing collimated detectors closer to the system under study.

In non-collimated version of RPT technique, radioactive tracer particle is identified by simultaneously monitoring counts data received by a set of usually 16-32

stationary NaI detectors arranged strategically around the system. It requires *in-situ* calibration prior to actual RPT experiments and development of position reconstruction algorithms to identify instantaneous particle position. However, it does not have any upper limit on tracking speed due to the use of stationary detectors. This has been used in this study and discussed in detail in next sub-sections.

4.1.3. Typical Set-up of RPT Technique. In a typical implementation of RPT technique around complex multiphase system an array of 16 to 32 scintillation detectors surrounds the system (Figure 4.1). These detectors are arranged strategically around the system in order to improve resolution and accuracy, which are main performance indicators of RPT technique.

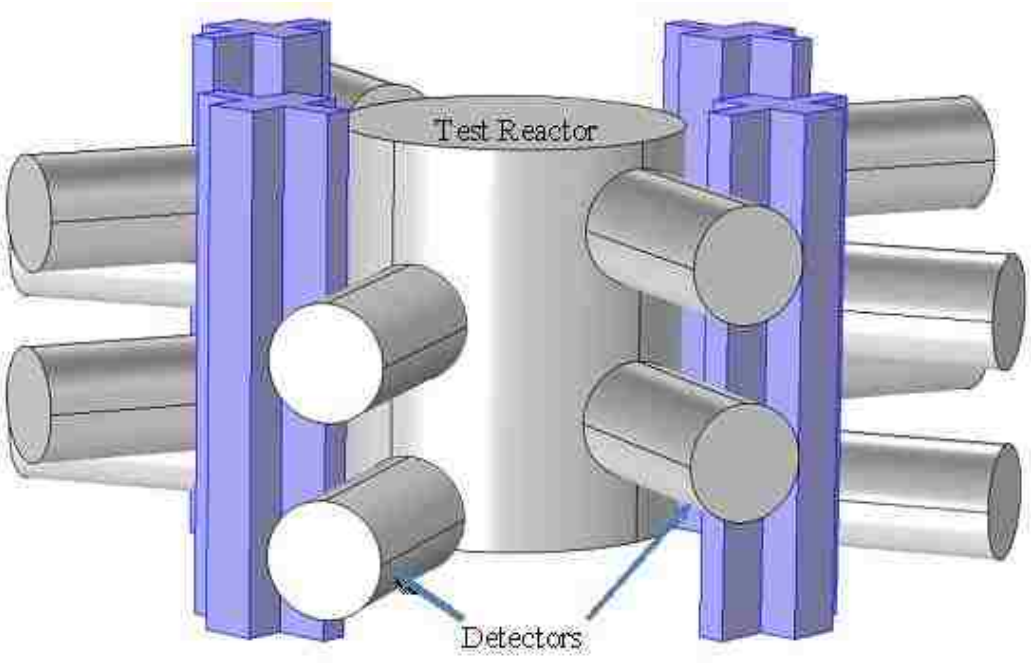

Figure 4.1 Typical RPT set-up

Research has been done to define the best configuration of detectors around the multiphase system which can provide best spatial resolution and accuracy (Roy et al., 2002). Each detector is usually aligned with the central axis of the system. The multiphase system under investigation is operated at normal conditions and tracer mimicking tracking phase is allowed to move freely in the system. The counts data recorded in different detectors are collected continuously and used to reconstruct instantaneous positions of tracer. Successive time differentiation of instantaneous position data provides information about instantaneous velocities. Ensemble averaging of obtained velocities can give important information about mean and fluctuating components of velocities at various system locations. This information can then be used to determine various turbulence parameters such as Reynolds stresses, turbulent kinetic energy and turbulent eddy diffusivities, etc. From the knowledge of instantaneous tracer positions a wealth of information about complete velocity field, overall and local residence time distribution, location and size of stagnant zones, if any, and other related turbulent parameters (such as turbulent kinetic energy, diffusivities, normal and shear stresses, etc.) can be obtained. A wavelet theory based filtering algorithm is usually used to remove white noise, if any, from reconstructed instantaneous position data (Degaleesan, 2002). Figure 4.2 illustrates flowchart representation of various data processing steps involved in RPT technique.

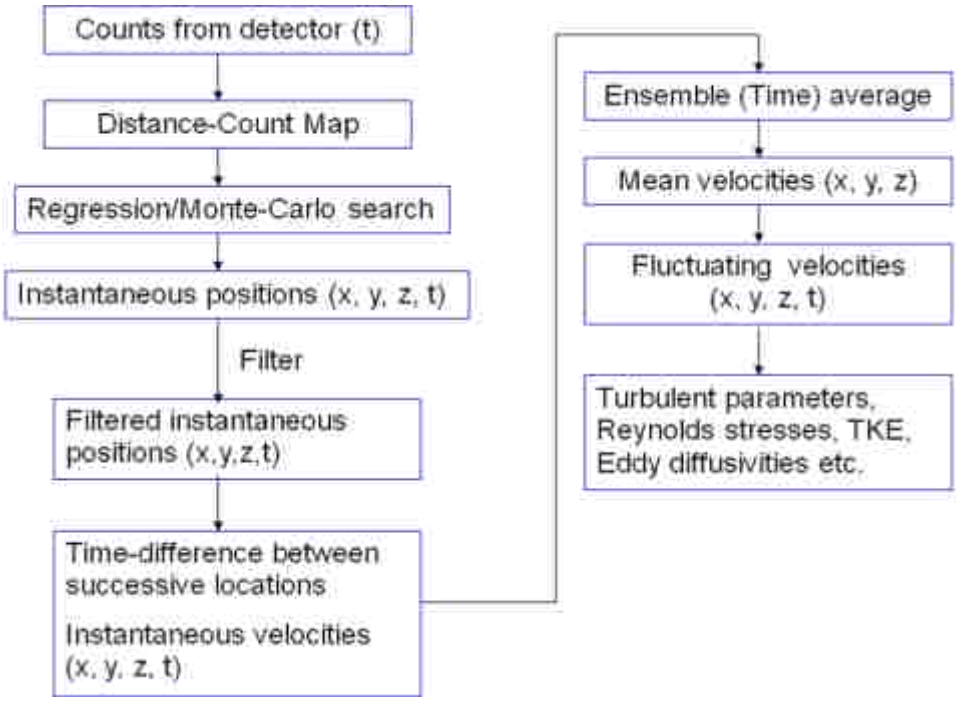

Figure 4.2 Flowchart representation of RPT data processing steps

4.1.4. Comparison with Other Techniques. RPT is one of the versatile and powerful techniques among the various velocimetry techniques. These velocimetry techniques can be broadly classified into two main categories:

1. Techniques using nuclear radiation such as RPT and positron emission particle tracking (PEPT)
2. Optics based techniques such as Particle Image Velocimetry (PIV), Laser Doppler Anemometry (LDA), etc.

Positron emission particle tracking (PEPT) uses positron emitting source. These positrons annihilate very close to their point of emission with free electrons and this results in the emission of two back-to-back gamma photons. They travel along the same line but in the opposite directions. With the help of sophisticated detection system (e.g.

gamma-ray camera, array of detectors surrounding the object etc.) , it is possible to locate the position of tracer in a 3-D domain (Ingram et al., 2007). The detection system, which works on the principle of coincidence detection of annihilation photons, is complicated and expensive as compared to RPT detection system. Also, there is an upper limit on operating conditions for use of PEPT due to low sensitivity and limited counting capability of detection system at higher velocities (Chaouki et al., 1997).

Particle image velocimetry (PIV) is a non-invasive flow visualization technique capable of quantifying the instantaneous flow field, as well as time-averaged flow patterns in planar laser illuminated region. It also allows measurement of local phase hold-ups in the multiphase systems (Chen and Fan (1992), Chen et al. (1999), Adrian (1991)). Particle image velocimetry (PIV), particle streak velocimetry (PSV), and particle tracking velocimetry (PTV) are the three variants of particle velocimetry based on the mode of operation. Typical PIV apparatus consists of a high resolution and high framing rate CCD camera, high power laser source, an optical arrangement to convert the laser output into a thin light sheet, associated electronics, and seeding nano-particles faithfully following the dynamics of phase under consideration. Matching the index of refraction of materials used in the experiments is necessary to avoid bending of the light at the interface of materials (Dominguez-Ontiveros and Hassan, 2009). The light bending phenomena will be pre-dominant in a multiphase system with higher volume fraction of dispersed phase. The velocity measurements obtained with particle velocimetry are in two-dimensional plane as opposed to full three-dimensional description of flow field obtainable using RPT.

LDA also known as Laser Doppler Velocimetry (LDV) works on the principle of 'Doppler effect' and is capable of providing point measurement of velocity (Durst et al., 1976). A coherent source of Laser is used to obtain two crossed beams. The seed particles are introduced into the system which follows the dynamics of the tracking phase. The seed particles size is large enough to scatter sufficient light for signal detection (to obtain good signal to noise ratio). Due to seeded particles, there is a shift in the frequency of the scattered light also known as Doppler frequency shift. Measurement of this shift can provide information about local velocity of fluid. The entire area of interest within the flow field is scanned by a crossed beam in a point-by-point manner and is the biggest disadvantage of this technique. Like other optical techniques, LDA is of limited use in highly opaque multiphase systems. However, high degree spatial resolution in velocity measurement is one of major advantage of LDA technique.

High penetration capability of gamma rays makes RPT technique suitable for visualization of flow through dense and opaque multiphase systems. This is one of the main advantages of RPT technique over optics based flow visualization techniques. Among different velocimetry techniques available, technique of RPT is not only accurate but provides data in a non-invasive manner without any limitations from system opacity. This avoids introduction of an intrusive probe which affects the flow dynamics. Hence, it is possible to capture the true multiphase flow dynamics with technique of RPT. Also, full information about the flow field in 3-D can be obtained using technique of RPT. It is worth to mention that RPT is the best suited technique for this study of granular flow in a PBR, as it has no limitations on operating conditions, system opacity, design and configuration of multiphase system. However, successful implementation and to obtain

reliable data using RPT technique requires specialized knowledge of radioactive tracer preparation, calibration methodology, development of protocols and procedures for safe handling of radioactive materials and carrying out work in compliance with it. Development of an efficient photon counting system is also crucial for successful demonstration of RPT technique. This requires an in-depth knowledge about basics of radiation detection principles, working principle of multi-channel counting system, nuclear instrumentation modules (NIM) and other related standards such as CAMAC (Computer Automated Measurement and Control). Also, the development of various mathematical models and position reconstruction algorithms is essential for particle trajectory reconstruction and for post-processing of position data in order to get various flow dynamics related parameters such as phase velocities, turbulent parameters, residence time distributions, etc.

4.1.5. Brief History of Use. As mentioned before, optics based flow visualization techniques cannot be used in highly opaque multiphase flow systems with larger volume fraction of dispersed phase. This is mainly due to the interference coming from phase interfaces which gives false results. High energy radiation based techniques (γ-ray or x-ray based) are suitable for such application as these radiations are unaffected by interaction with phase interfaces. These radiation based techniques work on the principle of *radio-opacity* i.e. differential attenuation of radiation based on density, and composition characteristics of attenuating material. The technique of RPT uses γ-ray emitting tracer which follows the dynamics of tracking phase. It was first qualitatively demonstrated by Kondukov et al. (1964) for fluidized bed application. Six scintillation detectors were used to track the tracer motion. Due to lack of sophisticated data

acquisition system, limited information was obtained. Similar problems were reported with the system developed by Meek (1972), Velzen et al. (1974). Meek's study used tracking set-up consisting of six detectors and was designed to move along with the tracer. Prior calibration of detector response was carried out to determine successive tracer locations. This tracking set-up was unable to track the tracer continuously. Lin et al. (1985) demonstrated improved version of RPT technique in a study of solids motion in fluidized beds. An efficient photon counting system along with concept of redundancy (having large number of scintillation detectors) was implemented in this study. The data acquisition system was further improved by Moslemian (1987) in which digital pulse counters were used. This helped in achieving faster sampling rates and thus improved resolution. This upgraded version of the RPT technique can be considered as a second generation which was able to give experimental data on solids velocities and turbulence parameters in fluidized beds. Co-operative research effort allowed upgrades of this system to be built at Florida Atlantic University (FAU) and at Chemical Reaction Engineering Laboratory (CREL) , Washington University in St. Louis (CREL-WU). Third generation of RPT was developed at CREL-WU by Devanathan (1991) to study the hydrodynamics of liquid phase in bubble columns. IBM macro assembly language was used to write new data acquisition programs and important information about liquid velocities and turbulence parameters for different bubble columns was obtained. The fourth generation of RPT was developed at CREL-WU by Yang (1992) in which the signal processing and data acquisition system was improved. Data acquisition programs were written in C language. This version of RPT was used extensively in hydrodynamics study of various multiphase reactor configurations at CREL-WU. Multi-particle

radioactive particle tracking (MPRPT) set-up is fifth generation RPT technique, compact and cheaper in nature, was also developed as a part of hydrodynamics study of anaerobic digesters (Vesvikar, 2006). This technique can track up to 8 different tracers simultaneously due to development of advanced electronic data acquisition system in collaboration with Oak Ridge National Lab (ORNL). Also, substantial development related to data filtering methods (Degaleesan, 1997), calibration apparatus and methodology (Luo, 2005), particle position reconstruction algorithms (Rammohan, 2001; Rados, 2003; Bhusarapu ,2005) has been carried out over the last 15-20 years. An upgraded version of RPT electronics and data acquisition program has been developed as a part of current work which could be considered as a sixth generation of RPT technique. This newer version of RPT technique was applied for the study of granular flow in a PBR.

4.1.6. Working Principle of RPT. Newton's inverse square law (Goats, 1988) is applicable for an isotropic point gamma source. According to this law, the intensity of radiation emitted by a point source is inversely proportional to the square of the distance from that source. If a hypothetical point detector is used to detect gamma radiations, counts recorded in the detector will be inversely proportional to square of the distance between gamma source and the detector. If there is an attenuating medium present in between the source and the detector, there will be an additional exponential decrease in counts with respect to distance and density according to Beer-Lambert law (Wentworth, 1966). When radiations of energy less than 1 MeV are emitted from mono-energetic radiation source and pass through an attenuating medium, different photon interactions such as Compton scattering, and photoelectric absorption are observed (Knoll, 2000).

Due to the attenuation, there will be build-up of low energy photons which causes broadening of energy spectrum. This build-up is caused by Compton scattering of photons due to the material in-between the detector and the source and Compton scattering in the detector, which partially deposits photon energy. These low energy photons will lower the fraction of useful un-scattered gamma energy photons (also known as Photo-peak fraction) traveling in a straight line from source to the detector. Hence, these low energy photon counts need to be removed by using appropriate energy discrimination level. In actual RPT experiments, a point source (also known as tracer) is moving inside a cylindrical vessel (prototype of multiphase system). There will be an attenuation of gamma photons due to the system inventory in between the tracer and the detector. An array of NaI scintillation detectors are arranged strategically around the multi-phase system and continuously measures photon counts above certain threshold. Various detector arrangements such as two-detectors per plane and adjacent plane detectors staggered at 45° (Roy, 2000), two-detectors per plane and adjacent plane detectors staggered at 90° (Degaleesan, 1997), three-detectors per plane (Bhusarapu, 2005; Luo, 2005), six detectors and eight detectors per plane (Vesavikar, 2006) have been used in the past RPT based studies. Roy et al. (2002) recommended symmetric distribution of detectors around the system and an alternate staggering of adjacent plane detectors. Roy et al. suggested that better resolution and good sensitivity in position reconstruction is achievable with four detectors per plane. In this work, an arrangement consisting of four detectors per plane and alternate staggering of adjacent plane detectors at 45° was used. RPT technique relies on detection and counting of un-scattered gamma rays traveling in a straight line from the tracer to the detector (i.e. photo-peak fraction).

The number of counts recorded in a given detector is a measure of the radius of an approximately spherical surface with the detector at its center and the tracer particle located on the surface. Theoretically, three detectors are sufficient to determine position of the tracer as three spheres can intersect only at one point (Chaouki et al., 1997). Due to the statistical nature of radioactive decay process and non-isotropic attenuating medium between the tracer and the detector, more number of detectors are required in the RPT technique. There are either phenomenological or empirical approaches to account for the relation between the number of photons counted in the detector and the location of the tracer particle. An analytical solution to the inverse problem of RPT, i.e. finding the instantaneous tracer position based upon instantaneous counts received in the detectors, is not possible. This problem is solved by performing a set of calibration experiments at the same operating conditions as those of actual RPT experiments. Calibration curves relating photo-peak counts with the tracer position are generated for each detector. These calibration curves along with the counts data recorded during actual experiments are used in the position reconstruction step of a RPT technique to find an instantaneous position of the particle and other parameters related to velocity field.

4.1.7. Mathematical Model Governing the Forward Problem of RPT. Non-collimated detectors based RPT technique relies on counting of un-scattered gamma-rays i.e. those contributing to photo-peak. These un-scattered gamma rays travel in a straight line path from the tracer to the detector. Figure 4.3 show schematic of the tracer location and NaI detector in a column under investigation. Theoretically, the number of photo-peak counts C recorded by the detector in a sampling time interval T is given by (Tsoulfanidis, 1983)

$$C = \frac{T\upsilon A\phi\varepsilon}{1+\tau\upsilon A\phi\varepsilon} \qquad (4.1)$$

where,

A – Strength of point radioactive source placed at a location (x,y,z) inside a dense medium in cylindrical vessel

ν – Number of gamma rays emitted per disintegration (property of radioisotope)

ϕ – Peak to total (Photo-peak) ratio

τ – dead time of detector per recorded pulse

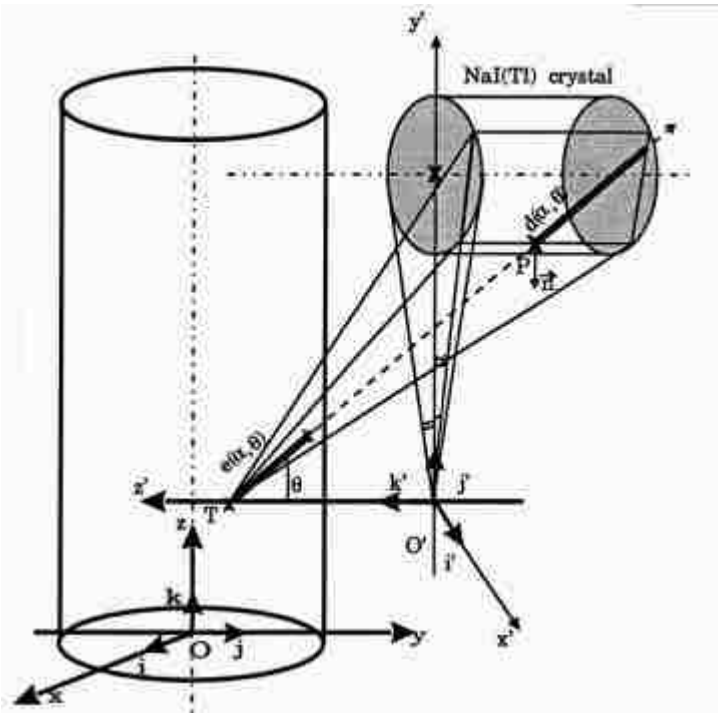

Figure 4.3 Schematic of the tracer location and NaI detector in a column under investigation (from Larachi et al., 1997)

ε – Total detection efficiency i.e. the probability of un-scattered gamma rays emerging from the source interacting with detector material which is given by equation 4.2 (Moens et al., 1981)

$$\varepsilon = \iint_{\Omega} \frac{\underline{r}.\underline{n}}{r^3} f_1 f_2 d\Sigma \qquad (4.2)$$

where,

Ω – Solid angle subtended by the detector surface at the tracer location

$\underline{n}$ – External unit vector normally perpendicular to dΣ

dΣ – Infinitesimal detector surface area

r – Distance between the tracer and the point on the surface of the detector

f_1 – Probability of non-interaction of gamma-rays emitted within solid angle Ω inside the material in the cylinder and cylinder wall and is given by

$$f_1 = \exp(-\mu_r e_r - \mu_w e_w) \qquad (4.3)$$

f_2 – Probability of interaction of these gamma-rays along the distance inside the detector

$$f_2 = 1 - \exp(-\mu_d d) \qquad (4.4)$$

where,

μ_r, μ_w, μ_d – attenuation coefficients of the reactor inventory, reactor wall, and detector material, respectively. Attenuation coefficient (μ) is a product of mass attenuation coefficient (μ/ρ) times the density of material (ρ).

e_r, e_w, d – path length traveled by photon in the reactor medium, reactor wall, and detector, respectively.

The system of equations 4.1 thru 4.4 is the set of equations governing the forward problem of RPT describing relationship between location of tracer particle and recorded count rate. It is difficult to estimate the solid angle (Ω) subtended by the detector surface at the unknown tracer location. Within this solid angle the parameters such as e_r, e_w, d are not same, but rather they are function of unknown position of the tracer and the direction in which gamma rays are emitted. Also, it is difficult to estimate accurate value of μ_r i.e. attenuation coefficient of reactor inventory due to its dependency on unknown tracer position and flow conditions. Hence, an analytical solution to the forward problem of RPT is not possible and is solved by carrying out *in-situ* RPT calibration.

4.1.8. Need for RPT Calibration. The exact calculation of total detection efficiency (equation 4.2) demands solving surface integral which contains variables dependent on unknown tracer position over an unknown solid angle. It is difficult to estimate detection efficiencies for situations encountered in RPT experiments (i.e. point source located at unknown locations inside an attenuating material and situated off the central axis for most of the times). All the above mentioned analytical difficulties invoke common practice of using semi-empirical modeling approaches to obtain various dependent and independent parameters of the model given by equations 4.1 thru 4.4 for particular system (Moslemian et al., 1992). This requires carrying out RPT calibration experiments at the same operating conditions as that of actual RPT experiments mimicking the attenuation of emitted gamma rays received by detectors. This was to provide data for estimation of model parameters of semi-empirical models. During RPT calibration, a radioactive particle is kept at known locations in the system and time averaged counts data is recorded in all the detectors. This provides relationship between

source-detector distance and counts recorded by all the detectors. Hence, obtained data is used to plot calibration curves for each detector. The inverse problem of position reconstruction uses this calibration data for reconstruction of instantaneous position of the tracer. There are different position reconstruction algorithms (Devnathan,1991; Degalessan,1997; Rados,2003; Rammohan,2002; Ong,2003; Bhusarapu,2005; Vesavikar, 2006; Shaikh, 2007; Han, 2007) developed over the years to find out instantaneous position of the tracer based on counts recorded in the detectors. Also, computational methodology based on Monte Carlo simulation method (Mosorov and Abdullah, 2011) has been used in conjunction with series of calibration experiments to obtain much needed model parameters and to obtain a map of gamma- ray counts vs. distance for large number of calibration positions. Each point on this computer generated map gives relationship between the tracer-detector distance and corresponding gamma-ray counts recorded by the detectors (Larachi et al., 1997).

4.1.9. RPT Position Reconstruction Algorithm. The main aim of RPT position reconstruction algorithm is to find instantaneous position of the tracer particle based on the counts recorded in a set of detectors with least possible reconstruction error. There are four main types of RPT position reconstruction algorithms (Rados,2003; Gupta,2002; Larachi et. al,1997; Rammohan,2002; Bhusarapu, 2005) which are as follows.

- Weighted Least Square Regression Method
- Monte Carlo Method
- Feed Forward Neural Network Method
- Cross-Correlation Based Method involving Semi-Empirical Model

Weighted least square regression method assumes that intensity of radiation or counts received in a detector is a function of the distance between the center of the detector crystal and the tracer location. In principle, four detectors can identify unknown location of the tracer. However, due to statistical nature of radioactive decay process a redundancy in number of detectors is required to apply the weighted least-squares method of position reconstruction. Based on the calibration curve obtained using calibration experiments and from the cubic spline fitting (Devnathan,1997), the most probable location is identified from the application of weighted least-square regression to the counts registered in all the detectors. This method has poor accuracy and resolution in dense flows (Degaleesan, 1997). This is due to the basic assumption that counts recorded depend only on the particle-detector distance and independent of the geometry of the system, attenuating medium, etc. Rados (2003) developed a new approach to take into account lateral arcs present in the detector calibration curve also known as *band-effect*. A 3^{rd} order beta spline with 9 coefficients was fitted to the experimental calibration data and unknown particle position was reconstructed through a non-linear least square approach. This new approach of position reconstruction was demonstrated in slurry bubble column systems and found to be giving satisfactory results.

Monte Carlo Method (Gupta, 2002; Yang et al., 1993) accounts for the effect of geometry, solid angle and characteristics of an attenuating medium. This method generates a very fine grid of calibration points. The modeling of an attenuating medium in between the tracer and the detector is usually carried out by using holdup distribution profile. However, the effect of flow conditions on the attenuating medium is either taken as a constant (Larachi et al., 1994) or estimated using a time-averaged holdup profile

(Gupta, 2002). The change in the intensity of counts with changes in the holdup distributions is large. Using constant holdup value or time-averaged hold-up profile, where its constants are estimated by regression, introduces errors into the computationally expensive and sophisticated Monte Carlo based model. This is one of the main drawbacks of this method.

Feed Forward Neural Network Method (Godfroy et al., 1999) uses a black-box model employing neural network. In this method, part of the calibration data is used to estimate large number of neural network constants and gain confidence. Remaining calibration data is used as a test data to validate the neural network model. The main drawback of this method is that the model used does not have any physical significance and employs huge number of fitting parameters (~ 160), which can restrict its applicability.

Cross-correlation based position reconstruction algorithm (Bhusarapu, 2005) is a two-step approach in which a cross-correlation based search method is used to locate the tracer particle position and a semi-empirical model relating counts to the position of the tracer particle is used for further mesh refinement. This semi-empirical model is a mechanistic simplification of actual complex mathematical model (given by equations 4.1 thru 4.4) relating the counts intensity (C) recorded in the detector to the position of the γ-rays emitting tracer particle. This model takes into account effect of geometry as well as the attenuating medium in between the tracer particle and the detector. It has been found to work satisfactorily in gas-solid flows. In PBR study, calibration experiments suggested that counts received at the detectors are not only a function of distance between the tracer and the detector but also of the attenuation characteristics of a

medium in between the tracer and the detector. Hence, a cross-correlation based position reconstruction algorithm was used in this PBR study.

4.2. RPT TECHNIQUE BASED STUDY OF GRANULAR FLOW IN A PBR

RPT technique is capable of providing information about three-dimensional pebbles flow, velocity and its components, overall and local residence time distribution, stagnant zones, pebbles occurrence, Lagrangian trajectory and other related solids flow dynamic parameters in a non-invasive manner. However, the implementation of RPT around continuous pebbles recirculation experimental set-up (mimicking PBR cold flow operation) is more involved, challenging and time consuming. It demands carrying out following tasks before, during and after RPT experiments to obtain useful information.

- Development of continuous pebble recirculation experimental set-up suitable for implementation of RPT which is already described in Section 3.
- Design and fabrication of mechanical structure for fixing detectors systematically around test reactor, detector centering and laser alignment with the central axis of a test reactor.
- Development of a radioactive tracer particle capable of mimicking the pebbles flow dynamics.
- Development of calibration apparatus and methodology suitable for the study of granular flow in a PBR.
- Up-gradation of multi-channel scintillation detector based counting system.
- Performing RPT calibration experiments and generating detector calibration curves.

- Carrying out actual RPT experiments.
- Development of position reconstruction algorithms suitable for study of granular flow in a PBR and reconstructing instantaneous tracer particle position
- Processing obtained position data to get useful information about pebbles trajectories, velocity profile, residence time distribution, etc.

RPT technique is non *off-the-shelf* in nature as far as its application to multiphase flow systems is concerned. Hence, proper implementation of RPT for the study of complex multiphase systems requires an in-depth understanding about basics of RPT technique and carrying out above mentioned tasks in a systematic manner. The main steps in application of RPT technique for the study of granular flow in PBR includes preparation of tracer particle, arrangement of detectors, electronic system for data acquisition, design and development of RPT manual calibration apparatus and calibration methodology, implementation of cross-correlation based position reconstruction algorithm, etc. These various steps are discussed in detail in next paragraphs.

4.2.1. Preparation of RPT Tracer Particle Suitable for PBR Study. The RPT technique is based on following the motion of a single radioactive particle (γ-emitter) in whole system domain. Development of a radioactive tracer particle suitable for particular study is a challenging and pivotal task in order to obtain reliable RPT technique results. The main characteristic of a radioactive tracer is to mimic the dynamics of phase to be tracked. It should meet the following requirements (Computer automated radioactive particle tracking (CARPT) manual, 2007):

- The density of tracer should match with the density of phase to be tracked

- It should contain a suitable radioactive source of appropriate strength to ensure good measurement statistics (high signal to noise ratio) and should not saturate detectors. Longer half-life of radioisotope is desirable to avoid decay correction and reasonable working life.
- When tracking solid phase, tracer should have the same size and shape as that solids, whereas it should be as small as possible for tracking of liquid phase to reduce the drag force
- It should be rigid, thermally and mechanically stable at the operating conditions of the experiment

Tracer preparation task involves selection of suitable radioisotope, activity selection, particle size selection and fabrication, sealing of particles inside vials, irradiation of sealed vials in high flux nuclear reactor, preparation of radioactive tracer particle inside hot glove box, sealing radioactive particle inside tracer particle, density matching and initial testing of tracer particle for contamination in tumbler. Tracer preparation is the bottleneck activity in implementation of RPT around any multiphase system and involves lot of activities and involvement of number of internal and external agencies such as Radiation safety, Missouri University Research Reactor (MURR) Columbia, Missouri, etc.

4.2.1.1 Choice of radionuclide. The source strength reduces to half of its initial value in one half-life. The half-life of selected radionuclide should be an order of magnitude higher than that of total duration of given set of experiments. This will ensure that there is no significant reduction in the activity of source during experiment. This is particularly important for long lasting experiments such as slow flow of pebbles in a

PBR. Feasibility study of using Scandium-46 and cobalt-60 based tracer particle was carried out. It was decided to use cobalt-60 based tracer particle due to its prolonged half-life (~5.2 years) as compared to shorter half-life of scandium-46 (half-life ~84 days) and lesser irradiation time requirement in nuclear reactor. Use of cobalt-60 is suitable for this study of granular flow as the movement of pebbles is very slow and will not require any half- life correction unlike scandium-46.

4.2.1.2. Source activity selection. It is essential to have source of sufficient strength from better statistics and reliable measurements point of view. This will ensure that high signal to noise ratio is observed even in the distant location of the source from the detector. At the same time, selected strength value should not saturate detectors when source is very close to the detector. Based on these two opposing requirements, minimum radioactivity of tracer particle for given size of reactor and attenuating medium is decided. Particles of source strength in between 150-500μCi have been used in past RPT experiments (Computer automated radioactive particle tracking (CARPT) manual, 2007). A strong source of radioactivity is required for study of granular flow in a PBR due to presence of highly attenuating glass marbles. A radioactive Co-60 source of 500μCi strength was chosen for this PBR study. The calculations for tracer mass and subsequent phase density match calculations were done based on this chosen source strength and by following reported calculation procedure (Computer automated radioactive particle tracking (CARPT) manual, 2007). It can be found in appendix B.

4.2.1.3. Manufacturing of Cobalt particles, sealing inside quartz vials and irradiation in nuclear reactor. The Co-60 particles were manufactured out of Cobalt block by compressing a small piece of the Cobalt between two hardened steel plates. A

small piece of the foil was placed into a small recess in a carbon block and heated with a TIG welding torch to form the Cobalt particle. The batch of Cobalt particles (~600µm in diameter) was manufactured as per the above mentioned procedure by John Kreitler, Medical School machine shop of Washington University in St. Louis. After it, these particles were inspected under Hi-Rox optical microscope and scanning electron microscope (SEM) at Material Research Center (MRC) of Missouri S&T for their size, shape, purity and defects if any. Good Co-particles were picked, sealed in a quartz vial at MO-SCI Corporation, Rolla and sent to Missouri University research reactor (MURR), Columbia, Missouri for irradiation.

4.2.1.4. Actual preparation of tracer. A hot glove box (Figure 4.4) was necessary to perform safe handling of radioactive particles received after irradiation in nuclear reactor.

Figure 4.4. RPT Glove box

Hot glove box suitable for RPT tracer preparation houses optical Microscope with LCD screen, arrangement for safe cutting of irradiated vials, and subsequent tracer preparation related activities. These activities include

1. Opening of irradiated vials inside glove box with the help of glass-cutters and vial holder and retrieving radioactive cobalt particles safely (Please refer appendix A for glass vial cutting procedure),
2. Washing of particles inside a container filled with water and drying them, testing of washed water in liquid scintillation counting system (located in Schrenk Hall) for loose contamination, if any
3. Particle integrity inspection under microscope
4. Procuring of ½" Teflon particle from CIC balls and central hole drilling with the help from Adam Lenz
5. Putting radioactive Cobalt particle inside tracer particle with the help of tweezers
6. Sealing of tracer particle using screw cap to secure radioactive particle
7. Density matching with that of glass marbles (Please refer appendix B)
8. Testing of tracer inside tumbler for contamination, if any

A Number of dry runs were carried out on dummy vials containing cobalt particles to demonstrate vial handling and opening procedure. The vial containing actual radioactive particle was opened after number of dry runs and tracer particle suitable for PBR study was prepared by following step- by-step procedure mentioned above. Figure 4.5 shows schematic diagram and actual picture of RPT tracer particle used in this PBR study.

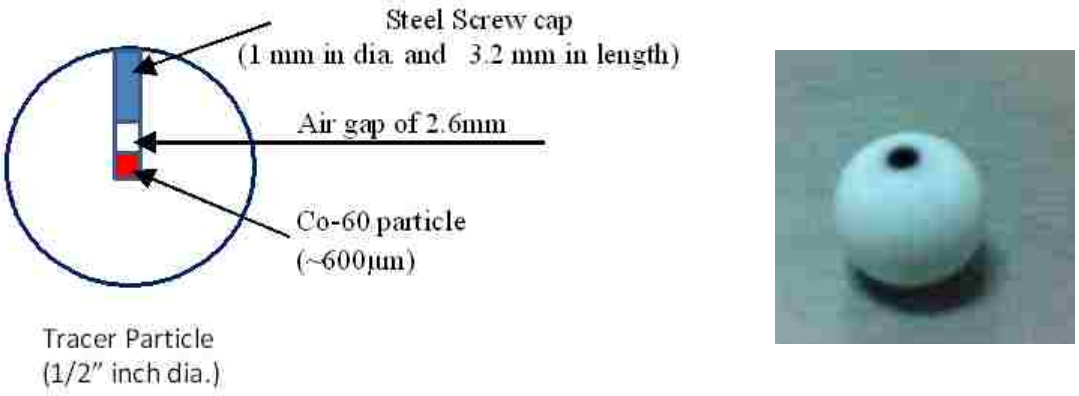

a. Schematic diagram b. Actual picture

Figure 4.5. RPT tracer particle

4.2.2 RPT Detector Arrangement. In this study, an array of sixteen NaI scintillation detectors (Canberra 802-2×2) along with pre-amplifiers (Canberra 2007P) were arranged strategically around the continuous pebble recirculation experimental set-up. The number of detectors was 4 per plane (at 90° to in-plane neighboring detectors). The adjacent out-of-plane detectors on same column post were staggered at 45° in order to improve accuracy and resolution (Roy et al., 2002). 3.25" of distance was maintained between two neighboring in-plane arrangements of detectors. The schematic of the detector arrangement is shown in Figure 4.6a and 4.6b. The detector centering and alignment with respect to central axis of test reactor is crucial from accurate distance calculations and was carried out using dummy detectors containing lasers in the center.

4.2.3. RPT Multi-channel Data Acquisition System. The previous version of RPT multi-channel data acquisition system was a combination of components from two different standards : Nuclear Instrumentation Module (NIM) and Computer Automated Measurement and Control (CAMAC) standards.

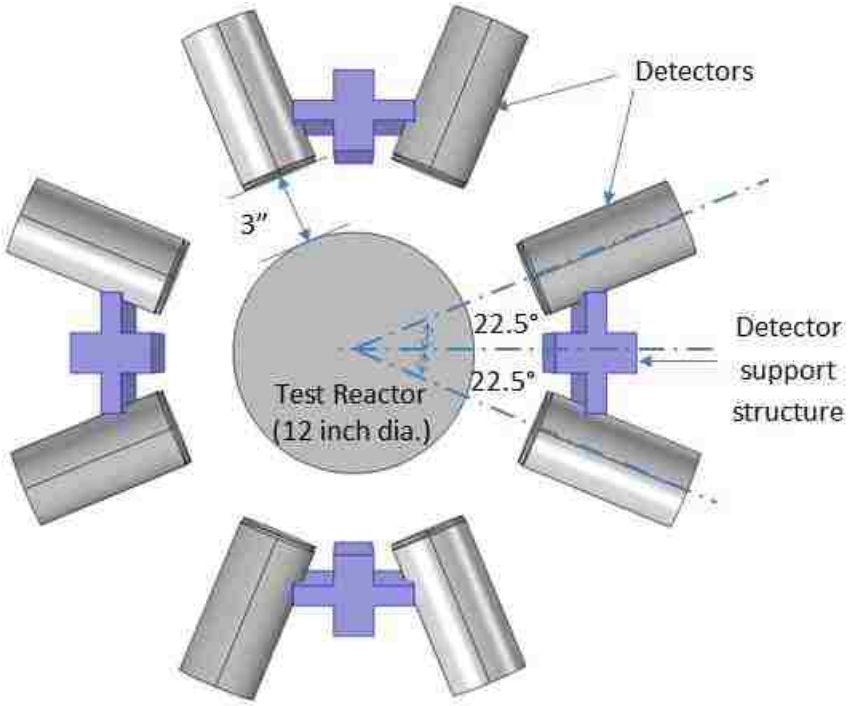

a. Top view

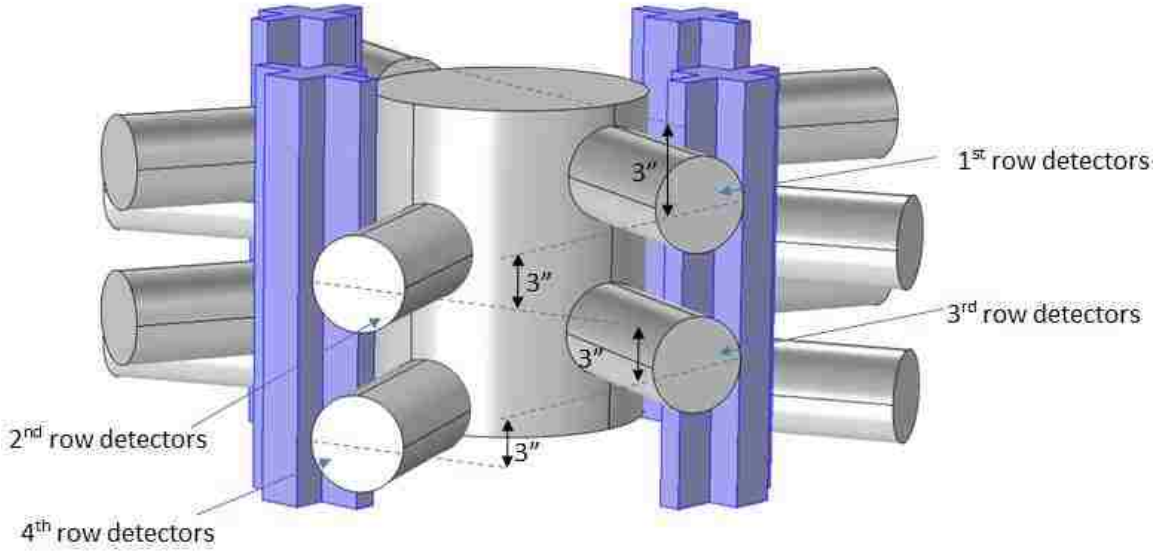

b. Side view

Figure 4.6 Schematics of RPT detector arrangement

Previous design used General Purpose Interface Bus (GPIB) based crate controller (Kinetics Systems 3988-G3A) and List sequencing crate controller (3982-Z1B) to read humongous multi-channel counts data coming from the scalars, stores it temporarily in the buffer memory and transfers them to PC in a systematic manner using GPIB. As these components became obsolete, a critical change was required in the hardware configuration of RPT. This demanded finding a suitable replacement for controller and reprogramming of data acquisition system without making major changes to hardware architecture.

Figure 4.7 shows the schematics of data acquisition system of sixth generation RPT technique used in this study. Red color indicates modifications in terms of new components / new communication standards / new DAQ programs to the architecture of RPT data acquisition system. The newly developed GUI (graphical user interface) based data acquisition program and CC-USB controller (CC-USB controller from Weiner Inc.) were tested extensively and demonstrated the success of implementation. The newly developed RPT data acquisition system has three modes of operation: *Track*, *Calibration*, *MCA* (Multichannel Analyzer). In *Track* mode, actual particle tracking experiments are carried out. It requires user to provide input of sampling frequency, total sampling time, and threshold settings on discriminator. Calibration mode is used to perform RPT calibration by providing input of tracer particle position and recording counts in each detector at user defined sampling frequency. In MCA mode, gamma spectroscopy is carried out for each detector to find out the position of photo-peak in each detector channel. Figure 4.8 shows the results of gamma spectroscopy for Co-60 test source and for Cs-137 and Co-60 test sources together.

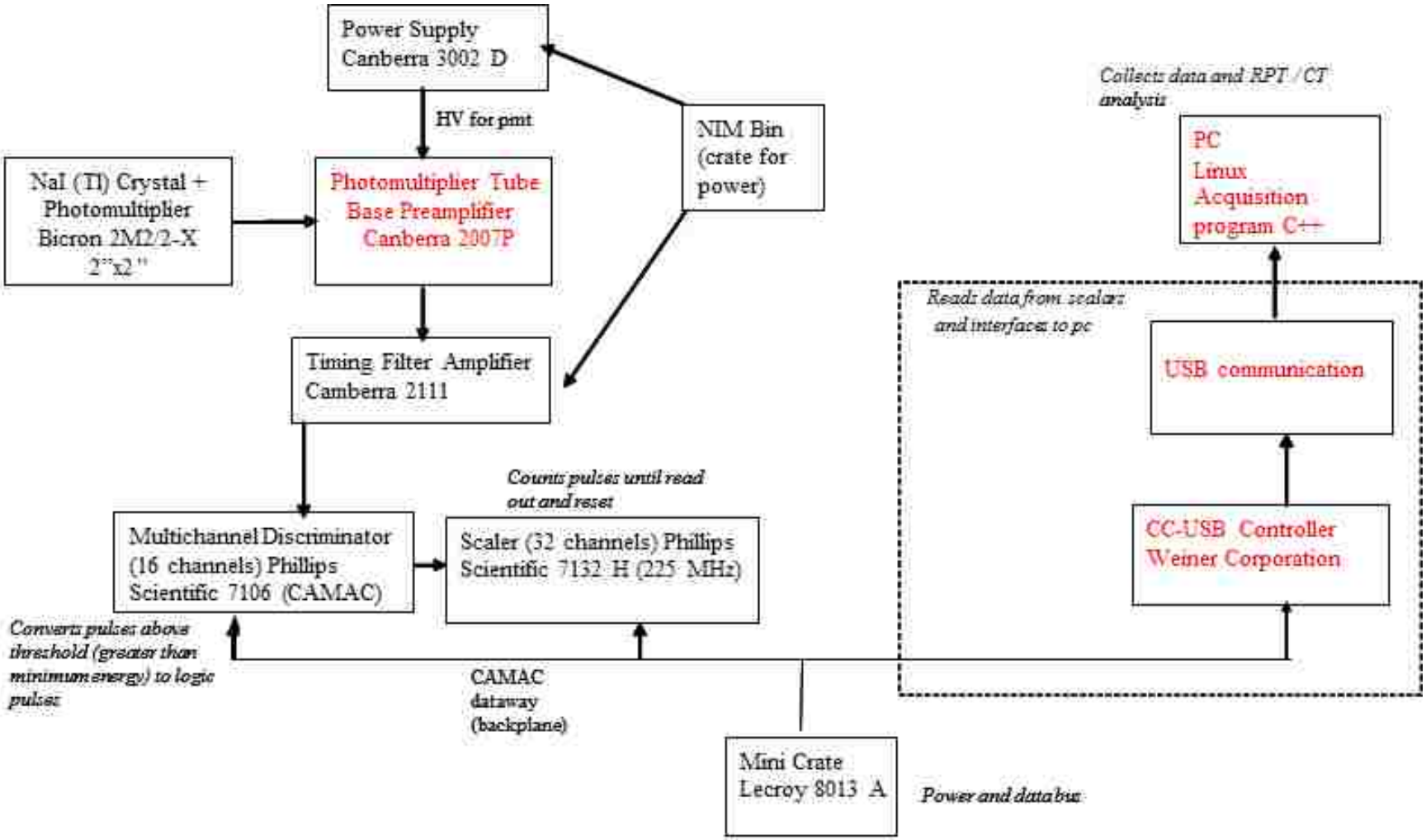

Figure 4.7. Modified RPT electronics for data acquisition (Red color indicates new components/standards/Programs)

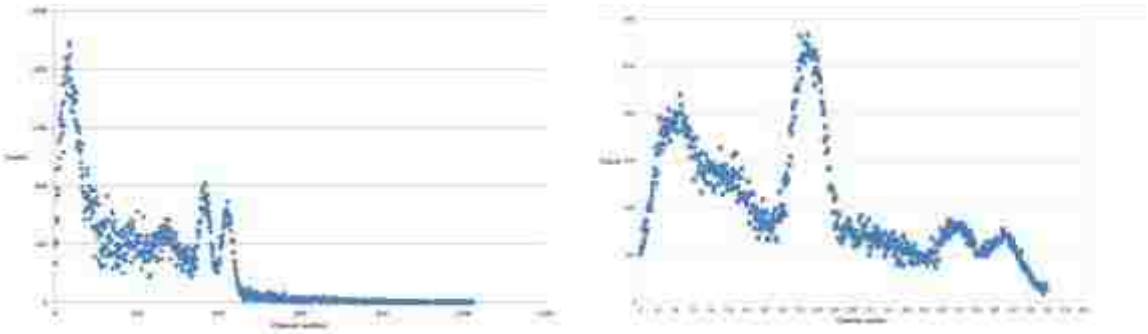

a. Co-60 spectrum **b**. Combined Cs-137 and Co-60 spectrum

Figure 4.8 Spectrum results obtained using modified RPT electronics

Due to the hardware limitations, one value of threshold is set for all channels. This requires synchronization of photo-peaks in all the channels. This is usually done by varying fine and coarse gains on timing filter and amplifiers. Reprogramming to incorporate all the above mentioned modes and associated troubleshooting consumed significant amount of time. The newly developed data acquisition system was used extensively in RPT experiments related to study of granular flow in a PBR. More details about newly developed DAQ program can be found out in appendix C.

4.2.4. RPT Calibration. An analytical solution to the forward problem of RPT, i.e. finding the instantaneous tracer position based upon counts data received in the detectors, is not possible. This problem is solved by performing a set of calibration experiments at the same operating conditions as those of actual RPT experiments. RPT calibration involves placing radioactive particle at known locations inside multiphase system using automatic/ manual calibration apparatus and recording photo-peak counts in each detector. This data is then used to generate calibration maps relating counts with position, which will be helpful in position reconstruction step. A calibration

methodology, which involves a manual calibration device, suitable for pebble bed reactor study was designed, and developed as a part of current research. Figure 4.9 shows schematic diagram and actual picture of calibration apparatus.

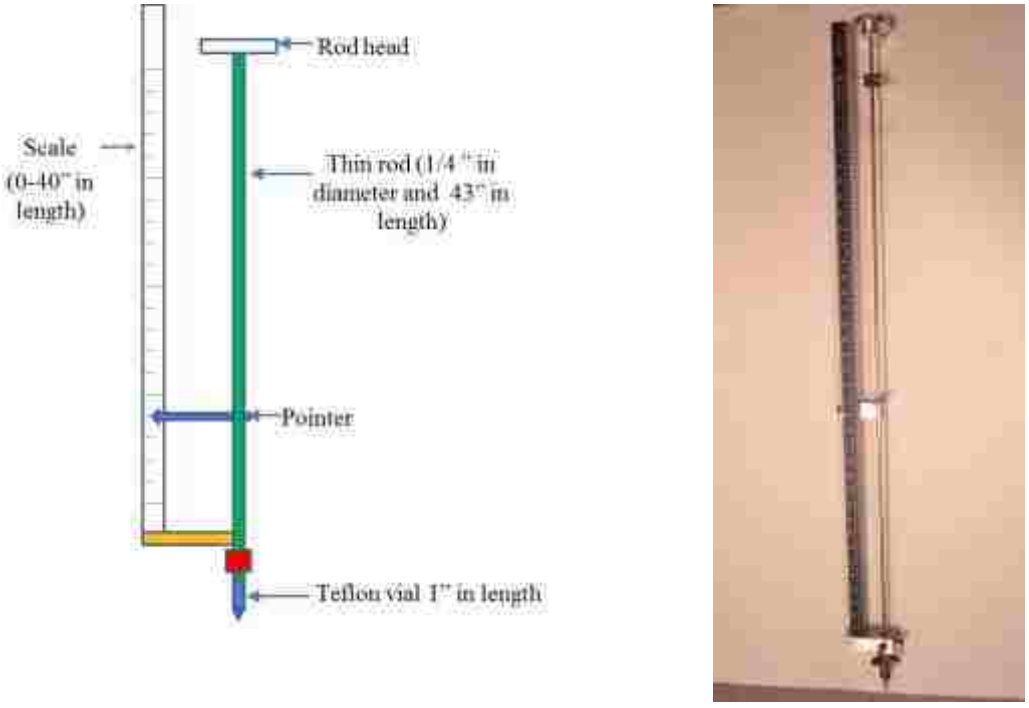

a. Schematic diagram b. Actual picture

Figure 4.9 Calibration apparatus

Basically, it consists of a rod (1/4” in diameter and 43” in length) having a Teflon vial (1” in length) at the tip to contain the radioactive particle. With the help of a guide bush arrangement, the rod can slide in/out to place radioactive particle at any height. The exact position can be recorded with the help of a scale (Range: 0 to 40”) attached to the rod. This rod can be placed at selected radial positions with the help of threaded holes in the top plate mounted on the test reactor. Once particle is placed at known positions,

counts data can be recorded by running data acquisition program in calibration mode. This design allowed having calibration points in bottom conical region which is essential in position reconstruction. Radioactive tracer particle was used in synchronization of photo-peaks in all the detector channels. This synchronization was carried out by adjustment of coarse and fine gains on timing filter and amplifier (Canberra Model No. 2111). The radioactive tracer particle was placed at different radial (0 cm, 7.62 cm and 13.97 cm) and azimuthal positions (0° thru 360° in steps of 45°) at different vertical heights (incremental steps of 2 cm) with the help of a manual calibration apparatus and photo-peak counts in each detector were recorded for each position (Figure 4.10) . A total 376 positions were used to carry out RPT calibration.

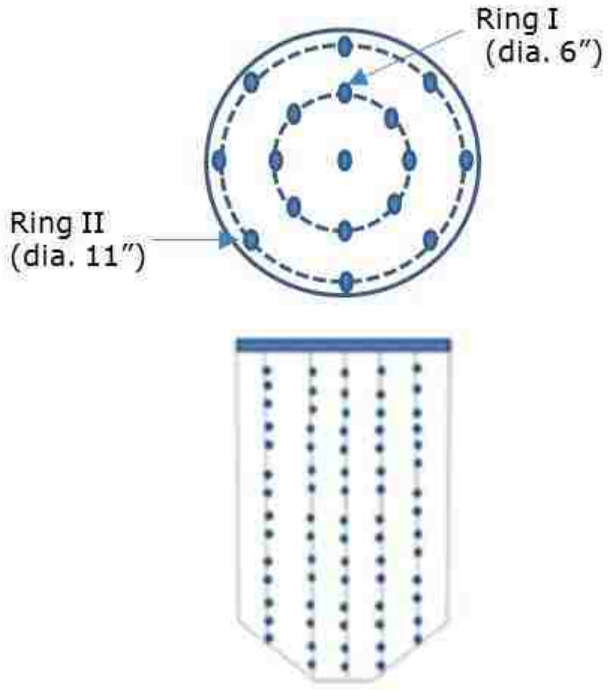

Figure 4.10 Calibration grid (376 points)

4.2.5. Experimental Assessment of Pebble Beds as Static Packed Beds Approximation. The slow and dense granular flow in a PBR is currently approximated by the study of static packed beds (duToit, 2002). However, there are no such experimental studies that have been carried out to support the conclusions of the published research. Hence, there is a need to compare packing characteristics between static packed beds and the moving beds encountered in PBRs (packed beds with slow and dense granular flow). To find out the effect of pebble movement on packing characteristics, three sets of experiments were carried out as a part of RPT calibration. In each set of experiments, a radioactive tracer containing a Co-60 particle was placed at different heights (in increments of 1 cm) along the central axis of the test reactor and for each position tracer photo-peak counts were recorded in each detector channel (Figure 4.11).

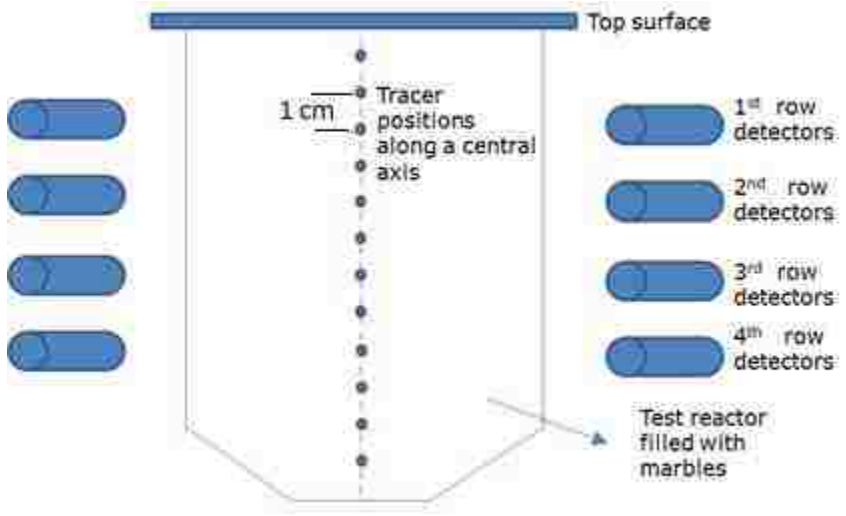

Figure 4.11 Experimental set-up for comparison of packing characteristics between static packed beds and the moving beds of PBR

This whole exercise was repeated for three different cases: These cases are as follows:

Case 1: Static packed bed case

Case 2: Moving bed case with maximum exit flow rate of ~ 40 marbles per minute

Case 3: Moving bed case with controlled exit flow rate of ~ 12 marbles per minute

The obtained photo-peak counts data in these three different cases were analyzed to check effect of movement of pebbles on structural characteristics of packed beds and is discussed in next paragraphs.

4.2.6. Implementation of Cross-correlation Based Position Reconstruction Algorithm for PBR Study (Bhusarapu, 2005). Calibration curves generated for each detector indicate that there is a spread in counts readings for same tracer-detector distance. This suggests that counts received at the detectors are not only function of tracer-detector distance but also of the attenuation characteristics of a medium in between the tracer and the detector. Cross-correlation based method (Bhusarapu, 2005) is a two-step approach in which cross-correlation based search is used for locating tracer particle position and a semi-empirical model is used to relate counts recorded to the position of emitting tracer particle. This semi-empirical model is a mechanistic simplification of actual complex mathematical model (Equation 4.1) relating the counts (C) recorded in the detector to the position of tracer particle emitting γ-radiation(Chaouki et al., 1997). This mechanistic model takes into account geometry as well as the attenuating medium in between the particle and the detector. It provided satisfactory results in gas-solid flows (Bhusarapu, 2005) and hence, was chosen in this PBR study.

RPT calibration experiments are usually performed prior to actual RPT experiments. In this study, 376 calibration positions were used. Using manual calibration apparatus, Co-60 particle was placed at various known locations and counts were recorded in all 16 detectors surrounding the system. Hence, there is a unique series of counts (C_{calib}) recorded in N_d (number of detectors used) detectors corresponding to each calibration position. Cross-correlation based method is a two-step approach and these two steps are as follows.

4.2.6.1. Step I – Finding cross-correlation coefficient. The series of counts obtained in all the detectors for some known position of a tracer particle during a calibration and similar series of counts obtained during an actual experiment (C_{run}) at a given instant of time can be analyzed to provide an estimate of match between the two counts series. This is quantified in terms of a cross-correlation coefficient ($R_{run,\,calib}$) (Equation 4.5). The zero lag of a cross-correlation function is an auto-correlation function, which has maximum value of 1.

$$R_{run,\,calib_k}(0) = \sum_{i=1}^{N_d} \frac{C_{calib\,(i)}}{\sum_{j=1}^{N_d} C^2{}_{calib\,(j)}} \cdot \frac{C_{run\,(i)}}{\sum_{j=1}^{N_d} C^2{}_{run\,(j)}} \qquad (4.5)$$

where $C_{calib}(i)$, series of counts obtained in detector i= 1 to N_d at a given tracer position during a calibration experiment and $C_{run}(i)$ series of counts obtained in detector i=1 to N_d, where N_d is the total number of detectors.

Hence, when the unknown tracer position during an actual experiment is the same as that of a known calibration position, zero lag of normalized cross-correlation function will be equal to one. Therefore, the problem of finding unknown tracer position is

reduced to matching the counts data received in all the detectors to the information obtained for a known calibration position. This is the step I of a cross-correlation based position reconstruction algorithm.

4.2.6.2. Step II – Establishing additional calibration datasets at refined level by using semi-empirical model. Step II is fitting of simplified mathematical model over region of interest (ROI) to refine the experimental calibration grid and establishing additional calibration datasets. RPT calibration is time consuming and labor intensive and is carried out at finite number of positions depending on accessibility to the system. During actual RPT experiments, the tracer particle follows the dynamics of tracking phase and visits locations in the systems which are usually different than experimental calibration positions. Hence, there is a need to derive additional calibration datasets using RPT calibration experiments and a suitable mathematical model. This newly established calibration datasets at refined mesh level along with *in-situ* experimental calibration datasets can then solve the problem of identifying unknown tracer position based on the counts recorded in the detectors. A semi-empirical model (equation 4.6) is used to derive additional calibration datasets which was proposed and developed by Bhusarapu (2005) based on the key parameters of equation 4.1 (mainly geometry, the medium attenuation characteristics and the detector efficiency). This semi-empirical model is a mechanistic simplification of an actual complex mathematical model relating the counts intensity (C) to the position of tracer particle emitting γ-radiation (given by equations 4.1 thru 4.4).

$$C = \underbrace{\frac{k_1}{d^2}}_{1} . \underbrace{exp\left(-k_2\, d_x - k_3\, d_y - k_4\, d_z\right)}_{2} \underbrace{1 - exp(-\mu_d k_5)}_{3} \qquad (4.6)$$

where,

C – Counts recorded in the detector

$k_{1,2,3,4,5}$ – Model fitted parameters

k_1 – Model fitted parameter proportional to the solid angle subtended by the detector at the tracer location (**units** – cm^2)

$k_{2,3,4}$ – Effective mass attenuation coefficients (as fitted parameters) of the medium in between the tracer and the detector in x, y and z directions respectively (**units** – 1/cm)

d – Distance of the tracer from the center of the detector crystal ((**units** – cm)

d_x, d_y, d_z – x, y and z components of the distance of the tracer from the center of detector crystal (**units** – cm)

μ_d- Mass attenuation coefficient of the detector material (**units** – 1/cm)

k_5 –Length of travel of the photon in the detector crystal (**units** – cm)

This model takes into account the geometry (thru model parameter k_1) as well as the attenuating medium effects in between the tracer and the detector (thru model parameters $k_{2,3,4,5}$). Term 1 of equation 4.6 is corresponding to an inverse square law and k_1 is a parameter representing the solid angle subtended by the detector at the tracer location. According to inverse square law, counts intensity is inversely proportional to the square of the tracer-detector distance. Term 2 is corresponding to the attenuation characteristics of a heterogeneous medium in between the tracer and the detector. $k_{2,3,4}$ are effective mass attenuation coefficients in x, y and z directions, respectively. Term 3 is corresponding to the detector efficiency. k_5 is a parameter corresponding to the travel length of the photon in the detector material. In this manner, this semi-empirical model takes into account geometry as well as the attenuation characteristics of a medium in between the tracer and the detector and the detector efficiency. Figure 4.12 illustrates this two-step approach of cross-correlation based position reconstruction algorithm.

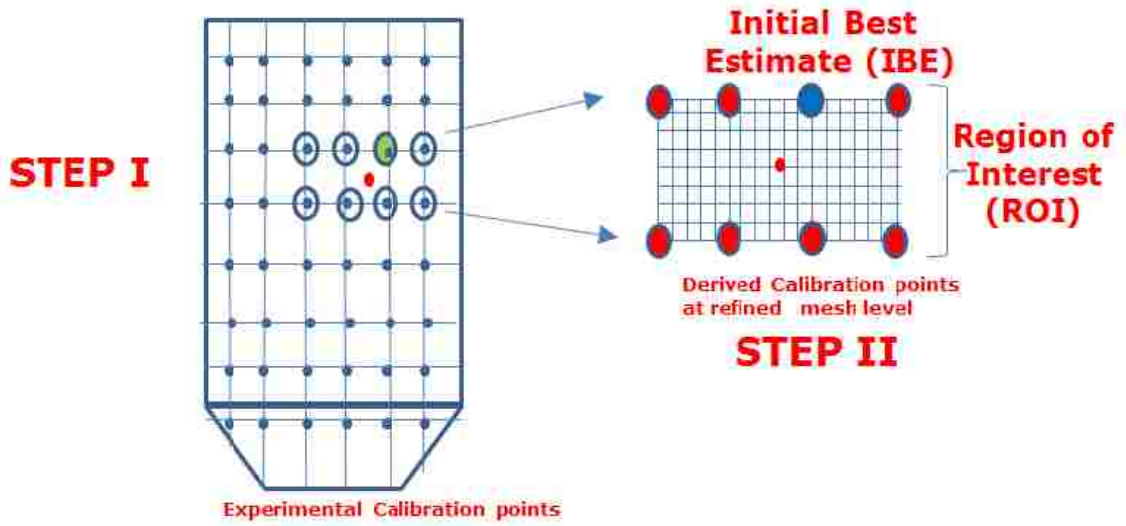

Figure 4. 12 Schematics of two-step position reconstruction approach

Step I of cross-correlation based position reconstruction algorithm finds cross-correlation coefficient ($R_{run,\,calib_k}(0)$) using Equation 4.5 for each experimental calibration data point and finds region of interest (ROI) from the whole domain. It involves finding initial best estimate (IBE) point with the maximum value of cross-correlation coefficient ($R_{run,\,calib_k}(0)$) and then finding neighboring points around it to form ROI. In Step II, a semi-empirical model which is a mechanistic simplification of actual complex mathematical model (given by set of equations 4.1 thru 4.4) is fitted over this ROI and model parameters ($k_{1,2,3,4,5}$) are found out using experimental calibration data. These model parameters are then used to establish additional refined calibration data points at finer grid level. Typically, a finer grid of estimated calibration points (Δr =10mm (in radial direction), $\Delta\theta$=15° (in azimuthal direction), Δz =5mm (in axial direction)) is established in step II. After establishing additional calibration datasets, step

I is repeated and a point with maximum value of $R_{run,\,calib_k}(0)$ is found out. This two-step process is repeated until convergence criterion of 1- $R_{run,\,calib_k}(0)$ ≤0.005 is achieved. This is done by choosing a point with the second maximum value of cross-correlation coefficient as IBE point and forming ROI around it and repeating two-step process. This approach provided satisfactory results and met convergence criterion. This entire two-step approach was implemented in a single MATLAB program (Please refer appendix D) and was used to reconstruct the unknown position of a tracer particle. Before applying this cross-correlation based position reconstruction algorithm on an actual RPT experimental data, it was necessary to validate this algorithm and estimate reconstruction errors. This was carried out by treating counts data corresponding to some of known calibration positions as unknown test datasets. This test data was removed from calibration dataset in order to necessitate second step of this position reconstruction algorithm. Obtained results of this validation exercise are explained in sub-section 4.4.3.

4.2.7. RPT Experiments. During RPT experiments, the radioactive tracer particle was seeded at different radial positions and allowed to move freely with the rest of pebbles (glass marbles) while the detectors kept collecting counts continuously at a frequency of 6 Hz. A sampling frequency of 6 Hz was chosen because of slow movement of the pebbles. It is the smallest sampling frequency possible with the new DAQ system of RPT. At smaller sampling frequencies, signal-to-noise ratio is better due to the larger sampling time. During these experiments, tracer was seeded at different radial positions using seeding tube and was tracked continuously using detectors until it leaves the system from the bottom opening. The obtained RPT results are discussed in results sub-sections.

4.3. RESIDENCE TIME DISTRIBUTION SET-UP TO MEASURE PEBBLES OVERALL RESIDENCE TIME IN A NON-INVASIVE MANNER

The time spent by pebbles at a particular position in the core (local residence time) and total time taken by pebbles from their entry into the core to its exit from the core (global residence time) is a crucial information for devising refueling strategies, burn-up estimation, and fuel mechanical damage point of view. The effect of different initial seeding positions of pebbles on these residence times will be an important knowledge. Also, such a study can provide insight on non-idealities associated with pebbles flow in the core. Hence, an experimental study of pebbles overall RTD is carried out using two collimated detectors based RTD set-up. Figure 4.13 shows a schematic diagram and actual picture of RTD set-up implemented around continuous pebble recirculation experimental set-up.

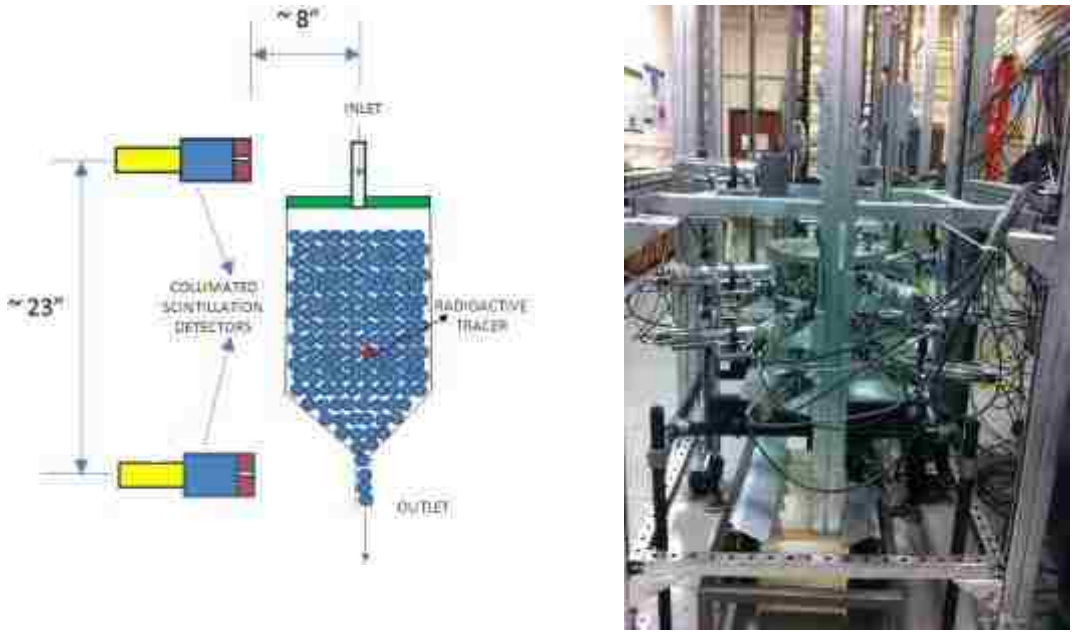

a. Schematic diagram b. Actual picture

Figure 4.13 RTD set-up

A dedicated residence time distribution (RTD) set-up consisting of two collimated scintillation detectors was implemented around the continuous pebble re-circulation experimental set-up along with the technique of RPT (Figure 4.13). This set-up is capable of measuring pebbles overall residence time in the test reactor in a non-invasive manner. It uses same radioisotope based tracer same used in the RPT study. The tracer contains Co-60 radioactive particle (initial strength of 500μCi) enclosed inside Teflon tracer particle which has same shape, size and density as that of ½" diameter glass marbles. A lead collimator for scintillation detectors is fabricated using water-jet machining facility available with Missouri S&T. The slit in the collimator is 2" in length, 1" thick and has a width of 1mm (Figure 4.14). When the tracer is in the plane of horizontal slit, maximum counts are recorded. This principle is used to record the time of entry and exit of tracer from which overall residence time of pebbles can be determined in a non-invasive manner.

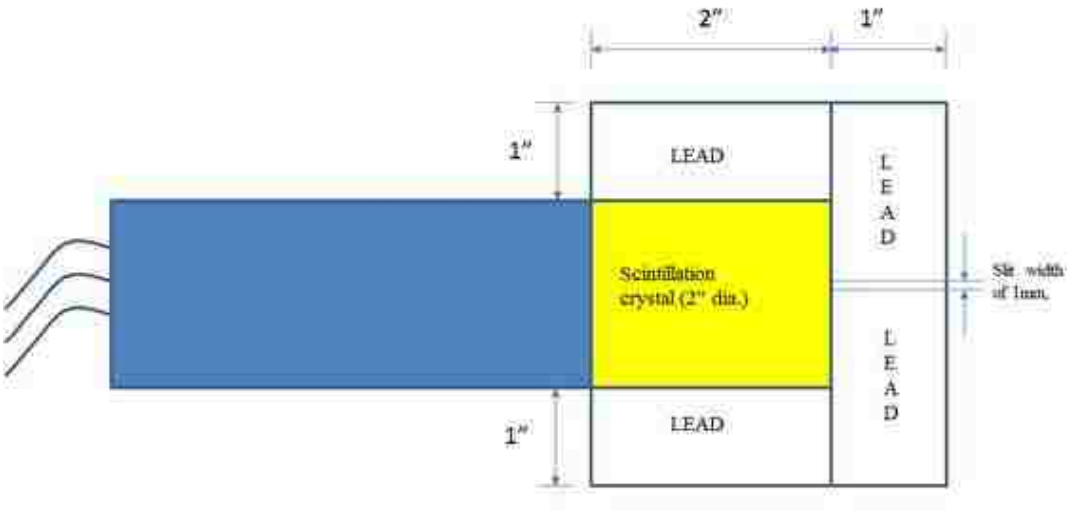

Figure 4. 14 Lead collimator used in RTD set-up

Figure 4.15 shows counts response of top and bottom collimated detectors. A peak in the counts recorded in both the detectors is observed when the tracer is in the plane of collimator slit. This information is then used to find out overall residence time of the tracer for different initial seeding positions of the tracer.

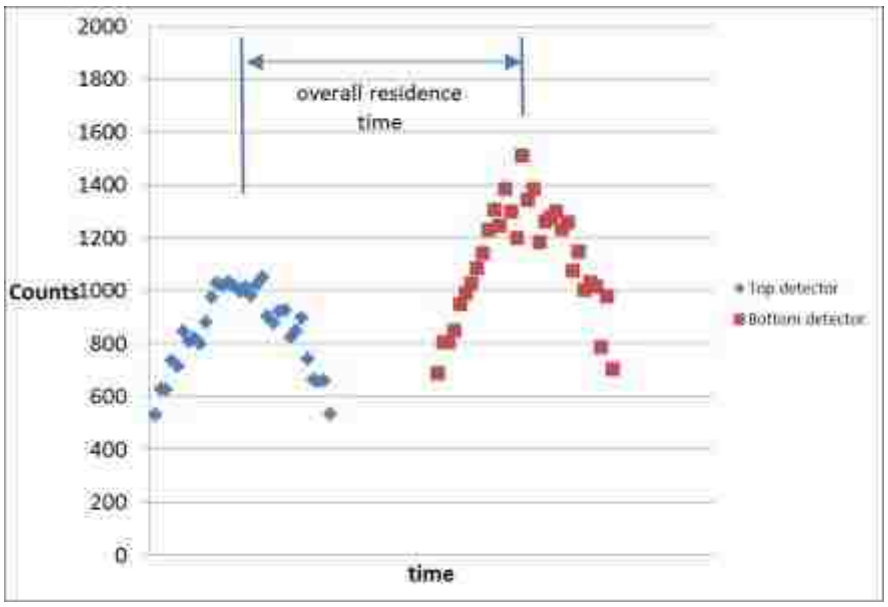

Figure 4.15 Counts response of top and bottom collimated detectors of RTD set-up

4.4 RESULTS AND DISCUSSIONS

4.4.1. Assessment of 'Pebble Bed as Static Packed Beds' Approximation. If the distribution of pebbles would have changed significantly due to the movement of pebbles, it would change the attenuation characteristics of the heterogeneous medium in between the tracer and detectors and will be subsequently reflected in photo-peak counts

data. The photo-peak counts data obtained for three different cases is plotted on the same graph for each detector. The in-plane detectors (four per plane) are arranged symmetrically around the column (Figure 4.6) and hence data corresponding to a single detector from each row is shown in the Figure 4.16 for the sake of brevity. These representative detectors from each row are mounted on the same column of detector support structure. The other three detectors from the same row exhibited same trend as shown by a representative detector from that row.

The tracer was always placed below the horizontal plane of 1^{st} row detectors. Hence, photo-peak counts recorded in 1^{st} row detectors are found to decrease with increase in the distance between tracer placement position and the top surface of the test reactor. On the other hand, tracer is always placed above the horizontal plane of 4^{th} row detectors. Hence, photo-peak counts recorded in 4^{th} row detectors are found to increase with the increase in the distance between tracer placement position and the top surface of the test reactor.

For 2^{nd} and 3^{rd} row detectors, the tracer is initially placed above their horizontal level and afterwards below their horizontal level. Hence, photo-peak counts recorded in 2^{nd} and 3^{rd} row detectors are found to increase initially and then decrease with increase in the distance between tracer placement position and the top surface of the test reactor. A peak in the photo-peak counts data is observed for 2^{nd} and 3^{rd} row detectors. The distances from the top surface of the test reactor corresponding to these observed peaks are different for 2^{nd} and 3^{rd} row detectors and are due to the fact that 2^{nd} and 3^{rd} low detectors are mounted at different horizontal levels.

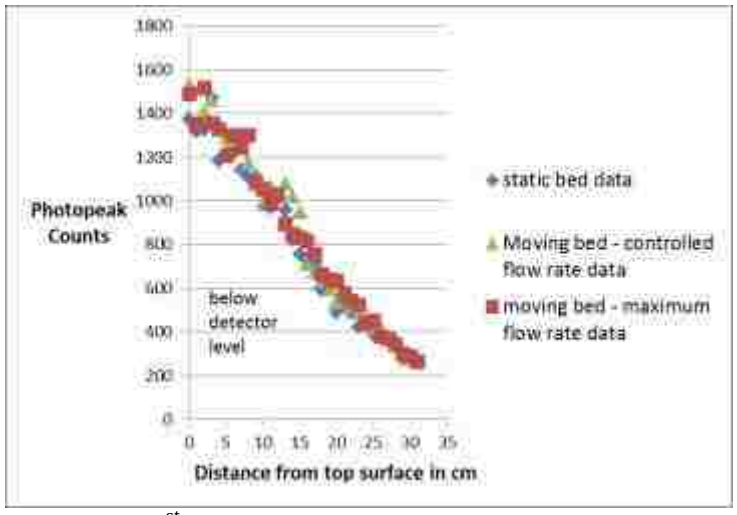

a. 1st row representative detector response

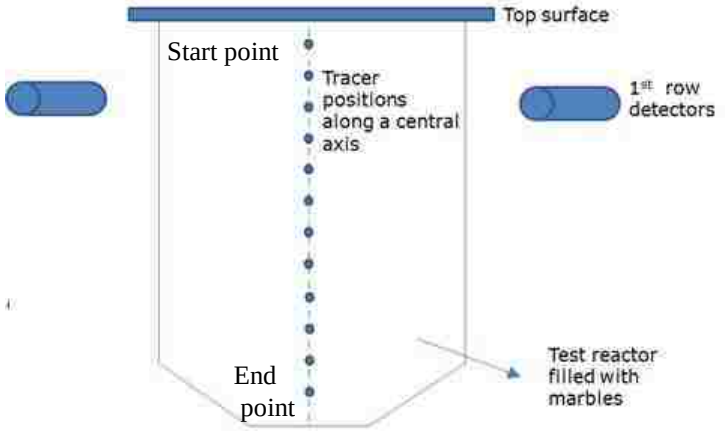

b. Tracer positions w.r.t. 1st row detectors

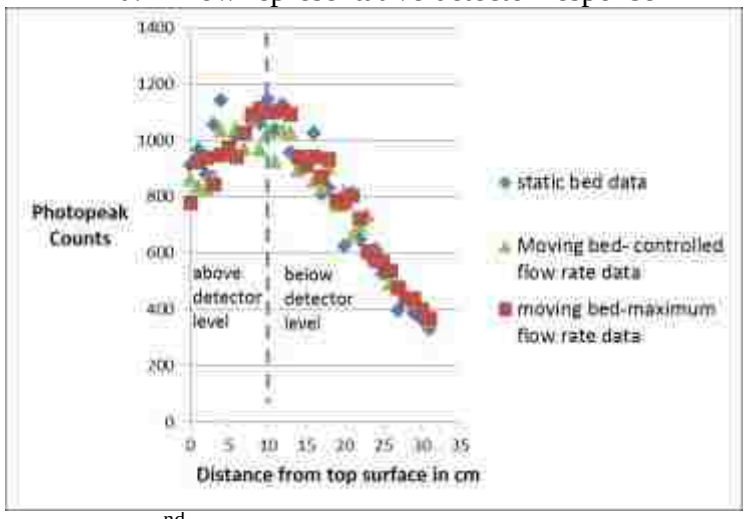

c. 2nd row representative detector response

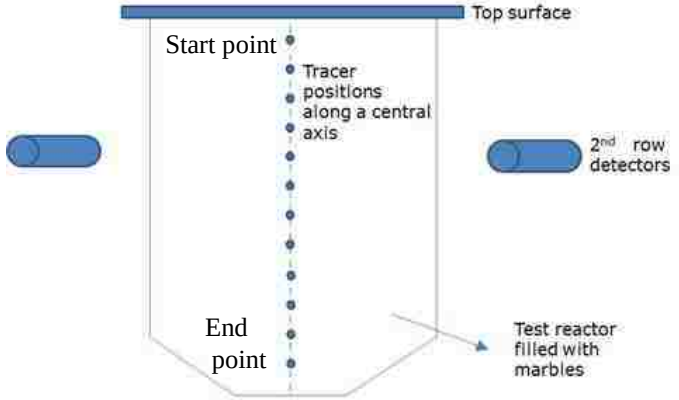

d. Tracer positions w.r.t. 2nd row detectors

Figure 4.16 Comparison of photo-peak counts data for three cases

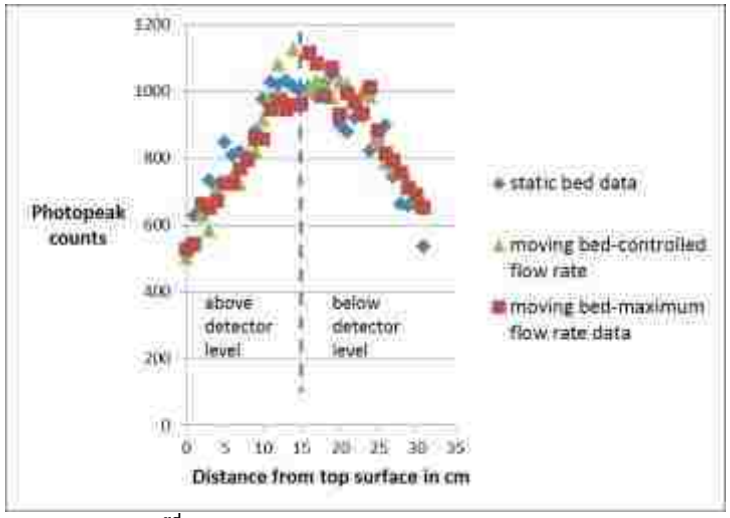

e. 3rd row representative detector response

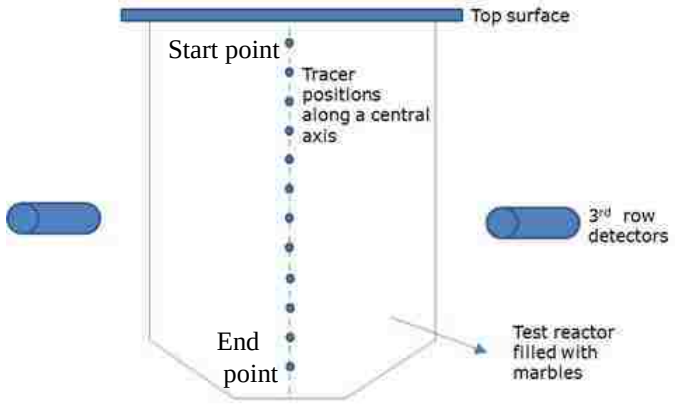

f. Tracer positions w.r.t.3rd row detectors

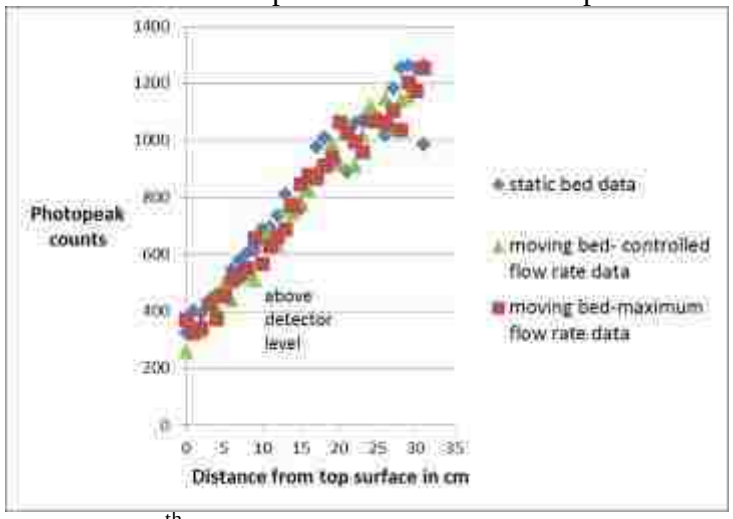

g. 4th row representative detector response

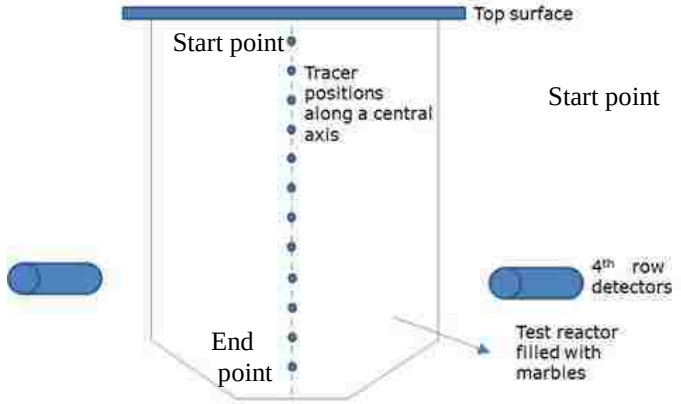

h. Tracer positions w.r.t. 4th row detectors

Figure 4.16 Comparison of photo-peak counts data for three cases cont.

The average absolute relative error (AARE) and standard deviation (σ) for case 2 (Moving bed case with exit flow rate of ~ 40 marbles per minute)/Case 3 (Moving bed case with controlled exit flow rate of ~ 12 marbles per minute) with respect to case 1 (static packed bed case) is calculated using equations 4.7 and 4.8 (Shaikh, 2007).

$$AARE = \frac{1}{N}\sum_{1}^{N}\frac{Counts_{Case\ 2/case\ 3} - Counts_{Case\ 1}}{Counts_{Case\ 1}} \quad (4.7)$$

$$\sigma = \sqrt{\sum_{i=1}^{N}\frac{\left(\left|\frac{Counts_{Case\ 2/case\ 3} - Counts_{Case\ 1}}{Counts_{Case\ 1}}\right| - AARE\right)^2}{N-1}} \quad (4.8)$$

Where N= no. of measurement points

For 1st row detectors, average absolute relative error (AARE) and standard deviation (σ) between case 3 (controlled flow rate case) and case 1 (static bed case) was found to be 8.07% and 6.15%, respectively, whereas AARE and standard deviation between case 2 (maximum flow rate case) and case 1 (static bed case) was found to be 7.94% and 6.74%. Similarly for 2nd row detectors, average absolute relative error (AARE) and standard deviation between (case 3) controlled flow rate case and case 1 (static bed case) was found to be 9.16% and 7.25%, respectively, whereas AARE between case 2 (maximum flow rate case) and case 1 (static bed case) was found to be 7.85% and 6.55%. Similarly for 3rd row detectors, average absolute relative error (AARE) and standard deviation between case 3 (controlled flow rate case) and case 1 (static bed case) was found to be 8.39% and 6.43%, respectively, whereas AARE and standard deviation between case 2 (maximum flow rate case) and case 1 (static bed case) was found to be 7.85% and 5.55% respectively. Similarly for 4th row detectors, AARE and standard deviation between case 3 (controlled flow rate case) and case 1 (static bed case)

was found to be 10.18% and 6.64% respectively, whereas AARE and standard deviation between case 2 (maximum flow rate case) and case 1 (static bed case) was found to be 9.12% and 6.38 % respectively. These values of AARE and standard deviation for different cases, considering the Poisson distribution of radioactive decay process, are smaller in magnitude. This suggests that attenuation characteristics of the medium in between the tracer and the detectors are not changing significantly due to the movement of pebbles. Hence, slow and dense granular flow encountered in a PBR could be represented by the examination of static packed beds depending on the type of measurement and the parameters to be investigated. This is an important finding which justifies the use of packed bed geometry in the experimental investigation of gaseous coolant dynamics and the determination of solids hold-up and voidage instead of the design and construction of complex experiments involving continuous pebble recirculation experimental set-up. However, additional experimental/computational work is required to investigate further and validation of methodology to check the effect of pebbles movement on the structural characteristics of the bed.

4.4.2 RPT Calibration Results. RPT calibration experiments for 376 positions of tracer (Figure 4.11a) were carried out for two different conditions. 1. Static packed bed condition 2. Moving bed condition (controlled flow rate of 12 marbles per minute). The parity plot of counts data (Figure 4.17) confirms that PBR could be well approximated by static packed beds, depending on the parameters to be studied. AARE and standard deviation between counts data for static packed bed case and moving bed case was found to be 9.31% and 7.22%, respectively.

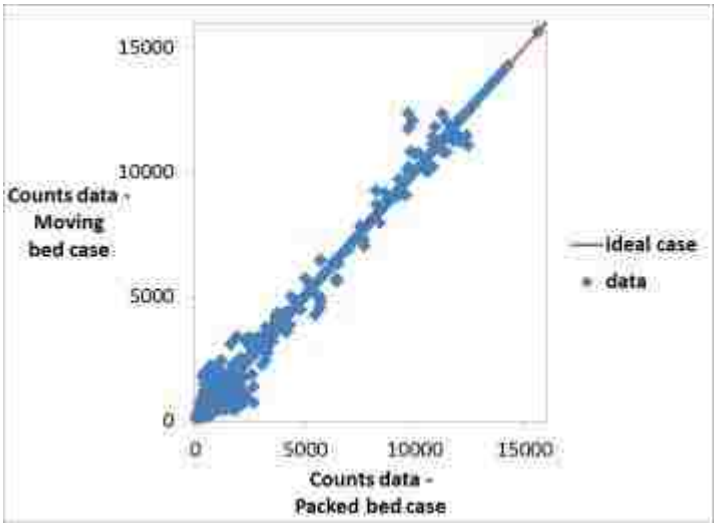

Figure 4.17 Parity plot

Calibration curves (Figure 4.18) generated for each detector indicated that there is a spread in counts readings for the same tracer-detector distance. This suggests that counts received at the detectors are not only function of tracer-detector distance but also of the attenuation characteristics of medium in between the tracer and the detector.

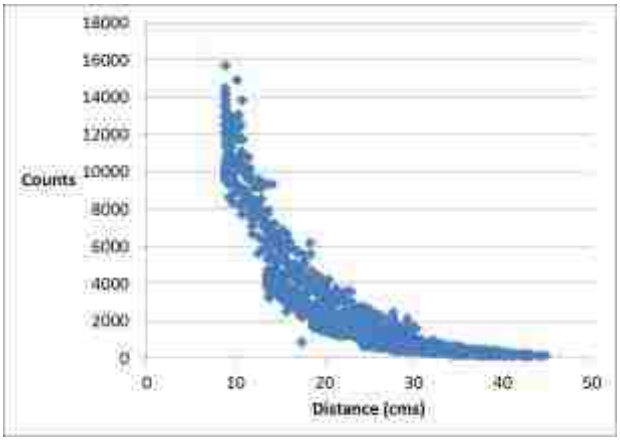

Figure 4.18 RPT detector calibration curve for PBR study

This spread in counts also known as '*band effect*' is due to highly un-isotropic attenuating medium. Solid angle subtended at the tracer by the detector plays an important role towards this *'band effect'*. At larger tracer-detector distances, effect of solid angle diminishes and less spread in counts is observed. At smaller tracer-detector distances, effect of solid angle is dominant and hence, broader spread in recorded counts is observed. This spread of counts for the same distance of tracer from the detector poses additional challenges during the position reconstruction step. Hence, a cross-correlation based position reconstruction algorithm, which takes into account the geometry as well as the attenuating medium effects, is used in this PBR study (Bhusarapu, 2005).

4.4.3. RPT Position Reconstruction Validation Results. The Obtained validation results of position reconstruction algorithm for test datasets are plotted in Figure 4.19. Results of this validation exercise are also tabulated in Table 4.1. The reconstruction errors obtained by using this reconstruction algorithm were less than 0.5 cm. The position reconstruction algorithm properly predicted x and y co-ordinates of unknown position in all cases. Mostly reconstruction error has been observed in the z-direction (maximum % error of 5.26%). This suggests that detector counts are less sensitive to z-coordinate of tracer position as compared to x and y co-ordinates. This position reconstruction algorithm was then applied to RPT experimental data to get more information about pebbles flow field.

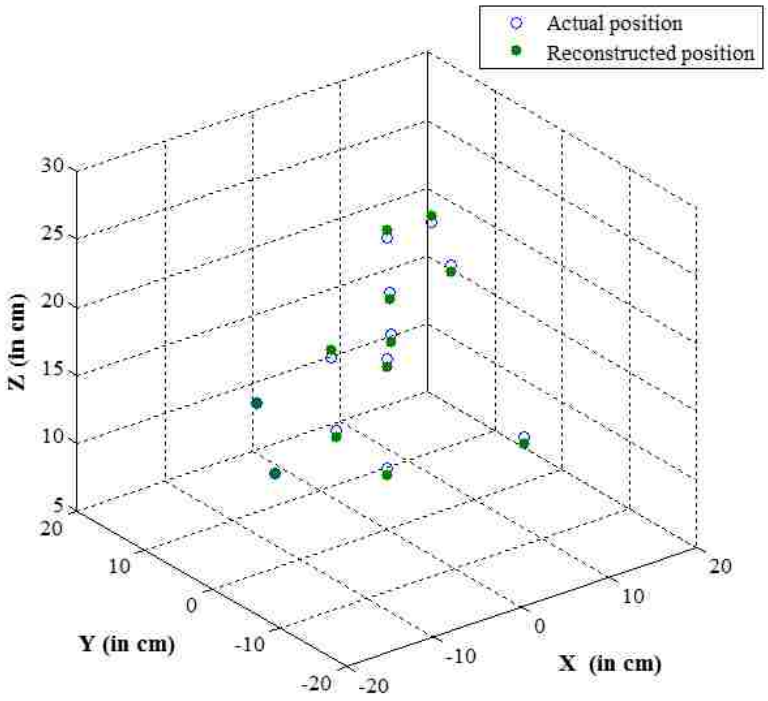

Figure 4.19 Validation of position reconstruction algorithm results

Table 4.1 Position reconstruction algorithm validation results

Actual position co-ordinates			**Reconstructed position co-ordinates**			**Error**	**% error**
x	**y (in mm)**	**z**	**x**	**y (in mm)**	**z**	**(in mm)**	
13.75	-2.46	9.00	13.75	-2.46	9.50	0.50	5.26
-13.92	1.23	17.00	-13.92	1.23	17.00	0.00	0.00
-8.36	-11.19	27.00	-8.36	-11.19	27.50	0.50	1.82
-2.28	4.54	11.00	-2.28	4.54	11.50	0.50	4.35
3.39	3.79	17.00	3.39	3.79	17.50	0.50	2.86
5.08	0.00	27.00	5.08	0.00	26.50	0.50	1.89
0.00	0.00	9.00	0.00	0.00	9.50	0.50	5.26
0.00	0.00	17.00	0.00	0.00	17.50	0.50	2.86
0.00	0.00	27.00	0.00	0.00	26.50	0.50	1.89
-0.45	-10.15	27.00	-0.45	-10.15	27.50	0.50	1.82
1.34	10.07	15.00	1.34	10.07	14.50	0.50	3.45
-7.86	6.43	9.00	-7.86	6.43	9.00	0.00	0.00

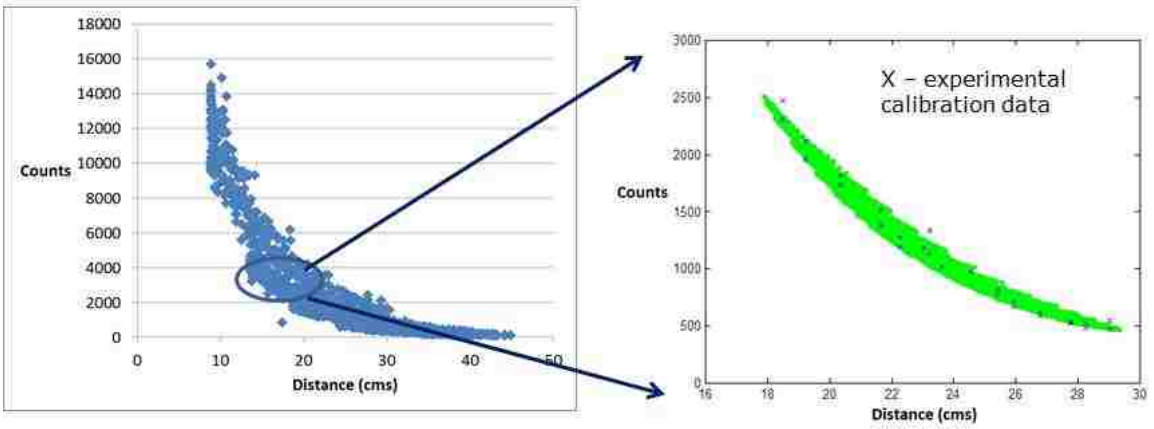

a. Calibration curve b. Estimated calibration data

Figure 4.20 Estimated calibration datasets after mesh refinement using semi-empirical model

The semi-empirical model is used in step II of position reconstruction step and it should capture the band effect which was seen in the RPT detector calibration curve. Figure 4.20a shows typical calibration curve for any RPT detector obtained during study of granular flow in a PBR and Figure 4.20b shows estimated calibration datasets after mesh refinement. Estimated calibration datasets in Figure 4.20b is also exhibiting '*band effect*' which was seen in detector calibration curve.

4.4.4. RPT Experiments Trajectories Results. By using calibration curves and cross-correlation based position reconstruction algorithm, lagrangian trajectory of the radioactive tracer is reconstructed. The obtained results about tracer trajectories in two and three dimensions, velocity vector plot for different initial seeding positions are shown in Figure 4.21 and 4.22.

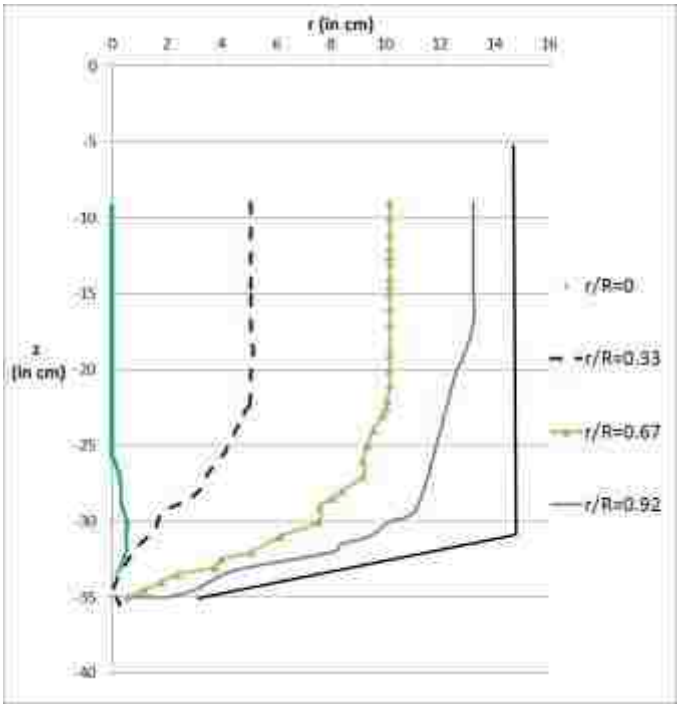

a. Two-dimensional tracer trajectories obtained using RPT

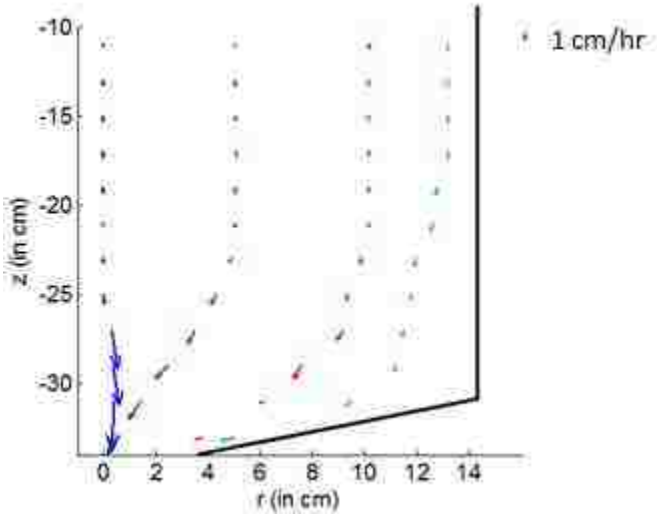

b. Velocity vector plot (Length of arrows proportional to magnitude of velocity)

Figure 4.21 RPT results

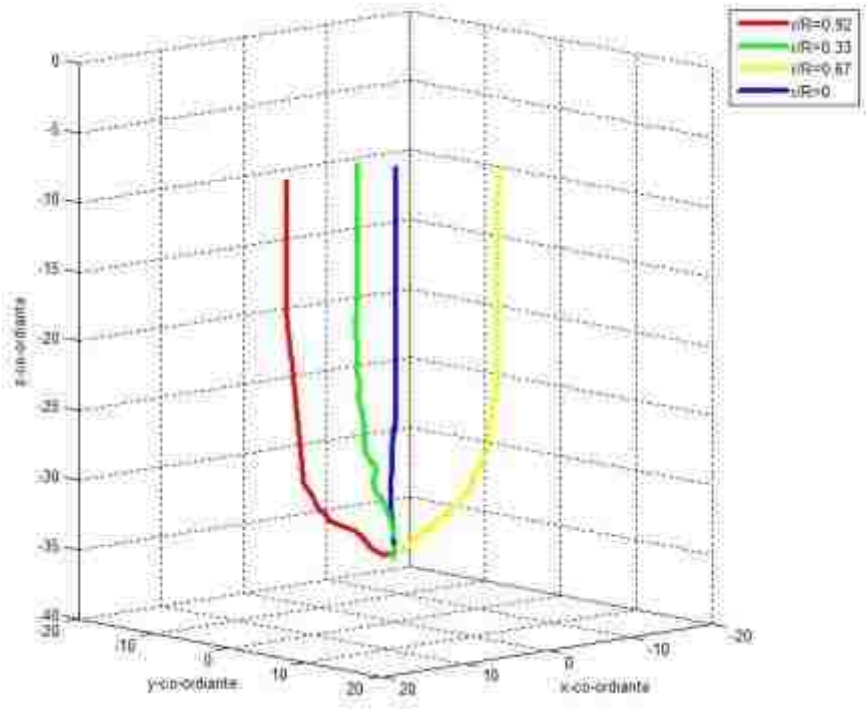

Figure 4.22 Three-dimensional tracer trajectories obtained using RPT

A plug-type flow is observed in the upper cylindrical region of reactor for all seeding positions. Tracer seeded at the center follows a shortest straight line path. Tracers seeded away from the center initially follow a straight line path in the upper portion of the reactor. Afterwards, tracer starts moving towards the center of a test reactor and a radial movement of tracer is observed. (Figure 4.21 and Figure 4.22). Tracer seeded close to the wall follows a longest path. The length of tracer trajectories is calculated for each seeding position. A shortest trajectory length of 26.74 cm is found for the initial seeding position at the center (r/R of 0). The tracer trajectory length increases with change in dimensionless initial seeding position from the center towards outer periphery. A highest trajectory length of 35.44 cm (32.54% increase with respect to shortest trajectory length)

is observed for the initial tracer seeding position close to the wall (r/R of 0.92). The values of trajectory length and percentage increase with respect to the shortest trajectory length are tabulated in Table 4.2.

Table 4.2 Tracer trajectory length values for different initial seeding positions

	Tracer initial seed position Dimensionless radial position (r/R)			
	0	**0.33**	**0.67**	**0.92**
Trajectory length (in cm)	26.74	29.23	32.4	35.44
% increase with respect to shortest trajectory length	--	9.31	21.17	32.54

4.4.5. Effect of Initial Seeding Position on Pebbles Overall Residence Time. RTD experimental set-up is used to carry out experiments at different initial seeding position of a radioactive tracer particle. The obtained results about overall residence time for different initial seeding positions of a tracer are as shown in Figure 4.23 and 4.24. Figure 4.23 represents overall RTD results in time units, whereas Figure 4.24 represents overall RTD results in terms of transit number (Gatt, 1973) calculated by equation 4. 9.

$$\textbf{Transit number} = \frac{\text{No.of pebbles recirculated between the seeding of the tracer and it's exit}}{\text{total number of pebbles in the bed}} \quad (4.9)$$

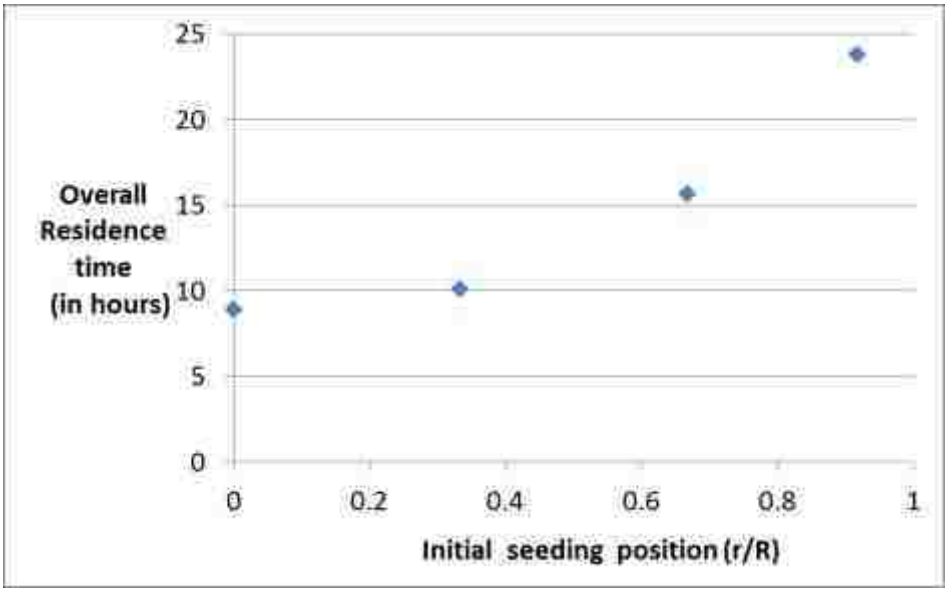

Figure 4.23 Overall pebbles residence time in hours

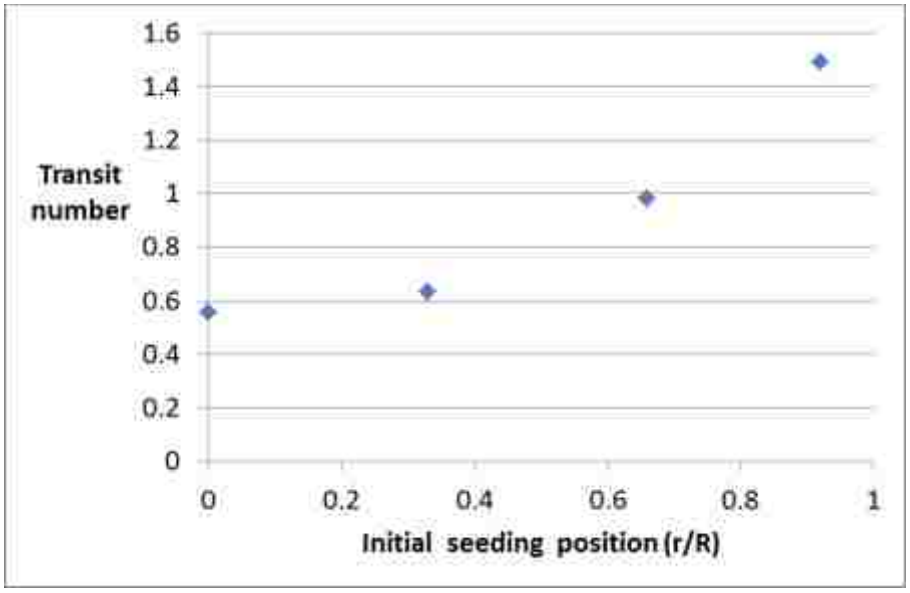

Figure 4.24 Overall pebbles residence time in terms of transit number

Transit number of 1 indicates that the whole bed inventory is recirculated between the initial seeding of the tracer and its exit. In Gatt's study (1973), it has been reported that transit number increases as the seeding distance from the center of the bed increases. To check the effect of initial seeding radius, 4 number of experiments were carried out. Tracer was initially seeded at different dimensionless radial positions (r/R) of 0, 0.33, 0.67 and 0.92. It is found that overall residence time/transit number increases at a slower rate for dimensionless radial positions (r/R) between 0 and 0.33, whereas it increases at a faster rate for dimensionless radial positions above (r/R) of 0.33 and is highest in a region close to the wall. This also suggests that there is a possibility of faster moving zone of pebbles close to the center. It has been discussed further while discussing RPT velocity profile results. Transit number for initial dimensionless seeding position (r/R) of 0.67 is found to be close to 1. For particles between initial dimensionless seeding position (r/R) of 0.67 and the outer periphery, more than one bed inventory needs to be recirculated before tracer leaves the system.

4.4.6. Zonal Residence Time of Pebbles. RPT results are analyzed to provide more information about residence time in different zones and average zonal velocities. The whole reactor was divided into three zones: Zone I (from the height of 10 to 20 cm), Zone II (from the height of 20-30 cm) and Zone III (from the height of 30 to 36 cm) as shown in Figure 4.25a. The obtained results about zonal residence times are tabulated in Table 4.3 and are shown in Figure 4.25b thru 4.25d.

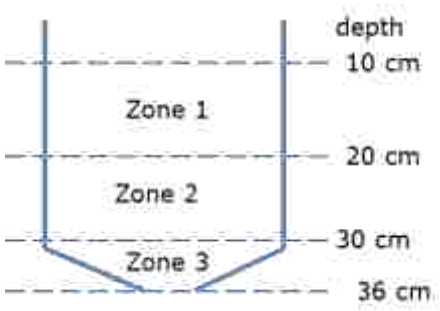

a. Zone-wise division of reactor

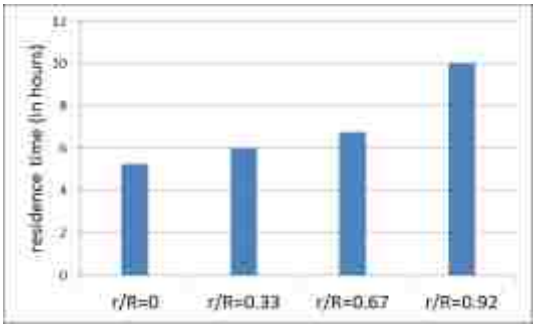

b. Zone -1 residence time

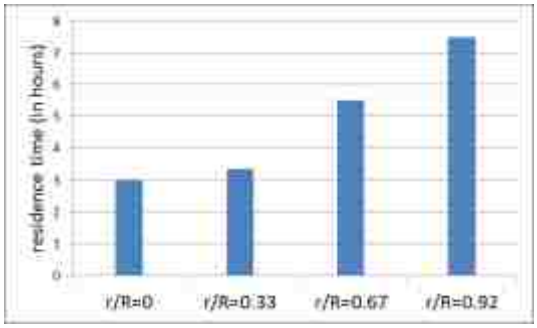

c. Zone -2 residence time

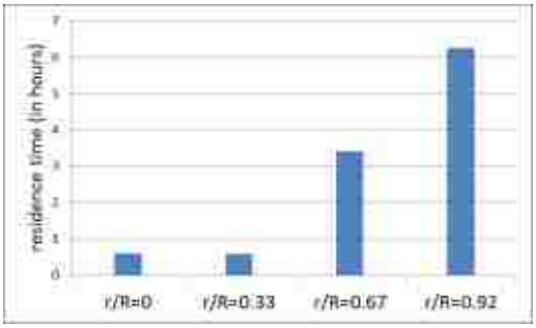

d. Zone-3 residence time

Figure 4.25 Zonal residence time results obtained using RPT

Table 4.3 Overall/Zonal residence times for different initial seeding positions of tracer (Values in brackets represents % of overall residence time)

	Residence time in hours			
	r/R= 0	**r/R= 0.33**	**r/R= 0.67**	**r/R= 0.92**
Zone 1	**5.25** (59.3%)	**6** (59.4%)	**6.75** (43.1%)	**10** (42.1%)
Zone 2	**3** (33.9%)	**3.5** (34.7%)	**5.5** (35.1%)	**7.5** (31.6%)
Zone 3	**0.6** (6.8%)	**0.61** (5.9%)	**3.42** (21.8%)	**6.27** (26.3%)
Overall	**8.86** (100%)	**10.1**(100%)	**15.67**(100%)	**23.77**(100%)
increase with respect to shortest residence time	--	14.1%	76.9%	168.2%

It is found that zonal residence time for each zone increases with increase in the value of dimensionless initial seeding position (i.e. from center towards wall). RTD set-up results about overall residence time of tracer/transit number for different initial seeding positions (Figure 4.24) exhibited the same trend. The values of zonal residence time are highest for dimensionless initial seeding position (r/R) of 0.92 among all initial seeding positions. The zonal residence time as a percentage of overall residence time is calculated and tabulated in brackets next to absolute value in Table 4.3. It is observed that the zonal residence time as a percentage of overall residence time decreases from zone 1 to zone 2 and further from zone 2 to zone 3 for all seeding positions. Percent increase in zonal residence time for dimensionless initial seeding positions (r/R) of 0.33, 0.67 and 0.92 are calculated using corresponding zonal residence time for dimensionless initial seeding position (r/R) of 0 and are tabulated in Table 4.4. Highest percentage increase (~ 943% increase) in zonal residence time was observed for zone 3 of initial seeding position of (r/R) 0.92.

Table 4.4 Percentage increase in zonal residence time values

Initial seeding position	**% increase in zonal residence time with respect to Initial seeding position r/R=0**		
	Zone 1	**Zone 2**	**Zone 3**
r/R= 0.33	14.29	16.67	1.67
r/R= 0.67	28.57	83.33	468.33
r/R= 0.92	90.48	150.00	943.33

4.4.7. Average Zonal Velocities and Overall Average Velocities. Zonal residence times are indicative of average zonal velocities in respective zones. Lesser zonal residence time is an indication of higher average velocity in that respective zone and vice versa. Figure 4.26 represents z-component of average zonal velocities for different initial seeding positions of the tracer calculated using Equation 4.10.

$$\mathrm{z-component\ of\ average\ zonal\ velocities} = \frac{\mathrm{tracer\ movement\ in\ z-direction}}{\mathrm{zonal\ residence\ time\ in\ hours}} \quad (4.10)$$

Smallest z-component of average zonal velocities are observed (Table 4.5) in all the three zones for dimensionless initial seeding position (r/R) of 0.92 i.e. close to the wall, whereas highest z-component of average zonal velocities are observed in all the three zones for dimensionless initial seeding position (r/R) of 0 i.e. at the center. In zone 3, the difference between average zonal velocities for seeding positions (r/R) of 0.92 (close to the wall) and 0 (at the center) becomes much more pronounced (0.96 cm/hr versus 10 cm/hr). This pronounced velocity difference (941% higher average zone III velocities for initial seed position (r/R) of 0 with respect to (r/R) of 0.92) has already been reported in Pebble Bed Modular Reactor, safety analysis report (2000) and RPT experiments are capturing it. It is discussed further while comparing velocity radial profile results of the RPT technique with DEM simulation results in section 6. It is noteworthy to mention that z-component of average zonal velocity is increasing from zone 1 to zone 2 and further from zone 2 to zone 3 for dimensionless initial seeding position (r/R) of 0 and 0.33. For dimensionless initial seeding position (r/R) of 0.67 and 0.92, it increases from zone 1 to zone 2 but decreases from zone 2 to zone 3.

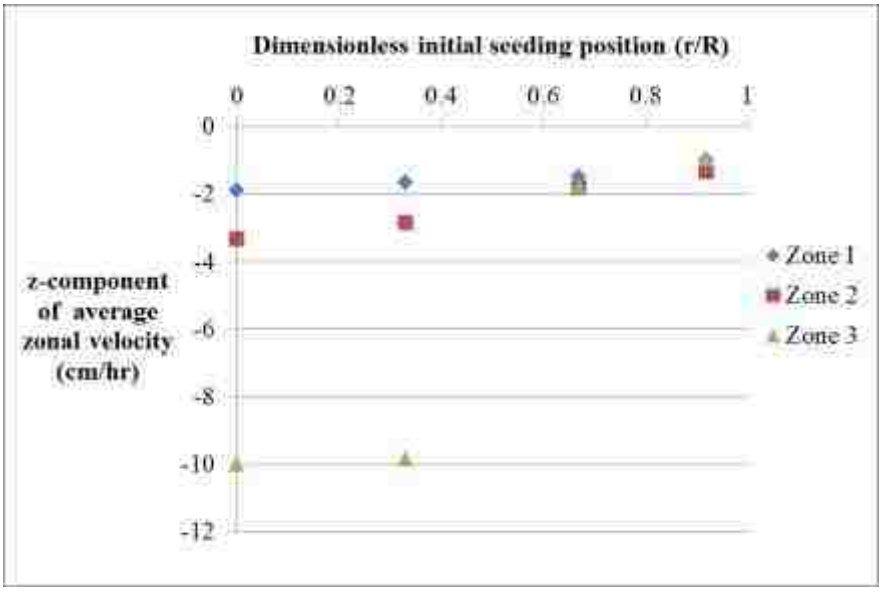

Figure 4.26 z-component of average zonal velocity for different initial seeding positions

Table 4.5 z-component of average zonal velocities for different initial seeding positions

	Tracer initial seed position (dimensionless radial position (r/R))				
	0	**0.33**	**0.67**	**0.92**	
z-component of average zonal velocity (cm/hr)	1.90	1.67	1.48	1.00	**ZONE 1**
	3.33	2.86	1.82	1.33	**ZONE 2**
	10.00	9.84	1.75	0.96	**ZONE 3**

Radial movement of the tracer particle in zone 2 and zone 3 is the main reason for this decrease in z-component of average zonal velocities. This is evident from increase in the values of r-component of average zonal velocities from zone 2 to 3 for these seed positions. Tracer when initially seeded close to the center is spending significantly less time in zone 3 as compared to its combined residence time in zones 1 and 2. Faster movement (evident from highest average zonal velocities) and shortest path to travel

(indicated by shortest trajectory length of 26.74 cm) are the main reason for smallest overall residence time for initial seeding position at the center. Slower movement (evident from smallest average zonal velocities) and longest path to travel (indicated by highest trajectory length of 35.44 cm) are the main reason for highest overall residence time for initial seeding position close to the wall.The radial movement of tracer was predominantly observed in zone 2 and zone 3 for initial seeding position (r/R) of 0.33, 0.67 and 0.92 (Table 4.6). Highest radial movement of tracer was observed in zone 3 for initial seeding position (r/R) of 0.92.

Table 4.6 Radial movement of tracer particle for different initial seeding positions

	Tracer initial seed position (dimensionless radial position (r/R))				
	0	0.33	0.67	0.92	
Radial movement of tracer particle (in cm)	0.00	0.00	0.00	0.61	**ZONE 1**
	-0.47	3.40	2.60	1.90	**ZONE 2**
	0.47	1.39	6.95	9.36	**ZONE 3**

In zone 1 for all initial seeding positions except r/R of 0.92, no radial movement of tracer is observed. In zone 2, highest radial movement of tracer (3.4 cm) was observed for initial seeding position r/R of 0.33. Radial movement of tracer in r-direction towards the center is considered as ‘positive’, whereas tracer movement away from the center is considered as ‘negative’. The tracer is moving towards the center in all zones for all initial seeding positions except in zone 2 for initial seeding position r/R of 0 (at the center). An outward movement of 0.47cm was observed in zone 2 for this initial seeding

position at the center. This outward movement could be caused by the random nature of packing at the center of the bed. In zone 2, radial movement of tracer gradually decreases from 3.40 cm (for r/R of 0.33) to 1.90 cm (for r/R of 0.92), whereas in zone 3, radial movement of tracer gradually increases from 1.39 cm (for r/R of 0.33) to 9.36 cm (for r/R of 0.92). The r-component of average zonal velocities for different initial seeding positions is calculated by using equation 4.11 and is tabulated in Table 4.7. In zone 2, r-component of average zonal velocities gradually decreases from 0.97 cm/hour (for r/R of 0.33) to 0.25cm/hour (for r/R of 0.92), whereas in zone 3, it gradually reduces from 2.32 cm (for r/R of 0.33) to 1.49 cm (for r/R of 0.92).

$$\mathrm{r-component\ of\ average\ zonal\ velocities} = \frac{\text{tracer movement in r-direction}}{\text{zonal residence time in hours}} \quad (4.11)$$

Table 4.7 r-component of average zonal velocities for different initial seeding positions

	Tracer initial seed position (dimensionless radial position (r/R))				
	0	0.33	0.67	0.92	
r-component of average zonal velocity (in cm/hour)	0.00	0.00	0.00	0.06	**ZONE 1**
	-0.16	0.97	0.47	0.25	**ZONE 2**
	0.82	2.32	2.02	1.49	**ZONE 3**

Tracer's overall average velocity for each initial seeding position is calculated by using equation 4.12 and is tabulated in Table 4.8.

$$\mathrm{Overall\ average\ velocity} = \frac{\text{trajectory length in cms}}{\text{overall residence time in hrs}} \quad (4.12)$$

Table 4.8 Overall average velocity of tracer for different initial seed positions

	Tracer initial seed position Dimensionless radial position (r/R)			
	0.00	**0.33**	**0.67**	**0.92**
Tracer average velocity (in cm/hour)	3.02	2.89	2.07	1.49
% decrease with respect to overall average velocity for seed position at the center	--	4.20	31.49	50.60

Overall average velocity of tracer for initial seed position (r/R) of 0 (at the center) is 3.02 cm/hour, whereas it is 1.49 cm/hour for initial seed position (r/R) of 0.92 (near the wall). Overall average velocity for initial seed position near the wall decreases by ~50 % with respect to the initial seed position at the center. This also indicates that tracer when seeded at the center is moving faster (~102 % increase) with respect to the initial seed position near the wall.

4.4.8. Velocity Radial Profile – RPT Results. RPT results were analyzed for estimation of tracer velocities. Figure 4.27a shows locations of control volumes (CV) 1 and 2. These control volumes are 1 cm thick and are located at a depth of 11cm (CV1) and 27 cm (CV2) from the top surface of the test reactor. Obtained velocity results for CV1 and CV2 is shown in Figure 4.27b. A plug-flow type velocity radial profile is observed for CV1 in the upper region. The velocity profile is nearly uniform except in a region close to the wall. This suggests that pebbles move collectively as a solid mass in the upper region. A velocity radial profile with pronounced concavity near the central region is observed for CV 2. This indicates that tracer when initially seeded at the center (r/R of 0) is moving much faster than when initially seeded near the wall (r/R of 0.92).

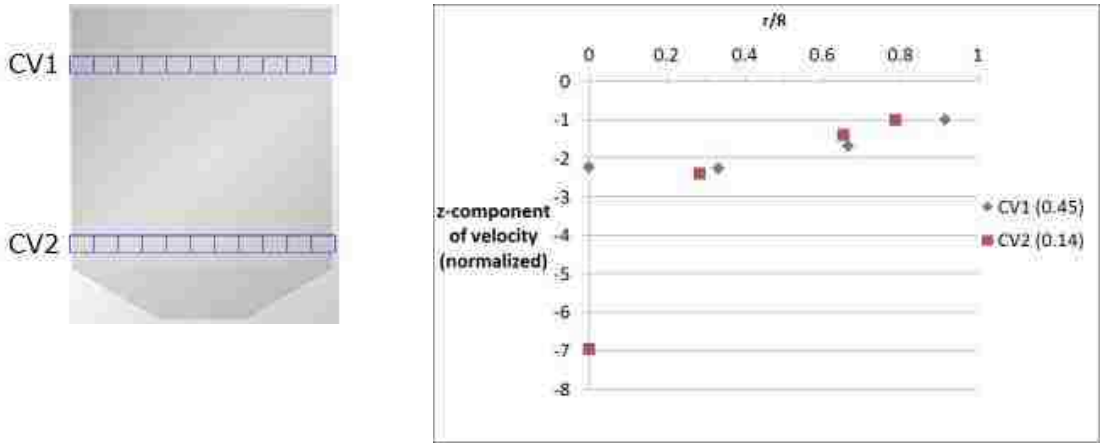

a. Locations of control volume (CV)

b. Pebbles velocity radial profile (numbers in bracket indicates mass flow index) (MFI) values)

Figure 4.27 Pebbles velocity radial profile obtained using RPT

This observation has been consistent with PBMR safety analysis report (PBMR SAR, 2000) and has also been confirmed by RPT results about zonal residence times and average zonal velocities. Many of previous studies failed to capture this pronounced concavity in velocity radial profile. The main possible reason for not capturing this effect could be use of 180° half model which introduces "wall-effect". Also, values of mass flow index (MFI), which is calculated using equation 4.13 (Nederman, 1992) are found out for both CV's.

$$\text{MFI} = \frac{\text{velocity close to the wall } (V_{wall})}{\text{velocity at the center}(V_{center})} \quad (4.13)$$

The mass flow is observed for values of mass flow index (MFI) greater than 0.3 and funnel flow is observed for values of mass flow index less than 0.3 (Johansson and Jenike, 1962). In mass flow, there is a simultaneous motion of all the particles as a solid

mass. In funnel/core flow, there is a rapid movement of particles in the center which are surrounded either by slowly moving or stagnant particles. The obtained value of MFI for CV1 suggests that there is a mass flow suggesting a simultaneous motion of all particles as a solid mass. Also, the obtained value of MFI for CV2 suggests that there is a funnel flow indicating that the particles in the center are moving much faster than outer ones close to the wall. This is also evident from the velocity radial profile obtained for CV2. This observation has been consistent with observations of RTD experiments suggesting possibility of faster moving zone of particles close to the center.

The obtained experimental results from RPT and RTD techniques are serving as a benchmark data. The assessment of DEM simulation results using this experimental benchmark data is carried out and discussed in Section 6.

4.5. SUMMARY

The following are the highlights of work carried out and key findings of this section with regards to pebbles flow field

- Implementation of advanced radioisotopes based non-invasive flow visualization techniques such as RPT and RTD around continuous pebble re-circulation experimental set-up is carried out.
- Development of Cobalt-60 based tracer (500μCi strength) mimicking the pebbles (glass marbles) is demonstrated and utilized in RPT and RTD experiments.

- Design and development of manual RPT calibration apparatus suitable for study of granular flow in a PBR is achieved and used in RPT calibration experiments to generate calibration curve for each detector.
- Calibration curves generated for each detector indicate that there is a spread in photo-peak counts readings for the same tracer-detector distance. This suggested that counts received at the detectors are not only a function of tracer-detector distance; but also of the attenuation characteristics of the medium in between the source and the detector and the detector efficiency.
- RPT calibration experiments under different operating conditions of bed (moving/static packed beds) suggested that PBR could be represented by the examination of static packed beds, depending on the type of measurement and parameters to be investigated.
- A cross-correlation based position reconstruction algorithm, which takes into account the geometry as well as the attenuating medium effects, is established and implemented. Before applying this cross-correlation based position reconstruction algorithm on an actual RPT experiments data, it is validated using counts data for known positions and position reconstruction error is estimated. A maximum reconstruction error of 5 mm in the z-direction is observed.
- RPT experiments are carried out by seeding tracer at different dimensionless radial positions (r/R) of 0, 0.33, 0.67 and 0.92 and tracking it using an array of scintillation detectors surrounding the system.

- By using the calibration curves and cross-correlation based position reconstruction algorithm, instantaneous position of a radioactive tracer is reconstructed. This instantaneous position data is used to provide more information about Lagrangian trajectories and their length, overall and zonal residence time, overall and zonal average velocities, velocity radial profile, flow patterns etc.
- Tracer initially seeded at the center follows a straight line path which is the shortest one (trajectory length of 26.74 cm). Tracers initially seeded at non-radial positions (r/R) of 0.33, 0.67 and 0.92 follows straight line path in the upper portion of the reactor. Afterwards, tracer moves radially towards the bottom central opening. Tracer initially seeded near the wall follows a longest path (trajectory length of 35.44 cm).Tracer seeded at the center moves faster (~102%) than when is seeded near the wall.
- Overall residence time/transit number increases with change in dimensionless initial seeding position (r/R) from the center towards the wall (169 % increase is observed for r/R of 0.92 with respect to r/R of 0) .
- Zonal residence times are used to calculate average zonal velocities in respective zones. Smaller values of z-component of average zonal velocities are observed in all the three zones for initial seeding position (r/R) of 0.92 (close to the wall). On the other hand, larger values of z-component of average zonal velocities are observed in all the three zones for initial seeding position (r/R) of 0 (at the center).

- In zone 3, the difference between z-components of average zonal velocities for initial seeding position close to the wall and at the center is more pronounced (0.96 cm/hour versus 10 cm/hour). This observation is consistent with previous observations reported in PBMR safety analysis report.
- It is observed that average zonal velocity of tracer gradually increases from zone 1 to 2 and further from zone 2 to 3 for all the seeding positions.
- Radial movement of the tracer has been observed in zone 2 and zone 3 for all initial seeding positions except at the center. Highest radial movement of 9.36cm in zone 3 is observed for initial seeding position (r/R) of 0.92.
- Overall average velocity of tracer is calculated for each seeding position using trajectory length values and overall residence time. It is found that overall average velocity of tracer for initial seed position r/R of 0 (at the center) is 3.02 cm/hr. This is ~102 % higher than the overall average velocity of tracer for initial seed position r/R of 0.92 (near the wall). This indicates that tracer when seeded at the center is moving faster than when seeded near the wall.
- Velocity radial profile results obtained using RPT suggested a plug flow type velocity profile in the upper cylindrical region, whereas velocity profile with pronounced concavity is observed near cylinder-cone transition point which are consistent with predictions based on mass flow index calculations.

5. DESIGN, DEVELOPMENT AND DEMONSTRATION OF OPERATIONAL FEASIBILITY OF NOVEL DYNAMIC RPT CALIBRATION TECHNIQUE

An analytical solution to the inverse problem of RPT, i.e. finding the instantaneous tracer position based upon instantaneous counts received in the detectors, is not possible. This problem is solved by performing a set of calibration experiments at the same operating conditions as those of actual RPT experiments. Calibration curves, map of photo-peak counts relating to the tracer positions, are generated for each detector. It provides relationship between the source-detector distance and photo-peak counts recorded by the detectors, which are used during inverse problem of position reconstruction. Usually, RPT calibration is carried out *in-situ* and in an invasive manner. There are major shortcomings of conventional calibration methodology due to which it has limited applicability in practical applications. As a part of this work, design and development of novel, non-invasive and dynamic calibration RPT technique is carried out to overcome shortcomings of conventional calibration methodology and has been discussed in detail in next sub-sections.

5.1. INTRODUCTION AND MOTIVATION FOR THE DEVELOPMENT OF DYNAMIC RPT CALIBRATION TECHNIQUE

Previously, different techniques have been used to place the radioactive particle at known locations inside the multi-phase system. Broadly, these techniques can be classified into manual and automatic calibration methods. There are different manual calibration methods (CARPT Manual, 2007):

1. A vertically graduated rod

2. A vertical nylon line with cylindrical lead piece

3. A vertical swivel and fishing line

4. A horizontally graduated rod.

In all these manual calibration methods, the radioactive tracer particle is placed safely at known locations in the system and photo-peak counts are recorded. Manual calibration is tedious and time consuming. Also, positioning accuracy of placing tracer particle at exact locations is poor as compared to automatic calibration apparatus. Automated calibration apparatus makes use of stepper motors for automated movement of a long rod in three directions (x, y, z or r, θ, z). The rod contains radioactive tracer particle at its tip in the vial. Due to the static and invasive nature of conventional RPT calibration methodology, it has limited applicability for practical applications. The major shortcomings of conventional RPT calibration methodology are as follows:

1. During RPT calibration particle is held **static** at known locations, whereas particle moves during actual RPT experiments. This introduces error in position reconstruction step known as 'dynamic bias' (Rammohan, 2002). It is not a major issue in the study of slow granular flow in a PBR but poses challenges in study of highly turbulent flows.
2. Existing calibration method is **invasive** in nature. The tracer particle needs to be placed at known locations with the help of a manual/automatic calibration apparatus. Hence, multiphase system needs to be designed from accessibility point of view (ports/holes suitable for entry of rod containing radioactive particle).

3. It is difficult to perform RPT calibration in high pressure and or high temperature multiphase systems due to its invasive nature and system safety considerations.
4. During RPT calibration, the tracer particle is placed at known locations and held static for certain duration to get time-averaged counts data. This procedure is time consuming and cumbersome especially with manual calibration apparatus.
5. RPT technique cannot be applied on industrial scale systems due to its existing calibration method. A use of short-lived radioisotopes based tracer particle and some non-invasive methodology of RPT calibration are desirable for study of industrial scale systems. Such a technique, if developed will be an industrial analogue of *catheterization* procedure widely used in hospitals for diagnostics purposes.

To overcome these shortcomings and to make the RPT technique viable for practical applications, advancement in its existing calibration methodology is essential. There is a need to develop and demonstrate a new dynamic and non-invasive calibration equipment and associated methodology. As a part of this work, design and development of novel, non-invasive and dynamic calibration RPT technique is carried out to overcome above mentioned shortcomings of current calibration methodology. This calibration technique makes use of three collimated detectors mounted on a moving platform and its concept of locating the tracer particle position in a non-invasive manner. Additionally, this technique has conventional fixed detectors which records counts data for identified tracer particle position. The conceptual and engineering design of novel RPT calibration technique, its various systems and sub-systems are described in detail in next sub-sections.

5.2. DESIGN AND DEVLOPMENT OF RPT CALIBRATION TECHNIQUE

As a part of this work, novel, non-invasive and dynamic technique known as calibration RPT is designed; developed and its operational feasibility has been demonstrated. This novel design can carry out RPT calibration in a dynamic and non-invasive manner. This technique is a synergistic combination of fixed detectors and three collimated detectors based RPT techniques (Figure 5.1). This technique retains advantages of both the RPT techniques while combining them and overcomes their limitations during individual use.

Figure 5.1. Synergistic combination of fixed detectors based conventional RPT technique (Han, 2007) and collimated detectors based RPT technique (Shehata , 2005; Wang 2011)

In fixed detectors based RPT technique, the instantaneous tracer particle position is identified by continuously recording counts data received by a set of Sodium Iodide scintillation detectors (usually 16-32 No.) arranged strategically around the system. A

position reconstruction algorithm makes use of recorded counts data from actual experiments and *in-situ* calibration data to reconstruct the instantaneous tracer particle position. In fixed detectors based RPT technique, usually a large number of stationary and non-collimated detectors (16 to 32) are used. Fixed detectors based RPT technique is non-invasive in nature but relies heavily on its existing invasive calibration method.

Moving collimated detectors based RPT technique has been used in Gatt's study (1973). Prof. Robin Gardener and his research group from North Carolina State University (NCSU) has developed advanced version of moving collimated detectors based RPT technique and demonstrated its application for study of granular flow in a pebble bed reactor (Shehata, 2005; Wang 2011). It consists of a set of three collimated detectors, having narrow slits on front side, mounted on a moving horizontal platform (Figure 5.1). This platform can be moved up/down in vertical direction. When the plane of the slit in the collimator aligns with the tracer particle, a peak in counts data is observed. This principle is used to identify position co-ordinates of tracer particle. A collimated detector having horizontal slit (middle detector in Figure 5.1) is fixed to the moving platform. This detector gives information about z-coordinate of the tracer particle. The other two collimated detectors are having vertical slits and can swing around a fixed pivot point on this moving horizontal platform. These detectors provide information about in-plane position co-ordinates of the tracer particle (x and y or r and θ) in a non-invasive manner. Stepper motors are used for up-down movement of horizontal platform and rotary swinging movement of the collimated detectors. This method doesn't require any *in-situ* calibration to identify the instantaneous position co-ordinates of the tracer particle unlike the fixed detectors based RPT technique. However, this method

involves real time tracking of an unknown motion of the tracer particle. Hence, its performance has limitations due to the upper limit on particle tracking speed. This limitation is usually due to the slower up-down movement of the heavy platform. Also, use of well collimated detectors demands stronger radioactive source for better signal-to-noise (S/N) ratio.

In this novel calibration technique, collimated detectors based RPT technique is being used to provide position information of the tracer particle while carrying out actual RPT experiments. RPT calibration and actual tracking experiments can be carried out simultaneously and separate calibration step used in the fixed detectors based RPT technique can be avoided. In short, necessary position data about calibration positions can be identified with the help of moving collimated detectors based RPT technique, whereas the counts data associated with respective calibration positions can be recorded with the help of fixed detectors. In this manner, this novel RPT calibration equipment can overcome static and invasive nature of existing calibration method and increase its applicability for industrial applications. The major limitation of moving collimated detectors based RPT technique is upper limit on tracking speed due to slower movement of the moving platform. This limitation can be overcome by design of RPT experiments. The moving platform will be fixed at certain heights and at these different heights number of calibration positions will be derived with the help of RPT calibration equipment while carrying out actual RPT experiments. This new calibration RPT technique is capable of providing fewer calibration data points in a dynamic and non-invasive manner. This technique can be integrated with the step II of position reconstruction method where the collected data can be used to obtain the fitted model

parameters of equations. These fitted model parameters will be used to generate additional calibration datasets at refined level. The conceptual and engineering design of this novel RPT calibration equipment is explained in the following paragraphs.

5.2.1. Conceptual Design. The schematic diagram of novel and dynamic RPT calibration equipment is as shown in Figure 5.2. It consists of fixed non-collimated detectors, in addition to three collimated detectors mounted on a moving horizontal platform. This horizontal platform can be moved up-down with the help of stepper- motor operated ball screws. The dimensions of horizontal platform were selected such that movement of horizontal platform will not obstruct data collection and recording of fixed non-collimated detectors. Out of these three collimated detectors, two will be having collimators with narrow vertical slit in the front. These collimated detectors with vertical slit can swing relative to the moving platform with the help of stepper motors and drive mechanism.

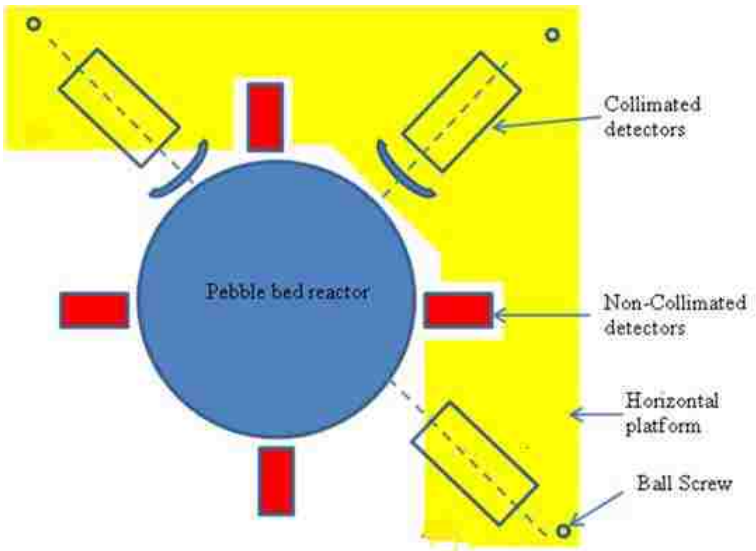

Figure 5.2 Schematics of novel dynamic RPT calibration experimental set-up

The third detector fixed to the moving platform will be having a collimator with narrow horizontal slit. This detector will provide information about z-coordinate of the tracer particle, whereas two swinging collimated detectors will provide information about the in-plane position co-ordinates (x, y or r, θ co-ordinates) of the tracer particle in the horizontal plane pre-determined by the collimated detector fixed to the platform. These three collimated detectors, mounted on a moving platform, are capable of providing position co-ordinates of the tracer particle in a non-invasive manner and fixed detectors surrounding the system can record counts data for these identified positions of the tracer particle. The locations data identified by three collimated detectors of RPT calibration technique will form a set of calibration data which can be used in position reconstruction step. There are two ways to carry out position reconstruction step: 1. Generate large amount of calibration datasets and use conventional reconstruction approach of curve fitting (Rados, 2003). It is good for systems where counts are function of source-detector distance only. 2. Generate a reasonable amount of calibration dataset and use a mechanistic model approach (Bhusarapu, 2005) or use Monte Carlo approach based simulation methods (Gupta, 2002) to estimate additional calibration dataset at refined level. In this manner, sufficient information required to generate detector calibration curves can be obtained. Therefore, step 2 can be integrated with the new RPT calibration technique. RPT calibration and actual experimentation can be carried out simultaneously with the help of this new RPT calibration equipment. This conceptual design of novel and dynamic RPT calibration technique is transformed into engineering design and is explained in the following paragraphs.

5.2.2. Engineering Design of Novel RPT Calibration Technique. RPT Calibration technique consists of a mechanical structure mounted on wheels, a horizontal platform which can move with respect to the stationary mechanical structure and on which three collimated detectors are mounted, ball screw mechanism to move this platform up and down, chain and sprocket mechanism for synchronous rotation of these ball screws, stepper motor and bi-slides for collimated detectors swinging movement about respective pivot point, quadrature encoders for feedback about the position of detectors, radiation detection and data acquisition system for both collimated and fixed detectors. The RPT calibration technique is mounted on guided wheels and jack assembly so that it can be moved easily to any location and held fixed, if required. The RPT calibration technique has been erected around continuous pebble recirculation experimental set-up containing test reactor of 1foot in diameter and 1foot in height (Figure 5.3).

The entire RPT calibration technique is broadly divided into three systems comprising of various sub-systems and components

a. Mechanical structure

b. Motion control system

c. Radiation detection system

The detailed description about each system is discussed in the following paragraphs.

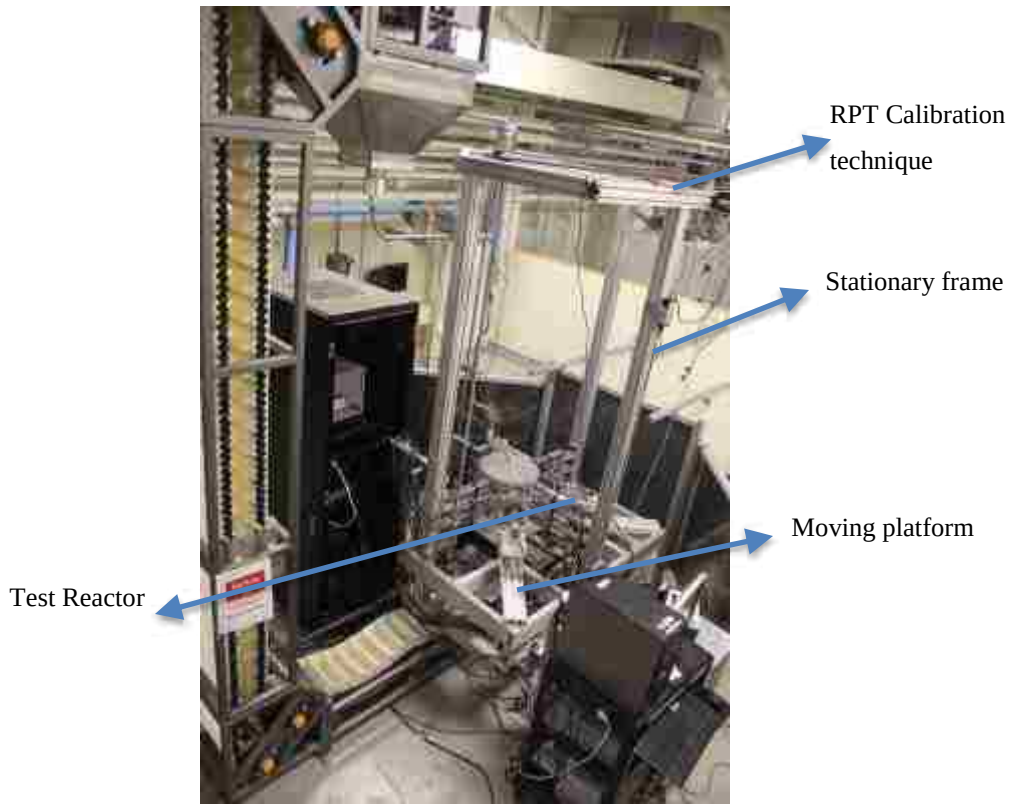

a. Implementation of novel RPT calibration technique around continuous pebble recirculation experimental set-up

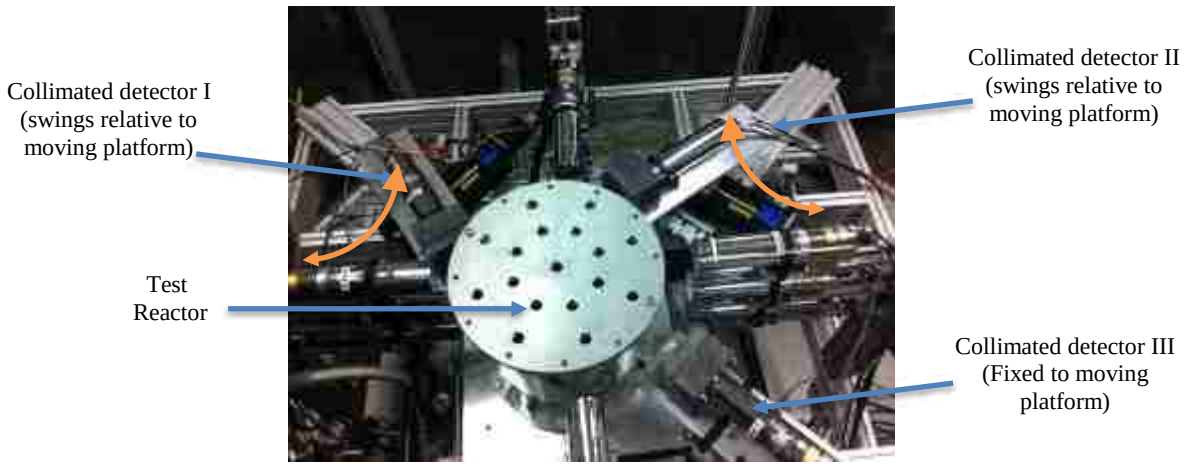

b. RPT calibration equipment (top view)

Figure 5.3 RPT calibration technique

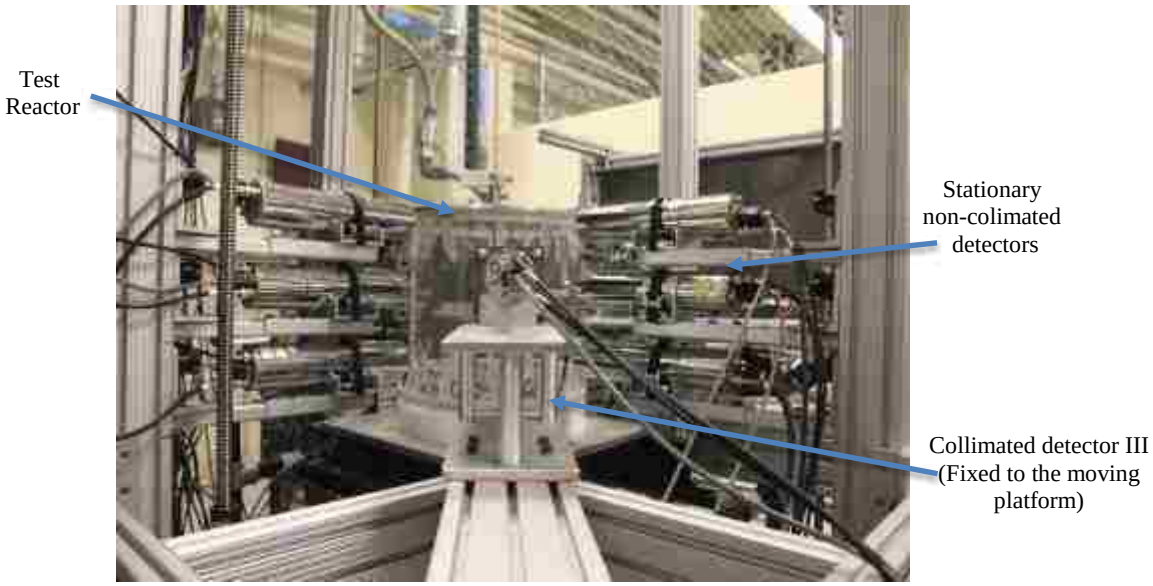

c. RPT calibration equipment (side view)
Figure 5.3 RPT calibration technique cont.

5.2.2.1. Mechanical structure. RPT Calibration technique mechanical structure (Figure 5.4) consists of a stationary frame mounted on guided wheels and jack assembly (Figure 5.5a) and a horizontal moving platform with respect to the stationary frame (Figure 5.5b). Stationary frame is made out of 3030-LITE (Make: 80/20 Inc.) which is a 3.0" x 3.0" T-slotted aluminum profile made from 6105-T5 aluminum. Stationary frame consists of 4 3030-LITE column posts of 90 inch in length. These four column posts are connected to the top and bottom using five side frames made out of 3030-LITE. This altogether forms mechanical structure of RPT calibration equipment (Figure 5.4). Four 3030-LITE column posts guide up and down movement of a moving platform. The fixed and non-collimated detectors are mounted on these four column posts of stationary frame. Stationary frame is mounted on four swivel caster ratchet. These casters have leveling

pads which allows keeping RPT Calibration components stationary, if required and compensating for uneven floors. Also, these casters allow precise centering of RPT calibration components around any test reactor. The stationary frame has an arrangement at the top to hold three ball screws and associated bearings, chain and sprocket mechanism to rotate these ball screws, spur gear stepper motor to drive this chain and sprocket mechanism, etc. The stepper motor with gear box rotates ball screws and rotary motion of ball screws is converted into linear motion of the moving platform using screw nuts mounted on the moving platform. The moving platform has 5 sides and is made out of various 15 series T-slotted aluminum profiles.

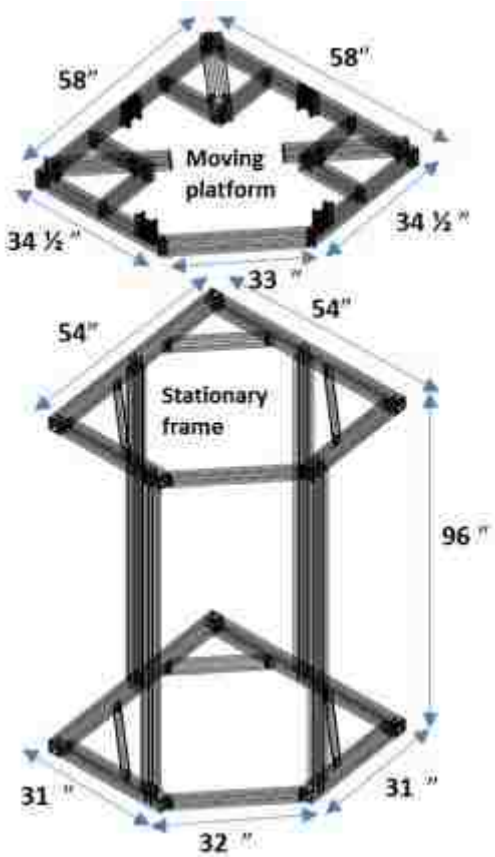

Figure 5.4 Exploded view of RPT Calibration technique mechanical structure

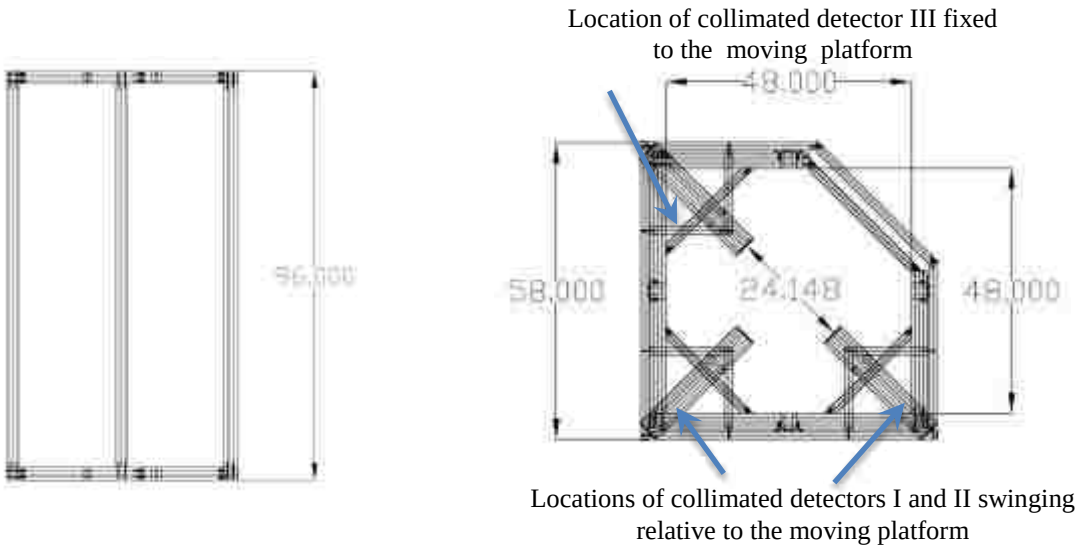

a. Stationary frame (front view) b. Moving platform (top view)

Figure 5.5 Calibration RPT mechanical structure

Note. All dimensions are in inches

The three collimated detectors and associated motion system components such as stepper motor, drive mechanism etc. are mounted on this moving platform. The relative locations of three collimated detectors on moving platform are as shown in Figure 5.5. The collimated detectors I and II, capable of swinging movement with respect to the moving platform, have a vertical slit in the front collimator. The collimated detector III, fixed to the moving platform, has horizontal slit in the front collimator. The design of collimator is discussed in detail in next sub-sections. The horizontal platform can be moved up-down in fine increments using spur geared stepper motor and ball screw-nut type mechanism. This movement in vertical direction helps in carrying out RPT calibration experiments at different heights. Corner diagonal piece of a moving platform has been made removable. This helps in the implementation of RPT calibration technique around test reactor without any difficulty.

5.2.2.2. Motion control system. The moving platform needs to be moved up-down with respect to the stationary frame. A spur geared stepper motor (Model No. PK296B2A-SG18 from Velmex Inc.) drives three ball screws (3/4 ×13/64×8 feet). These ball screws are mounted on stationary frame and are rotated with the help of chain and sprocket mechanism installed on top side of the mechanical structure. This spur geared stepper motor is driven by a VXM stepper motor controller. A collimated detector III, having horizontal slit, is mounted on a moving platform and does not move relative to it (Figure 5.6). This collimated detector III can identify z co-ordinate of tracer position.

Figure 5.6 Collimated detector III having horizontal slit fixed to the moving platform

Lead has a half value layer (HVL) of 0.49” for Co-60 source. A half value layer is related to shielding performance of materials and reduces original strength of a radioative source by a half value. Hence, 1” thick lead on front and sides of the detector

is selcted which provides roughly 2 HVL's of shielding resulting into 75% reduction of original intensity. Figure 5.7 shows schematics of a collimated detector with detailed dimensions. The slit in the collimator is 2" in length to cover detector, 1" thick and has a width of 1mm. A slit width of 1mm is chosen for the collimators of all three detectors based on the recommendations of previous work (Shehata, 2005 and Wang, 2011).

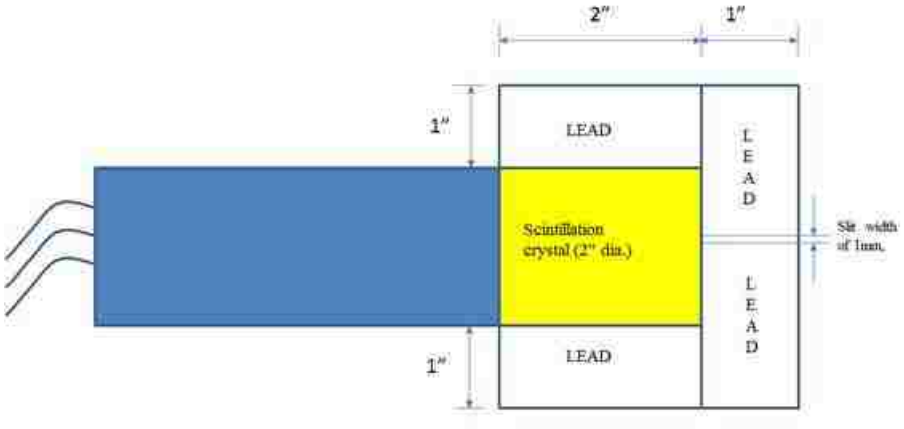

Figure 5.7 Collimated detector schemnatic diagram

The modular design of the collimator gives flexibility to rotate the front portion of the collimator by 90° in either direction. In this manner, it is possible to have horizontal or vetical slit in front of the detector. The collimated detector III, fixed to the moving platform, has a horizontal slit, whereas other two collimated detectors I and II , swinging in a horizontal plane relative to the moving platform, have vertical slits. The collimator used in this study covers crystal portion only of Sodium Iodide scintillation detectors (2" in length) and hence light in weight. This improved design allows faster

tracking speed without putting excessive torque requirement on the stepper motors. This is a notable difference between the RPT calibration technique and previously developed collimated detectors based RPT set-ups. These two detectors are mounted on moving horizontal platform (Figure 5.8a and 5.8b) and can be swung in a horizontal plane about a pivot point with the help of separate stepper motors (National Instruments, Model No. T23NRLH-LNN-NS-00) and precision slide mechanism (Bi-slide from Velmex Inc.). These collimated detectors I and II, capable of swinging movement, have adjustable pivot point and can swing about a pivot point to scan the entire test reactor. The location of pivot point can be adjusted which helps in optimizing total angular movement of collimated detectors. There is an opposing requirement on the placement of collimated detectors with respect to the test reactor from radiation detection and motion control point of view. For better signal-to-noise ratio (S/N), these collimated detectors need to be placed as close as possible to the test reactor. However, this demands wider swinging movement of the detectors I and II to scan the entire test reactor. If these collimated detectors are placed far away from the test reactor, narrower swinging movement of the detectors will be required to cover the same diameter test reactor. The design of swinging movement mechanism in RPT calibration equipment allows having pivot point far away from the test reactor and placing collimated detectors as close as possible to the test reactor for better signal-to-noise ratio (S/N). This is one of the distinct advantageous features of this RPT calibration technique.

a. Top view of swinging collimated detectors I/II

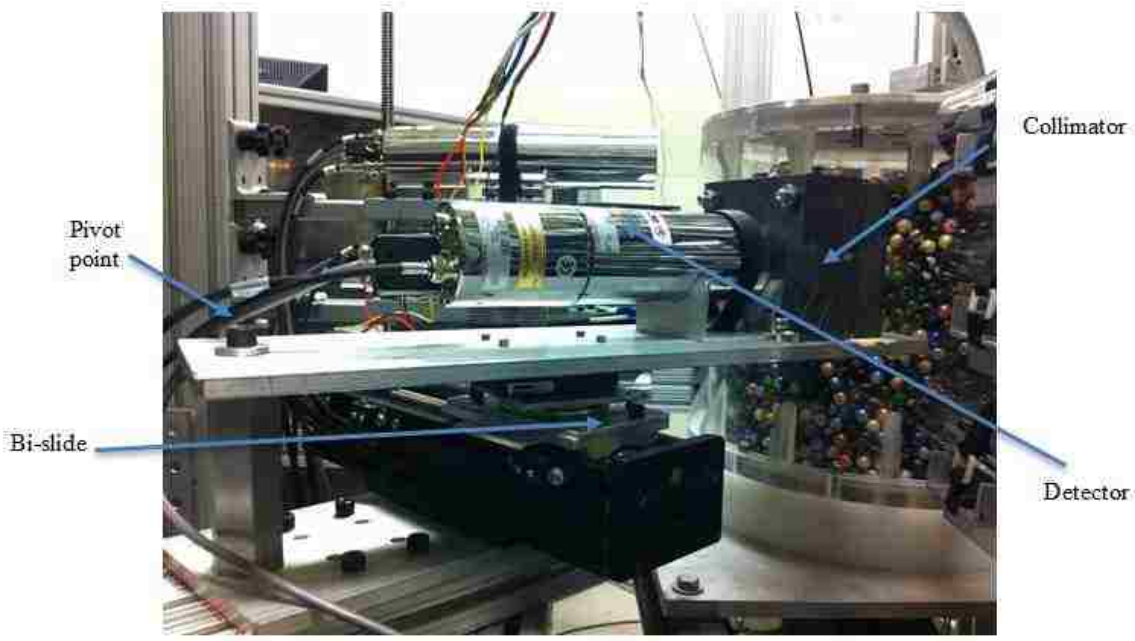

b. Side view of swinging collimated detectors I/II

Figure 5.8 Swinging collimated detectors I/II

Figure 5.9 shows block diagram of motion control system used for swinging movement of the collimated detectors. To control the movement of stepper motors, a four axis servo/stepper motor controller from National Instruments (Model No. PCI-7354) is used, which is installed on motherboard of a personal computer. The operation of stepper motors is controlled by the train of logic pulses of zeros and ones. The motion controller converts motion commands generated by the motion control software (LabVIEW) into a train of logic pulses. The motion controller conveys the targeted position to the stepper motor in terms of number of steps. The stepper motor drive receives these pulses from the motion controller and based on that sends a power signal to drive the stepper motor to reach the target position. The stepper motor used for swinging movement of the collimated detectors has its own power supply (Powervolt Inc., Model No. BVU75) which supplies power to the stepper motor thru a stepper motor drive from National Instruments (Model No. P70530). LabVIEW - motion control software from National Instruments, offering graphical programming environment, is installed on a personal computer.

Figure 5.9 Block diagram of motion control system for swinging movement of the collimated detectors

In-house developed LabVIEW program is used to control the movement of stepper motors, to get position feedback from the encoders mounted on stepper motors, to acquire and process counts data from the collimated detectors I and II. The position feedback through quadrature encoders mounted on the shaft of stepper motors is used to identify instantaneous angular position of the collimated detectors I and II. Peak counts are recorded in collimated detectors I and II when the plane containing vertical slit aligns with the tracer particle. Based on the observed peak counts in the collimated detectors and corresponding encoder feedback about the angular position of the collimated detectors, it is possible to find in-plane position co-ordinates (x,y - Cartesian co-ordinate system or r,θ - cylindrical co-ordinate system) of the tracer particle. The feedback from the encoder is obtained in terms of arbitrary counts and converted into angular position co-ordinates of collimated detectors by carrying out encoder calibration. This is explained in detail in appendix F.

5.2.2.3. Radiation detection system. RPT Calibration equipment synergestically combines moving collimated detectors based RPT technique with fixed non-collimated detectors based RPT technique. Radiation detection and data acquisition system components of stationary detectors based RPT technique are already described in Section 4. Radiation detection and data acquisition system of moving collimated detectors consists of 2'×2' NaI Scintillation detectors (Canberra Model No. 802), Pre-amplifier (Canberra Model No. 2007P), Timing filter and amplifier (Canberra Model No.2111), NIM power supply 2000, USB multifunction DAQ device (National Instruments Model No. USB-6221), and BNC cables to connect various components. Figure 5.10 represents a Block diagram of LabVIEW interface between radiation detection and motion control

system for collimated detectors of RPT Calibration equipment. The multifunction DAQ device converts pulses coming from amplifiers into a digital voltage signal which are measured and counted in a LabVIEW environment. A LabVIEW program has been developed to acquire detector signals, provide information about count rates in arbitrary units and write recorded data to files for further processing, to carry out motion control of stepper motors used to swing the collimated detectors, provide encoder feedback about angular positions of collimated detectors. This LabVIEW program is an interface between radiation detection and motion control system.

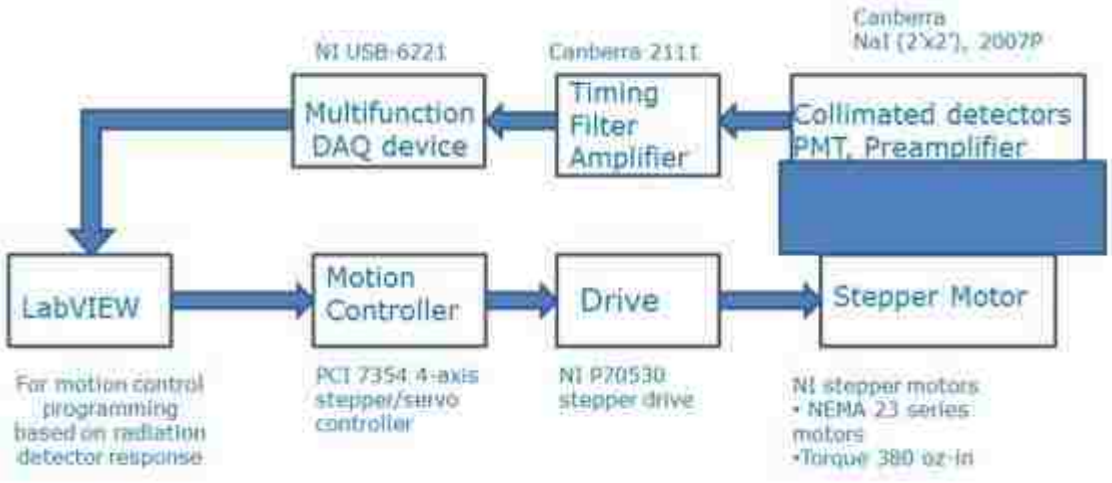

Figure 5.10 Block diagram of LabVIEW interface between radiation detection and motion control system for collimated detectors of RPT Calibration equipment

5.2.3. Detector Response as a Function of Angular Position. Collimated detectors I and II having vertical slit can swing about their respective pivot point to scan entire test reactor. The number of counts recorded in the detector depends on source-detector distance, the intensity of a source, attenuation characteristics of the medium in between, detector geometry, solid angle subtended at the detector by a source etc. Due to the collimator, counts recorded in the detector become a strong function of angular orientation of collimator slit with respect to the radioactive source. Figure 5.11 shows typical counts response of the collimated detector having vertical slit for different angular positions of the collimated detector with respect to a radioactive tracer particle.

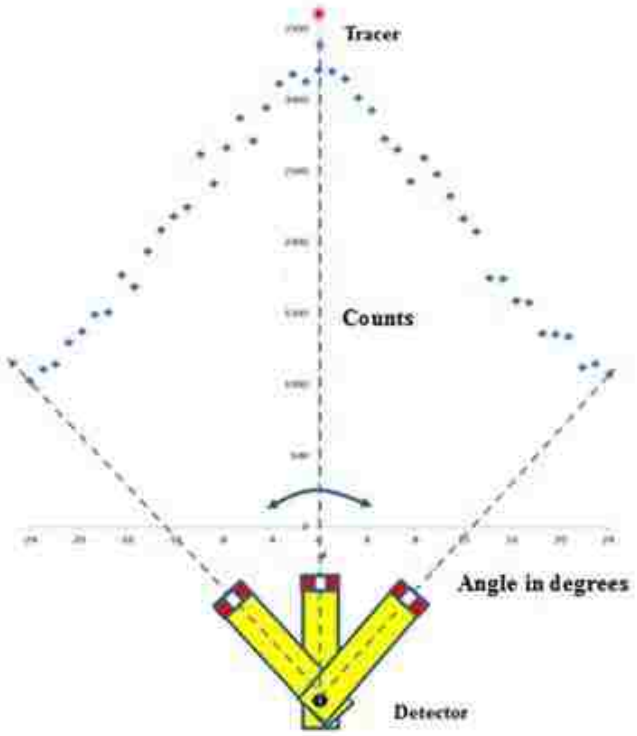

Figure 5.11 Counts rate response of the collimated detector as a function of the angular position

The radioactive tracer particle is in the horizontal plane passing through the central axis of a collimated detector. The typical counts response of the collimated detector is a bell shaped curve. When the plane containing vertical slit in the collimated detector is in the alignment with the tracer particle, a maxima in the counts recorded is observed. For other orientations of a vertical slit in the collimator, lesser counts are recorded. The observance of peak in the recorded counts when slit in the collimator aligns with the tracer particle is used to identify one of in-plane position co-ordinates of a radiaoctve tracer particle. Hence, two rotary collimated detectors I and II having vertical slits can identify in-plane angular positions co-ordinates (θ_1 and θ_2) of a tracer particle. The information about in-plane angular position co-ordinates corresponding to a maxima in the count rates can be obtained based on the position feedback from the encoders mounted on the stepper motors. In-house developed LabVIEW program continuously acquires and writes collimated detectors I and II counts rate data and position feedback from the encoders to data files. This counts rate data is then analyzed to find maxima in the count rate and then cross-correlated with the position feedback from the encoders to identify corresponding angular co-ordinates (θ_1 and θ_2) of the collimated detectors I and II. These angular position co-ordinates can then be converted into cartesian (x,y) or cylinderical co-ordinates (r,θ) using suitable expressions described in the next section. Third collimated detector having a horizontal slit is fixed to a moving horizontal platform. A maximum in the counts rate is observed for this collimated detector when it's horizontal slit is in alignment with the tracer particle. This provides information about the z co-ordiante of the tracer particle. In this manner, it is possible to identify unknown position of the tracer particle in a non-invasive manner with the help of three collimated

detectors mounted on a moving horizontal platform. The collimators used have a narrow slit of 1mm width and hence counts recorded in the collimated detectors are reduced siginificantly. This demands closer placement of the collimated detectors with respect to the test reactor and or use of a stronger radioactive source. In the study carried out at Massachussettes Institute of Technology (M.I.T) using collimated detectors (M.I.T., 2002), Na-24 radioactive source of 1 mCi strength has been used. Alreay prepared and tested Co-60 based tracer particle (500 μCi radioactve strength) has been used in this study. More information about this tracer particle can be found out in Section 4.

5.2.4. In-plane Measurement. Figure 5.12 shows schematics of a typical in-plane measurement to deduce in-plane cartesian (x,y) or cylinderical co-ordinates (r,α) from the angular position co-ordinates θ_1 and θ_2 of collimated detectors I and II.

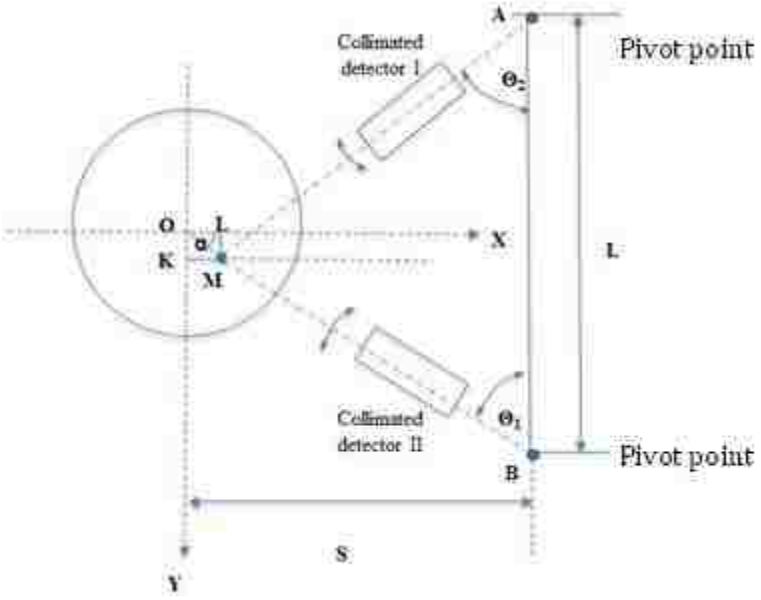

Figure 5.12 Schematic diagram of typical in-plane measurement (θ_1 and θ_2)

The information about angular position co-ordinates of collimated detectors is obtained from the position feedback of encoders mounted on stepper motors. Typically, a moving platform is fixed at certain height and entire test reactor is scanned using collimated detectors I and II. When tracer is in alignment with the vertical plane containing slit in the collimator, peak counts are recorded in the collimated detectors. In-house developed LabVIEW program continuously records and writes counts rate data and encoder feedback. The encoder feedback is then converted into angular position co-ordinates by making use of encoder calibration procedure (Appendix G). Let us assume that θ_1 and θ_2 are the in-plane angular position co-ordinates of the tracer particle obtained based on the encoder position feedback and counts rate response of collimated detectors I and II. A set of equations 5.1 thru 5.6 is then used to find out position co-ordinates (r and α in cylindrical co-ordinate system or x and y in Cartesian co-ordinate system) of the tracer particle from the in-plane angular position co-ordinates θ_1 and θ_2 (Shehata, 2005).

$$r = OM = \sqrt{OL^2 + LM^2} \qquad (5.1)$$

$$OL = S - \frac{L*\tan\theta_1*\tan\theta_2}{\tan\theta_1+\tan\theta_2} \qquad (5.2)$$

$$LM = L\left[\frac{1}{2} - \frac{\tan\theta_2}{\tan\theta_1+\tan\theta_2}\right] \qquad (5.3)$$

$$\alpha = \tan^{-1}\left(\frac{LM}{OL}\right) \qquad (5.4)$$

$$x = r * \cos\alpha \qquad (5.5)$$

$$y = r * \sin\alpha \qquad (5.6)$$

where,

L - Distance between pivot points of collimated detectors I and II

S- Distance between central axis of a test reactor and horizontal line passing through the pivot points of collimated detectors I and II. Table 5.1 summarizes known and unknown parameters for a typical in-plane measurement.

Table 5.1 Known and unknown parameters for typical in-plane measurement

Known parameters	**Unknown parameters**
S , L, z co-ordinate for plane of measurement	θ_1 , θ_2 or x, y

5.2.5. Stepwise Procedure for Deriving Position Co-ordinates of a Tracer Particle Using RPT Calibration Technique. The stepwise procedure to derive tracer particle in-plane position co-ordinates in a non-invasive manner using RPT calibration equipment is as follows:

Step 1: The horizontal moving platform of RPT calibration technique is fixed at some arbitrary height. The horizontal working plane to derive calibration data points is fixed in order to avoid vertical up-down movement of the heavy moving platform. It can be moved and fixed to different heights and steps 2 thru 4 can be repeated to derive additional calibration data points at each height.

Step 2: The moving collimated detectors I and II are swung around their respective pivot points to scan the entire test reactor. In-house developed LabVIEW program continuously collects and writes counts rate data recorded in the collimated detectors I and II and associated position feedback from the encoders.

Step 3: The counts rate data for each collimated detector is then analyzed to find maxima in the counts rate and corresponding feedback about angular position of collimated detectors I and II is obtained from the encoders. The encoder feedback about position is in arbitrary counts readings which is then converted into angular position co-ordinates (θ_1 and θ_2) of the collimated detectors I and II.

Step 4: The angular position co-ordinates θ_1 and θ_2 , corresponding to the identified tracer particle position, are then converted into r and α co-ordinates (for cylindrical co-ordinate system) or into x and y co-ordinates (for Cartesian co-ordinate system) using equations 5.1 thru 5.6.

5.2.6. Experiments to Demonstrate Operational Feasibility of RPT Calibration Technique. The operational feasibility of above described RPT calibration Technique needs to be demonstrated for known positions of the tracer particle. Hence, two separate sets of experiments were carried out. Tracer particle was held stationary at known locations in 1st set of experiments, whereas it was moving along a straight line path in a controlled manner in 2nd set of experiments. These feasibility experiments were carried out using the radioactive tracer particle used in the RPT and RTD studies and has already been described in Section 4. Co-60 based tracer particle of 500μCi radioactive strength was found to be weaker to carry out these experiments in a test reactor completely filled with the glass marbles. Additionally, these glass marbles have significant attenuation of γ-rays coming from the Co-60 tracer particle. Hence, these experiments were carried out in an empty test reactor. Initial hand-calculations suggested that tracer particle of at least 1mCi strength is required to carry out such feasibility experiments in a test reactor of 1 foot diameter completely filled with the glass marbles.

Such a strong source might saturate fixed non-collimated detectors. This can be avoided by increasing gap between the front face of fixed non-collimated detectors and the outer periphery of the test reactor.

5.2.6.1. 1st set of experiments. For 1st set of experiments, tracer was placed at known locations inside a test reactor and held stationary with the help of a manual calibration apparatus previously described in Section 4. Figure 5.13 shows schematic diagram of experimental arrangement for 1st set of experiments. The moving platform of RPT calibration technique was moved in the vertical direction and aligned with the tracer particle.

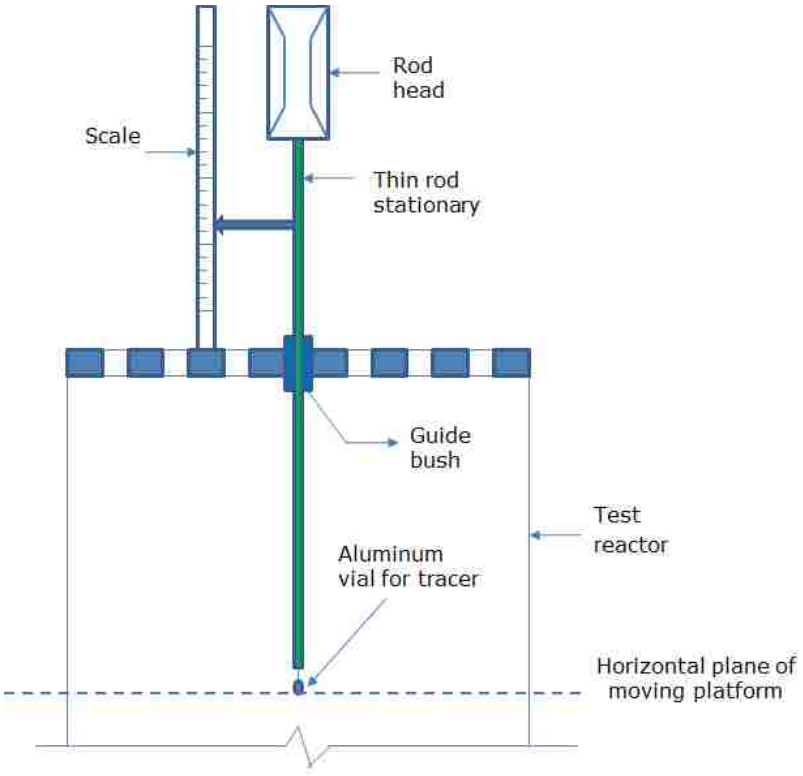

Figure 5.13 Schematic diagram of experimental arrangement for 1st set of experiments.

This ensures that plane containing horizontal slit in the collimated detector III, fixed to the moving platform, passes through the tracer particle.The counts rate data recorded in this collimated detector and laser alignment were used for this alignment. Afterwards, collimated detectors I and II were continuously swung about their respective pivot points to scan entire test reactor. The radiation counts rate data along with encoder feedback about position was continuously acquired and written to data file with the help of in-house developed LabVIEW program. The radiation counts rate data and encoder feedback about the angular position of collimated detectors I and II was then cross-correlated to find out angular position co-ordinates of the collimated detectors I and II corresponding to recorded maxima in the radiation counts rate data. These angular position co-ordinates were then used to find out in-plane position co-ordinates of the tracer particle (r and α co-ordinates and then x, y co-ordinates) using mathematical expressions given by equations 5.1 thru 5.6. A total four number of experiments were carried out under 1st set of experiments. Obtained results about the in-plane position co-ordinates were compared with the actual known tracer particle position to estimate reconstruction errors. It is discussed in detail in next sub-sections.

5.2.6.2. 2nd set of experiments. In 2nd set of experiments, the moving platform of RPT calibration technique was fixed at mid-height of the test reactor (6” from the top of the reactor). Figure 5.14 shows schematics of experimental arrangement for 2nd set of experiments. The tracer particle was kept in a vial at the tip of a long rod of manual calibration apparatus. This rod of the manual calibration apparatus was allowed to move vertically downwards in a controlled manner. A string was tied to this long rod at its top end and wrapped around top mechanical structure of RPT calibration technique.

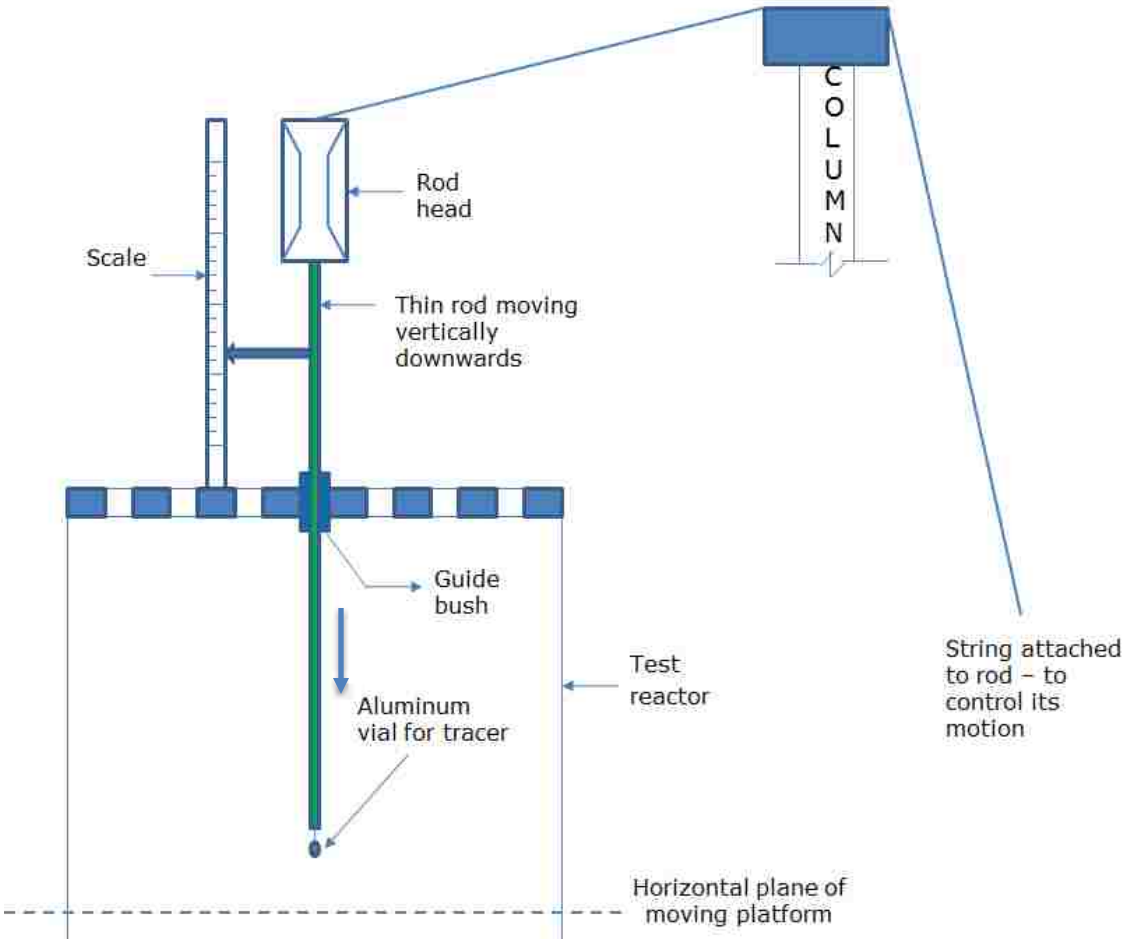

Figure 5.14 Schematic diagram of experimental arrangement for 2nd set of experiments.

This string was manually released to move the rod vertically downwards along with vial containing radioactive tracer particle in a controlled manner.The moving tracer particle initially approaches the horizontal plane of the moving platform, crosses it at one instant and goes away from it. This movement of the tracer particle was stopped before it touches the bottom surface of the test reactor. The collimated detectors I and II were swung continuously to scan entire test reactor during this vertically downward movement

of the tracer and counts rate data along with position feedback from the encoders were acquired and written to data files with the help of a LabVIEW program. The radiation counts rate data and encoder feedback about the angular position of collimated detectors I and II were then cross-correlated to find out angular position co-ordinates of the collimated detectors I and II. These angular position co-ordinates were then used to find out in-plane position co-ordinates of the tracer particle (r and θ co-ordinates and then x, y co-ordinates) using mathematical expressions given by equations 5.1 thru 5.6. A total four number of experiments were carried out under 2^{nd} set of experiments. In case of 2^{nd} set of experiments, r and θ or x and y co-ordinates of the moving tracer particle were constant. The z co-ordinate of the tracer particle was only changing due to its vertically downward movement. However, the moving platform was fixed at mid-height of the test reactor. Obtained results about the in-plane position co-ordinates of tracer particle for 2^{nd} set of experiments were then compared with the actual in-plane position co-ordinates to estimate reconstruction errors. It is discussed in detail in next paragraphs.

5.3. RESULTS AND DISCUSSIONS

To demonstrate operational feasibility of newly designed and developed RPT calibration equipment, 2 sets of experiments as described earlier were carried out. The radiation counts rate data and encoder position feedback obtained in each experiment was analyzed to provide results about in-plane position co-ordinates of the tracer particle.

5.3.1. 1st Set of Experiments (Tracer Held Static). During one cycle of scan (Figure 5.15), collimated detectors I/II starts scanning from one end of a test reactor (point P), goes to the other end of a test reactor (point Q) and then comes back to the initial starting point (point P).

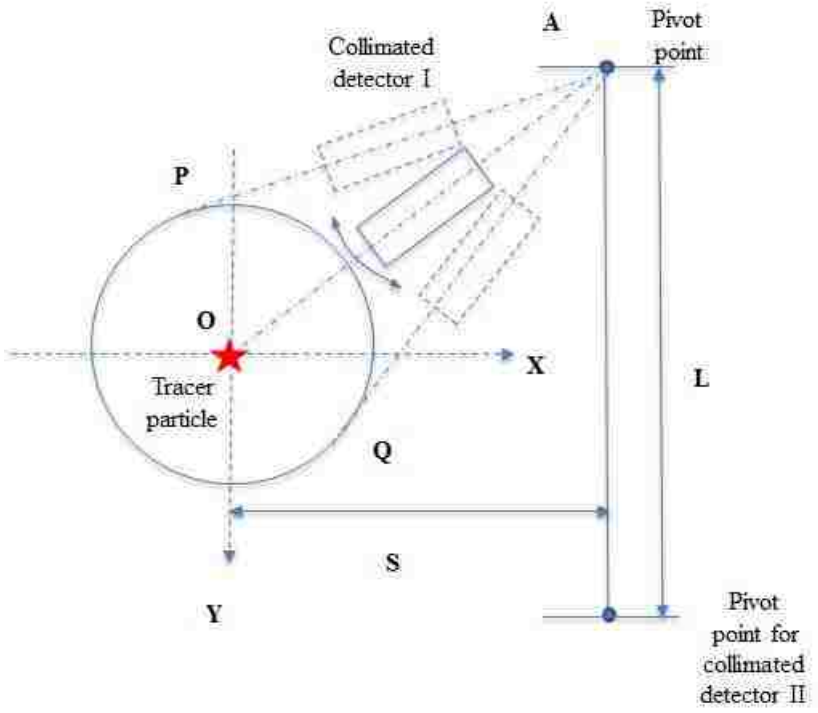

Figure 5.15 One scanning cycle of collimated detectors I/II

This forward and backward swinging movement of collimated detectors in a horizontal plane about its pivot point was repeated several times during each experiment. Figure 5.16 shows a typical counts rate response of collimated detector I/II during one

scanning cycle. The tracer was held stationary at the center of a test reactor with the help of a manual calibration apparatus. A typical bell-shaped counts rate response curve was obtained for one scanning cycle of collimated detectors I/II. A peak was observed in the recorded counts rate data of the collimated detectors when the plane containing vertical slit in the collimator passes through the tracer particle (represented by line OA in Figure 5.15). The minimum in the counts was observed when the vertical slit in the collimated detector is not in alignment with the tracer particle (represented by line PA or QA in Figure 5.15) and makes wider angle with angular position represented by line OA)

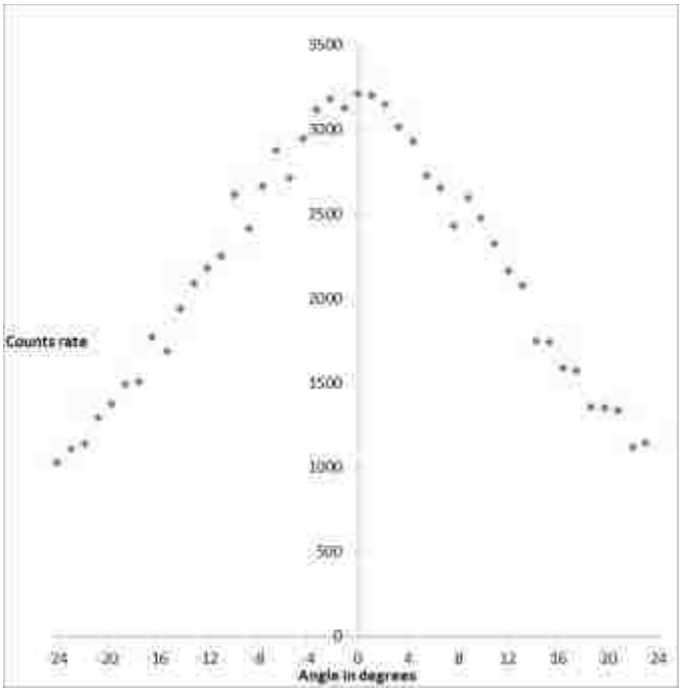

Figure 5.16 Counts rate response of collimated detectors I/II - tracer held stationary for one scanning cycle

Figure 5.17 shows counts rate response of collimated detectors I/II obtained over several cycles of scan. Multiple peaks having roughly same value were observed in the recorded counts rate data. The encoder feedback about detector position was analyzed to find out angular positions of collimated detectors I and II corresponding to instances when peaks in the counts rate were observed. The tracer was held stationary at 4 different positions and counts rate data along with encoder position feedback were obtained over several scanning cycles of collimated detectors. Obtained data was analyzed to find out in-plane position co-ordinates of the tracer particle using step-wise procedure mentioned before. The exact in-plane position co-ordinates of the tracer particle during these experiments were known beforehand and hence used to estimate position reconstruction errors.

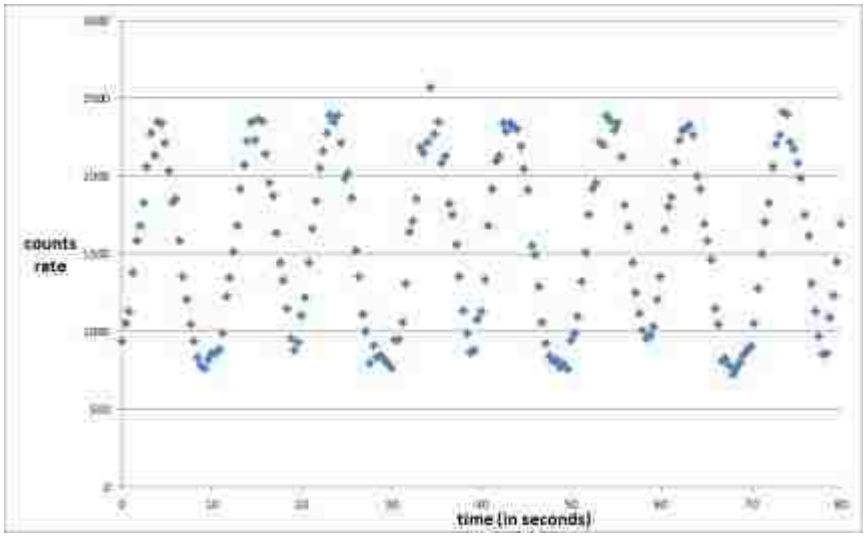

Figure 5.17 Counts rate response of collimated detectors I/II – tracer is held stationary at the center of a test reactor (obtained over several cycles of scan)

Table 5.2 presents position reconstruction results obtained using RPT calibration equipment and it was analyzed further to estimate reconstruction errors. Reconstruction error is the absolute difference between actual and reconstructed position. It was found that maximum reconstruction accuracy achievable with the RPT calibration equipment is within 3.4 mm, whereas minimum reconstruction accuracy achievable with the RPT calibration equipment is within 1mm for experiments in which the tracer particle was held stationary.

Table 5.2. Position reconstruction results – Tracer is stationary

Actual Position (in cms)		**Reconstructed position** (in cms)		**Reconstruction error** (in cms)	
X co-ordinate	Y co-ordinate	X co-ordinate	Y co-ordinate	X co-ordinate	Y co-ordinate
0	0	-0.23	0.25	0.23	0.25
13.97	0	14.15	0.15	0.18	0.15
0	13.97	-0.1	13.7	0.1	0.27
5.39	5.39	5.7	5.05	0.31	0.34

5.3.2. 2nd Set of Experiments (Tracer Moving). In 2nd set of experiments, tracer was moved vertically downwards along a straight line path with the help of calibration apparatus and its speed was manually controlled by a string attached to it (Figure 5.14).

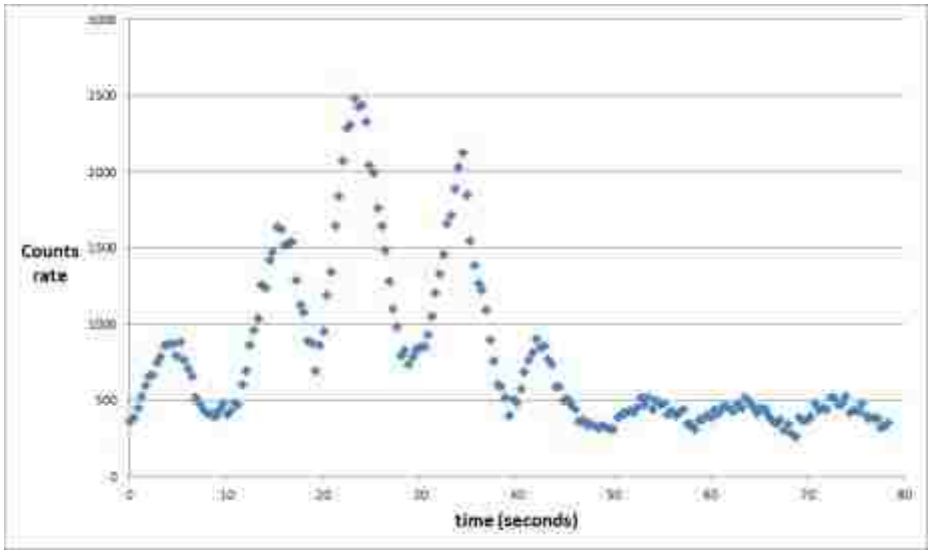

a. Counts rate response of collimated detector I during movement of tracer particle

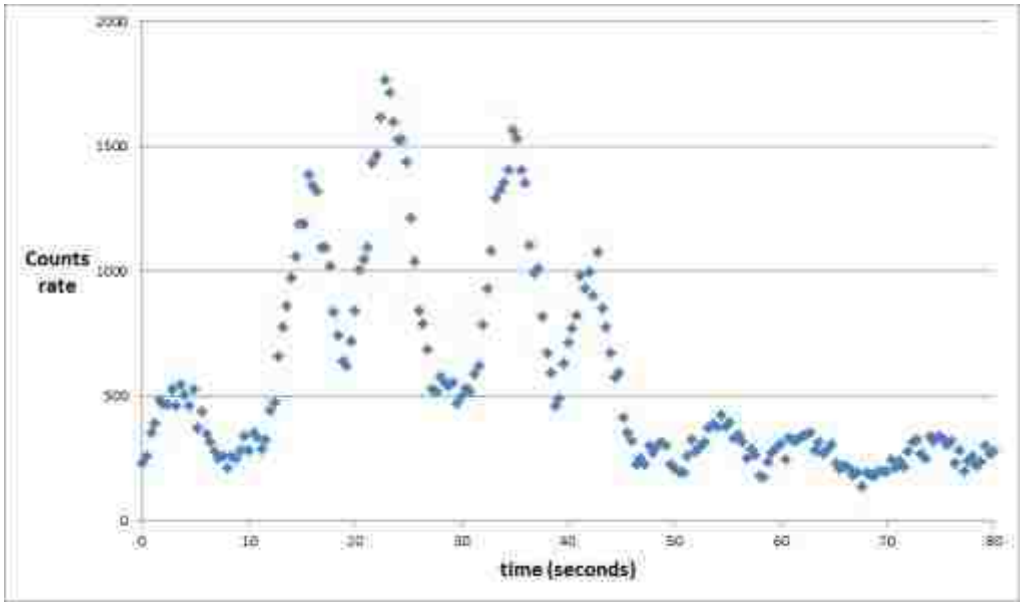

b. Counts rate response of collimated detector II during movement of tracer particle

Figure 5.18 Counts rate response of collimated detectors I and II

The tracer particle was moved vertically downwards along a straight line path at an average speed of ~0.3 cm/sec. The moving platform of RPT calibration technique was fixed at mid-height of the test reactor. Figure 5.18a and 5.18b represents the counts rate response of collimated detectors I and II during this downward movement of a tracer particle along a straight line path. Multiple peaks of gradually increasing values were observed when the tracer approaches horizontal plane of stationary held moving platform. Once it crosses the horizontal plane of moving platform, multiple peaks of gradually decreasing values were observed. Each peak is corresponding to an instant when the tracer particle is in the plane of vertical slit in the collimated detectors I/II. A highest value peak in the counts rate data is corresponding to an instant when the moving tracer particle is in the plane of the vertical slit in the collimated detectors I/II and in the horizontal plane of the moving platform on which these collimated detectors I/II are mounted. The encoder feedback about angular positions of collimated detectors I and II corresponding to highest value peaks in the counts rate data were then used to estimate in-plane tracer position co-ordinates. The exact position of a tracer particle during these experiments was known beforehand and was used to estimate position reconstruction errors. Table 5.3 presents position reconstruction results obtained using RPT calibration equipment when the tracer particle was moving. It was found that maximum reconstruction accuracy achievable with the RPT calibration equipment is within 5.9 mm, whereas minimum reconstruction accuracy achievable with the RPT calibration equipment is within 1.2 mm for experiments in which tracer particle was moving in a straight line path.

Table 5.3. Position reconstruction results – Tracer is moving

Actual Position (in cms)		**Reconstructed position** (in cms)		**Reconstruction error** (in cms)	
X co-ordinate	Y co-ordinate	X co-ordinate	Y co-ordinate	X co-ordinate	Y co-ordinate
0	0	-0.12	0.37	0.12	0.37
13.97	0	14.56	0.32	0.59	0.32
0	13.97	-0.19	13.5	0.19	0.47
5.39	5.39	5.05	5.1	0.34	0.29

Reconstruction accuracy can be further improved by using stronger radioactive tracer particle, reducing scanning speeds of collimated detectors, demonstrating in smaller size test reactors etc. The results of preliminary operational feasibility experiments suggested that it is possible to use RPT calibration technique to develop dynamic and non-invasive calibration methodology for the RPT technique. However, additional experimentation with a stronger radioactive source and in test reactors of different sizes needs to be carried out to further demonstrate RPT calibration equipment's operational feasibility and improve its accuracy.

5.4 ADVANTAGES AND LIMITATIONS OF NOVEL AND DYNAMIC RPT CALIBRATION TECHNIQUE

Previously described and newly developed RPT calibration technique has some advantages and disadvantages which are discussed in detail in next sub-section

5.4.1. Advantages of RPT Calibration Equipment. The main advantages of newly developed RPT calibration technique are as follows.

1. RPT Calibration technique can identify the position of a tracer particle in a non-invasive manner. Using RPT calibration equipment, it is possible to carry out *in-situ*

calibration in a non-invasive manner and has a potential for use in industrial applications. However, a lot of work needs to be carried out to demonstrate its operational feasibility in different multiphase systems and to improve its accuracy.

2. With the help of RPT calibration technique, it is possible to carry out RPT calibration and actual RPT experiments simultaneously.
3. Moving platform, on which collimated detectors are mounted, can be fixed at different heights and calibration positions corresponding to instances when the moving tracer particle crosses horizontal plane of the moving platform can be derived. This kind of design of RPT experiments helps to overcome limited tracking capability in vertical direction as reported in previous studies (Shehata, 2005).

5.4.2. Limitations of RPT Calibration Technique. The main limitations of RPT calibration technique are as follows:

1. Due to the use of collimators with narrow slit widths, counts recorded in the collimated detectors are reduced significantly and this demands use of a stronger radioactive tracer particle and or placing collimated detectors close to the multiphase system. However, use of a stronger radioactive source might lead to a saturation of fixed non-collimated detectors. This can be avoided by placing fixed non-collimated detectors away from the multiphase system.
2. Usually, moving platform is fixed at certain height and calibration positions at that height are derived when the tracer particle crosses horizontal plane of a moving platform. Hence, it is not practical to obtain large number of calibration positions with the help of RPT calibration technique. Use of multiple moving platforms, each having three collimated detectors, can provide large number of calibration positions at

different heights simultaneously. A few number of experimental calibration positions obtained using RPT calibration technique can be combined with Monte-Carlo method based simulations or can be used to estimate model parameters of a semi-empirical model (Equation 4.6) discussed and used earlier in sub-section 4.2.6.2, which is a mechanistic simplification of an actual complex mathematical model relating counts rate with the tracer-detector distance. However, additional work needs to be carried out to demonstrate this hybrid approach.

5.5 SUMMARY

As a part of this work, design and development of novel and dynamic RPT calibration equipment, which is a synergistic combination of fixed non-collimated detectors based RPT technique and collimated detectors based RPT technique, was carried out. The conceptual and engineering design of RPT calibration equipment, its various systems and sub-system was described in detail. Typical counts rate response of collimated detectors during a swinging movement shows a peak in the counts rate corresponding to an instant when the plane containing slit in the collimator aligns with the tracer particle. This principle was used to identify unknown tracer position co-ordinates in a non-invasive manner. RPT Calibration equipment was implemented around continuous pebbles recirculation experimental set-up and its operational feasibility was demonstrated by carrying out two sets of experiments. In 1^{st} set of experiments, tracer particle was held stationary at known locations with the help of a manual calibration apparatus. In 2^{nd} set of experiments, tracer particle was moved vertically downwards along a straight line path in a controlled manner with the help of a manual calibration

apparatus and by releasing attached string. The obtained reconstruction results about tracer particle position were compared with actual known position and reconstruction errors were estimated. It suggested that it is possible to identify tracer position using RPT calibration equipment with a maximum reconstruction accuracy of 5.9 mm. This new equipment development is a first and important step towards making RPT technique viable for practical applications. However, additional work needs to be carried out to demonstrate operational feasibility of this equipment in different multiphase systems of various sizes and to improve upon its reconstruction accuracy.

6. DISCRETE ELEMENT METHOD BASED INVESTIGATION OF GRANULAR FLOW IN A PEBBLE BED REACTOR

The flow of pebbles in a PBR is a good example of slow and dense type granular flow. Experimental benchmarking investigation of such flows to validate models and simulations using conventional optics based techniques has certain limitations and hence; radio-isotopes based flow visualization techniques such as RPT are suitable for such investigation. It is impractical to carry out experimental investigation in an actual scale PBR due to the large scale and safety issues. However, experimental benchmarking study in a scaled set-up mimicking cold flow operation of a PBR is possible and feasible. On the other hand, discrete element method (DEM) based simulations are capable of providing wealth of information about granular flow in an actual scale PBR but needs to be validated first using benchmark experimental data. This is one of the main objectives of this PhD work. In current work EDEM ^{TM} (Experts in Discrete Element Method - a commercial DEM code from DEM solutions Ltd., UK) was used to simulate a slow and dense granular flow and the experimental results discussed earlier using RPT technique are used as a benchmark data to evaluate the DEM results as part of the models and simulations validation steps.

6.1. DISCRETE ELEMENT METHOD

Discrete element method (DEM) is a numerical approach based upon the force balance method and is used to compute the motion of a large number of particles (Cundall and Strack, 1979). In DEM, all particles are tracked individually by taking into

account all the forces acting on each particle and finding the resultant accelerations, velocities and displacements of each particle. It is based on soft sphere approach, proposed by Cundall and Strack (1979). This soft sphere approach allows particles to deform during contact. However, particles are treated as a rigid body in DEM and their deformation during contact is taken into account in contact force models. DEM calculations alternate between the application of Newton's second law of motion and force-displacement law *also known as* contact force model at the contact points. The linear and angular momentum balance according to Newton's second law for the i^{th} particle can be given by (Iwashita, and Oda, 1998, Zhou et al., 1999, Rao and Nott, 2008)

$$m_i \frac{dv_i}{dt} = m_i b + \sum_{j=1}^{k_i} F_{ij} \qquad \text{Linear momentum balance} \quad (6.1)$$

$$I'_i \frac{d\omega_i}{dt} = \sum_{j=1}^{k_i} (T_{ij} + M_{ij}) \quad \text{Angular momentum balance} \quad (6.2)$$

where,

m_i : Mass of particle 'i'

v_i : Linear velocity of center of mass of i^{th} particle

b : Body force per unit mass

F_{ij} : Force exerted on particle 'i' by a particle 'j' which is in contact with it

k_i : Number of particles in contact with particle 'i'

I'_i : Moment of inertia

T_{ij} : Torque exerted on particle 'i' due to the tangential component of the contact force between particles i and j and is given by

$$T_{ij} = R_{(i)}\boldsymbol{n} \times F_{ij} \qquad (6.3)$$

where, R_i is the radius of sphere i and $\times$ denotes the cross product of two vectors.

M_{ij} – Rolling friction torque exerted by particle *j* on particle *i*

The rolling friction torque $\boldsymbol{M_{ij}}$ is necessary to take into account hysteresis losses associated with the deformation of the particles during rolling (Zhou et. al, 1995). Linear velocities are measured with respect to a co-ordinate system which is at rest related to the surface of the earth whereas; angular velocities are measured with respect to a co-ordinate system, origin of which, coincides with the center of mass of particle 'i'.

Contact force model (expressions for F_{ij}) describes how the particles in contact are interacting with each other. It models particle-particle and container wall-particle interaction behavious. Contact force model provides closure equations to DEM based simulations and it involves contact forces components in normal and tangential directions.

$$F_{ij}=F_{n_{ij}}+F_{t_{ij}} \qquad (6.4)$$

where,

F_{ij} = Contact force for interaction between particle i and j

$F_{n_{ij}}$ = Normal component of contact force for interaction between particle i and j

$F_{t_{ij}}$ = Tangential component of contact force for interaction between particle i and j

The calculation of contact forces is carried out using phenomenological contact force models. There is a lack of contact force models developed from the first principles (Rao and Nott, 2008) and this demands assessment of available contact force models with benchmark experimental data.

After calculating contact forces at each contact point, Newton's second law of motion is solved to find out resultant accelerations of each particle from which new velocities and positions of each particle are found out using suitable integration schemes. Specialized numerical integration algorithms such as central difference time integration scheme, velocity Verlet and the leap-frog algorithm, Newmark-β method etc. are widely used in DEM methodologies (Rougier et al., 2004). The central difference numerical integration scheme is a second-order time integration scheme and its equations are as follows

$$v_{t+\Delta t/2} = v_{t-\Delta t/2} + \Delta t * a \quad (6.5)$$

$$r_{t+\Delta t/2} = r_t + \Delta t * v_{t+\Delta t/2} \quad (6.6)$$

where, $v_{t+\Delta t/2}$ is the new velocity at time $\mathrm{t} + \Delta \mathrm{t}/2$ and $v_{t-\Delta t/2}$is the velocity at time $\mathrm{t} - \Delta \mathrm{t}/2$, a is the acceleration evaluated at r_t, r_t is the position of particle at time t and $r_{t+\Delta t/2}$is the new position at time $t + \Delta t/2$.

6.1.1. Contact Forces. Figure 6.1 shows interaction of two particles i and j in contact with each other. These two particles are having radii of R_i and R_j respectively. These particles have linear and angular velocities of V_i, V_j and ω_i, ω_j, respectively. n_{ij} is the unit vector along the line joining center of particles i and j pointing from particle i towards particle j. r_i and r_j are position vectors of particle i and j respectively.

The normal overlap (ξ_n) between two particles can be calculated as

$$\xi_n = \left(R_i + R_j\right) - \left|r_i + r_j\right| \quad (6.7)$$

The unit vector n_{ij} along the line of contact pointing from particle i to particle j is

$$n_{ij} = \frac{r_j - r_i}{\left|r_i - r_j\right|} \quad (6.8)$$

The relative velocity ($V^{\overline{rel}}$) of the point of contact becomes

$$V^{\overline{rel}} = V_j - V_i + (\omega_j \times R_j) - (\omega_i \times R_i) \quad (6.9)$$

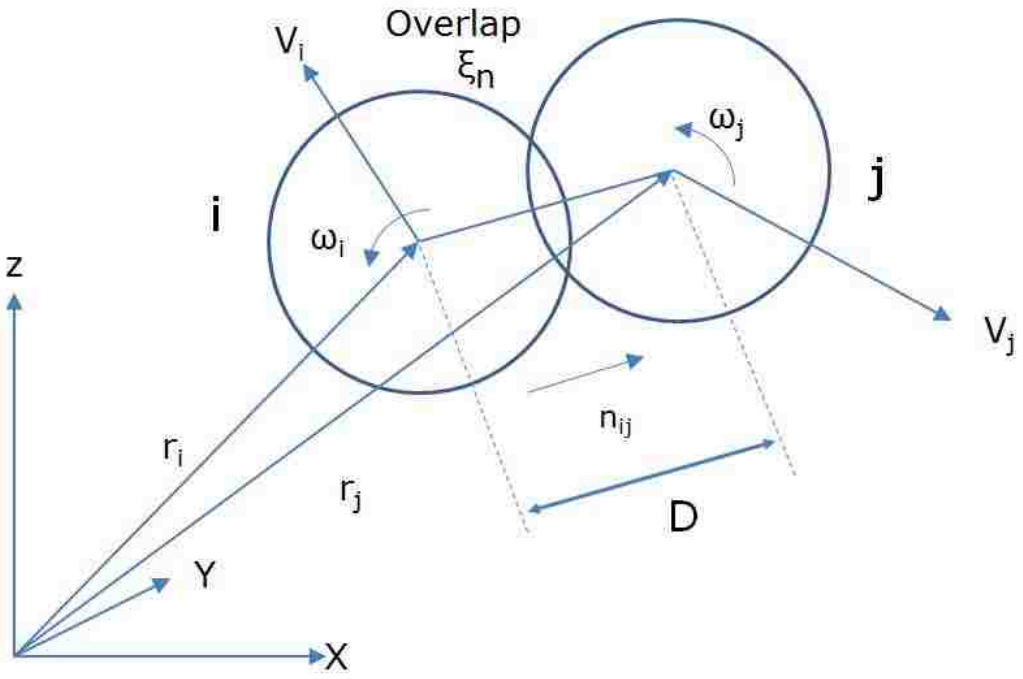

Figure 6.1 Typical particle-particle interaction

The normal($V_n^{\overline{rel}}$) and tangential ($V_t^{\overline{rel}}$) components of relative velocity are

$$V_n^{\overline{rel}} = (V_{ij}.n_{ij}).n_{ij} \quad (6.10)$$

$$V_t^{\overline{rel}} = (V_{ij} \times n_{ij}) \times n_{ij} \quad (6.11)$$

The overlap between the two particles is represented as a system of linear /non-linear springs, dashpots in both normal and tangential directions. It is convenient to calculate the contact forces (F_{ij}) spring and dashpot models (equation 6.12). The spring

(linear/non-linear) represents elastic restoration force and the dashpot represents dissipation of kinetic energy due to the inelastic collisions. Friction characteristics of particle-particle or particle-wall interaction in tangential directions are modeled using slider. Figure 6.2 represents the shcematic of the spring-dashpot system used to model particle contact forces (F_{ij}) in normal and tangential directions. The spring stifness coefficients in the normal and tangential directions are k_n and k_t , respectively. Similarly, the damping coefficients in the normal and tangential directions are C_n and C_t , respectively.

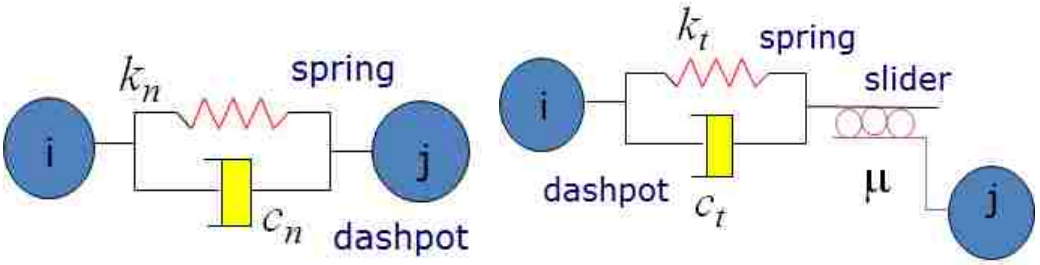

a b

Figure 6.2 Schematic of the spring-dashpot system used to model contact forces
a. Normal direction model b. Tangential direction model

In normal direction model, the spring and dashpot are in parallel. The spring provides an elastic restoration force while the dashpot dissipates energy during contact (Figure 6.2a). The normal component of the contact force ($F_{n_{ij}}$) exerted on particle in the normal direction is given by

$$F_{n_{ij}} = -\left(\underbrace{k_n \, \xi_n}_{F_n^s} + \underbrace{C_n V_n^{\overline{rel}}}_{F_n^d} \right) \quad (6.12)$$

where, k_n , C_n , $V_n^{\overline{rel}}$ and $\boldsymbol{\xi}_n$ are the stiffness(or "spring constant") , the damping coefficient, relative velocity and the overlap between particles, respectively, in the normal direction. The normal component of the contact force ($F_{n_{ij}}$) can be decomposed into the spring force (F_n^s) and the dashpot force (F_t^d). These forces are calculaed using suitable expressions discussed in next paragraphs.

In tangential model, the spring is in series with a coulombic friction sliding element. The spring allows the particle to respond elastically, while the sliding friction element allows particles to slide against each other (Figure 6.2b). The tangential force (F_t) exerted on particle in the tangential direction is given by

$$\boldsymbol{F_{t_{ij}}} = -\left(\underbrace{k_t \, \xi_t}_{F_t^s} + \underbrace{C_t V_t^{\overline{rel}}}_{F_t^d} \right) \quad (6.13)$$

where, k_t , C_t , $V_t^{\overline{rel}}$ and $\boldsymbol{\xi}_t$ are the stiffness(or "spring constant") , the damping coefficient, relative velocity and the overlap between particles respectively, in the tangential direction. The tangential component of the contact force ($\boldsymbol{F_{t_{ij}}}$) can be decomposed into the spring force ($\boldsymbol{F_t^s}$) and the dashpot force ($\boldsymbol{F_t^d}$). These forces are calculaed using suitable expressions discussed in next paragraphs. The overlap between the particles (ξ) and their relative velocities ($\mathbf{V}_{ij}$) in the normal and tangential directions are calculated first and then contact forces in the normal and tangential directions are evaluated through expressions specific to chosen contact force models . The Hertz–Mindlin contact model (EDEM user manual, 2010) was used in this work.

6.1.2. Hertz–Mindlin Contact Force Model. There are numerous contact force models available with EDEM ™. Hertz-Mindlin contact model (with no-slip between) is used widely and was used in current work. A contact force model using Hertzian theory to model normal direction interaction (Hertz,1882) and Mindlin theory to model tangential direction interaction (Mindlin and Deresiewicz, 1953) is known as *Hertz-Mindlin contact force model*. Figure 6.3 is a schmeatic representation of Hertz–Mindlin contact force model. Following are the main reasons for using this contact model in current work

- Represents dry granular media properly
- Default contact model in EDEM™ - accurate and efficient force calculation
- Consists of non-linear spring, dashpot and slider

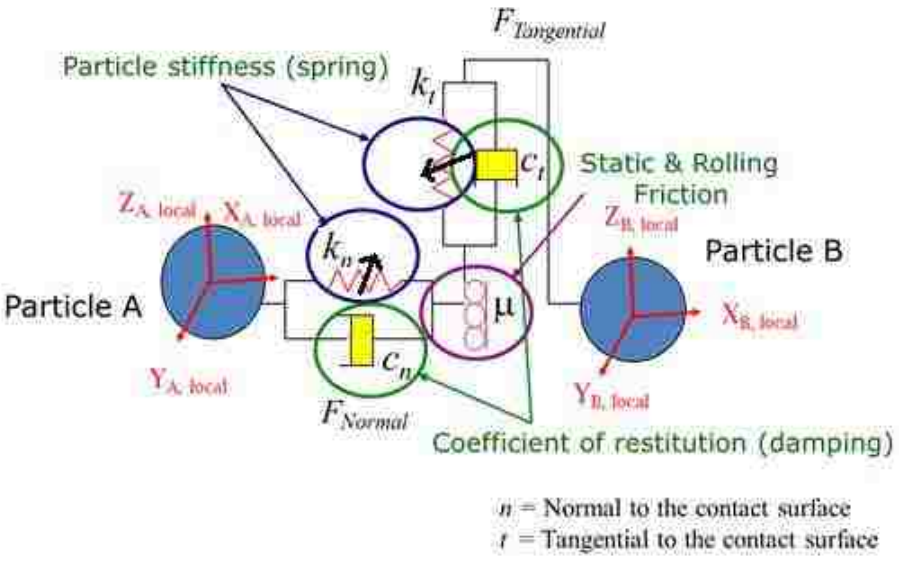

Figure 6.3. Schematic representation of Hertz–Mindlin contact force model

6.1.2.1 Normal contact force model. Normal component of Hertz–Mindlin contact force model is represented by the combination of non-linear spring and dashpot (Figure 6.4).

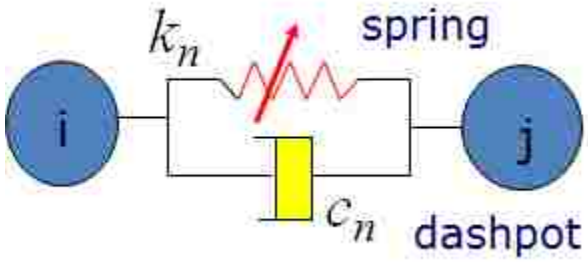

Figure 6.4. Normal Contact Force Model

The normal spring force ($\boldsymbol{F_n^s}$) is calculated as follows

$$F_n^s = \frac{4}{3} * \mathrm{E}^* * \sqrt{\mathrm{R}^*} * \xi_{\mathrm{n}}^{3/2} \qquad (6.14)$$

where, the equivalent Young's Modulus E* is defined as

$$\frac{1}{\mathrm{E}^*} = \frac{1-\nu_{\mathrm{i}}^2}{\mathrm{E_i}} + \frac{1-\nu_{\mathrm{j}}^2}{\mathrm{E_j}} \qquad (6.15)$$

The equivalent R* is defined as

$$\frac{1}{\mathrm{R}^*} = \frac{1}{\mathrm{R_i}} + \frac{1}{\mathrm{R_j}} \qquad (6.16)$$

where, E_i, ν_i, R_i and E_j, ν_j, R_j are the Young's modulus, Poisson ratio and radius of particles i and j in contact with each other.

The normal damping force ($\mathbf{F_n^d}$) is given by

$$F_n^d = -2 * \sqrt{\frac{5}{6}} * \beta * \sqrt{S_n * m^*} * V_n^{\overline{rel}} \quad (6.17)$$

where, $m^*$is the equivalent mass and is given by

$$\frac{1}{\mathrm{m}^*} = \frac{1}{m_i} + \frac{1}{m_j} \quad (6.18)$$

$V_n^{\overline{rel}}$ is the normal component of the relative velocity and is given by

$$\beta = \frac{lne}{\sqrt{ln^2 e + \pi^2}} \quad (6.19)$$

e as the coefficient of restitution and

$$S_n = 2 * E^* \sqrt{R^* * \xi_n} \quad (6.20)$$

6.1.2.2 Tangential contact force model. Tangential component of Hertz–Mindlin contact force model is represented by a combination of non-linear spring, dashpot and slider (Figure 6.7).

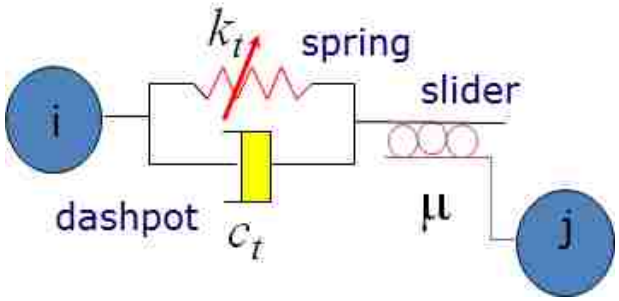

Figure 6.5 Tangential Contact Force Model

The tangential force (F_t) depends on the tangential overlap (ξ_t) and the tangential stiffness (S_t)

$$F_t^s = -S_t * \xi_t \quad (6.21)$$

where, S_t is defined as

$$S_t = 8G^* \sqrt{R^* \xi_n} \qquad (6.22)$$

G^* is the equivalent shear modulus. The tangential damping force ($\mathbf{F_t^d}$) is given by

$$F_t^d = -2 * \sqrt{\frac{5}{6}} * \beta * \sqrt{S_t * m^*} * \overline{V_t^{rel}} \qquad (6.23)$$

where, $\overline{V_t^{rel}}$ is the relative tangential velocity.

The tangential force (F_t) is limited by Coulomb friction force which is $\mu_{static} * F_n$. μ_{static} is the coefficient of static friction. If the tangential force (F_t) exceeds $\mu_{static} * F_n$, it is assumed that sliding is going to occur. The tangential contact force (F_t) is then replaced by $F_t = - \mu_{static} * F_n$. For Simulations in which rolling friction is important, it is accounted for by applying a torque (T_i) to the contacting surfaces

$$T_i = -\mu_{rolling} F_n R_i \qquad (6.24)$$

where, $\mu_{rolling}$ is the coefficient of rolling friction, R_i is the distance of the contact point from the center of mass. More information about the Hertz-Mindlin contact force model and associated equations can be found in related references (EDEM™ Manual, 2010; Tsuji et al., 1992).

6.1.3. Tasks Carried Out Under DEM based Study. The slow and dense granular flow in a PBR has been approximated by static packed beds in previous studies (duToit, 2002). Also, first step in any DEM based analysis is to pack the particles inside a confined geometry. Packing algorithms available with commercial codes such as EDEM™ are used without any detailed validation exercise. In most cases, average porosity results of numerical packing are compared with available experimental

benchmark data, which is not sufficient. Also, the nature of packing affects subsequent motion of particles in granular flow problems. Hence, there is a need to perform validation study of numerically simulated packing structures with the available experimental benchmark data which was carried out as a part of this work. The radial porosity profile is a good indicator of local bed structure and was used along with average porosity values for this validation study. Also, EDEM^{TM} based parametric sensitivity study of interaction properties was carried out as a part of this work. Such study helped in determining the sensitivity of packed bed structural properties to interaction characteristics and highlighted important interaction characteristics from experimental determination and reliable simulation point of view. The packing algorithm used in EDEM^{TM} demands proper input of elasticity (material properties) and frictional (interaction properties) parameters which are not readily available in the literature for materials and interactions of interest. It is recommneded to determine experimentally these paramters of interest, in case of it's unavailability, by developing simple experimental set-ups.

It is of interest to identify the flow pattern in bunker-type geometries (upper cylindrical portion with a conical bottom hopper). Typically, mass /funnel/ mixed type flows are observed in these kind of geometries. The flowing packings of pebbles were simulated in EDEM™. These simulations were analyzed for prediction of different flow regimes for different bottom cone angles, velocity profiles, trajectories of tagged pebbles etc. Obtained EDEM™ results for pebble trajectories and velocities were compared with RPT experiments results for an assessment of DEM contact force models. The main activities carried out as a part of this DEM based study are as follows

- Experimental determination of interaction properties of interest by developing simple experimental set-ups and use of these properties in EDEM^{TM} based simulations.
- EDEM™ based validation study of numerically simulated packing structures with available benchmark data and parametric sensitivity study of interaction properties.
- Characterization of velocity field in terms of trajectories, velocity profiles, etc.
- Identification of flow patterns i.e. mass/funnel/mixed flow in PBR type geometries.
- Assessment of contact force models used in DEM by comparing simulation results with experimental benchmark data

6.2. PACKED BEDS STRUCTURES

Proper representation of three dimensional complex packed beds structure is essential; since local flow and transport characteristics of the fluid flowing through the voids are closely coupled with the local bed structure. Literature review suggested that much effort has been made by many researchers in the development of computer simulations for random packing of mono-sized spheres inside cylindrical geometries (Visscher and Bolsterli, 1972; Clarke and Wiley, 1987; Cooper, 1988; Soppe, 1990; Nolan and Kavanagh, 1992; Bagi, 2005; Mueller, 2005; Salvat et al., 2005; Zamponi, 2008; Li and Ji, 2012). The packing results obtained using numerical packing algorithms have been validated with available experimental benchmark data (Mueller, 1992; Mueller, 2005).

6.2.1. Classification of Numerical Packing Algorithms. These numerical packing methods can be classified into two types: Sequential model and Collective model. In sequential model, spheres are packed one by one based on some rules to ensure randomness of packing and no overlap is allowed between spheres. Typical examples of sequential model include

- Monte Carlo based rejection sampling trial methods (Cooper, 1988)
- Gravitational deposition methods (Mueller, 2005)
- Domain triangulation methods (Bagi, 2005)

In collective model, spheres are generated randomly permitting overlaps, and collective rearrangement is carried out to eliminate overlaps. Collective packing algorithms are more time consuming as compared to sequential models. These numerical packing algorithms can also be classified into two types: Geometry-based model and Dynamics-based model. In geometry-based model, realistic forces are not taken into account, whereas in dynamics based approach realistic forces are taken into account. The packing in DEM is based on collective and dynamics approach and requires intensive computational efforts. It will be of interest to assess numerically simulated packing structures in EDEM^{TM} with that of one simulated using numerical packing codes which have been already validated. Mueller's packing code is based on sequential and geometry based approach (Mueller, 2005) and was used to provide benchmark data for this assessment study. This evaluation study provided recommendations/suggestions for accurate simulations of packed bed structures in EDEM™. This is essential; as the simulated packed beds are used in CFD analysis of packed bed or in DEM based study of solids movement for pebble bed reactor applications.

6.2.2. Structural Properties of Packed Beds. The structure of packed beds is very complex and affects local fluid, heat and mass transport phenomena (Zhang et al., 2006). Various structural properties such as mean/average/bulk porosity (ε_{avg}) (Kuroki et al., 2009), radial distribution of particle centers (Mariani et al., 2001), cumulative fraction of particle centers as a function of radial co-ordinate (Mariani et al., 2009), axially averaged radial porosity profile (Mueller, 1992; Mueller, 2005; Sederman et al., 2001), and co-ordination number (Silbert et al., 2002) can be used to characterize structure of packed beds.

Mean/average/bulk porosities (ε_{avg}) can be determined based on number of particles, volume of each particle and volume of the container. Traditionally, mean porosity, a global indicator of bed structure, has been used for validating numerically simulated packed bed structures which is not sufficient due to its averaging effect.

Axially averaged radial porosity variation profile is a signature characteristic of packed beds and a good indicator of the local bed structure. Axially averaged radial porosity variation profile exhibits typical shape of damped oscillations, with higher values of porosity/voidage at the wall and decreasing towards center (Figure 6.6). The local bed structure is crucial from transport phenomena point of view and local changes in porosity can lead to large variations in the predicted velocity profile, especially near the wall. Accurate knowledge of local porosity in packed beds is also important from heat transfer and stability analysis and control point of view.

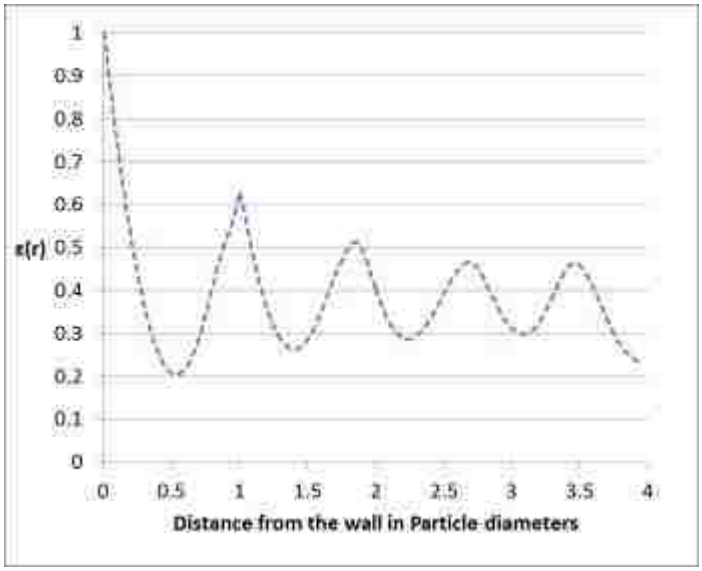

Figure 6.6 Axially averaged radial porosity variation profile (aspect ratio of 7.99) - EDEM^{TM} results

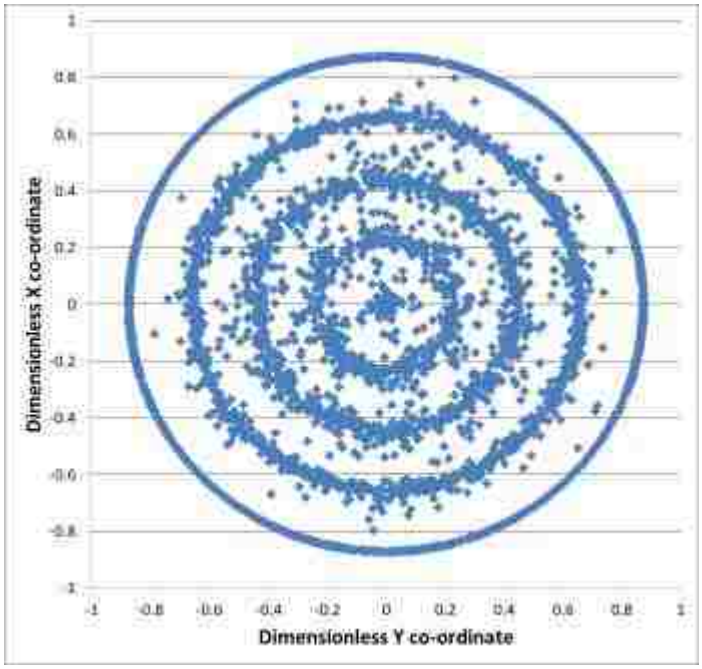

Figure 6.7 Distribution of particle centers (aspect ratio of 7.99) - EDEM^{TM} results

Distribution of particle centers, when viewed from the top, is a qualitative indicator of bed structure (Figure 6.7). There is a well ordered first layer against the wall. Almost all the sphere centers, in this first layer adjacent to the wall, are positioned at one sphere radius (one-half sphere diameter). It is impossible for sphere particle centers to exist in the region between the wall and one-half of a sphere particle diameter for mono-sized spherical particles. There are 2^{nd}, 3^{rd}, 4^{th} and so on layer of particles depending on aspect ratio of packed beds. In ideal situations, no sphere particle centers would exist between the first and second layer and so on. The location of these layers dictates the corresponding minima in the radial porosity variation profile. In actual packed beds, there is a dispersion of particle centers away from these ordered layers. It has been reported that that this dispersion is highly dependent on friction between particles. Distribution of particle centers is a qualitative indicator of bed structure and needs to be studied together with the radial porosity variation profile. Radial porosity variation profile along with mean porosity is a good indicator of local as well as global bed structure and hence was used in this validation study.

6.2.3. Need for Validation Study of Numerically Simulated Packing Structures. The local flow and transport properties are closely coupled with structural characteristics of packed beds. The input of bed structure, in terms of positions of the particle centers, is crucial for reliable CFD (Computational Fluid Dynamics) based analysis of single and two phase flows in packed beds. CFD based analysis is capable of providing detailed information about momentum, heat and mass transport phenomena occurring in packed beds (Mueller, 2005). Also, hydrodynamic and thermal models of packed beds require accurate knowledge about porosity profiles and associated solid

phase distributions (Mariani et al., 2009). Pore network modeling is increasingly becoming popular to study multiphase flows in porous media (Liapis et al., 1999, Meyers and Liapis, 1998). In these network models, void spaces are represented by a regular two- or three-dimensional lattice of wide pores connected by narrower throats. It solves fluid transport equations at the pore level. However, it requires complete description of packed beds structures in 3-D to map it onto a network of pores without sacrificing much of topographic information. The complete information about packed beds is usually provided in terms of center co-ordinates (x, y, z co-ordinates) and radius of each particle. Hence, the proper input of bed structure is required in various analyses and crucial for further reliable analysis. Hence, it is necessary to validate EDEM^{TM} simulated packing structures before performing EDEM^{TM} based numerical simulations of granular flow in a PBR.

6.3. EXPERIMENTAL DETERMINATION OF INTERACTION PROPERTIES

To assess EDEM™ based simulation results with corresponding experiments, all parameters involved in the simulations needs to be similar as that of in the experiments. A proper input of interaction parameters in DEM based simulations serves as a crucial link (plays a pivotal Role) between DEM based simulations and benchmark experiments as outlined in Figure 6.8.

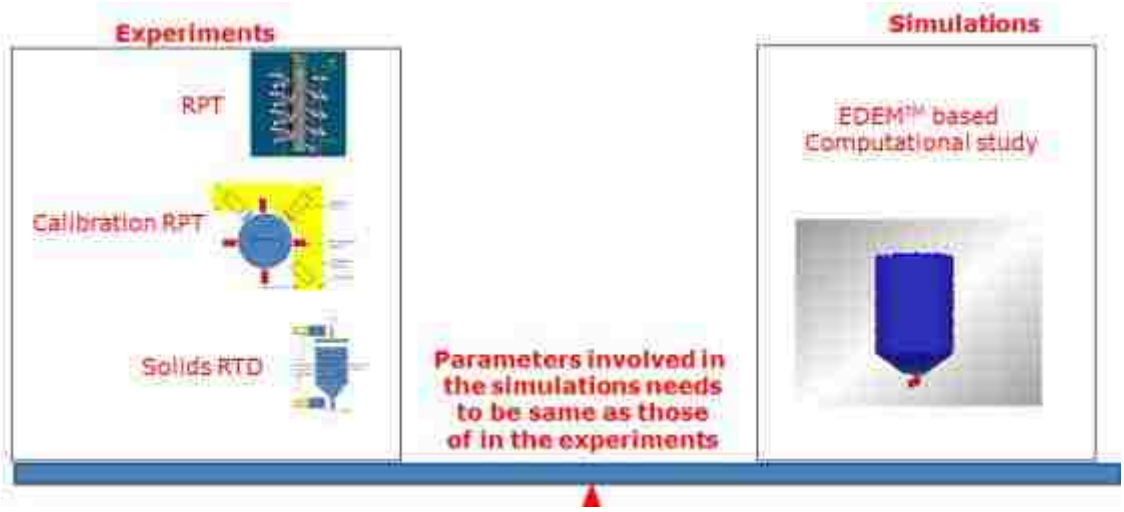

Figure 6.8 Fair assessment of DEM simulations with experiments

EDEM™ requires proper input of material properties such as density (ρ), Poisson ratio (ν), modulus of elasticity (E) and interaction properties such as coefficients of static (μ_{static}) and rolling friction ($\mu_{rolling}$) and the coefficient of restitution (COR). The static friction is the resistance that two solid objects will have before the onset of relative motion, and depends upon their respective surface roughness and the contact areas. It is expressed in terms of the coefficient of static friction (μ_{static}) (Rao and Nott, 2008). The rolling friction is a measure of the rolling resistance of a spherical object upon another spherical object or flat surface and occurs due to micro-slip at the contact. It is expressed in terms of the coefficient of rolling friction ($\mu_{rolling}$) (Bharadwaj et al., 2010). The coefficient of restitution is defined as the ratio of speeds of two objects before and after an impact (Rao and Nott, 2008). It has been reported that static friction is a key parameter and needs to be experimentally determined (Li et al., 2005; Khane et al., 2010). The interaction parameters of coefficient of static friction (μ_{static}) and coefficient of restitution

(COR) were determined by developing simple experimental set-ups involving the same materials as in the pebble bed test reactor. However, it is difficult to accurately measure coefficient of rolling friction and hence its values were chosen by referring to previous studies involving the same materials. These experimentally determined interaction parameters were used in the validation of EDEM™ simulated numerical packing and in the subsequent EDEM™ based simulations to properly model the flow of pebbles in a pebble bed test reactor.

6.3.1. Determination of Coefficient of Static Friction (μ_{static}). Static friction is the resistance that two solid objects will have before the onset of relative motion and it depends on their surface roughness and contact area.

A classical theory of friction, which treats the contact area as a point to point interaction, states that

$$\mu_{static} = \frac{F}{N} \qquad (6.25)$$

where μ_{static} is the coefficient of static friction, F is the frictional force, and N is the normal force. According to classical theory of friction, frictional effect between two particles made-up of same material and surface quality can be approximated as point-point contact for small contact area. Hence, the friction between two particles can be represented simplistically by a particle-plane wall interaction of the same material and surface condition. Hence, an experimental setup was developed as shown in Figure 6.9 which uses a cart with three glass marbles glued to its bottom. This cart was pulled along an acrylic and a glass surface to determine coefficient of static friction for glass-acrylic and glass-glass interaction.

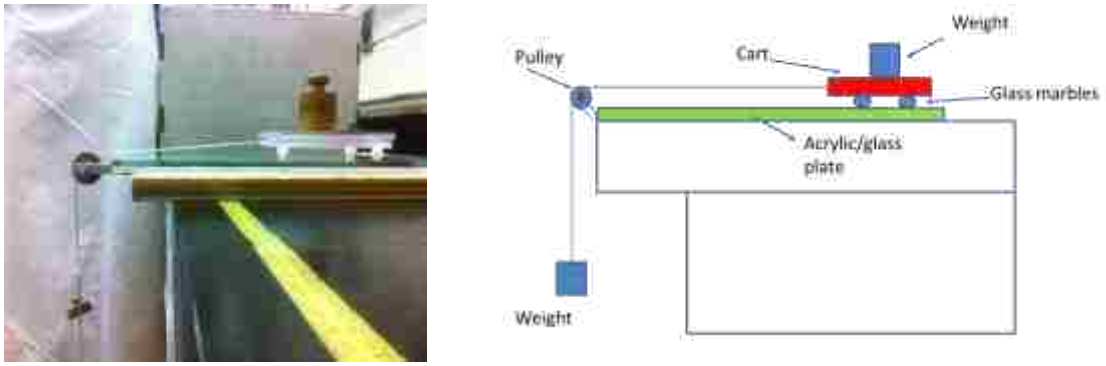

a. Picture of an actual set-up b. Schematic diagram of the set-up

Figure 6.9 Experimental set-up to measure static friction

A string was wrapped around the pulley with one end attached to the cart and the other attached to the pulling weight. In each trial, different amounts of weights were placed on top of the cart and weight at the pulling end side of the string were increased until the cart started moving from a stationary position. The values of the weights on the cart and the pulling end side were recorded in each case. Using this data, the coefficient of static friction was determined (Refer to Equation 6.23) for glass-glass and glass-acrylic interaction.

6.3.2. Determination of Coefficient of Restitution (COR). The coefficient of restitution (COR) is defined as the ratio of speeds of two objects before and after an impact. It can also be determined when an object is dropped on a stationary surface using the equation 6.26

$$COR = \sqrt{\frac{h}{H}} \qquad (6.26)$$

where, h is the height of the first bounce and H is the initial dropping height. A simple experimental set-up was developed where a glass ball was dropped from a certain height onto an acrylic and a glass surface. The height of the first bounce was recorded in each case. The COR was then calculated using equation 6.26. The measured values of μ_{static} and COR are tabulated in Table 6.1.

Table 6.1 Experimentally determined values of interaction parameters

Interaction	**Coefficient of Static Friction** (μ_{static})	**Coefficient of Restitution** COR
Glass-Acrylic	0.2178 ± 0.004	0.3818±0.072
Glass-Glass	0.2353 ±0.018	0.6455±0.072

6.3.3. Selection of Suitable Value of Coefficient of Rolling Friction ($\mu_{rolling}$)

Coefficient of rolling friction is one of the interaction parameters input to EDEM™. It is difficult to experimentally determine accurate value of this parameter and literature survey suggested a value of 0.005 is reasonable considering materials (Glass and acrylic) used in EDEM™ based simulations of a pebble bed test reactor.

These experimentally determined values of interaction parameters were used in EDEM™ based simulations of a pebble bed test reactor. This will assure fair assessment of EDEM™ based simulation results with corresponding experiments. EDEM™ based validation study of numerically simulated packing structures and parametric sensitivity study of interaction parameters was carried out and obtained results are discussed in next paragraphs.

6.4 SIMULATION OF PACKED BED STRUCTURES IN EDEM™: VALIDATION AND PARAMETRIC SENSITIVITY STUDY OF INTERACTION PROPERTIES

Most of the numerical packing codes used to pack spheres inside containers do not consider various interaction properties of the particles and/or containers. On the other hand, the DEM methodology considers different material and interaction properties and hence has the capability to simulate real system structural performance more precisely if proper input data is provided. In a discrete element method-computational fluid dynamics (DEM-CFD) coupled approach (Theuerkauf et al., 2006 ; Bai et al., 2009), DEM methodology is used to simulate the structure of packed beds and is subsequently imported to a CFD preprocessor to generate a mesh for CFD based analysis. A validation study of numerically simulated packing structures is essential before carrying out subsequent CFD based analysis. The main aim of this study is to validate numerically simulated packing structures in EDEM™ with available benchmark data. Mueller's numerical packing code (Mueller, 2005) is very well validated against experimental data about packed beds structure of spherical particles for wide range of aspect ratios and was used in this study. Traditionally, mean/average porosity (global indicator of bed structure) has been used for the validation of numerically simulated packed bed structures (Kuroki et al., 2009) which is not sufficient due to its averaging effect. An axially averaged radial porosity variation profile is a good indicator of local bed structure and was used along with mean porosity values for structural characterization of packed beds. The main objectives of this study are as follows:

- To make recommendations and/or suggestions about how to better simulate realistic packed bed structures in EDEM™ and henceforth perform additional reliable numerical analysis
- To perform a parametric sensitivity study of interaction parameters from a packed bed structural characterization point of view
- To highlight important interaction parameters which needs to be determined experimentally for the simulation of realistic packed beds in EDEM™

6.4.1. Simulation Set-up. The experimental work carried as a part of this work involved implementation of radioisotopes based technique such as RPT around a cold flow continuous pebble recirculation experimental set-up for the evaluation of solids dynamics. This continuous pebble recirculation experimental set-up, which simulates the flow of pebbles in a pebble bed test reactor, measures one foot in diameter and one foot in height. Glass marbles, ½" dia., model the pebbles and were packed inside acrylic test reactor. Obtained results of experimental investigation are serving as a benchmark data for EDEM™ based simulations of a PBR. EDEM™ based validation and parametric sensitivity study simulates reactor geometry (diameter aspect ratio, which is defined as the ratio of the diameter of the container to the diameter of the particles, in this case equal to 23.9) using glass marbles used in the experimental investigation. This study required an accurate input of material properties such as density, shear modulus and Poisson ratio, all of which were easily obtainable for most materials. The elastic properties of materials used in the current study are tabulated in Table 6.2. EDEM™ also requires an input of interaction properties such as the coefficients of static and rolling friction and the

coefficient of restitution (COR). The interaction parameters such as the coefficient of static friction and the coefficient of restitution were determined experimentally by developing simple experimental set-ups that use the same materials as those used in the pebble bed test reactor (Herbig et al., 2011).

Table 6.2. Elasticity properties of Glass and Acrylic **(Ref.** www.matweb.com**).**

	Glass	**Acrylic**
Density (kg/m^3)	1540	2170
Modulus of Elasticity (Pa)	$2.4*10^{10}$ Pa	$2.4*10^{10}$ Pa
Poisson Ratio	0.25	0.3

The determination of coefficient of rolling friction demands a cumbersome procedure and hence was not determined for this study. Instead, previously reported values of rolling friction in the literature for the interaction of the same materials were used in our EDEM^{TM} based simulations (Bhardwaj et al., 2010). The values of the various interaction parameters used in this study are shown in Table 6.3.

Table 6.3. Determined/chosen interaction parameters for interactions of interest.

	Glass-Glass	**Glass-Acrylic**
Coefficient of Static friction (μ_{static})	0.2178	0.2353
Coefficient of Rolling friction ($\mu_{rolling}$)	0.005	0.005
Coefficient of Restitution (COR**)**	0.3818	0.6455

6.4.2. Time Step. The time step chosen in EDEM^{TM} based simulations is a fraction of the critical time step for which the velocities and accelerations are assumed to be constant. A time step of 3.83E-06 sec, 60% of critical Rayleigh time step (Δt_c), was used in this EDEM^{TM} based study. Hence, resultant forces on any sphere will be determined exclusively by its interaction with the particles/wall with which it is in contact. The critical time-step is determined from the Rayleigh wave propagating on the surface of the smallest sphere and is given by:

$$\Delta t_c = \frac{\pi R_{min}}{\beta}\sqrt{\frac{\rho}{G}}, \qquad (6.27)$$

where ρ is the particle density, G is the shear modulus, β=0.8766+ 0.163ν and ν is the Poisson ratio. It took approximately 36 hours to achieve an equilibrium packing for each case using an Intel Core 2 Duo machine with 4GB of RAM.

6.4.3. Parametric Sensitivity Study of Interaction Properties. It is important to find out important interaction properties from packed beds structural characterization point of view and which needs to be determined experimentally, in case of their unavailability. To check sensitivity of packed beds structural properties to various interaction properties, simulation case matrix for an aspect ratio of 23.9 (Table 6.4) was prepared. Effect of interaction properties on structure of packed beds were investigated by carrying out EDEM^{TM} based simulations in which all cases from simulation case matrix were simulated. Simulation case matrix used two groups of parameters –the control group and the other known as test group. Experimentally determined values of coefficient of static friction ($\boldsymbol{\mu_{Static}}$), coefficient of rolling friction ($\boldsymbol{\mu_{rolling}}$) (value of which was chosen based on literature survey) and coefficient of restitution (**COR**) for glass-acrylic and glass-glass interaction formed the control group.

Table 6.4 Simulation case matrix

CASE	Particle-Wall interaction			Particle-Particle interaction			Average porosity Values
	Coefficient of Static Friction μ_{Static}	Coefficient of Rolling Friction $\mu_{Rolling}$	Coefficient of Restitution **COR**	Coefficient of Static Friction μ_{Static}	Coefficient of Rolling Friction $\mu_{Rolling}$	Coefficient of Restitution **COR**	ε_{avg}
1	✓	✓	✓	✓	✓	✓	0.4253
2	×	×	✓	×	×	✓	0.3856
3	✓	✓	✓	**H**	✓	✓	0.4359
4	✓	✓	✓	×	✓	✓	0.3847
5	×	✓	✓	✓	✓	✓	0.423
6	✓	✓	**H**	✓	✓	**H**	0.4037
7	✓	H	✓	✓	H	✓	0.4544
8	✓	×	✓	✓	×	✓	0.4136
9	×	×	×	×	×	×	0.3891
10	✓	✓	×	✓	✓	×	0.4265
11	×	×	×	✓	×	×	0.4123
12	✓	×	×	×	×	×	0.3951
13	✓	×	×	✓	×	×	0.425
14	H	✓	✓	✓	✓	✓	0.4283
15			Mueller's benchmark data				0.4192
16			Hypothetical case				0.4119

[a] ✓ - Determined value × - Neglecting the parameter **H** – High value

In test group, value of only one interaction parameter was varied i.e. either neglected or exaggerated as a big value (which may be non-physical) while the other parameters were maintained identical to the control group. In this manner, it was possible to identify and visualize effect of particular interaction parameter on structural properties and provided some general understanding about sensitivity of packed beds structure to interaction properties which is a crucial knowledge. EDEM^{TM} simulations were analyzed to provide results related to radial porosity variation profile and mean porosity values. These results were obtained for each test group and compared with control group results to check the effect of that particular interaction parameter.

Case 1 from simulation case matrix (Table 6.4) represents control group for this parametric study. Case 3 and 4 were test groups for coefficient of static friction between particle and wall. Case 6 and 10 were test groups for coefficient of restitution. Case 5 and 14 were test groups for coefficient of static friction between particles. Case 7 and 8 were test groups for coefficient of rolling friction. Case 9 neglects all interaction parameters used is EDEM^{TM} simulations, whereas case 11 and case 12 were simulated to check sensitivity of packed beds structural properties to static friction between particles and between particle-wall respectively. Case 13 was simulated to check combined effect of static friction between particles and between particle and the wall on the packed beds structure. Detailed information about value of each parameter for all the cases can be found in Table 6.3. Case 15 represents benchmark data obtained using Mueller's numerical packing code for aspect ratio of 23.9. Mueller's numerical packing code is validated against experimental data for wide range of aspect ratios. Mueller's packing code packs particles sequentially inside cylindrical container based on a dimensionless

packing parameter, whereas EDEM^{TM} makes use of force balance method. For each case, mean porosity (ε_{avg}) was determined by using information about number of particles, diameter of particles (dp), height (H) and diameter of cylindrical container (D). Obtained results about mean porosity for each case are tabulated in Table 6.4. Radial porosity variation profile was determined based on the methodology described by Mueller (Mueller, 1992) which uses position co-ordinates of particle centers and determines axially averaged radial porosity variation profile using integration of finite particle volumes intersecting with concentric rings. Axially averaged radial porosity variation profile is a signature characteristic of packed beds and was used along with mean porosity values to evaluate numerical packing results for different cases. Test groups results for each interaction parameter were compared with results obtained for control group to check the sensitivity of bed structure to that particular interaction parameter. These results are presented in next paragraphs.

6.4.3.1 Sensitivity of packed bed structure to static friction. Static friction between particles and between particle and wall are important interaction parameters and their effect on structure of packed beds was checked separately, whereas effect of COR and rolling friction on packed bed structure was studied collectively for particle-particle and particle-wall interaction.

6.4.3.1.1. <u>Static friction between particles</u>. Case 3 is a test group for static friction between particles in which high value of static friction between particles is considered, whereas case 4 is a test group for static friction between particles in which static friction is neglected. Case 1 is a control group which uses determined interaction parameters from Table 6.2. Figure 6.10.a. compares radial porosity variation profiles for

cases 3, 4 and 1. By neglecting friction between particles (Case 4), tighter packed beds are obtained which is also evident from average porosity values. Also, radial porosity variation profile for case 4 differs significantly when compared with case 1 at all radial positions. On the other hand, high value of static friction between particles (Case 3) damps out porosity variation profile quickly while moving towards the center. Also, average porosity values found to be higher than case 1 (control group) which indicates that loosely packed beds are obtained for higher value of static friction between the particles. It is evident that static friction between particles is a crucial input parameter from accurate packed bed structural characterization point of view. EDEM^{TM} based simulations must be provided with an accurate input of coefficient of static friction between the particles which can be determined experimentally for interactions of interest. It also confirmed previously reported findings that friction inhibits closer packing of particles in packed beds (Mariani et. al, 2009).

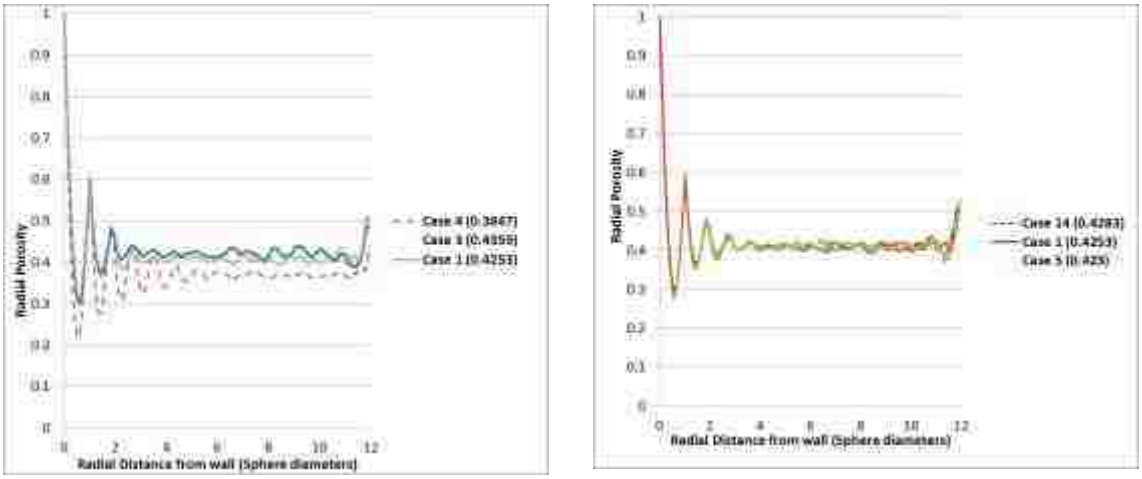

a. Static friction between particles b. Static friction between particle-wall

Figure 6.10 Sensitivity of packed bed structure to static friction

6.4.3.1.2. <u>Static friction between particle and wall.</u> Case 14 is a test group for static friction between particles and wall in which high value of static friction was considered, whereas case 5 is a test group for static friction between particle and wall was neglected. Figure 6.10.b. compares radial porosity variation profiles for cases 14, 5 and 1. Static friction between particle and wall doesn't affect average porosity values significantly, whereas radial porosity variation profile shows observable difference up to 3 particle diameters from the wall. There is no significant difference observed beyond 3 particle diameters from the wall up to the center. This indicates that particle-wall friction could be an important parameter, particularly in the region close to the wall. The average porosity values for case 1 and 5 are in closer agreement. However, their respective radial porosity variation profile indicated different local bed structures up to 3 particle diameters from the wall. By neglecting static friction between particle and wall, slightly tighter packed bed were obtained which is evident from radial porosity variation profile results and mean porosity values. This further illustrates that radial porosity variation profile is a signature characteristic of packed beds and should be used as an indicator for this validation study of numerically simulated packed bed structure.

6.4.3.2. Sensitivity of packed bed structure to COR. Figure 6.11 compares the radial porosity variation profiles for cases 10, 6 and 1. Case 6 is a test group for COR in which a high value of COR was considered, whereas case 10 was a test group for COR in which COR was neglected. COR values are usually between 0 and 1. A COR value of 0 represents a perfectly inelastic interaction, whereas COR value of 1 represents a perfectly elastic interaction.

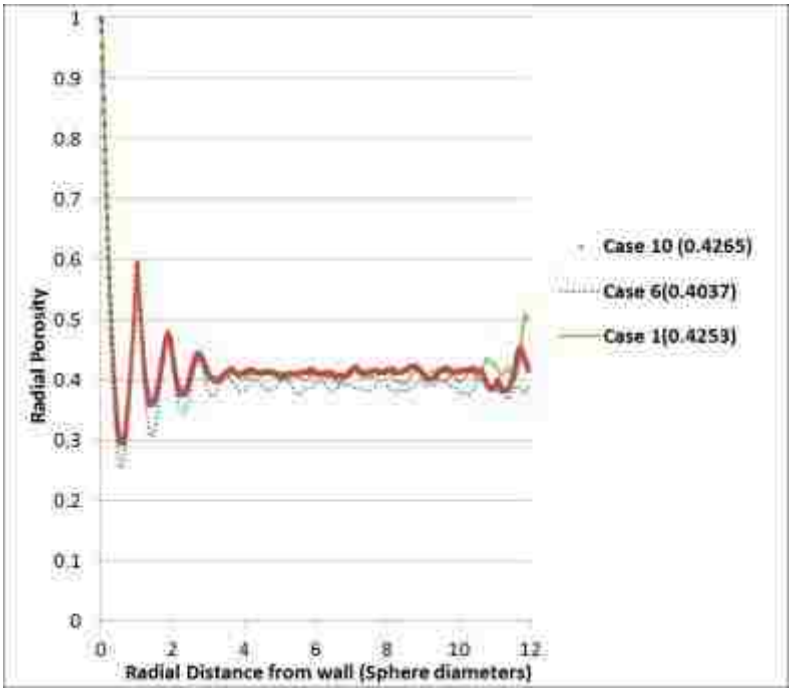

Figure 6.11 Effect of Coefficient of restitution (COR) on radial porosity variation profile (numbers in brackets represent average porosity values)

The case 6 porosity profile indicates that relatively tighter packed beds are obtained as compared with case 10 where a COR value of 0 is used. This is also evident from average porosity values. There is no significant difference observed between the porosity variation profile and average porosity values for cases 1 and 10. This suggests that packed bed structures are less sensitive to input of COR value in EDEM^{TM} based simulations and negligence of COR does not affect packed bed structural properties significantly. For higher values of COR, interaction becomes more of an elastic type which may cause closer packing of particles and result into dense packed bed structures. It suggested that a COR value of 1 should be avoided in EDEM^{TM} based simulations, if value of COR is unavailable.

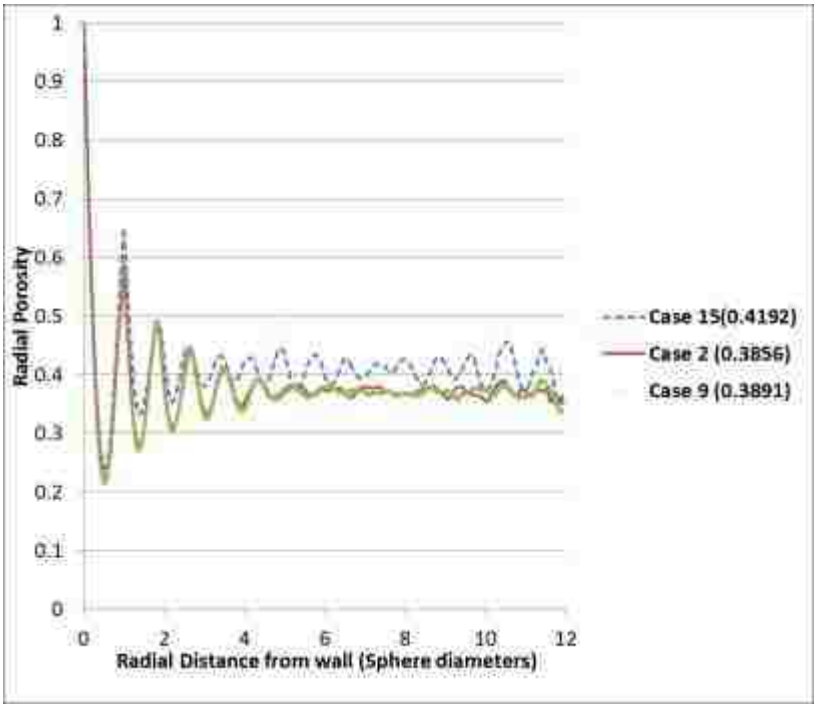

Figure 6.12 Comparison of radial porosity variation profile for Case 2 (Static and rolling friction parameters were neglected) Case 9 (COR along with static and rolling friction parameters were neglected).

This is necessary to avoid simulation of unrealistic tightly packed bed structures. Figure 6.12 compares cases 15, 2 and 9 to further test the effects of COR on packed bed structural properties. Case 9 neglects all interaction parameters used in EDEM^{TM} simulations. Case 2 neglects static and rolling friction parameters for particle-particle and particle-wall interactions. It supported previous observation that COR has negligible effect on the packed beds structural properties. It is confirmed by comparing porosity variation profile and average porosity values for cases 2 and 9. Also, it was confirmed that neglecting friction parameters results into more tightly packed beds.

6.4.3.3 Sensitivity of a packed bed structure to rolling friction. Case 7 is a test group for rolling friction where a high value of rolling friction was considered, whereas case 8 is a test group for rolling friction where rolling friction was neglected. Figure 6.13 compares the radial porosity variation profile results for cases 8, 7 and 1.

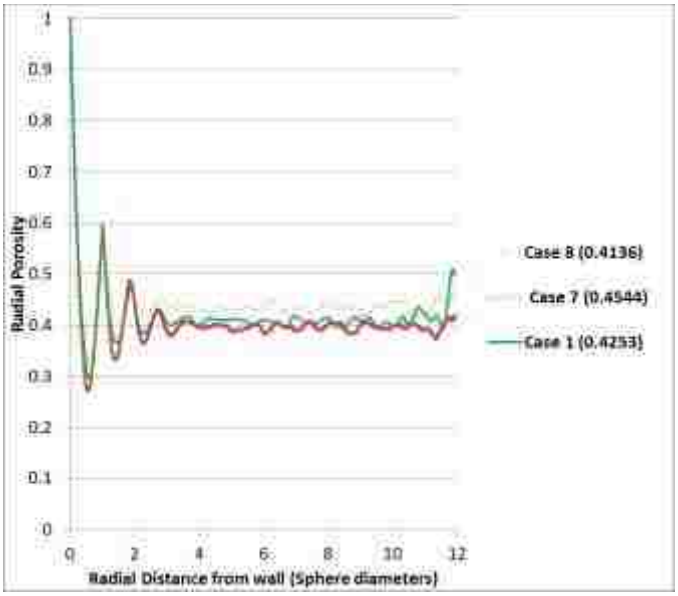

Figure 6.13. Effect of rolling friction on radial porosity variation profile (numbers in brackets represent average porosity values).

Neglecting rolling friction (case 8) results into relatively closer packing when compared with cases 1 and 7 in which rolling friction was considered. A higher value of rolling friction means more resistance to rolling motion between particles or between particles and the wall, which inhibits closer accommodation of particles. Loosely packed beds were observed when a higher value of rolling friction was used in case 7. The rolling friction value used in case 7 was 200 times higher than the nominal value used in

these DEM simulations (1 versus 0.005). This suggested that packed bed structures are less sensitive to rolling friction when compared with static friction characteristics. The experimental determination of an accurate value of rolling friction for interactions of interest is more involved and time consuming task and some uncertainty always exists with experimentally determined values. Hence, it is reasonable to neglect rolling friction characteristics in EDEM^{TM} based simulations of packed beds, in case of its unavailability.

6.4.4. Validation Study - Comparison with Benchmark Data. A comparison between Mueller's benchmark data (case 15) and the control group (case 1) is shown in Figure 6.14. The average porosity values are found to be in close agreement. The porosity variation profile obtained for the control group matches with the benchmark data to a great extent.

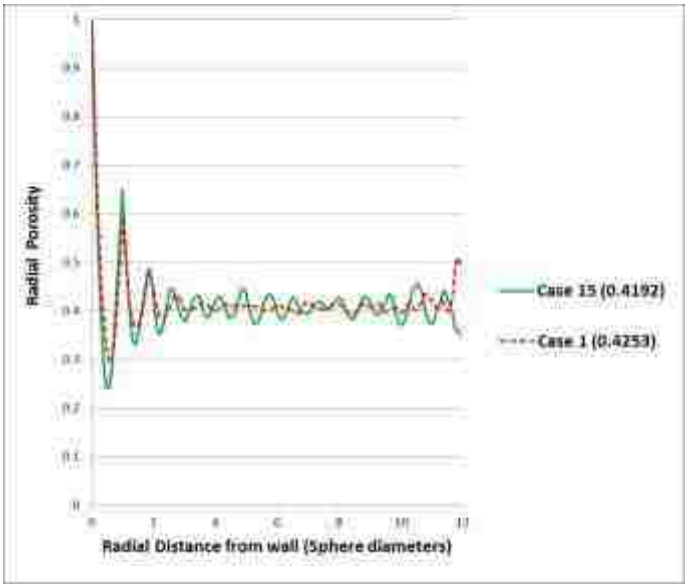

Figure 6.14 Comparison of radial porosity variation profile for Mueller's data and case 1 (which uses experimentally determined values of interaction parameters) (numbers in brackets represent average porosity values).

There are small observable mismatches up to 3 particle diameters from the wall but it matches to a greater extent beyond 3 particle diameters from the wall. The determination of the radial porosity variation profile requires input of particle center position information. The results of a hypothetical case (case 16) were obtained by combining particle center position information obtained for case 12 (where experimentally determined value of static friction between particle-wall was only considered) and case 11 (in which experimentally determined value of static friction between particles was only considered). The particle center position information from the cases 11 and 12 was combined in the following manner to obtain hypothetical case particle center position information. The first ring of particles close to the wall was generated using position data for case 12 (where only experimentally determined value of static friction between particle and wall was considered) and the remainder of particle position data was obtained from case 11 (in which experimentally determined value of static friction between particles was only considered). Figure 6.15 shows comparison of radial porosity variation profiles obtained for cases 1, 13, 15 and 16. Case 13 considers particle-particle and particle-wall static friction, whereas other interaction parameters such as COR and rolling friction were neglected.

The radial porosity variation profile for cases 13 and 1 are found to be in good agreement, as are the mean porosity values. Case 13 under-predicts the near-wall porosity variation profile as compared to benchmark data, which could be the main reason for slightly different average porosity values. There is a good match observed between the radial porosity variation profile for cases 15 (Mueller's benchmark data) and 16 (hypothetical case) and the mean porosity values are found to be in good agreement. The

hypothetical case results suggested that static friction for particle-particle and particle-wall interaction is an important parameter. If static friction between particles and particle-wall was considered collectively (case 13), it failed to match with benchmark data (case 15) especially in the near-wall region.

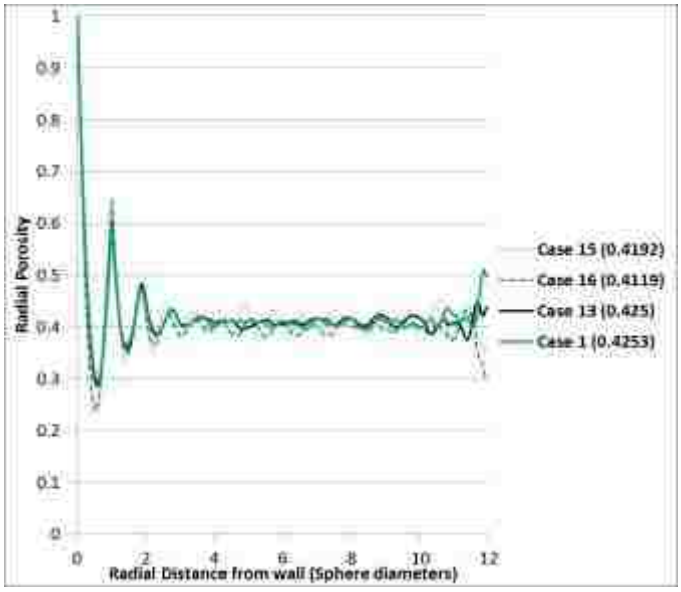

Figure 6.15 Comparison of radial porosity variation data between case 15 (Mueller's benchmark data), case 1 (which uses experimentally determined values of interaction parameters), case 16 (hypothetical case) and case 13 (which considers only static friction between particles and particle-wall).

This indicated that even though static friction for particle-particle and particle-wall interaction is important; considering it collectively fails to match with the benchmark data. On the other hand, the hypothetical case (case 16) considered static friction between the particle and the wall in the near wall region and static friction between particles in the region away from the wall. Case 16 simulated benchmark data

results to a greater extent and suggested a possibility of differential role played by static friction characteristics. In future, additional DEM simulations based comprehensive study for a wide range of aspect ratios may be required to further investigate the differential role played by static friction characteristics.

Existing empirical correlations for the mean porosity assumes that only diameter aspect ratio (ratio of container diameter (D) and particle diameter (d_P)) controls the packed beds structure (Theuerkauf et al., 2006). Results of this validation and parametric sensitivity study suggested that existing empirical correlations should include static friction characteristics in addition to diameter aspect ratio (D/d_P).

6.5. EDEM^{TM} BASED STUDY OF PEBBLES FLOW IN A PBR

Interaction properties required for EDEM^{TM} based simulations of granular flow in a PBR were determined experimentally by developing simple experimental set-ups. As a part of this work, investigation of granular flow in a PBR was carried out using EDEM^{TM}. The granular flow encountered in a PBR is slow and dense in natures where understanding about pebbles movement is crucial. The slow and dense granular flow was studied in the past (Choi et al., 2004) by faster flow regime in which particles drain from the vessel under gravity. The overall flow rate was found not to alter the geometry of the flow profile. The continuous pebbles recirculation experimental set-up is having control over pebbles exit flow rate and allows mimicking slow and dense granular flow. It is impractical to mimic such a slow flow in EDEM^{TM} due to intensive computational requirements. Hence, a faster flow regime without control over exit flow rate was simulated in EDEM^{TM} and is explained in next sub-section.

6.5.1. Simulation Set-up. In this EDEM^{TM} based simulation study, continuous pebble recirculation experimental set-up was modeled in a simplistic manner as a cylinder with conical bottom having an opening for draining of the marbles. In EDEM^{TM} based simulations, marbles drain under the influence of gravity as it is unrealistic to simulate slow granular flow in a PBR with the available computational resources. Obtained results were assessed using benchmark data of RPT experiments. The Hertz-Mindlin contact model (EDEM user manual, 2010) was used to model particle-particle and cylinder wall-particle interaction. Material properties and interaction parameters from table 6.2 and 6.3 were used in these simulations. The initial filling of test reactor geometry was carried out by blocking the bottom opening in the cone with a plate. The particles were generated randomly and allowed to settle down under gravity until static equilibrium condition was reached. After complete filling, the bottom plate was removed and draining of marbles was initiated. Time step of 1.53E-05 sec was used. These simulations were carried out for two different geometries with bottom half-cone angles of 30° and 60° by maintaining the same exit opening diameter. Height (H) and diameter (D) of cylindrical portion were 12” for both the geometries. Figure 6.16 shows two different geometries used in this simulation study.

6.5.2. Results. Obtained simulation data for both the geometries was analyzed to get results about streamlines, velocity field, positions of tagged particles as a function of time, mass flow index (MFI) values to predict prevailing flow patterns etc.

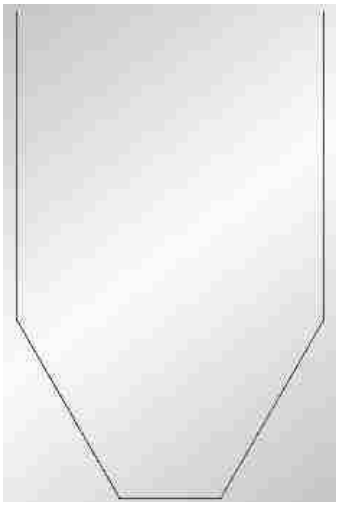

a. 30° bottom half-cone angle case

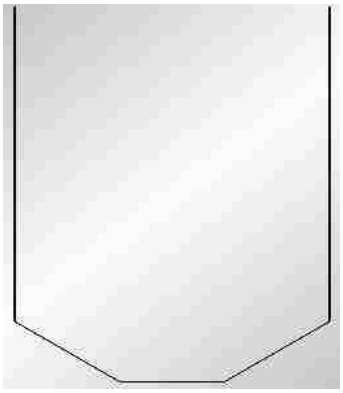

b. 60° bottom half-cone angle case

Figure 6.16 Simulation geometries

6.5.2.1. Streamlines results. Obtained streamlines results are presented in Figure 6.17. These streamlines results are obtained for a 10 mm thick slice. Streamlines results suggested that there is a plug-type flow in the top portion of cylinder, whereas converging-type flow near the bottom conical section. Particles close to the wall were found to be moving slowly as compared to rest of the particles For 30° bottom half-cone angle geometry, transition from plug to converging type flow is observed closer to the cylinder-cone transition point. For 60° bottom half-cone angle geometry, transition from plug flow to converging type flow is observed much earlier as compared to case of 30° bottom half-cone angle geometry. A fast moving zone was observed just above the exit opening in the both geometries.

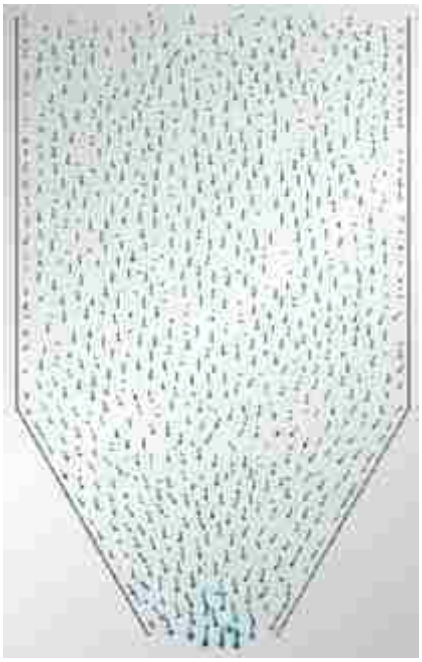

a. For geometry with 30° bottom half-cone angle

b. For geometry with 60° bottom half-cone angle

Figure 6.17 Streamlines results

6.5.2.2. Time-dependent positions of tagged particles. Figure 6.18 and 6.19 shows locations of tagged particles at different time instances. These particles were tagged at the start of discharge when they were at the same vertical level. It is clear from Figure 6.18 and 6.19 that particles at the center are moving much faster than the particles near the wall for both geometries. Also, a comparison between relative positions of tagged pebbles confirmed a plug type flow in the upper cylindrical region. Figure 6.18 suggests that pebbles are moving as a solid mass in the upper cylindrical region and has nearly uniform velocity profile except for a boundary layer effect. This has been further confirmed by simulation results for velocity radial profile.

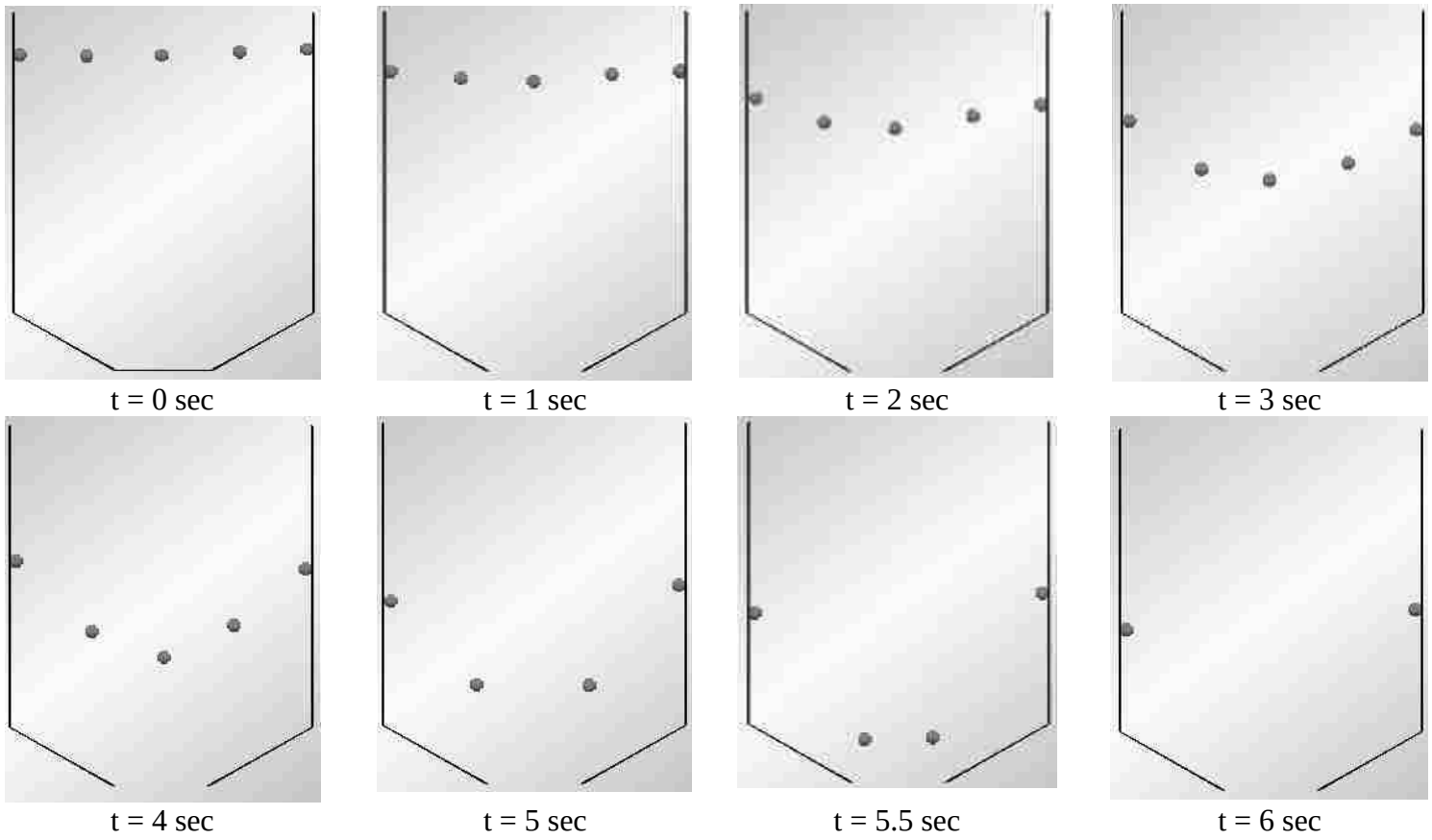

Figure 6.18 Time-dependent positions of tagged particles- for 60° degree cone angle

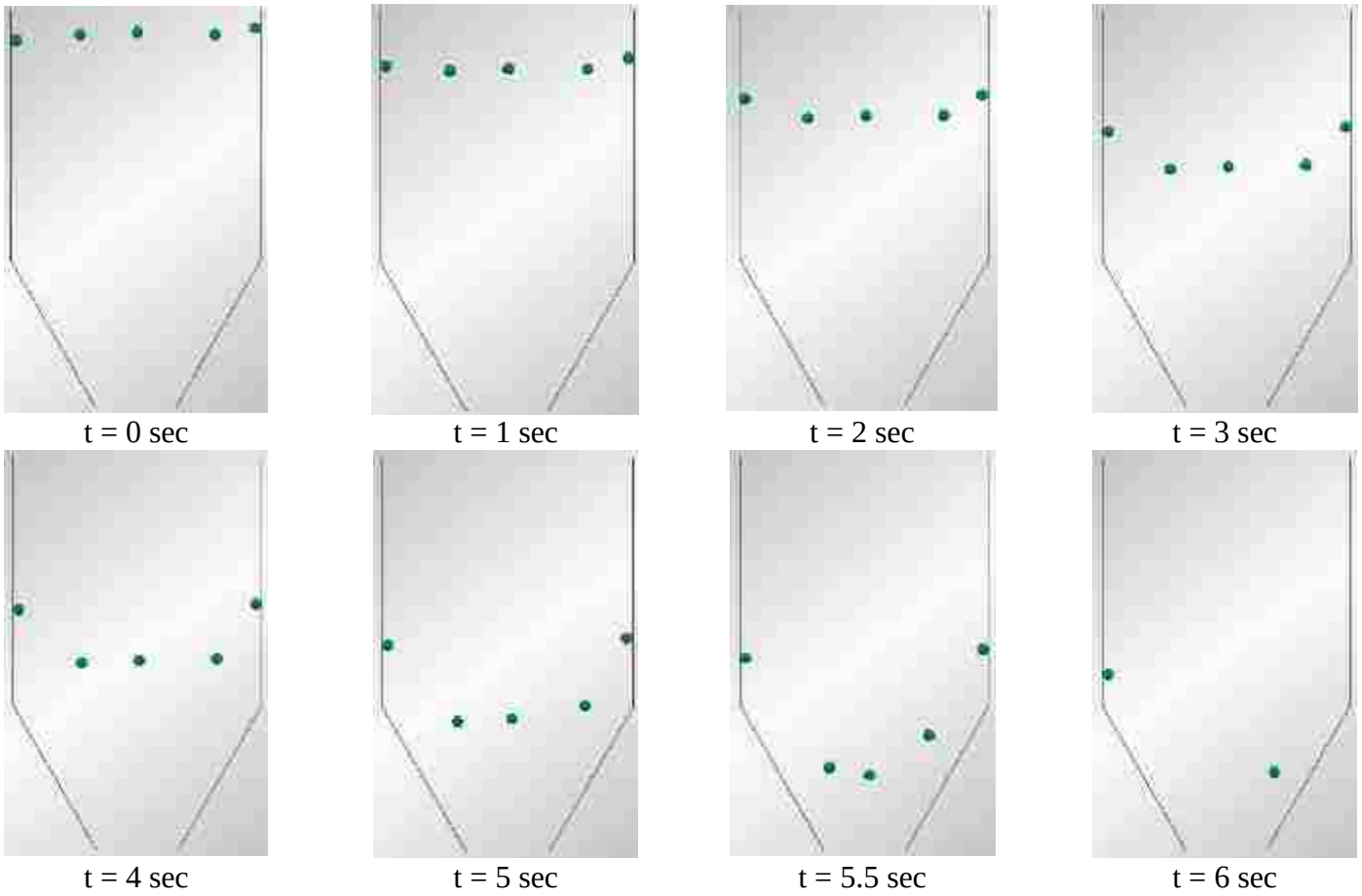

Figure 6.19 Time-dependent positions of tagged particles – for 30° degree cone angle

A pronounced concavity in relative positions of tagged pebbles is observed. This is due to the faster movement of particles at the center as compared to the particles at the wall. This pronounced concavity is observed predominantly in geometry with 60° half-cone angle. Also, this has been confirmed by velocity radial profile results of RPT experiments. M.I.T experiments were not able to capture this pronounced concavity in relative positions of particles at same instant of time. This pronounced concavity is a result of prominent difference in downward velocities of particles which seems to be a function of radial distance from the Centre of a test reactor. Particles at the Centre are having higher velocities as compared to particles near the wall and this resulted into pronounced concavity in relative positions of tagged particles and also in velocity radial profile. This also suggests a possibility of funnel type of flow in test reactor geometry with 60° half-cone angle. Direct observation of discharge process, which is described in next paragraphs, confirmed this observation.

6.5.2.3. Direct observation of discharge. Direct observation of discharge can provide useful information about various flow patterns in a PBR. A vertical slice of 10 mm thickness was selected and particles belonging to this slice were divided into different horizontal layers of same height. This was carried out at the beginning of the discharge process. These layers were colored alternatively with two contrasting colors (Red and Green). This division helped in identifying the movement of particles in respective layers and therefore, flow patterns in different geometries. Figure 6.20 shows snapshots of discharge process for two geometries at different instances of time. Plug type flow with a boundary layer of slower velocities was observed in the upper region and converging type flow was observed in the lower region.

60 ° angle

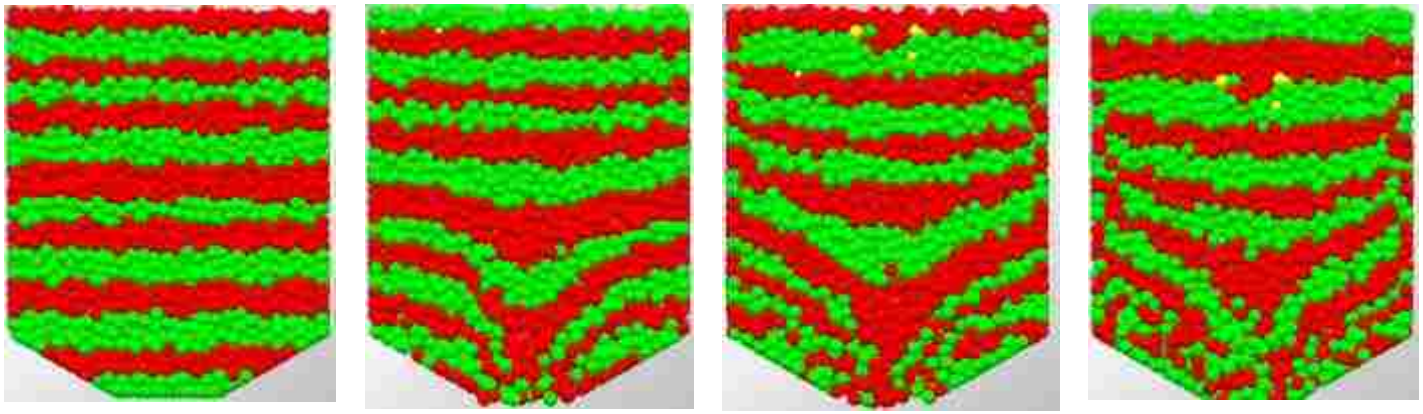

t= 0 sec **t= 1 sec** **t= 2 sec** **t= 3 sec**

30° angle

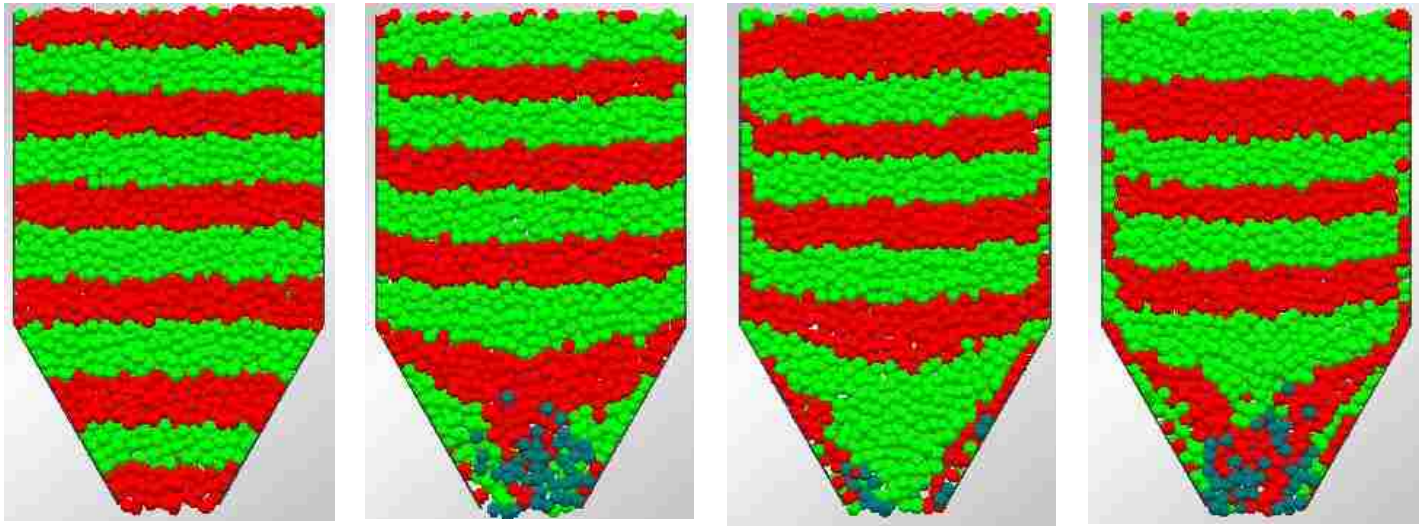

t= 0 sec **t= 1 sec** **t= 2 sec** **t= 3 sec**

Figure 6.20 DEM Simulation results – Direct observation of discharge

These observations are consistent with streamlines results and relative positions of tagged particles. Direct observation of discharge process suggested that transition from plug flow in the upper cylindrical region to converging type flow in the lower region is a function of bottom cone angle. This transition is happening somewhere near the cylinder-cone transition point for the case of geometry with 30° half-cone angle. In case of geometry with 60° half-cone angle, this transition is observed much before the cylinder-cone transition point. Direct observation of discharge did not indicate presence of any stagnant zones for both the geometries. However, particles close to the wall were found to be slowly moving and a mixing zone of red and green color particles was observed particularly for test reactor geometry with bottom half-cone angle of 60°. Mass flow of particles is observed when all the particles are moving simultaneously during the discharge. In funnel-type flow, particles within an internal channel above the bottom outlet are in motion, whilst the rest of the particles surrounding the channel are slowly moving /stationary. Mixed flow is an intermediate situation where the flow channel reaches the vertical wall at a point below the top surface (Nederman, 1992). More of mass-type flow is observed for test reactor geometry with 30° half-cone angle as compared to test reactor geometry with 60° half-cone angle. A funnel type flow is observed near lower conical portion for test reactor geometry with 60° half-cone angle. This funnel flow observation for 60° half-cone angle reactor geometry needs to be further verified by carrying out mass flow index (MFI) calculations and predicting prevailing flow patterns. There were some gray color particles observed in the conical section for test reactor geometry with 30° half-cone angle. These particles were not part of initial alternate layers in the selected vertical slice and might be diffusing into this

vertical slice as flow progressed. No such gray particles were observed for test reactor geometry with 60° half-cone angle. This suggested possibility of lateral diffusion of particles in the lower conical section, particularly for steeper bottom cones.

6.5.2.4. Velocity radial profile and mass flow index (MFI). Figure 6.21 represent the locations of control volumes (CV1 and CV2) in the test reactor geometries. These control volumes were used for plotting velocity radial profiles and MFI calculations. Figures 6.22a and 6.22b represents velocity radial profiles for both control volumes in geometries with half-cone angles of 30° and 60° respectively. These control volumes are 1 cm thick and are located at a depth of 11cm (CV1) and 27 cm (CV2) from the top of the test reactor. These control volumes are located at the same height, has same width and same number of bins in both test reactor geometries.

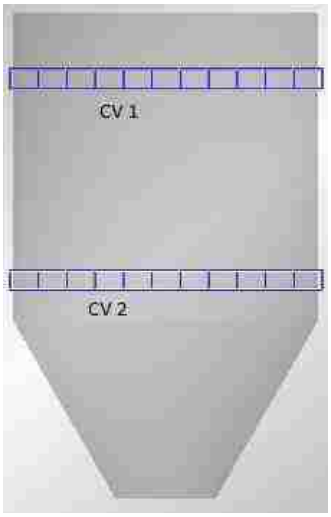

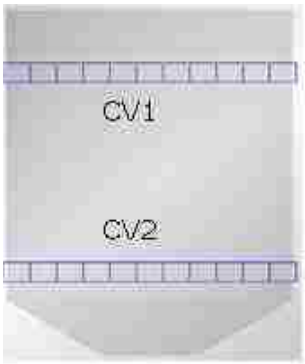

a. Test reactor geometry with 30° half-cone angle

b. Test reactor geometry with 60° half-cone angle

Figure 6.21 Locations of control volume

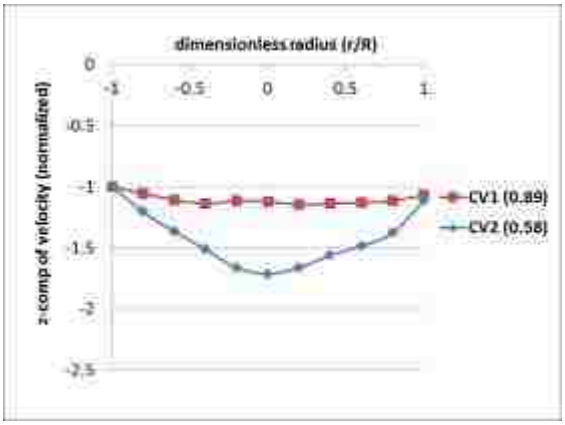

a. Test reactor geometry with 30° half-cone angle

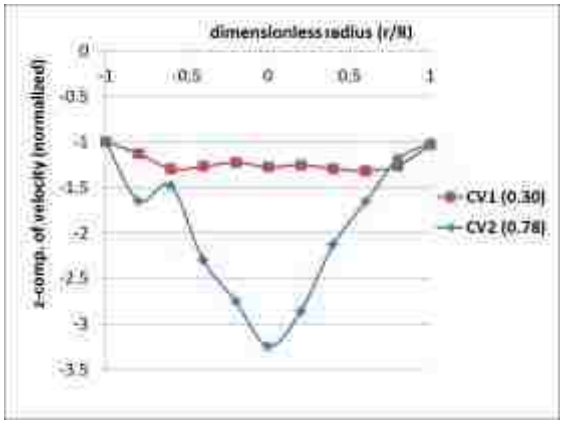

b. Test reactor geometry with 60° half-cone angle

Figure 6.22 EDEM^{TM} Results -Velocity radial profile
(values in bracket represents MFI values)

Velocity radial profiles for control volume 1 (CV1) for both test reactor geometries is nearly uniform, except for a slowly moving zone near the wall. This further confirmed observance of plug-type flow with a boundary layer in the upper cylindrical region. Velocity radial profile for control volume 2 (CV2) for test reactor geometry with 60° half-cone angle indicated pronounced concavity at the center in the velocity profile. Particles at the center were having much higher velocities as compared to the particles near the wall. On the other hand, velocity radial profile for control volume 2 (CV2) for geometry with 30° half-cone angle was parabolic in shape. Mass flow index (MFI) is an important indicator used to predict flow patterns and can be defined as the ratio of velocity of particles close to the wall to the velocity of particles at the center. If MFI>0.3, there is a mass flow. If MFI<0.3, it is an indicative of funnel-type flow. If MFI value is closer to 1, it suggests existence of uniform plug flow. Value of MFI in between 0.3 and

1 suggests existence of plug-type flow with a boundary layer effect. For test reactor geometry with 30° half-cone angle, MFI values obtained using velocity profiles predicted mass-type flow in CV1 and CV2. Direct observation of discharge also suggested mass-type flow pattern for test reactor geometry with 30° half-cone angle. For test reactor geometry with 60° half-cone angle, MFI values obtained using velocity profiles predicted mass flow for CV1 and funnel type flow for CV2. Direct observation of discharge also suggested the same for test reactor geometry with 60° half-cone angle (Figure 6.20). RPT results about velocity radial profile were compared with DEM simulation results in next paragraphs. Also, a comparison between pebble Lagrangian trajectories obtained using RPT and DEM simulation results was carried out.

6.5.2.5. Comparison of DEM simulation results with RPT experiments results. RPT results of velocity radial profile for test reactor are as shown in Figure 6.23a. RPT experiments were carried out for discrete number of seeding positions. Velocity radial profile results obtained using RPT experiments confirmed plug-type flow with a boundary layer effect for CV1. Also, a pronounced concavity in the velocity radial profile results has been observed for CV2. MFI values for both control volumes were calculated. Velocity of tracer near the wall was used as V_{wall} for MFI calculations. MFI values obtained using velocity profiles predicted existence of funnel-type flow for CV2, whereas existence of mass-type flow for CV1. The shape of velocity radial profile obtained using RPT experiments (Figure 6.23a) is in qualitative agreement with velocity profile results obtained using EDEM^{TM} simulations (Figure 6.22b). EDEM^{TM} based simulation results are in fair agreement with RPT experiments results.

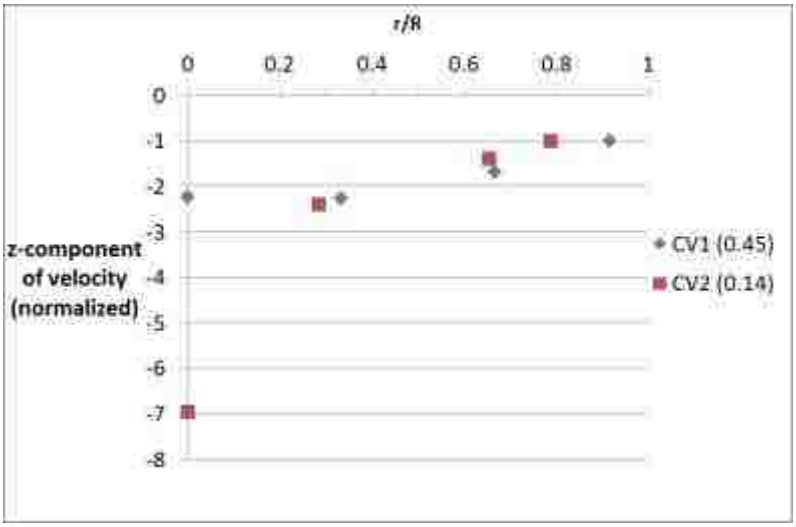

a. RPT results – Velocity profile

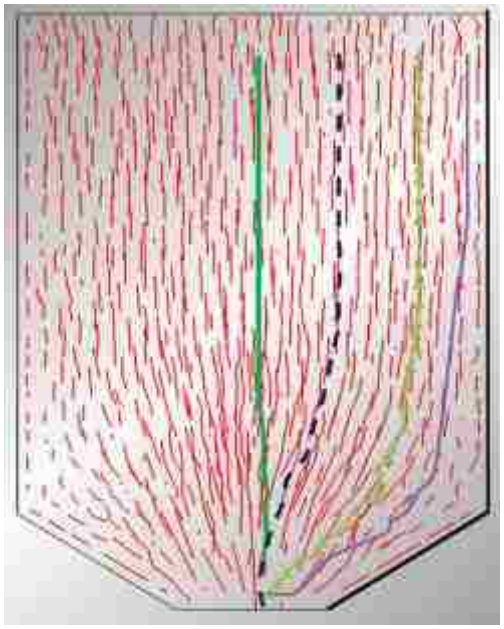

b. Comparison of streamlines results obtained using RPT experiments and EDEM^{TM} simulations

Figure 6.23 Assessment of DEM simulation results with RPT experiments

However, additional experimental investigation needs to be carried out for different sizes of test reactor, different bottom cone angles, and different sizes of pebbles to further assess DEM simulation results before using DEM for full scale reactor simulations.

6.6. SUMMARY

Discrete element method (DEM) based simulations are capable of providing crucial information about granular flows in a PBR. DEM requires calculation of contact forces which are evaluated using phenomenological models. There is a lack of contact force models developed from the first principles and this demands assessment of DEM simulation results using experimental benchmark data. DEM based study of granular flow in a PBR was carried out using EDEM^{TM} – commercial DEM based code. Following activities were carried out as a part of this EDEM^{TM} based study.

- Experimental determination of interaction properties such as coefficient of static friction and coefficient of restitution was carried out by developing simple experimental set-ups and these experimentally determined values were used in EDEM^{TM} based simulations.
- EDEM^{TM} simulated packing structures were evaluated with available benchmark data. Radial porosity variation profile along with mean porosity values were chosen for structural characterization of beds.
- EDEM^{TM} based parametric sensitivity study of interaction properties was carried out for diameter aspect ratio of 23.9 and important interaction properties from packed beds structural characterization point of view were

highlighted. It was found that static friction characteristics play an important role in packed beds structural characterization. Packed bed structures were found to be less sensitive to input of coefficient of restitution and coefficient of rolling friction. Results of this parametric study suggested that existing empirical correlations should include static friction characteristics in addition to diameter aspect ratio (D/d_P).

- Slow and dense granular flow in a PBR was studied by carrying out EDEM^{TM} based simulations. The continuous pebble recirculation experimental set-up was modeled in EDEM^{TM} in a simplistic manner as a cylinder with conical bottom having an opening for draining of the marbles. Characterization of velocity field in terms of streamlines, velocity profile, and various flow patterns was carried out. The effect of two different bottom half-cone angles of 30° and 60° on the flow field was studied.
- Results of streamlines, velocity radial profiles, and direct observation of discharge indicated a plug-type flow in the upper cylindrical region, whereas converging type flow near the bottom conical region. The transition from plug-type flow in the upper cylindrical region to converging type flow in lower region is found to be function of bottom cone angle. This transition found to be happening somewhere near the cylinder-cone transition point for the case of geometry with 30° half-cone angle. In case of geometry with 60° half-cone angle, smoother transition from plug-type flow to converging flow was happening much before the cylinder-cone transition point.

- Velocity radial profile for control volume 2 (CV2) for test reactor geometry with 60° half-cone angle indicated pronounced concavity at the center in the velocity profile. This indicated that particles at the center are having much higher velocities as compared to the particles near the wall. On the other hand, velocity radial profile for control volume 2 (CV2) for geometry with 30° half-cone angle is found to be parabolic in shape.
- Prediction of prevailing flow patterns i.e. mass/funnel/mixed flow in both test reactor geometries was carried out by calculating mass flow index (MFI) values. MFI values obtained using velocity profiles for test reactor geometry with 30° half-cone angle predicted mass type flow, whereas funnel type flow was predicted for test reactor geometry with 60° half-cone angle. These flow pattern predictions were consistent with direct observations of discharge and relative movement of tagged particles.
- Assessment of EDEM^{TM} simulation results using RPT experiments benchmark data was carried out and a fair agreement was observed in trajectory and velocity profile results. However, additional experimental investigation needs to be carried out for different sizes of test reactor, different bottom cone angles, and different sizes of pebbles to further assess DEM simulation results before using it for full scale reactor simulations.

7. CONCLUDING REMARKS AND RECOMMENDATIONS

In this section concluding remarks and summary of the key findings of this work alongside with recommendations for future work related to study of granular flow in pebble bed rectors are presented.

7.1. CONCLUDING REMARKS

As a part of this work, design and development of continuous pebble recirculation experimental set-up, mimicking flow of pebbles in a pebble bed reactor, is carried out. Experimental investigation of slow and dense granular flow of pebbles in a mimicked test reactor is carried out using advanced radioisotopes based flow visualization techniques such as RPT and RTD. RPT and RTD experiments provided benchmark information about Lagrangian trajectories in two and three-dimensions, overall and zonal residence times, overall and zonal average velocities, velocity radial profile, flow patterns etc. Also, DEM based simulations of granular flow in a test reactor are carried out using EDEM^{TM} – a commercial DEM code. The effect of two different half-cone angles of 30° and 60° on the pebbles flow field is studied. A comparison between DEM simulation results and experimental benchmark data is carried out for an assessment of contact force models used in DEM simulations. To make the RPT technique viable for practical applications, design and development of novel and dynamic RPT calibration equipment is carried out as a part of this work. The important achievements and findings related to various aspects of this work are summarized in this section. These findings are already discussed in detail in Sections 4 thru 6.

7.1.1. RPT and RTD Results. RPT and RTD experiments are carried out by seeding radioactive tracer particle at different initial seeding positions and provided useful information about Lagrangian trajectories, overall and zonal residence times, velocity field etc. RPT calibration experiments under different operating conditions of bed (moving/static packed beds) suggested that PBR could be represented by the examination of static packed beds, depending on the type of measurement and parameters to be investigated. Tracer initially seeded at the center moves faster and follows a shortest straight line path, whereas it moves slowly and follows a longest path when initially seeded near the wall. Overall residence time/transit number is found to increase with change in initial seeding position from center towards wall. The whole reactor is divided into three zones for analyses: Zone I (from the height of 10 to 20 cm), Zone II (from the height of 20-30 cm) and Zone III (from the height of 30 to 36 cm). It is found that zonal residence time for each zone increases with change in initial seeding position from center towards wall. The z-component of average zonal velocities is found to be smallest for initial seeding position of tracer close to the wall, whereas highest for initial seeding position of tracer at the center. It is observed that average zonal velocity of tracer gradually increases from zone 1 to 2 and further from zone 2 to 3 for all seeding positions. Radial movement of tracer particle is observed in zone 2 and zone 3 for all initial seeding positions except seeding position at the center. Overall average velocity results suggested faster movement of particles near the center with respect to particles near the wall. RPT results about velocity radial profile suggested existence of plug-type flow in the upper cylindrical region. A pronounced concavity in the velocity radial profile is observed in a region near cylinder-cone transition point. This is confirmed by results of

RPT about zonal residence times and average zonal velocities. It is noteworthy to mention that many of previous studies failed to capture this pronounced concavity in velocity radial profile. RPT and RTD experimental results provided benchmark data for assessment of DEM based simulation results.

7.1.2. Demonstration of Operational Feasibility of RPT Calibration Technique. As a part of this work, design and development of novel and dynamic RPT calibration technique, which is a synergistic combination of fixed detectors and collimated detectors based RPT techniques, is carried out. This technique makes use of three collimated detectors on a moving platform and its principle of operation to locate position of a tracer particle in a non-invasive manner. Additionally, this technique includes conventional fixed detectors which can record counts for identified tracer particle position. RPT Calibration equipment is implemented around continuous pebbles recirculation experimental set-up and its operational feasibility is demonstrated by carrying out two sets of experiments. In 1^{st} set of experiments, tracer particle was held stationary at known locations, whereas tracer particle was made to move vertically downwards in 2^{nd} set of experiments. Obtained position reconstruction results for two sets of experiments are compared with actual known position data and reconstruction errors are estimated. It is possible to identify tracer position in a non-invasive manner with reconstruction accuracy of 6mm using RPT calibration equipment. However, additional work needs to be carried out to demonstrate operational feasibility of this equipment in different multiphase systems and to improve upon its position reconstruction accuracy.

7.1.3. DEM Simulations Results. Discrete element method (DEM) based simulations, capable of providing crucial information about granular flows in a PBR, are carried out using EDEM^{TM} – a commercial DEM code. Experimental determination of interaction properties such as coefficient of static friction and coefficient of restitution is carried out by developing simple experimental set-ups and these experimentally determined values are used in EDEM^{TM} based simulations. EDEM^{TM} simulated packing structures are validated with available benchmark data. Radial porosity variation profile along with mean porosity values are chosen as indicators of bed structure for this validation exercise. EDEM^{TM} based parametric sensitivity study of interaction properties is carried out. It is found that static friction characteristics play an important role in packed beds structural characterization and suggested that existing empirical correlations should include static friction characteristics in addition to aspect ratio (D/d_P). Packed bed structures are found to be less sensitive to input of coefficient of restitution and coefficient of rolling friction.

The continuous pebble recirculation experimental set-up is modeled in EDEM^{TM} in a simplistic manner as a cylinder with conical bottom having an opening for draining of the marbles. The effect of two different half-cone angles of 30° and 60° on the flow field is studied. Results of streamlines, velocity radial profiles, and direct observation of discharge indicated a plug-type flow in the upper cylindrical region, whereas converging-type flow near the bottom conical region. The transition from plug-type flow in the upper cylindrical region to converging type flow in the lower region is found to be a function of bottom cone angle. This transition is happening somewhere near the cylinder-cone transition point for test reactor geometry with 30° half-cone angle. In case of geometry

with 60° half-cone angle, smoother transition from plug-type flow to converging flow is observed and happening much before the cylinder-cone transition point. Velocity radial profile obtained for control volume near conical region indicated pronounced concavity at the center for test reactor geometry with 60° half-cone angle. This suggested that particles at the center are having much higher velocities as compared to the particles near the wall. On the other hand, velocity radial profile for control volume near conical region is parabolic in shape for test reactor geometry with 30° half-cone angle. Mass flow index (MFI) values are calculated to predict the flow patterns i.e. mass/funnel/mixed flow in both test reactor geometries. MFI values obtained using velocity profiles for test reactor geometry with 30° half-cone angle predicted mass type flow, whereas funnel type flow is predicted for test reactor geometry with 60° half-cone angle. These flow pattern predictions are consistent with direct observations of discharge and relative movement results of tagged particles. Assessment of EDEM^{TM} simulation results using benchmark data of RPT experiments is carried out and a fair agreement is observed in results about Lagrangian trajectories and velocity profile. However, additional experimental investigation needs to be carried out for different sizes of test reactor, different bottom cone angles, and different sizes of pebbles to further assess DEM simulation results before using it for full scale reactor simulations.

7.2. RECOMMENDATIONS FOR FUTURE WORK

- Continuous pebble recirculation experimental set-up that measures one foot in diameter and one foot in height simulates the flow of pebbles in a pebble bed test reactor. Glass marbles of ½" dia. mimic the bed pebbles. This set-up can be modified

to accommodate bigger size pebbles, larger dia. and taller test reactors. It is recommended to carry out RPT and RTD experiments in larger size columns with bigger pebbles to provide more information about granular flow and inputs for the development of scale-up methodology for PBR's .

- RPT calibration experiments under different conditions of bed suggested that pebble bed can be approximated as static packed beds, depending on the type of measurement and parameters to be investigated. It is recommended to verify this approximation using computed tomography experiments around continuous pebble recirculation experimental set-up at different exit flow rate of marbles.
- The bottom cone angle has significant effect on the pebbles flow field and it is recommended to carry out experimental investigations for different bottom cone angles.
- It is recommended to carry out additional work to demonstrate operational feasibility of RPT calibration equipment in different multiphase systems and to improve upon its position reconstruction accuracy.
- Additional EDEM^{TM} based simulations for a range of aspect ratios needs to be carried out to ensure validity of results obtained using parametric sensitivity study of interaction properties and packing algorithm validation study for diameter aspect ratio of 23.9.
- It is recommended to carry out DEM based simulations of full-scale reactor geometry by using determined interaction properties for graphite pebbles and steel wall materials. There is an effect of temperature on interaction properties and should be taken into account while carrying out these full-scale reactor simulations.

APPENDIX A
GLASS VIAL OPENING PROCEDURE

GLASS VIAL OPENING PROCEDURE

- Take a swipe on the inside surface of the lead pig lid to check for contamination
- Gently drop vial out of lead pig into the big white tray.
- Take the dose rate reading in contact with vial using Ludlum survey meter kept inside glove box.
- Using the four pronged finger tool, place the vial into hole provided in shielding block.
- Hold vial using flat surface offered by scissors and score the vial using triangular diamond knife.
- Rotate the shielding block by 90 degree and score at new location. Make sure that vial will be scored roughly around entire periphery.
- Using the four pronged finger tool, place the vial inside plastic bag. Zip Lock the face of bag.
- Hold the bag remotely in one hand making sure not to touch the vial and using glass snapping tool, break the vial inside plastic bag.
- Make sure that particle containing portion of vial is upright while breaking the vial.
- Cut the bag close to portion containing vial. If possible using tweezers lift the particle containing half of vial and place it in silver petri dish.
  If particle comes out of vial, dump the entire content of bag in the silver petri dish gently.
- Using tweezers transfer the particles from petri dish into clean plastic vial.

- Place the plastic vial containing irradiated particles inside lead pig and put the lid on the pig.
- Dump the broken glass pieces into solid waste container. Put the petry dish used during this procedure into waste container.
- Using wet paper towel, clean the white tray and shielding block to remove dust generated during glass scoring, if any.
- Dump the used paper towels into solid waste container provided inside glove box.
- Take swipe sample of tray and block. Put the sample next to front transparent portion of wall.
- Use the Ludlum survey meter kept outside glove box & monitor dose rate to check contamination, if any.
- Make the glove box ready for particle washing procedure.
  It is recommended to follow principle of ALARA by minimizing exposure time, working remotely and behind shielding during glass vial cutting.

APPENDIX B
TRACER PARTICLE CALCULATIONS AND DENSITY MATCH

Tracer particle calculations and density match

The test reactor is filled with glass marbles having average diameter of ½". Hence, a tracer particle of ½" diameter needs to be used to match size and shape with glass marbles. Teflon is selected as a material of the tracer particle due to ease in machining, strength and integrity considerations and also from density matching point of view. A Cobalt particle having diameter of 600µm is selected for irradiation with neutrons in Missouri University Research Reactor (MURR). Bigger size cobalt particles are favorable due to lesser irradiation time requirement in the nuclear reactor. To accommodate this 600µm radioactive Cobalt particle, a hole of 1 mm diameter and ~7mm in length is drilled in a Teflon particle. The density of composite tracer particle is matched with that of glass marbles by matching their masses. The mass of this composite Teflon particle with a dummy cobalt particle and steel screw cap is matched with average mass of ½" glass marbles by selecting suitable length screw cap and adjusting air gap. A screw cap made from steel (1 mm diameter and 3.2 mm in length) is found to be matching the mass of composite tracer particle (2.48 grams) with average mass of glass marbles (2.49 grams).

APPENDIX C
NEW DAQ SYSTEM OF RPT –OPERATING MANUAL

OPERATING MANUAL FOR RPT-DAQ SOFTWARE

The new upgraded DAQ system of RPT technique makes use of CC-USB controller and DAQ software developed specifically for the technique of RPT technique. The CC-USB is a list mode CAMAC controller must occupy the right- most two slots on the CAMAC crate.

C.1 RUNNING THE DAQ SOFTWARE

The newly developed RPT data acquisition system has three modes of operation: Normal (tracks the particle), Calibration (used for RPT Calibration), LED setup (finds the position of photo-peak for each detector). When the desktop icon for '*Data Acquisition*' is double clicked it will start the data acquisition program. The main window of DAQ program will be as shown in Figure C.1.

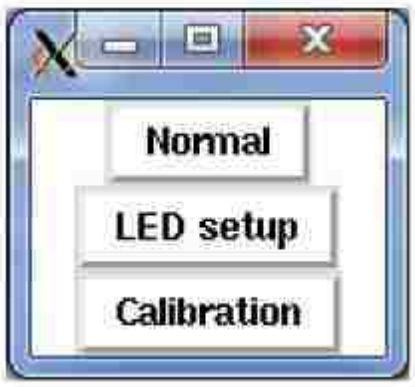

Figure C.1 DAQ modes of operation

Once mode is selected based on the task requirement, a user interface appropriate to that mode is displayed.

C.1.1 LED Setup mode. In LED setup mode, gamma spectroscopy is carried out for each detector to find the position of photo-peak in each detector channel. Due to the hardware limitations, one value of threshold is set for all channels. This requires synchronization of photo-peaks in all the channels. This is usually done by varying fine and coarse gain on timing filter and amplifiers.Selecting the LED setup mode brings up the following control panel.

Figure C.2 LED setup control

The dwell time is the number of seconds of data taking at each discriminator setting. The discriminator setting aka threshold is increased gradually from 0 to 1023. At each threshold value, counts data is collected for the set dwell time. Longer dwell times give better statistics, and may be required for weaker sources, but also require longer run times. Conversely, a shorter dwell time will give poorer statistics but will result in a faster run time. After acquiring data for all threshold levels, a spectrum is generated for each detector channel. This spectrum can be viewed for each channel by selecting the channel number in the array of radio buttons and clicking the Plot button provided on LED channel interface.

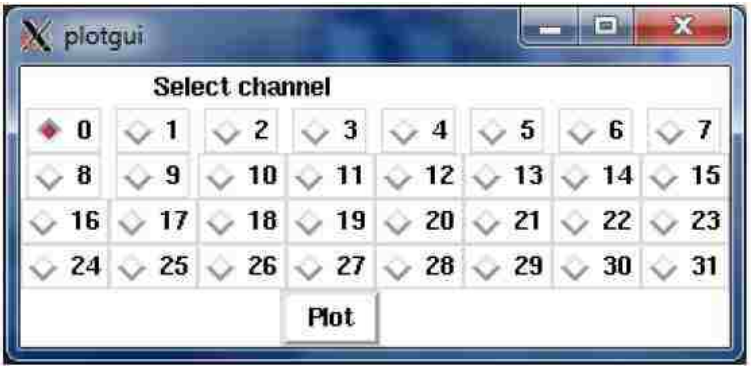

Figure C.3 LED plotting interface

Figure C.4 represents obtained spectrum results using upgraded DAQ system of RPT.

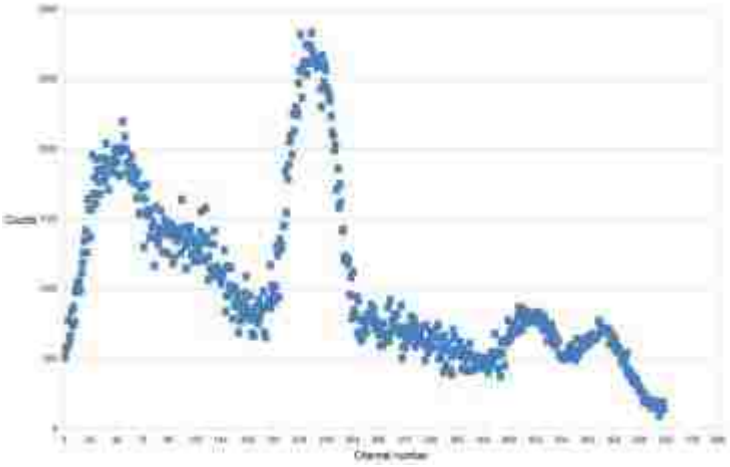

Figure C.4 Spectrum results obtained

C.1.2 Calibration Mode. Calibration mode is used to perform RPT calibration by providing input of tracer particle position and recording counts in each detector at user defined sampling frequency. Three windows are available. There is a window to run the DAQ program in calibration mode. User can manually provide data about position of tracer particle and select the sampling frequency (Figure C.5). The counts data can be recorded for a number of positions by clicking start button and can be saved in a .csv file.

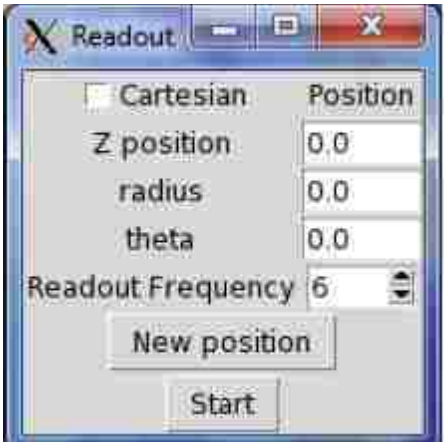

Figure C.5 Calibration Run Control Panel

There are two more windows available LED control panel (Figure C.6) and the scalar display window (Figure C.7). There is a provision to enable selected channels from an array of channels. User can provide input of threshold which will be obtained from the LED set-up mode. Two discriminators are used in the hardware configuration of RPT technique DAQ system. There is a provision to provide different threshold for these two different discriminators. Scalar display window is used for display and monitoring purposes .

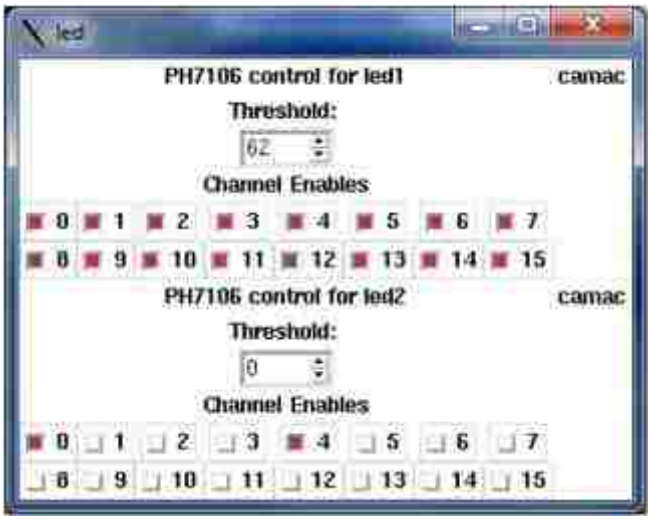

Figure C.6 LED Control Panel

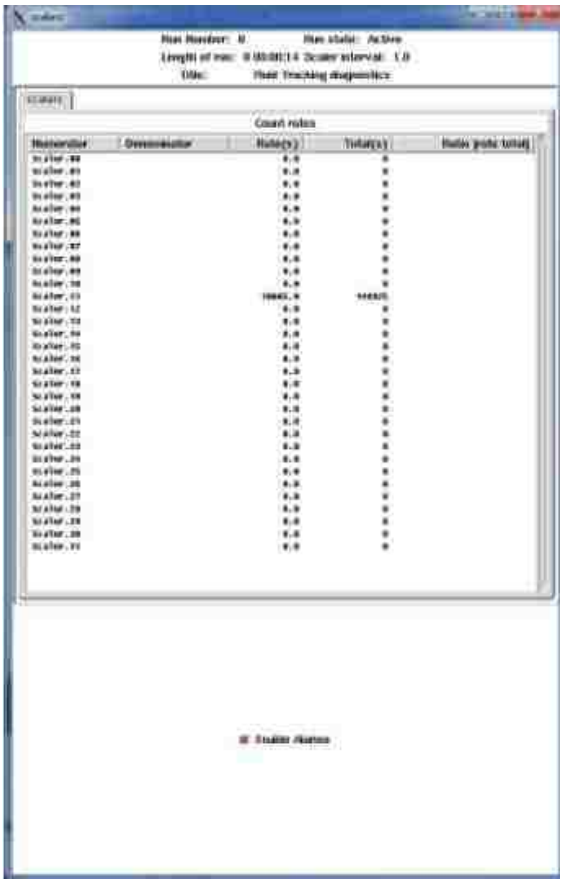

Figure C.7 Scalar display window

C.1.3 Normal Mode. In Normal mode, actual particle tracking experiments are performed. It requires user to provide input of sampling frequency, total sampling time, and threshold settings on discriminator. The readout window in normal mode and associated LED setup window has all these provisions. LED set-up window is similar to the one used in the calibration mode. At the end of sampling time, collected data in all the detectors can be saved in .csv format which will be used later in position reconstruction step.

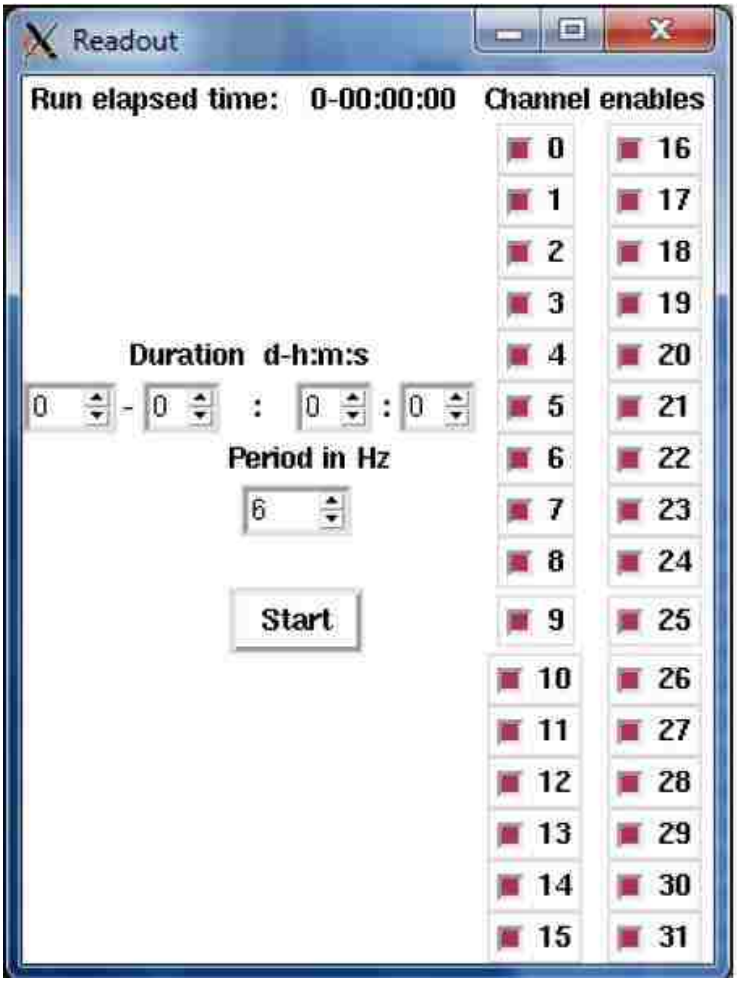

Figure C.8 Normal mode setup control panel

APPENDIX D
RPT POSITION RECONSTRUCTION MATLAB PROGRAM

```
**********************************************************************
% read data from run file
run= csvread('1a.csv');
% read data from calibration file
cali = csvread('cali.csv');
% read data from detector file
detector=csvread('crys.csv');

% read size of run file
size_run= size(run);%size of run file
run_row=size_run(1,1);%no. of rows in run file

% read size of calibration file
size_cali=size(cali);  %size of calibration file
cali_row=size_cali(1,1);%no. of rows in calibration file
cali_column=size_cali(1,2)-3;%no. of columns in calibration file

%nd = input('no of detectors\n')

%initializing matrix
sum_cali=zeros(1,cali_row);%matrix for square root of summation of no.s
in row of calibration matrix
sum_run=zeros(1,run_row);%matrix for square root of summation of no.s
in row of run matrix
%r=zeros(run_row,cali_row);
r1=zeros(cali_row,2,run_row);

%calculation of square root of summation of no.s  in row of calibration
matrix
for i=1:cali_row
    for j = 1:cali_column
       sum_cali(1,i)=sum_cali(1,i)+(cali(i,j)*cali(i,j));%calculation
of summation of no.s  in row of calibration matrix
    end
    sum_cali(1,i)=sqrt(sum_cali(1,i));%calculation of square root of
sum of no.s  in row of calibration matrix
end

%calculation of square root of summation of nos  in row of run matrix
%matrix
for i=1:100:run_row
    for j=1:size_run(1,2)
       sum_run(1,i) =sum_run(1,i)+run(i,j)*run(i,j);%calculation of
summation of no.s  in row of run matrix
    end
    sum_run(1,i)=sqrt(sum_run(1,i));%calculation of square root of sum
of nos  in row of run matrix
end
%calculation of r1
for i=1:100:run_row
    for k=1:cali_row
        for j=1:cali_column % no. of detectors

r1(k,1,i)=r1(k,1,i)+(cali(k,j)*run(i,j))/(sum_cali(1,k)*sum_run(1,i));
        end
```

```
        r1(k,2,i)=k;
        r1(k,3:5,i)=cali(k,cali_column+1:cali_column+3);
    end
end

rr1=r1;
%sort the r1
for i=1:100:run_row
    r1(:,:,i)=sortrows(r1(:,:,i),1);
    dlmwrite('r1.csv', r1(cali_row,:,i),'-append');
end
%% IBE

for row=1:100:run_row
Initial_best_esti=r1(cali_row,2,row)
ibe=Initial_best_esti;

ibe1=cali(ibe,cali_column+1:cali_column+3);
disp('1st Initial Best Estimation')
disp('    r       theta        z')
disp(ibe1)
ibe_x=cali(ibe,cali_column+1)*cos(cali(ibe,cali_column+2)*pi/180);
ibe_y=cali(ibe,cali_column+1)*sin(cali(ibe,cali_column+2)*pi/180);
ibe_z=cali(ibe,cali_column+3);
%flag=1-r(1,1);
%while flag>0.0001

z=cali(ibe,cali_column+3);%ibe z
r=cali(ibe,cali_column+1);%ibe r
thita=cali(ibe,cali_column+2);%ibe thita


ibe_best(1,1)=ibe;%row no.
ibe_best(1,2)=r1(cali_row,1,row);%r1
ibe_best(1,3:5)=ibe1;%ibe r,thita,z
ibe_best(1,6)=ibe_x;%ibe x
ibe_best(1,7)=ibe_y;%ibe y
ibe_best(1,8)=ibe_z;%ibe z

% flag1=0;
% flag2=0;
% z1=z-1;
% z2=z+1;
for i=1:cali_row
  %  while flag1~=1
    if cali(i,cali_column+1)==r && cali(i,cali_column+2)==thita &&
cali(i,cali_column+3)==z-1
        ibe_best(2,1)=i;%row no.
        ibe_best(2,2)=rr1(i,1,row);%r1
        ibe_best(2,3:5)=cali(i,cali_column+1:cali_column+3);%ibe
r,thita,z
        ibe_best(2,6)=ibe_best(2,3)*cos(ibe_best(2,4)*pi/180);%ibe x
        ibe_best(2,7)=ibe_best(2,3)*sin(ibe_best(2,4)*pi/180);%ibe y
        ibe_best(2,8)=ibe_best(2,5);%ibe z
        flag1=1;
```

```
    end
   % z1=z1-1;
    %end
    %while flag2~=1
    if cali(i,cali_column+1)==r && cali(i,cali_column+2)==thita &&
cali(i,cali_column+3)==z+1
        ibe_best(3,1)=i;%row no.
        ibe_best(3,2)=rr1(i,1,row);%r1
        ibe_best(3,3:5)=cali(i,cali_column+1:cali_column+3);%ibe
r,thita,z
        ibe_best(3,6)=ibe_best(3,3)*cos(ibe_best(3,4)*pi/180);%ibe x
        ibe_best(3,7)=ibe_best(3,3)*sin(ibe_best(3,4)*pi/180);%ibe y
        ibe_best(3,8)=ibe_best(3,5);%ibe z
        flag2=1;
    end
    %z2=z2+1;
   % end
end

if r==0
   j=0;
   ibe_best(4:27,3)=5.08;%r
   ibe_best(4:11,5)=z;%z
   ibe_best(12:19,5)=ibe_best(2,5);%z
   ibe_best(20:27,5)=ibe_best(3,5);%z
   ibe_best(4:11,8)=z;%z
   ibe_best(12:19,8)=ibe_best(2,8);%z
   ibe_best(20:27,8)=ibe_best(3,8);%z
   for i=4 : 27
       if i==12
           j=0;
       end
       if i==20
           j=0;
       end
       ibe_best(i,4)=j;%thita
       ibe_best(i,6)=ibe_best(i,3)*cos(ibe_best(i,4)*pi/180);%ibe x
       ibe_best(i,7)=ibe_best(i,3)*sin(ibe_best(i,4)*pi/180);%ibe y
       j=j+45;
       for a=1: cali_row
          if cali(a,cali_column+1)==ibe_best(i,3) &&
cali(a,cali_column+2)==ibe_best(i,4) &&
cali(a,cali_column+3)==ibe_best(i,5)
               ibe_best(i,1)=a;
               ibe_best(i,2)=rr1(a,1,row);
           end
       end
   end
elseif r==5.08
    ibe_best(4,3:4)=0;
    ibe_best(9,3:4)=0;
    ibe_best(14,3:4)=0;
    ibe_best(5:6,3)=5.08;%r for current plane
    ibe_best(7:8,3)=10.16;%r for current plane
    ibe_best(10:11,3)=5.08;%r for upper plane
    ibe_best(12:13,3)=10.16;%r for upper plane
```

```
    ibe_best(15:16,3)=5.08;%r for lower plane
    ibe_best(17:18,3)=10.16;%r for lower plane
    ibe_best(4:8,5)=z;%z for current plane
    ibe_best(9:13,5)=ibe_best(2,5);%z for upper plane
    ibe_best(14:18,5)=ibe_best(3,5);%z for lower plane
    ibe_best(4:8,8)=z;%z for current plane
    ibe_best(9:13,8)=ibe_best(2,5);%z for upper plane
    ibe_best(14:18,8)=ibe_best(3,5);%z for lower plane
    if thita==0
        ibe_best(5,4)=45;%THETA for current plane
        ibe_best(7,4)=22.5;
        ibe_best(10,4)=45;%THETA for upper plane
        ibe_best(12,4)=22.5;
        ibe_best(15,4)=45;%THETA for lower plane
        ibe_best(17,4)=22.5;
        ibe_best(6,4)=315;%THETA for current plane
        ibe_best(8,4)=337.5;
        ibe_best(11,4)=315;%THETA for upper plane
        ibe_best(13,4)=337.5;
        ibe_best(16,4)=315;%THETA for lower plane
        ibe_best(18,4)=337.5;
    elseif thita==315
        ibe_best(5,4)=0;%THETA for current plane
        ibe_best(7,4)=337.5;
        ibe_best(10,4)=0;%THETA for upper plane
        ibe_best(12,4)=337.5;
        ibe_best(15,4)=0;%THETA for lower plane
        ibe_best(17,4)=337.5;
        ibe_best(6,4)=270;%THETA for current plane
        ibe_best(8,4)=292.5;
        ibe_best(11,4)=270;%THETA for upper plane
        ibe_best(13,4)=292.5;
        ibe_best(16,4)=270;%THETA for lower plane
        ibe_best(18,4)=292.5;
    else
        ibe_best(5,4)=thita+45;%THETA for current plane
        ibe_best(7,4)=thita+22.5;
        ibe_best(10,4)=thita+45;%THETA for upper plane
        ibe_best(12,4)=thita+22.5;
        ibe_best(15,4)=thita+45;%THETA for lower plane
        ibe_best(17,4)=thita+22.5;
        ibe_best(6,4)=thita-45;%THETA for current plane
        ibe_best(8,4)=thita-22.5;
        ibe_best(11,4)=thita-45;%THETA for upper plane
        ibe_best(13,4)=thita-22.5;
        ibe_best(16,4)=thita-45;%THETA for lower plane
        ibe_best(18,4)=thita-22.5;
    end
    for i=4:18
       ibe_best(i,6)=ibe_best(i,3)*cos(ibe_best(i,4)*pi/180);%ibe x
       ibe_best(i,7)=ibe_best(i,3)*sin(ibe_best(i,4)*pi/180);%ibe y
       for a=1: cali_row
          if cali(a,cali_column+1)==ibe_best(i,3) &&
cali(a,cali_column+2)==ibe_best(i,4) &&
cali(a,cali_column+3)==ibe_best(i,5)
              ibe_best(i,1)=a;
```

```
                ibe_best(i,2)=rr1(a,1,row);
            end
        end
    end
elseif r==10.16
    ibe_best(4:5,3)=5.08;%r for current plane
    ibe_best(6:7,3)=13.97;%r for current plane
    ibe_best(8:9,3)=5.08;%r for upper plane
    ibe_best(10:11,3)=13.97;%r for upper plane
    ibe_best(12:13,3)=5.08;%r for lower plane
    ibe_best(14:15,3)=13.97;%r for lower plane
    ibe_best(4:7,5)=z;%z for current plane
    ibe_best(8:11,5)=ibe_best(2,5);%z for upper plane
    ibe_best(12:15,5)=ibe_best(3,5);%z for lower plane
    ibe_best(4:7,8)=z;%z for current plane
    ibe_best(8:11,8)=ibe_best(2,5);%z for upper plane
    ibe_best(12:15,8)=ibe_best(3,5);%z for lower plane

    if thita==22.5
       ibe_best(4,4)=45;
       ibe_best(6,4)=45;
       ibe_best(8,4)=45;
       ibe_best(10,4)=45;
       ibe_best(12,4)=45;
       ibe_best(14,4)=45;
       ibe_best(5,4)=0;
       ibe_best(7,4)=0;
       ibe_best(9,4)=0;
       ibe_best(11,4)=0;
       ibe_best(13,4)=0;
       ibe_best(15,4)=0;
   elseif thita==337.5
       ibe_best(4,4)=0;
       ibe_best(6,4)=0;
       ibe_best(8,4)=0;
       ibe_best(10,4)=0;
       ibe_best(12,4)=0;
       ibe_best(14,4)=0;
       ibe_best(5,4)=315;
       ibe_best(7,4)=315;
       ibe_best(9,4)=315;
       ibe_best(11,4)=315;
       ibe_best(13,4)=315;
       ibe_best(15,4)=315;
   else
       ibe_best(4,4)=thita+22.5;
       ibe_best(6,4)=thita+22.5;
       ibe_best(8,4)=thita+22.5;
       ibe_best(10,4)=thita+22.5;
       ibe_best(12,4)=thita+22.5;
       ibe_best(14,4)=thita+22.5;
       ibe_best(5,4)=thita-22.5;
       ibe_best(7,4)=thita-22.5;
       ibe_best(9,4)=thita-22.5;
       ibe_best(11,4)=thita-22.5;
       ibe_best(13,4)=thita-22.5;
```

```
        ibe_best(15,4)=thita-22.5;
     end
    for i=4:15
        ibe_best(i,6)=ibe_best(i,3)*cos(ibe_best(i,4)*pi/180);%ibe x
        ibe_best(i,7)=ibe_best(i,3)*sin(ibe_best(i,4)*pi/180);%ibe y
        for a=1: cali_row
           if cali(a,cali_column+1)==ibe_best(i,3) &&
cali(a,cali_column+2)==ibe_best(i,4) &&
cali(a,cali_column+3)==ibe_best(i,5)
                ibe_best(i,1)=a;
                ibe_best(i,2)=rr1(a,1,row);
            end
        end
    end
else
     ibe_best(4:5,3)=10.16;%r for current plane
     ibe_best(6:7,3)=13.97;%r for current plane
     ibe_best(8:9,3)=10.16;%r for upper plane
     ibe_best(10:11,3)=13.97;%r for upper plane
     ibe_best(12:13,3)=10.16;%r for lower plane
     ibe_best(14:15,3)=13.97;%r for lower plane
     ibe_best(4:7,5)=z;%z for current plane
     ibe_best(8:11,5)=ibe_best(2,5);%z for upper plane
     ibe_best(12:15,5)=ibe_best(3,5);%z for lower plane
     ibe_best(4:7,8)=z;%z for current plane
     ibe_best(8:11,8)=ibe_best(2,5);%z for upper plane
     ibe_best(12:15,8)=ibe_best(3,5);%z for lower plane

     if thita==0
        ibe_best(4,4)=22.5;
        ibe_best(6,4)=45;
        ibe_best(8,4)=22.5;
        ibe_best(10,4)=45;
        ibe_best(12,4)=22.5;
        ibe_best(14,4)=45;
        ibe_best(5,4)=337.5;
        ibe_best(7,4)=315;
        ibe_best(9,4)=337.5;
        ibe_best(11,4)=315;
        ibe_best(13,4)=337.5;
        ibe_best(15,4)=315;
    elseif thita==315
        ibe_best(4,4)=337.5;
        ibe_best(6,4)=0;
        ibe_best(8,4)=337.5;
        ibe_best(10,4)=0;
        ibe_best(12,4)=337.5;
        ibe_best(14,4)=0;
        ibe_best(5,4)=292.5;
        ibe_best(7,4)=270;
        ibe_best(9,4)=292.5;
        ibe_best(11,4)=270;
        ibe_best(13,4)=292.5;
        ibe_best(15,4)=270;
    else
        ibe_best(4,4)=thita+22.5;
```

```
        ibe_best(6,4)=thita+45;
        ibe_best(8,4)=thita+22.5;
        ibe_best(10,4)=thita+45;
        ibe_best(12,4)=thita+22.5;
        ibe_best(14,4)=thita+45;
        ibe_best(5,4)=thita-22.5;
        ibe_best(7,4)=thita-45;
        ibe_best(9,4)=thita-22.5;
        ibe_best(11,4)=thita-45;
        ibe_best(13,4)=thita-22.5;
        ibe_best(15,4)=thita-45;
    end
   for i=4:15
        ibe_best(i,6)=ibe_best(i,3)*cos(ibe_best(i,4)*pi/180);%ibe x
        ibe_best(i,7)=ibe_best(i,3)*sin(ibe_best(i,4)*pi/180);%ibe y
        for a=1: cali_row
           if cali(a,cali_column+1)==ibe_best(i,3) &&
cali(a,cali_column+2)==ibe_best(i,4) &&
cali(a,cali_column+3)==ibe_best(i,5)
                ibe_best(i,1)=a;
                ibe_best(i,2)=rr1(a,1,row);
            end
       end
   end
end
disp('Initial Best Estimation')
disp('     Row No.      R1      r      theta          z         x
y          z')
disp(ibe_best)
s=[row row];
%dlmwrite('ibe_best.csv', s, '-append');
dlmwrite('ibe_best.csv', ibe_best(1,:), '-append');

r=cali(ibe,cali_column+1);%ibe r
thita=cali(ibe,cali_column+2);%ibe thita
z=cali(ibe,cali_column+3);%ibe thita
x=2;
%if r=5.08 then take 1st five point of d_nn_xyz
if r==5.08
    %dividing best initial fit part into fine parts
    fine_mesh(1:3,1)=0;
    fine_mesh(1:3,2)=0;
    fine_mesh(1,3)=z;
    fine_mesh(2,3)=ibe_best(2,5);
    fine_mesh(3,3)=ibe_best(3,5);
    fine_mesh(1:3,4)=1;
    fine_mesh(1:3,5)=0;
    fine_mesh(1:3,6)=0;
    fine_mesh(1,7)=z;
    fine_mesh(2,7)=ibe_best(2,5);
    fine_mesh(3,7)=ibe_best(3,5);
    % thita!=315 is
    if thita~=315
        if ibe_best(4,4)>ibe_best(5,4)
            theta1=ibe_best(5,4);
            theta2=ibe_best(4,4);
```

```
        else
            theta1=ibe_best(4,4);
            theta2=ibe_best(5,4);
        end

    for i=0:5.08/5:5.08%dividing the radius from 0.73 to 7.62
        if i==0
            for k=ibe_best(2,5):0.5:ibe_best(3,5)+1%dividing height
with 0.5 cm
                fine_mesh(x,1)=i;%r
                fine_mesh(x,2)=0;%thita
                fine_mesh(x,3)=k;%z
                fine_mesh(x,4)=x;%no. of row
                fine_mesh(x,5)=i*cos(0*pi/180);%x
                fine_mesh(x,6)=i*sin(0*pi/180);%y
                fine_mesh(x,7)=k;%z
                x=x+1;
            end
        else
            if thita ~=0
                for j=theta1:22.5:theta2+1%dividing the angle with 7.5
degree
                    for k=ibe_best(2,5):0.5:ibe_best(3,5)+1%dividing
height with 0.2 cm
                        fine_mesh(x,1)=i;%r
                        fine_mesh(x,2)=j;%thita
                        fine_mesh(x,3)=k;%z
                        fine_mesh(x,4)=x;%no. of row
                        fine_mesh(x,5)=i*cos(j*pi/180);%x
                        fine_mesh(x,6)=i*sin(j*pi/180);%y
                        fine_mesh(x,7)=k;%z
                        x=x+1;
                    end
                end
            else
               for j=0:22.5:45%dividing the angle with 7.5 degree
                   for k=ibe_best(2,5):0.5:ibe_best(3,5)+1%dividing
height with 0.2 cm
                       fine_mesh(x,1)=i;%r
                       fine_mesh(x,2)=j;%thita
                       fine_mesh(x,3)=k;%z
                       fine_mesh(x,4)=x;%no. of row
                       fine_mesh(x,5)=i*cos(j*pi/180);%x
                       fine_mesh(x,6)=i*sin(j*pi/180);%y
                       fine_mesh(x,7)=k;%z
                       x=x+1;
                   end
               end
               for j=315:22.5:345%dividing the angle with 7.5 degree
                   for k=ibe_best(2,5):0.5:ibe_best(3,5)+1%dividing
height with 0.2 cm
                       fine_mesh(x,1)=i;%r
                       fine_mesh(x,2)=j;%thita
                       fine_mesh(x,3)=k;%z
                       fine_mesh(x,4)=x;%no. of row
                       fine_mesh(x,5)=i*cos(j*pi/180);%x
```

```
                    fine_mesh(x,6)=i*sin(j*pi/180);%y
                    fine_mesh(x,7)=k;%z
                    x=x+1;
                end
            end
        end
    end
end
 for i=5.08+(5.08/5):5.08/5:10.16%dividing the radius from 8.35 to
14.602
    for j=theta1:22.5:theta2%dividing the angle with 7.5 degree
        for k=ibe_best(2,5):0.5:ibe_best(3,5)%dividing height with
0.2 cm
            fine_mesh(x,1)=i;%r
            fine_mesh(x,2)=j;%thita
            fine_mesh(x,3)=k;%z
            fine_mesh(x,4)=x;%no. of row
            fine_mesh(x,5)=i*cos(j*pi/180);%x
            fine_mesh(x,6)=i*sin(j*pi/180);%y
            fine_mesh(x,7)=k;%z
            x=x+1;
        end
    end
end
else %if thita is 315
    for i=0:5.08/5:5.08%dividing the radius from 0.73 to 7.62
        if i==0
            for k=ibe_best(2,5):0.5:ibe_best(3,5)+1%dividing height
with 0.2 cm
                fine_mesh(x,1)=i;%r
                fine_mesh(x,2)=0;%thita
                fine_mesh(x,3)=k;%z
                fine_mesh(x,4)=x;%no. of row
                fine_mesh(x,5)=i*cos(0*pi/180);%x
                fine_mesh(x,6)=i*sin(0*pi/180);%y
                fine_mesh(x,7)=k;%z
                x=x+1;
            end
        else
            for j=270:22.5:360%dividing the angle with 7.5 degree
                for k=ibe_best(2,5):0.5:ibe_best(3,5)+1%dividing
height with 0.2 cm
                    fine_mesh(x,1)=i;%r
                    fine_mesh(x,2)=j;%thita
                    fine_mesh(x,3)=k;%z
                    fine_mesh(x,4)=x;%no. of row
                    fine_mesh(x,5)=i*cos(j*pi/180);%x
                    fine_mesh(x,6)=i*sin(j*pi/180);%y
                    fine_mesh(x,7)=k;%z
                    x=x+1;
                end
            end
            for j=0:22.5:45%dividing the angle with 7.5 degree
                for k=ibe_best(2,5):0.5:ibe_best(3,5)%dividing
height with 0.2 cm
                    fine_mesh(x,1)=i;%r
```

```
                        fine_mesh(x,2)=j;%thita
                        fine_mesh(x,3)=k;%z
                        fine_mesh(x,4)=x;% no. of rows
                        fine_mesh(x,5)=i*cos(j*pi/180);%x
                        fine_mesh(x,6)=i*sin(j*pi/180);% y
                        fine_mesh(x,7)=k;%z
                        x=x+1;
                    end
                end
            end
        end
        for i=5.08+(5.08/5):5.08/5:10.16%dividing the radius from 8.35
to 14.602
            for j=270:22.5:360%dividing the angle with 7.5 degree
                for k=ibe_best(2,5):0.5:ibe_best(3,5)%dividing height
with 0.2 cm
                    fine_mesh(x,1)=i;%r
                    fine_mesh(x,2)=j;%thita
                    fine_mesh(x,3)=k;%z
                    fine_mesh(x,4)=x;%no. of rows
                    fine_mesh(x,5)=i*cos(j*pi/180);%x
                    fine_mesh(x,6)=i*sin(j*pi/180);%y
                    fine_mesh(x,7)=k;%z
                    x=x+1;
                end
            end
            for j=0:22.5:45%dividing the angle with 7.5 degree
                for k=ibe_best(2,5):0.5:ibe_best(3,5)%dividing height
with 0.2 cm
                    fine_mesh(x,1)=i;%r
                    fine_mesh(x,2)=j;%thita
                    fine_mesh(x,3)=k;%z
                    fine_mesh(x,4)=x;% no. of rows
                    fine_mesh(x,5)=i*cos(j*pi/180);%x
                    fine_mesh(x,6)=i*sin(j*pi/180);% y
                    fine_mesh(x,7)=k;%z
                    x=x+1;
                end
            end
        end
    end
elseif r==10.16%if ibe at outter ring take first 6 ibe points
    %dividing best initial fit part into fine parts
    x=1;
    if thita~=315
        if ibe_best(4,4)>ibe_best(5,4)
            theta1=ibe_best(5,4);
            theta2=ibe_best(4,4);
        else
            theta1=ibe_best(4,4);
            theta2=ibe_best(5,4);
        end
        if thita~=0
            for i=5.08:5.08/5:13.97%dividing the radius from 8.35 to
14.602
```

```
                for j=theta1:22.5:theta2%dividing the angle with 15
degree
                    for k=ibe_best(2,5):0.5:ibe_best(3,5)%dividing
height with 0.2 cm
                        fine_mesh(x,1)=i;%r
                        fine_mesh(x,2)=j;% thita
                        fine_mesh(x,3)=k;%z
                        fine_mesh(x,4)=x;%no. of rows
                        fine_mesh(x,5)=i*cos(j*pi/180);%x
                        fine_mesh(x,6)=i*sin(j*pi/180);% y
                        fine_mesh(x,7)=k;%z
                        x=x+1;
                    end
                end
            end
        else
            for i=5.08:5.08/5:13.97%dividing the radius from 8.35 to
14.602
                for j=0:22.5:45%dividing the angle with 15 degree
                    for k=ibe_best(2,5):0.5:ibe_best(3,5)%dividing
height with 0.2 cm
                        fine_mesh(x,1)=i;%r
                        fine_mesh(x,2)=j;% thita
                        fine_mesh(x,3)=k;%z
                        fine_mesh(x,4)=x;%no. of rows
                        fine_mesh(x,5)=i*cos(j*pi/180);%x
                        fine_mesh(x,6)=i*sin(j*pi/180);% y
                        fine_mesh(x,7)=k;%z
                        x=x+1;
                    end
                end
                for j=315:22.5:345%dividing the angle with 15 degree
                    for k=ibe_best(2,5):0.5:ibe_best(3,5)%dividing
height with 0.2 cm
                        fine_mesh(x,1)=i;%r
                        fine_mesh(x,2)=j;% thita
                        fine_mesh(x,3)=k;%z
                        fine_mesh(x,4)=x;%no. of rows
                        fine_mesh(x,5)=i*cos(j*pi/180);%x
                        fine_mesh(x,6)=i*sin(j*pi/180);% y
                        fine_mesh(x,7)=k;%z
                        x=x+1;
                    end
                end
            end
        end
    else%thita = 315
        for i=5.08:5.08/5:13.97
            %dividing the radius from 8.35 to 14.602
            for j=270:22.5:315%dividing the angle with 7.5 degree
                for k=ibe_best(2,5):0.5:ibe_best(3,5)%dividing height
with 0.2 cm
                    fine_mesh(x,1)=i;%r
                    fine_mesh(x,2)=j;%thita
                    fine_mesh(x,3)=k;%z
                    fine_mesh(x,4)=x;% no. of rows
```

```
                    fine_mesh(x,5)=i*cos(j*pi/180);%x
                    fine_mesh(x,6)=i*sin(j*pi/180);% y
                    fine_mesh(x,7)=k;%z
                    x=x+1;
                end
            end
            for j=0:22.5:45%dividing the angle with 7.5 degree
                for k=ibe_best(2,5):0.5:ibe_best(3,5)%dividing height
with 0.2 cm
                    fine_mesh(x,1)=i;%r
                    fine_mesh(x,2)=j;%thita
                    fine_mesh(x,3)=k;%z
                    fine_mesh(x,4)=x;% no. of rows
                    fine_mesh(x,5)=i*cos(j*pi/180);%x
                    fine_mesh(x,6)=i*sin(j*pi/180);% y
                    fine_mesh(x,7)=k;%z
                    x=x+1;
                end
            end
        end
    end
elseif r==0% if ibe at center
    x=1;
    for i=0:5.08/5:5.08%dividing the radius from 0.762 to 7.62
        if i==0
            for k=ibe_best(2,5):0.5:ibe_best(3,5)+1%dividing height
with 0.5 cm
                fine_mesh(x,1)=i;%r
                fine_mesh(x,2)=0;%thita
                fine_mesh(x,3)=k;%z
                fine_mesh(x,4)=x;%no. of rows
                fine_mesh(x,5)=i*cos(j);%x
                fine_mesh(x,6)=i*sin(j);%y
                fine_mesh(x,7)=k;%z
                x=x+1;
            end
        else
            for j=0:22.5:360%dividing the angle with 15 degree
                for k=ibe_best(2,5):0.5:ibe_best(3,5)+1%dividing height
with 0.2 cm
                    fine_mesh(x,1)=i;%r
                    fine_mesh(x,2)=j;%thita
                    fine_mesh(x,3)=k;%z
                    fine_mesh(x,4)=x;%no. of rows
                    fine_mesh(x,5)=i*cos(j);%x
                    fine_mesh(x,6)=i*sin(j);%y
                    fine_mesh(x,7)=k;%z
                    x=x+1;
                end
            end
        end
    end
elseif r==13.97
    x=1;
    if thita~=315
        if ibe_best(6,4)>ibe_best(7,4)
```

```
            theta1=ibe_best(7,4);
            theta2=ibe_best(6,4);
        else
            theta1=ibe_best(6,4);
            theta2=ibe_best(7,4);
        end
        if thita~=0
            for i=10.16:5.08/5:13.97%dividing the radius from 8.35 to
14.602
                for j=theta1:22.5:theta2%dividing the angle with 15
degree
                    for k=ibe_best(2,5):0.5:ibe_best(3,5)%dividing
height with 0.2 cm
                        fine_mesh(x,1)=i;%r
                        fine_mesh(x,2)=j;% thita
                        fine_mesh(x,3)=k;%z
                        fine_mesh(x,4)=x;%no. of rows
                        fine_mesh(x,5)=i*cos(j*pi/180);%x
                        fine_mesh(x,6)=i*sin(j*pi/180);% y
                        fine_mesh(x,7)=k;%z
                        x=x+1;
                    end
                end
            end

        else
            for i=10.16:5.08/5:13.97%dividing the radius from 8.35 to
14.602
                for j=0:22.5:45%dividing the angle with 15 degree
                    for k=ibe_best(2,5):0.5:ibe_best(3,5)%dividing
height with 0.2 cm
                        fine_mesh(x,1)=i;%r
                        fine_mesh(x,2)=j;% thita
                        fine_mesh(x,3)=k;%z
                        fine_mesh(x,4)=x;%no. of rows
                        fine_mesh(x,5)=i*cos(j*pi/180);%x
                        fine_mesh(x,6)=i*sin(j*pi/180);% y
                        fine_mesh(x,7)=k;%z
                        x=x+1;
                    end
                end
                for j=315:22.5:345%dividing the angle with 15 degree
                    for k=ibe_best(2,5):0.5:ibe_best(3,5)%dividing
height with 0.2 cm
                        fine_mesh(x,1)=i;%r
                        fine_mesh(x,2)=j;% thita
                        fine_mesh(x,3)=k;%z
                        fine_mesh(x,4)=x;%no. of rows
                        fine_mesh(x,5)=i*cos(j*pi/180);%x
                        fine_mesh(x,6)=i*sin(j*pi/180);% y
                        fine_mesh(x,7)=k;%z
                        x=x+1;
                    end
                end
            end
```

```
        end
    else%thita = 315
        for i=10.16:5.08/5:13.97
            %dividing the radius from 8.35 to 14.602
            for j=270:22.5:315%dividing the angle with 7.5 degree
                for k=ibe_best(2,5):0.5:ibe_best(3,5)%dividing height
with 0.2 cm
                    fine_mesh(x,1)=i;%r
                    fine_mesh(x,2)=j;%thita
                    fine_mesh(x,3)=k;%z
                    fine_mesh(x,4)=x;% no. of rows
                    fine_mesh(x,5)=i*cos(j*pi/180);%x
                    fine_mesh(x,6)=i*sin(j*pi/180);% y
                    fine_mesh(x,7)=k;%z
                    x=x+1;
                end
            end
            for j=0:22.5:45%dividing the angle with 7.5 degree
                for k=ibe_best(2,5):0.5:ibe_best(3,5)%dividing height
with 0.2 cm
                    fine_mesh(x,1)=i;%r
                    fine_mesh(x,2)=j;%thita
                    fine_mesh(x,3)=k;%z
                    fine_mesh(x,4)=x;% no. of rows
                    fine_mesh(x,5)=i*cos(j*pi/180);%x
                    fine_mesh(x,6)=i*sin(j*pi/180);% y
                    fine_mesh(x,7)=k;%z
                    x=x+1;
                end
            end
        end
    end
end
dlmwrite('fine_mesh.csv', fine_mesh(1,:), '-append');
%plotting fine_mesh with new ibe
scatter3(fine_mesh(:,5),fine_mesh(:,6),fine_mesh(:,7),'+');
%hold on;
scatter3(ibe_best(:,6),ibe_best(:,7),ibe_best(:,8),'*');
% ---------------------------------------------------------------------
%% detector
for i = 1:16
    detector_xyz(i,1) = detector(i,1) * cos((detector(i,2))*pi/180);%x
    detector_xyz(i,2) = detector(i,1) * sin((detector(i,2))*pi/180);%y
    detector_xyz(i,3)= detector(i,3); %z
end
% detector_xyz
%---------------------------------------------------------------------

%% procedure to calcuate k2,k3,k4 i.e. 'k'
if r==5.08
    num_bf=18;
elseif r==10.16
     num_bf=15;
elseif r==0
    num_bf=27;
elseif r==13.97
```

```
    num_bf=15;
end
%num_bf=5;
%taking count of new ibes in matrix 'c'
for i=1:num_bf
    c(i,1:16)=cali(ibe_best(i,1),1:16);
end
%calculating dx,dy ,dz & d for nn_ibe w. r.t. detector
for j=1:16
    for i=1:num_bf
        dx(j,i)=sqrt((detector_xyz(j,1)-ibe_best(i,6))^2);
        dy(j,i)=sqrt((detector_xyz(j,2)-ibe_best(i,7))^2);
        dz(j,i)=sqrt((detector_xyz(j,3)-ibe_best(i,8))^2);
        d(j,i)=sqrt((dx(j,i))^2 + (dy(j,i))^2+(dz(j,i))^2);
        end
end
%creating A & B matrix
for j=1:16
  for i=1:num_bf-1
   a(i,1)=log(c(i,j)/c(i+1,j));
    d_data(i,1)=2*log(d(j,i+1)/d(j,i));
    B(i,1)=(a(i,1)-d_data(i,1));
    A(i,1)=-(dx(j,i)-dx(j,i+1));
    A(i,2)=-(dy(j,i)-dy(j,i+1));
    A(i,3)=-(dz(j,i)-dz(j,i+1));
  end

k=lsqnonneg(A,B);
k1(j,:)=k;

end

disp('Values of K')
disp('     k2        k3          k4')
disp(k1)

% ------------------------------------------------------------------
%% procedure to calculate count for fine mesh
size_fm= size(fine_mesh);
fm_row=size_fm(1,1);
sum_fm=zeros(1,fm_row);
fm_r1=zeros(fm_row,2,run_row);

for i=1:fm_row  %no. of fine mesh points
    for j=1:16
        fm_dx(i,j)=sqrt((detector_xyz(j,1)-fine_mesh(i,5))^2);
        fm_dy(i,j)=sqrt((detector_xyz(j,2)-fine_mesh(i,6))^2);
        fm_dz(i,j)=sqrt((detector_xyz(j,3)-fine_mesh(i,7))^2);
        fm_d(i,j)=sqrt((fm_dx(i,j))^2+(fm_dy(i,j))^2+(fm_dz(i,j))^2);
        fm_c(i,j)=(c(1,j)*d(j,1)^2*exp((-k1(j,1)*fm_dx(i,j))-
(k1(j,2)*fm_dy(i,j))-(k1(j,3)*fm_dz(i,j))))/(fm_d(i,j)^2*exp((-
k1(j,1)*dx(j,1))-(k1(j,2)*dy(j,1))-(k1(j,3)*dz(j,1))));
    end
end
```

```
%fm_c(1,:)
%------------
%% procedure for calculating r for fine mesh
for i=1:fm_row
    for j = 1:16
       sum_fm(1,i)=sum_fm(1,i)+(fm_c(i,j)*fm_c(i,j));
    end
    sum_fm(1,i)=sqrt(sum_fm(1,i));
end

%for i=1:run_row
    for k=1:fm_row
        for j=1:16

fm_r1(k,1,1)=fm_r1(k,1,1)+(fm_c(k,j)*run(row,j))/(sum_fm(1,k)*sum_run(1
,row));%r
        end
        fm_r1(k,2,1)=k;%fine mesh row no.
        fm_r1(k,3:5,1)=fine_mesh(k,1:3);%r, thita, z
    end
%end
%sortting
fm_r1(:,:,1)=sortrows(fm_r1(:,:,1),1);
%fm_r1
%
flag=1-fm_r1(fm_row,1,1);
flag

new_points(1,1:3)=fine_mesh(fm_r1(fm_row,2,1),5:7);%fine mesh x,y,z
new_points(1,4:6)=fine_mesh(fm_r1(fm_row,2,1),1:3);%fine mesh r, thita,
z
new_points(1,7)=fm_r1(fm_row,1,1);%r1
new_points(1,8)=fm_r1(fm_row,2,1);%fine mesh row no.

for i=1:fm_row-1
    new_points(i+1,1:3)=fine_mesh(fm_r1(fm_row-i,2,1),5:7);
    new_points(i+1,4:6)=fine_mesh(fm_r1(fm_row-i,2,1),1:3);
    new_points(i+1,7)=fm_r1(fm_row-i,1,1);%r1
    new_points(i+1,8)=fm_r1(fm_row-i,2,1);%fine mesh row no.
end
b=1;
for i=1:fm_row
    for j=1:num_bf
        if ibe_best(j,3)==new_points(i,4) &&
ibe_best(j,4)==new_points(i,5) && ibe_best(j,5)==new_points(i,6)
            np_in_ibe(b,1:8)=new_points(i,1:8);
            b=b+1;
        end
    end
end
% disp('New Points In The Initial Best Estimation')
% disp('     x         y         z         r        theta        z
R1      row no.')
% disp(np_in_ibe)
```

```
%dlmwrite('np_in_ibe.csv', s, '-append');
dlmwrite('np_in_ibe.csv', np_in_ibe(1,:), '-append');
format short
for i=1:50
    new_points_r1(i,1:7)=new_points(i,1:7);
end
% disp('New Points')
% disp('     x         y         z         r        theta        z
R1      row no.')
% disp(new_points_r1)

dlmwrite('points.csv', new_points_r1(1,:), '-append');

csvwrite('new_points.csv',new_points)
hold on;
scatter3(new_points(1:6,1),new_points(1:6,2),new_points(1:6,3),'*');
ylabel('Y')
xlabel('X')
zlabel('Z')
end
%-------------------------------------------------------------------
```

APPENDIX E

POSITION COORDINATES OF THE RPT DETECTORS

Table E.1 Position Coordinates of the RPT detectors

Detector	z, cm	r, cm	θ, °
1	7.62	22.86	112.5
2	15.24	22.86	67.5
3	22.86	22.86	112.5
4	30.48	22.86	67.5
5	7.62	22.86	22.5
6	15.24	22.86	337.5
7	22.86	22.86	22.5
8	30.48	22.86	337.5
9	7.62	22.86	202.5
10	15.24	22.86	157.5
11	22.86	22.86	202.5
12	30.48	22.86	157.5
13	7.62	22.86	292.5
14	15.24	22.86	247.5
15	22.86	22.86	292.5
16	30.48	22.86	247.5

APPENDIX F
CALIBRATION OF ENCODERS USED IN RPT CALIBRATION EQUIPMENT

RPT Calibration Equipment Encoder Calibration

Typically the position feedback from the encoder is obtained in some arbitrary counts readings. It is necessary to convert this feedback into angular position co-ordinates of the collimated detectors I and II. Figure F.1 shows schematic diagram of encoder output calibration.

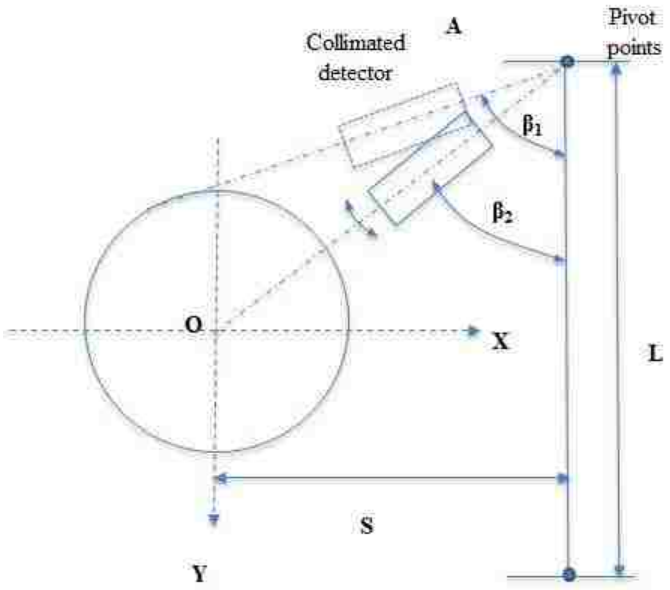

Figure F.1 Schematic diagram of encoder output calibration

The encoder is mounted on the shaft of stepper motor and gives feedback in terms of arbitrary counts. The central axis of a test reactor under study is treated as a first reference position for the calibration of encoder output. The encoder counts are reset to zero when the vertical slit in the swinging collimated detectors is aligned with the central

axis of a test reactor. The corresponding angular position of the collimated detector is identified as β_2. This alignment is carried out using dummy detectors of same size containing lasers in the center. In order to convert encoder counts reading into angular position co-ordinates, another known reference position is required. Usually, an angular position (β_1) of the collimated detector, for which vertical plane passing through the slit in the collimator is tangential to the outer periphery of a test reactor, is treated as another known reference position. For given distance between two pivot points (L) and distance of a central axis of a test reactor from the horizontal line S, these angular positions β_1 and β_2 can be calculated analytically. The encoder output in terms of arbitrary counts for these two reference positions can provide a conversion factor. This conversion factor can then be used to convert position feedback from the encoders into angular position co-ordinates of swinging collimated detectors.

BIBLIOGRAPHY

[1] U.S. D.O.E. Nuclear Energy Research Advisory Committee and the Generation IV International Forum, A Technology Roadmap for Gen-IV Nuclear Energy Systems (Dec. 2002)

[2] Boer B., Optimized core design and fuel management of a pebble-bed type nuclear reactor, Ph.D. thesis, Delft University of Technology, Delft, Netherlands (2009)

[3] Li, Y., Xu, Y., Jiang, S., DEM simulations and experiments of pebble flow with monosized spheres, *Powder Technology* 193 (3) , pp. 312-318 (2009)

[4] Terry W.K., Gougar H.D. and Ougouag, Direct deterministic method for neutronics analysis and computation of asymptotic burn-up distribution in a re-circulating pebble-bed reactor, *Annals of Nuclear Energy*, 29, pp.1345-1364 (2002)

[5] Yang, X., Hu, W., Jiang, S., Experimental Investigation on feasibility of two-region-designed pebble-bed high-temperature gas-cooled reactor, *Journal of Nuclear Science and Technology*, 46 (4) , pp. 374-381 (2009)

[6] Rycroft C., Grest G., Landry J., and Bazant M., Analysis of granular flow in a pebble-bed nuclear reactor, *Phys. Rev. E.*, 74, 021306 (2006)

[7] Al-Dahhan, M., Radioisotopes applications in industry: an overview, *Atoms for Peace: International Journal* , 2 (4), pp. 324 - 337 (2009)

[8] Shenoy, A., et al., Report 910720, Revision 1, General Atomics (1996)

[9] INL, Next Generation Nuclear Plant Research and Development Program Plan, INL/EXT-06-11804 (2008)

[10]Tak, N.-I., Kim, M.-H., Lim, H.S., Noh, J.M. , A Practical Method for Whole-Core Thermal Analysis of a Prismatic Gas-Cooled Reactor, *Nuclear Technology*, 177 (3) , pp. 352-365 (2012)

[11]Lee, H.C., Jo, C.K., Shim, H.J., Kim, Y., Noh, J.M., Decay heat analysis of VHTR cores by Monte Carlo core depletion calculation, *Annals of Nuclear Energy* , 37 (10) , pp. 1356-1368 (2010).

[12] Fogler, H.S., Elements of chemical reaction engineering, Fourth ed. , John Wiley & Sons, New York, 867-1005 (2005).

[13] Sie, S.T., Consequences of catalyst deactivation for process design and operation, *Applied Catalysis A: General* 212 (1-2), pp. 129-151 (2001)

[14] Kesava Rao, K., Nott, Prabhu R., An introduction to granular flow, Cambridge University Press (2008)

[15] Cundall P.A., Strack O.D.L.,A discrete numerical model for granular assemblies, *Geotechnique*, 29, 47–65(1979)

[16] Li Y., Xu Y., Thornton C., A Comparison of Discrete Element Simulations and Experiments for 'Sandpiles' composed of Spherical Particles, *Powder Technology* 160, 219-228 (2005)

[17] Kadak, A.C., and Bazant M.Z., Pebble flow experiments for pebble bed reactors, 2nd International Topical meeting on High Temperature Reactor Technology , Beijing, China (2004)

[18] Gatt, F.C., Flow of spheres and near spheres in cylindrical vessels, part IV, Australian Energy commission, Lucas Heights (1973)

[19] Shehata A., A New Method for Radioactive Particle Tracking, Ph.D. Thesis, North Carolina State University, Raleigh, North Carolina (2005)

[20] du TOIT, C. The Numerical Determination of the Variation on the Porosity of the Pebble-Bed Core, Proceedings of the conference on High-Temperature Reactors, Petten, The Netherlands, European Nuclear Society (2002)

[21] Nedderman, R. M. , Statics and Kinematics of Granular Materials, Cambridge University Press (1992)

[22] http://www.ornl.gov/info/ornlreview/v36_1_03/article_01.shtml (ORNL Review-nuclear power and research reactors) [Accessed December 12th , 2013]

[23] AGE, AVR- Experimental High Temperature Reactor:21 Years of Successful Operation for a Future Energy Technology, The society for Energy Technologies, Dusseldorf (1990)

24] Shehata, A. H. and Gardner, R. P., "A new method for tracking of single radioactive particles", 5th World Congress on Industrial Process Tomography, Bergen, Norway, pp.187-195 (2007)

[25] Deutsch, G.P., Flow of granular material from silos-paper No. 3.3. presented on Symposium on movement of Gran. Material and Struct., Fluid flow and heat transfer in packed beds, AAECRE Lucas heights (1967)

26] Matthew Aichele, Lars Gronning, Tanya Burka, Nicolas Hernandez, Jaehyuk Choi, Jeff Hung, Rhett Creighton, William Kennedy, Jacob Eapen, Scott Mahar, Dandong Feng, Marina Savkina, Catherine Goff, Dean Wang, Pebble Dynamics in PBMR – Experiments and Modeling, MIT Nuclear Engineering Design Report (2002)

[27] PBMR Safety Analysis Report, Document No. 001929-207/4, Rev. B, 6-17 (PBMR, 2000)

[28] Xu,Y.H., and Sun,Y.L., Status of the HTR programme in China, IAEA TCM on High Temperature Gas Cooled Reactor Application and Future Prospects ECN, Petten, The Netherlands (1997)

[29] Jiang, S.Y., Yang, X.T., Tang, Z.W., Wang, W.J., Tu, J.Y., Liu, Z.Y., Li, J., Experimental and numerical validation of a two-region-designed pebble bed reactor with dynamic core, *Nuclear Engineering and Design* 246 , pp. 277-285 (2012)

[30] Yang, X.T., Hu, W.P., Jiang, S.Y., Wong, K.K.L., Tu, J.Y., Mechanism analysis of quasi-static dense pebble flow in pebble bed reactor using phenomenological approach, *Nuclear Engineering and Design* 250 , pp. 247-259 (2012)

[31] Wang Z., A Dual Measurement System for Radioactive Tracer Pebble Tracking in PBRs, PhD Thesis, North Carolina State University, Raleigh, North Carolina (2011)

[32] Li, Y., Xu, Y., Jiang, S., DEM simulations and experiments of pebble flow with monosized spheres, *Powder Technology* 193 (3) , pp. 312-318 (2009)

[33] Iwashita, K., Oda, M., Rolling resistance at contacts in simulation of shear band development by DEM, *Journal of Engineering Mechanics* 124 (3) , pp. 285-292 (1998)

[34] Zhou, Y.C., Wright, B.D., Yang, R.Y., Xu, B.H., Yu, A.B., Rolling friction in the dynamic simulation of sandpile formation, Physica A: Statistical Mechanics and its Applications 269 (2) , pp. 536-553 (1999)

[35] Hertz, H., Über die berührung fester elastischer Körper (On the contact of rigid elastic solids) J. reine und angewandte Mathematik 92, pp. 156-171 (1882)

[36] Fan, L.S., and Zhu, C., Principles of Gas-Solids Flows, Cambridge University Press, Cambridge (1998)

[37] Mindlin, R.D., Compliance of elastic bodies in contact, *Journal of Applied Mechanics*, 16, 259-268 (1949)

[38] Roycroft, C.H., Multi-scale modeling in granular flow, PhD Thesis, Massachusetts Institute of Technology, Cambridge (2007)

[39] Choi, J., Kurdrolli, A., Rosales, R.R., Bazant M.Z., Diffusion and mixing in gravity-driven dense granular flows, *Physical Review Letters*, 92 (17), 301-4304 (2004)

[40] Nedderman, R. M., and Tüzün, U., Kinematic Model for the Flow of Granular-Materials, *Powder Technology*, vol. 22, no. 2, pp. 243-253 (1979)

[41] Mueller, G.E., Radial void fraction distributions in randomly packed fixed beds of uniformly sized spheres in cylindrical containers, *Powder Technology*, 72, 269-275 (1992)

[42] Goodling, J.S., Vachon, R.I., Stelpflug, W.S., Ying, S.J., Khader, M.S., Radial porosity distribution in cylindrical beds packed with spheres, *Powder Technology* 35 (1), 23-29 (1983)

[43] Mariani, N.J. , Salvat, W.I., Campesi, A. , Barreto, G.F. , Martinez, O.M., 2009, Evaluation of structural properties of cylindrical packed beds using numerical simulations and tomographic experiments, *International Journal of Chemical Reactor Engineering* 7, Art. No. A82 (2009)

[44] Cogliati, J.J. , Ougouag, A.M. , PEBBLES: A Computer Code for Modeling Packing, Flow and Re-circulation of Pebbles in a Pebble Bed Reactor, 3rd International Topical Meeting on High Temperature Reactor Technology, Sandton, South Africa, (2006)

[45] Kloosterman, J.L. and Ougouag, A. M., Spatial Effects in Dance-off Factor Calculations for Pebble-Bed HTR's, Mathematics and Computation, Supercomputing, Reactor Physics and Nuclear and Biological Applications Palais des Papes, Avignon, France, September 12-15, 2005, on CD-ROM, American Nuclear Society, LaGrange Park, IL (2005)

[46] Cogliati, J.J., Pebble bed pebble motion: Simulation and Applications, PhD thesis, Idaho State University (2010)

[47] Benenati, R.F. , Brosilow, C.B. , Void Fraction Distribution in Beds of Spheres, *AICHE Journal* 8 pp. 359-361 (1962)

[48] Ougouag, A.M., Cogliati, J.J., 2007, Earthquakes and pebble bed reactors: Time-dependent densification, Joint International Topical Meeting on Mathematics and Computations and Supercomputing in Nuclear Applications (2007)

[48] Li, Y. and Ji, W., Pebble Flow Simulation Based on a Multi-Physics Model, *Trans. Am. Nucl. Soc.* 103, 323-325 (2010)

[49] Li, Y. and Ji, W., Study on Pebble-Fluid Interaction Effect in Pebble Bed Reactors, *Trans. Am. Nucl. Soc.*, 105, 524-525 (2011)

[50] Li, Y. and Ji, W., Pebble Flow and Coolant Flow Analysis Based on a Fully Coupled Multi-Physics Model, *Nuclear Science and Engineering*, 173, 150-162 (2013)

[51] Li, Y. and Ji, W., A Collective Dynamics-based Method for Initial Pebble Packing in Pebble Flow Simulation, *Nuclear Engineering and Design*, **250**, 229-236 (2012)

[52] González-Montellano, C., Ayuga, F., Ooi, J.Y., Discrete element modeling of grain flow in a planar silo: Influence of simulation parameters, *Granular Matter* 13 (2) , pp. 149-158 (2010)

[53] Anand, A., Curtis, J.S., Wassgren, C.R., Hancock, B.C., Ketterhagen, W.R.: Predicting discharge dynamics from a rectangular hopper using the discrete element method (DEM). *Chem. Eng. Sci.* 63(24), 5821–5830 (2008)

[54] Johanson, J.R., Jenike, A.W., Bulletin 116: Stress and velocity fields in gravity flow of bulk solids. Salt Lake City, UT (1962)

[55] EN 1991–4, Actions on structures. Silos and tanks (2006)

[56] Jenike, A.W. Bulletin 108, Gravity flow of bulk solids. Salt Lake City, UT (1961)

[57] Jenike, A.W., Bulletin 123, Storage and flow of solids. Salt Lake City, UT (1964)

[58] Xu, Y., Kafui, K.D., Thornton, C., Lian, G., Effects of material properties on granular flow in a silo using DEM simulation, *Particulate Science and Technology* 20 (2) , pp. 109-124 (2002)

[59] Balevičius, R., Kačianauskas, R., Mróz, Z., Sielamowicz, I., Analysis and DEM simulation of granular material flow patterns in hopper models of different shapes, *Advanced Powder Technology* 22 (2) , pp. 226-235 (2011)

[60] Lee, K. O., Particle Tracking Using Molecular Dynamics Simulation For Pebble Bed Reactors, PhD Thesis, North Carolina State University, Raleigh, North Carolina (2011)

[61] Choi, J., Kudrolli, A. and Bazant, M.Z., Velocity profile of granular flows inside silos and hoppers. *Journal of Physics - Condensed Matter*, Vol. 17, No. 24, pp. S2533-S2548 (2005)

[62] Lee, K.O. , Wang, Z. , Eapen, J., Gremaud, P.A. , Gardner, R.P. , Azmy, Y.Y. , A compressible kinematic model for particle flow in Pebble Bed Reactors, *Trans. American Nucl. Soc.*, 101, pp. 915–916 (2009)

[63] Beverloo, W.A., Leniger, H.A. & Vandevelde, J. , The Flow of Granular Solids through Orifices. *Chemical Engineering Science*, Vol. 15, No. 3-4, pp. 260 (1961)

[64] Kadak A. C., A future for nuclear energy: Pebble bed reactors, *Int. J. Critical Infrastructures*, Vol. 1, No. 4, pp. 330-345 (2005)

[65] Khane V., Abdul Mohsin R., Al-Dahhan M.H., Study of Solids Dynamics in PBR using Radioactive Particle Tracking Technique, *Transactions of American Nuclear Society*, Vol. 103, pp.193-194 (2010)

[66] Khane V., Mueller G.E., Al-Dahhan M.H., Pebble Bed Reactor as Static Packed Bed, *Transactions of American Nuclear Society*,Vol. 105, pp.704-705(2011)

[67] Sen, R.S., Viljoen, C.F., The re-evaluation of the AVR melt-wire experiment with specific focus on different modeling strategies and simplifications, *Nuclear Engineering and Design* 251 , pp. 306-316 (2012)

[68] Lin, J.S. , Chen, M.M., and Chao B.T., A novel radioactive particle tracking facility for measurement of solids motion in gas fluidized beds, *AIChE J*., 31, 465-473 (1985)

[69] Vesavikar M., Understanding hydrodynamics and performance of anaerobic digesters, DSc thesis, Washington University, St. Louis (2006)

[70] Moslemian, D., Devanathan, N. and Duduković, M.P., Radioactive particle tracking for investigation of phase recirculation and turbulence in multiphase systems, *Rev. Sci. Instrum.*, 63(10), 4361-4372 (1992)

[71] Roy S., Larachi F., Al-Dahhan M.H., Duduković M.P., Optimal design of radioactive particle tracking experiments for flow mapping in opaque multiphase reactors, *Applied Radiation and Isotopes*, 56, pp. 485–503 (2002)

[78] Ingram A., Hausard M., Fan X., Parker D. J., Seville J.P.K., Finn N. , and M. Evans, Portable Positron Emission Particle Tracking (PEPT) for Industrial Use, The 12th International Conference on Fluidization - New Horizons in Fluidization Engineering Art.60, pp. 494-504 (2007)

[79] Chaouki, J., Larachi, F., and Duduković, M.P., Noninvasive Tomographic and Velocimetric Monitoring of Multiphase Flows, *Ind. Eng. Chem. Res.*, 36, pp. 4476-4503 (1997)

[80] Chen, R.C., and Fan, L.S., Particle image velocimetry for characterizing the flow structure in three-dimensional gas-liquid-solid fluidized beds, *Chem. Eng. Sci.*, 47, pp. 3615-3622 (1992)

[81] Chen, J., Kemoun, A., Al-Dahhan, M.H., Duduković, M.P., Lee, D.J., and Fan, L.-S., Comparative hydrodynamics study in a bubble column using computer-automated radioactive particle tracking (CARPT)/computed tomography (CT) and particle image velocimetry (PIV), *Chemical Engineering Science* 54 (13-14), pp. 2199-2207 (1999)

[82] Adrian, R.J. , Particle-imaging techniques for experimental fluid mechanics, *Annual Review of Fluid Mechanics*, Vol. 23, pp. 261–304 (1991)

[83] Dominguez-Ontiveros, E.E., and Hassan, Y.A., Non-intrusive experimental investigation of flow behavior inside a 5 × 5 rod bundle with spacer grids using PIV and MIR, *Nuclear Engineering and Design* 239 (5), pp. 888-898 (2009)

[84] Durst, F., Melling, A., and Whitelaw, J.H., Principles and practice of laser Doppler anemometry, Academic Press, London (1976)

[85] Kondukov N.B., Kornilaev A.N., Skachko I.M., Akhromenkov, A.A., and Kruglov A.S., An investigation of the parameters of moving particles in a fluidized bed by a radioisotropic method, *Int. Chem. Eng.*, 4, 43-47 (1964)

[86] Van Velzen, D., Flamm H.J., Langenkamp H., and Casile A., Motion of solids in spouted beds, *Canadian J. Chem. Eng.*, Vol. 52, 156-161 (1974)

[87] Meek C.C., Statistical characterization of dilute particulate suspensions in turbulent fluid fields, PhD Thesis, University of Illinois, Urbana, Illinois (1972)

[88] Lin, J.S., Chen, M.M. and Chao, B.T., A novel radioactive particle tracking facility for measurement of solids motion in gas fluidized beds, *AIChE J.*, Vol. 31, No. 3, 465-473 (1985)

[89] Moslemian, D., Study of solids motion, mixing and heat transfer in gas-solid fluidized beds, PhD Thesis, University of Illinois, Urbana, Illinois (1987)

[90] Devnathan, N., Investigation of Liquid Hydrodynamics in Bubble columns via Computer Automated Radioactive Particle Tracking (CARPT), D.Sc., St. Louis, Missouri, (1991)

[91] Yang, Y.B., Devnathan, N., and Duduković, M.P., Liquid backmixing in bubble columns, *Chemical Engineering Science*, 47(9-11), pp.2859-2864 (1992)

[92] Degaleesan, S., Fluid dynamic measurements and modeling of liquid mixing in bubble columns, D.Sc. Thesis, Washington University, St.Louis, Missouri (1997)

[93] Luo, H.P., Analyzing and Modeling of Airlift Photo-bioreactors for Microalgal and Cyanobacteria Cultures, D.Sc. Thesis, Washington University, St. Louis, Missouri (2005)

[94] Rados, N., Slurry Bubble Column Hydrodynamics, D.Sc. Thesis, Washington University, St. Louis, Missouri (2003)

[95] Rammohan, A., Characterization of single and multiphase flows in stirred tank reactors, D.Sc. Thesis, Washington University, Saint Louis, Missouri (2002)

[96] Bhusarapu, S., Solids flow mapping in gas solid risers, DSc thesis, Washington University St. Louis Missouri (2005)

[97] Wentworth, W.E., Dependence of the Beer-Lambert absorption law on monochromatic radiation: An experiment in spectrophotometry, *Journal of Chemical Education* 43 (5), pp. 262-264 (1966)

[98] Goats, G.C., Appropriate use of the Inverse Square Law, *Physiotherapy* 74 (1), pp. 8 (1988)

[99] Knoll, G.F., Radiation detection and Measurement, 3rd edition, John Wiley and Sons Inc., Section 10, pp. 308-312 (2000)

[100] McCabe, W.L., Smith, J.C., Harriott, P., Unit Operations of Chemical Engineering, Fifth Edition, McGraw-Hill, Inc., New York (1993)

[101] Luo, X., Li, X., Yu, S., Nuclear graphite friction properties and the influence of friction properties on the pebble bed, *Nuclear Engineering and Design* 240 (10) , pp. 2674-2681 (2010)

[102] Tsoulfanidis, N., Measurement and Detection of Radiation, McGraw-Hill, New York, NY, pp. 73–76 (1983)

[103] Moens, L., De Donder, J., Xi-lei, L., De Corte, F., De Wispelaere, A.,Simonits, A., and Hoste, J., Calculation of the absolute peak efficiency of gamma-ray detectors for different counting geometries , *Nuclear Instruments and Methods*187 (2-3), pp. 451-472 (1981)

[104] Pommé, S., Alzetta, J.P. , Uyttenhove, J. , Denecke, B. Arana, G. and Robouch, P., Accuracy and Precision of Loss-Free Counting in γ-ray Spectrometry, *Nucl. Instr. & Meth. Phys. Res. Sec. A* (422), pp.388-394 (1999)

[105] Mostoufi, N., Kenned, G., Chaouki, J., Decreasing the sampling time interval in radioactive particle tracking, *Canadian Journal of Chemical Engineering* 81 (1), pp. 129-133 (2003)

[106] Larachi, F., Kennedy, G., Chaouki, J., A γ-ray detection system for 3-D particle tracking in multiphase reactors, *Nuclear Inst. and Methods in Physics Research*, A 338 (2-3), pp. 568-576 (1994)

[107] Gupta, P., Churn-turbulent bubble columns: experiments and modeling, D. Sc. Thesis, Washington University, St. Louis, Missouri (2002)

[108] Godfroy, L., Larachi, F., Kennedy, G., Grandjean, B., Chaouki, J., On-line flow visualization in multiphase reactors using neural networks, *Applied Radiation and Isotopes* 48 (2), pp. 225-235 (1997)

[109] Yang, Y.B., Devanathan, N., and Duduković, M.P., Liquid Backmixing in Bubble Columns via Computer-Automated Radioactive Particle Tracking (CARPT), *Experiments in Fluids*, 16, 1-9 (1993)

[110] Godfroy, L., Larachi, F., Chaouki, J., Position and velocity of a large particle in a gas/solid riser using the radioactive particle tracking technique, *Canadian Journal of Chemical Engineering* 77 (2) , pp. 253-261 (1999)

[111] Degaleesan, S., Duduković, M.P., Pan, Y. , Application of wavelet filtering to the radioactive particle tracking technique, *Flow Measurement and Instrumentation* 13 (1-2) , pp. 31-43 (2002)

[112] CARPT Manual- Introduction to Radioactive Particle Tracking for Potential Users, Chemical Reaction Engineering Laboratory (CREL), Washington University, St. Louis, Missouri (2007)

[113] Khane, V., Mueller G.E., and Al-Dahhan M.H, Experts in Discrete Element Modeling (EDEM) Validation for Packed Bed Structural Properties, AIChE-2010 Annual Meeting, Salt Lake City, Utah (2010)

[114] Bharadwaj, R., Ketterhagen, W.R., Hancock, B.C. , Discrete element simulation study of a Freeman powder rheometer, *Chemical Engineering Science* 65 (21),5747-5756 (2010)

[115] Ergun S., *Chem. Eng. Prog.* 48, pp.89-94 (1952)

[116] Mueller, G.E., Numerically packing spheres in cylinders, *Powder Technology*, 159,105-110 (2005)

[117] Mueller, G.E., Radial porosity in packed beds of spheres. *Powder Technology*., 203, 626-633 (2010)

[118] Mosorov, V., Abdullah, J., MCNP5 code in radioactive particle tracking, *Applied Radiation and Isotopes* 69 (9) , pp. 1287-1293 (2011)

[119] Salvat, W.I., Mariani, N.J., Barreto, G.F., Martínez, O.M., An algorithm to simulate packing structure in cylindrical containers, *Catalysis Today* 107-108 , pp. 513-519 (2005)

[120] Visscher, W.M., Bolsterli, M., Random packing of equal and unequal spheres in two and three dimensions. *Nature* 239, 504–507 (1972)

[121] Zamponi, F., Mathematical physics— packings close and loose. *Nature* 453, 606–607 (2008)

[122] Soppe, W., Computer-simulation of random packings of hard-spheres, *Powder Technology*, 62, 189–197 (1990)

[123] Nolan, G.T., Kavanagh, P.E., Computer-simulation of random packing of hard spheres , *Powder Technology*, 72, 149–155 (1992)

[124] Clarke, A.S., and Wiley, J.D., Numerical-simulation of the dense random packing of a binary mixture of hard-spheres—amorphous metals. *Phys. Rev. B* 35, 7350–7356 (1987)

[125] Cooper, D.W., Random-sequential-packing simulations in three dimensions for spheres. *Phys. Rev. A* 38, 522–524 (1988)

[126] Bagi, K., An algorithm to generate random dense arrangements for discrete element simulations of granular assemblies. *Granul. Matter* 7, 31–43 (2005)

[127] Kuroki, M., Ookawara, S., Ogawa, K., A high-fidelity CFD model of methane steam reforming in a packed bed reactor, *Journal of Chemical Engineering of Japan*, 42 (SUPPL. 1), 73-78 (2009)

[128] Theuerkauf, J., Witt, P., Schwesig, D., Analysis of particle porosity distribution in fixed beds using the discrete element method, *Powder Technology* 165 (2), 92-99 (2006)

[129] Bai, H., Theuerkauf, J., Gillis, P.A., Witt, P.M., A coupled DEM and CFD simulation of flow field and pressure drop in fixed bed reactor with randomly packed catalyst particles, *Industrial and Engineering Chemistry Research* 48 (8), 4060-4074 (2009)

[130] Zhang, W., Thompson, K.E., Reed, A.H., Beenken, L., Relationship between packing structure and porosity in fixed beds of equilateral cylindrical particles, *Chemical Engineering Science* 61 (24) , pp. 8060-8074 (2006)

[131] Mariani, N.J., Martínez, O.M., Barreto, G.F., Computing radial packing properties from the distribution of particle centers, *Chemical Engineering Science* 56 (20), pp. 5693-5707 (2001)

[132] Sederman, A.J., Alexander, P., Gladden, L.F., Structure of packed beds probed by Magnetic Resonance Imaging, *Powder Technology* 117 (3) , pp. 255-269 (2001)

[133] Silbert, L.E., Ertas, D., Grest, G.S., Halsey, T.C. & Levine, D. , Geometry of frictionless and frictional sphere packings, *Physical Review E*, Vol. 65, No. 3 (2002)

[134] Herbig, T. Khane, V., Mueller, G.E., Al-Dahhan, M.H., Determination of Interaction Parameters for EDEM^{TM} Based Simulations of Pebble Bed Test Reactor Transactions of American Nuclear Society, Vol. 105, pp.701-702 (2011)

[135] http://engineershandbook.com/Tables/frictioncoefficients.htm [Accessed December 15th , 2013]

[136] EDEM™ User Manual, DEM Solutions (USA) Inc., Edinburgh, Scotland (2010)

[137] Tsuji, Y., Tanaka, T., Ishida, T., Lagrangian numerical simulation of plug flow of cohesionless particles in a horizontal pipe. *Powder Technol.* 71(3), 239–250 (1992)
[138] Mindlin R.D., Deresiewicz, H., Elastic Spheres in contact under varying oblique forces, Transactions of ASME, Series E. *Journal of Applied Mechanics* 20, 327-344 (1953)

[139] Claxton, K.T., A review of Pebble Bed Reactors and the Characteristics of Packed Beds, Journal of Nuclear Energy. Parts A/B. *Reactor Science and Technology* 20 (9) , pp. 735-777 (1966)

[140] Sederman, A.J., Johns, M.L., Alexander, P., Gladden, L.F., Structure-flow correlations in packed beds, *Chemical Engineering Science* 53 (12) , pp. 2117-2128 (1998)

[141] Bai, B., Liu, M., Lv, X., Yan, J., Yan, X., Xiao, Z., Correlations for predicting single phase and two-phase flow pressure drop in pebble bed flow channels, *Nuclear Engineering and Design* 241 (12) , pp. 4767-4774 (2011)

[142] Association of German Engineers (VDI), the Society for Energy Technologies (publ.) , AVR - Experimental High-Temperature Reactor, 21 Years of Successful Operation for A Future Energy Technology, pp. 9–23. ISBN 3-18-401015-5 (1990)

[143] Ong, B. C., Experimental investigation of bubble columns hydrodynamics: effect of elevated pressure and superficial gas velocity, D.Sc. Thesis, Washington University, Saint Louis (2003)

[144] Boyalakuntla, D.S. and Pannala, S., Summary of Discrete Element Model (DEM) Implementation in MFIX (2006)

[145] Liapis, A.I., Meyers, J.J., Crosser, O.K., Modeling and simulation of the dynamic behavior of monoliths: Effects of pore structure from pore network model analysis and comparison with columns packed with porous spherical particles, Journal of Chromatography A 865 (1-2) , pp. 13-25 (1999)

[146] Meyers, J.J., Liapis, A.I., Network modeling of the intraparticle convection and diffusion of molecules in porous particles packed in a chromatographic column, Journal of Chromatography A 827 (2) , pp. 197-213 (1998)

[147] Rougier, E., Munjiza, A., John, N.W.M., Numerical comparison of some explicit time integration schemes used in DEM, FEM/DEM and molecular dynamics, International Journal for Numerical Methods in Engineering 61 (6) , pp. 856-879 (2004)

[148] Han, L, Hydrodynamics, back-mixing, and Mass Transfer in a Slurry Bubble Column Reactor for Fischer-Tropsch Alternative Fuels, DSc Thesis, Washington University, Saint Louis (2007)

VITA

Vaibhav B. Khane was born in Kolhapur, Maharashtra, India. In February 2003, he received his Bachelors of Engineering (BE) in Mechanical Engineering from the Shivaji University, Kolhapur. After bachelors, he joined one year Orientation course for Engineering Graduates and Science post-graduates (OCES-2004 batch) in Nuclear Engineering in September 2004. After successful completion of training, he joined as a Scientific Officer-C with Nuclear Power Corporation of India Ltd. He worked with NPCIL for nearly three years in capacity of system commissioning engineer for TAPP 3 & 4, main plant operation engineer for KGS 1 & 2. In 2007, he came to USA to pursue Masters of Science (MS) in Nuclear Engineering at Missouri University of Science and Technology (Missouri S&T), Rolla, Missouri. In December 2009, he received his MS in Nuclear Engineering from Missouri University of Science and Technology in Rolla. After successful completion of MS, he joined PhD program in Department of Chemical and Bio-chemical Engineering at Missouri S&T in the spring of 2010. His main area of research is in bench-scale experimentation, development of advanced radioisotopes based flow visualization techniques, modeling and simulation of multiphase flow systems using DEM and CFD based codes. In May 2014, he received his Ph.D. in Chemical Engineering from Missouri University of Science and Technology, Rolla.

Vaibhav Khane has been a student member of the American Nuclear Society (ANS) since 2007. Also he has been a student member of the American Society for Mechanical Engineers (ASME) since 2007. He was inducted into Alpha Nu Sig 2009.